ON THE EFFECTS OF VISCOELASTICITY

IN STIRRED TANKS

by N. GÜL ÖZCAN-TAŞKIN

A thesis submitted to The Faculty of Engineering

of The University of Birmingham for the degree of DOCTOR OF PHILOSOPHY

School of Chemical Engineering

University of Birmingham

Birmingham, U.K.

April, 1993

ABSTRACT

Mixing viscoelastic fluids is common to many chemical and biochemical process industries where the rheological properties of the bulk change considerably over the time course. The objectives of this study were to investigate the effects of viscoelasticity in mechanically agitated vessels (on: *i*- the power consumption and flow patterns in single phase and gassed systems, *ii*- mixing time under unaerated conditions and *iii*- cavities in the presence of gas) and to study the performance of InterMIGs in comparison to the classical six bladed disc turbines. Model viscoelastic fluids prepared exhibited only slight shear thinning properties (Boger fluid type), hence the effects of viscoelasticity could be studied in the absence of other rheological properties. Results obtained with these fluids were compared to those with viscous Newtonian glycerol covering the transitional flow regime ($50 < Re < 1000$). Additionally, some work was also conducted in water for a preliminary characterisation of InterMIGs.

In the relatively low range of Elasticity numbers ($El < 3.5 \times 10^{-3}$) covered, secondary flow patterns were not reversed. The power drawn under unaerated conditions was higher in viscoelastic fluids (at a given Reynolds number) for both impeller types that had to compete with mutually opposing viscoelastic forces.

An experimental set-up to measure mixing times in viscous fluids (using the fluorescent dye-fibre optic technique) was installed. Reduced secondary circulations in viscoelastic fluids resulted in longer mixing times.

Power consumption under aeration was also higher in viscoelastic fluids than that in Newtonian glycerol. Different from the findings under unaerated conditions, this enhancement was independent of the level of viscoelasticity. Cavities, hence the power drawn under aeration, were in general stable with respect to the variations in the gas flow rate in viscous fluids. This stability was found to be accentuated by viscoelasticity.

InterMIGs underwent viscoelastic effects more severely on account of the complicated interaction of the viscoelastically driven flows with the flows associated with the inner and outer blades of these impellers. They presented a better choice in low and high viscosity Newtonian fluids and their performance was comparable to that of a single Rushton turbine in viscoelastic fluids.

Dedicated to my mother

Ayla OZCAN

and my father

Halil OZCAN

ACKNOWLEDGEMENTS

I am greatly thankful to my parents, Ayla and Halil ÖZCAN without whose support this work could not have started.

I would like to thank Professor Alvin W. NIENOW for his encouragement and suggestions,

and Dr A.J. Barker for his general guide as the post-graduate tutor throughout this work.

I would also like to thank the technical staff of the Mixing Group particularly those who changed the impellers despite their lack of enthusiasm for "handling sticky fluids" :

Mr Sid Chatwin, who provided continuous support during the experimental stage of this study, for his meticulous work for various modifications and maintanence of T61;

Mr Geoff Bartlett, who was involved in the installation of the mixing time measurement equipment, especially for the PMT module he recovered from a forgotten corner of the Department;

Mr Bob Badham, Mr Bob Sharpe and Mr John Homer for their various contributions;

as well as Mrs Wendy Keil for her efforts to fit appointments for me;

and Ms G. Wheeler for the photography work she managed to finish at the very last moment.

Among many people, with whom I had various discussions, I would like to acknowledge Prof. L. Choplin (Laval Univ., Canada), Prof. J. Norton

(Elec. Eng. Dept., Birmingham Univ.), Dr T. Taskin (GEC-Alsthom), Dr N. Berovic (Physics Dept., Birmingham Univ.), Dr W. Bujalski, Dr R. Oliver and A. Kowalski (Chem. Eng., Birmingham Univ.), Dr M. Cooke (ICI) for the interest they have shown and advice they have offered.

I cannot pass without mentioning the efforts that Dr Tamer TASKIN, who has been my partner throughout this study, has shown to be a patient person, my brother, Alpay ÖZCAN, who has always cheered me up from miles away.

Thursday evenings I spent with my students at the Brasshouse Centre: Janey, Ken, Robin, Ruth, Philip, Karen, David, Julie, Tracey and many others as well as my collegues Roula King, Tayfun Caga will be part of the colourful memories.

I will always remember my lab-mates and office-mates- especially Shaliza for all those times we laughed and worked together in the darknesses of G29, Mick and others.

I would finally like to thank Dr C.D. Rielly, Dr M.R. Mackley as well as "the Mackley crew" and the Post-doc Soc: to mention a few, Dean Ilievski, Feng Zhao, John Craven, Nigel Sherman, Paul Stonestreet, Ping Gao, Riaz Ahmed, Rob Marshall Suk Pannu and others for making my days in Cambridge possible and so enjoyable.

TABLE OF CONTENTS

CHAPTER I INTRODUCTION

I.1 MAJOR AREAS OF INTEREST AND MOTIVATIONS

Two major areas of interest of this research have been the effects of viscoelasticity in mechanically agitated vessels and the characterisation of the performance of a relatively new type of impeller in such systems.

The mixing of viscous fluids that also exhibit other rheological properties, is commonly carried out in stirred tanks in many industrial applications. The process can also require the contact of the liquid phase with gas. Several examples can be found in fermentation, food, pharmaceutical, paint and polymer industries where the viscosity of the bulk liquid increases and a complex rheological behaviour is built up during the process[2,3,72,74] due to a chemical or a biochemical reaction. All these changes affect the reactor performance in particular in batch and semi-batch processes. The initial liquid may be Newtonian with a very low viscosity. Microbial growth and excretion of extracellular metabolites in the fermentation and pharmaceutical industries (e.g. xanthan and mycelial fermentations), the addition of additives in the food industry (e.g. gums) and the production of polymers during polymerization reactions drastically increase the viscosity. The flow behaviour of the bulk liquid also deviates from that of Newtonian exhibiting shear thinning, viscoelastic properties with a yield value. These changes in the bulk rheology considerably alter the flow patterns, the pumping capacity of the impeller, the power demand, the mixing times, the mechanism of bubble break up, heat and mass transfer rates which in turn affect the product yield. Hence, they are significantly important to process design.

Studies in the field of mixing are generally carried out with model fluids due to the complexities arising from the time- dependent variation of

the physical properties of real fermentation broths or other industrial fluids and also because these allow visual observations that cannot be made with opaque fluids generally handled in stainless steel equipment. Despite increasing interest in viscous non-Newtonian fluids[13,69,76,77,78,132], a majority of the previous studies were carried out in water and water-like fluids- mainly Newtonian sugar or low concentration polymer solutions were used covering the turbulent flow regime. Although the study of these fluids is essential for a basic and preliminary understanding of many phenomena, they are far from simulating the rheologically complex behaviour of fermentation broths or other viscous fluids processed in industry. Shear thinning behaviour is one of the non-Newtonian fluid properties which has been extensively studied. The effects of viscoelasticity, on the other hand, are not so well understood due to the coexistence of this fluid property with others. Most viscoelastic fluids also exhibit other rheologically complex behaviour. Results obtained with such fluids have therefore been difficult to interpret in terms of viscoelasticity or another fluid property. Findings of researchers differ considerably. Mixing viscoelastic fluids is however quite common to many industrial applications. All the examples given above (polymer and bio-polymer production, mixing food additives, etc) exhibit viscoelastic behaviour. Viscoelastic fluid properties are known to interfere with the flow patterns induced by the impeller, even reverse them, resulting in changes in the power drawn, mainly on account of the non-zero normal stress differences. One motivation of this study came from the need of a better understanding of the role of viscoelasticity in mechanically agitated systems. Model fluids that exhibit viscoelasticity in the absence of other complex rheological behaviour (the so-called **Boger fluids**) were used for this purpose. These were also highly viscous and the transitional flow regime was covered.

Among the traditional impellers, six bladed disc turbines or Rushton

turbines are commonly used for gas dispersion purposes in low viscosity fluids. These are operated at high speeds; they create high local shear rates and the good momentum transport allows the energy from the impeller to be dissipated throughout the bulk. Gate and anchor impellers, which are large in size reaching the far corners of the vessel and helical impellers (screw or ribbon), which are operated slowly, are generally preferred for blending high viscosity fluids. These have an excellent pumping capacity, but their performance in low viscosity liquids and in particular for dispersing gas is known to be fairly poor. One or the other from the classical impeller types can be recommended for a given low or high viscosity range. For processes, where the rheological properties of the bulk change, the problem rises in the choice of a suitable impeller that would perform reasonably well during various stages of the process despite the changes in rheology. Another motivation of this study originated from the need of using alternative, new design impellers. **InterMIGs** were therefore studied. These impellers are recently reported to have successful applications for various purposes in both British[22] and German industries[41,125,133,134]. Hence, in this project it was aimed on one hand to study the effects of viscoelasticity on the flow patterns and power consumption in single phase systems and under aeration, on mixing time under unaerated conditions and cavities for aerated systems. On the other hand, the energetic aspects of mixing viscous fluids with InterMIGs was investigated in comparison to the classical six bladed disc turbines.

Most experimental facilities used were already available in the Department. A new experimental set-up for measuring mixing time using the **fluorescent dye- fiber optic technique** was installed during the course of this study since conventional techniques present various disadvantages for mixing time measurements in viscous fluids. The results presented in the

following chapters of this thesis are from the author's own work unless otherwise stated. Some of these results were presented as publications[86,87,88] which can be found in the Appendix.

I.2 LAYOUT OF THESIS

Following this introduction, Chapter II is on the rheology of model fluids used in this study. Chapters from III to VIII are concerned with various aspects of mixing studies: Chapters III to V are about the studies under unaerated conditions and VI to VII under aerated conditions. These chapters (II to VIII) are all individually constructed. Each is opened with a brief introduction, after which the relevant background theory, experimental results obtained during this study and discussions are given and then closed with a concluding section. Various equipment used is described in the relevant chapters (II, III, V and VI) and only briefly specified in others. Chapter IX contains general conclusions.

In Chapter II, the rheology of model fluids used in mixing experiments are presented, with more emphasis on viscoelastic fluids. The equipment used for measuring rheological properties is also described. The third and fourth chapters are concerned with the flow pattern observations and power characteristics of InterMIGs and Rushton turbines; Chapter III covers Newtonian fluids and Chapter IV viscoelastic fluids. Mixing equipment used throughout this study is detailed in Chapter III. The efficiency of the two types of impellers with variations on their geometry was studied measuring mixing time at a specific power input. Chapter V is allocated to mixing time studies where the performance of these impellers under unaerated conditions is evaluated in relation to fluid rheology. An experimental set-up designed for measuring mixing time in highly viscous fluids was installed during the course of this study. This fluorescent dye-fiber optic technique is described

in Chapter V.

Chapters VI, VII and VIII are concerned with the flow pattern and cavity observations and power characteristics of InterMIGs and Rushton turbines under aerated conditions. Chapters VI and VII cover studies with Newtonian fluids in the turbulent and transitional flow regimes respectively. In Chapter VI, additional equipment and techniques for aerated conditions are introduced. Studies on the effects of fluid viscoelasticity on flow patterns, cavities and power consumption for aerated conditions are presented Chapter VIII.

Despite the individual character of each chapter, they are strongly interrelated. In the results and discussions sections of many chapters, attributions and comparisons are made to the findings reported in other chapters. In Chapter IX, which contains major findings and conclusions, suggestions are also made for future work.

CHAPTER II RHEOLOGY OF MODEL FLUIDS

II.1 INTRODUCTION

The changes in rheological properties over the time course of batch and semi-batch processes is common to many applications in the food, fermentation and pharmaceutical industries. These changes result in significant modifications to the flow patterns, power requirements, heat and mass transfer rates. In order to study the importance of these properties, model fluids simulating the rheology of biological media have been used in mixing studies avoiding complexities that arise from continuous changes in the course of time. These fluids, which are mostly transparent, are also suitable for visual observations that can not be made in (bio)reactors.

This chapter is concerned with rheology where general concepts and fluids of different flow behaviour relevant to applications in mixing and particularly to the experimental aspects of this work are briefly introduced in Sections II.2 and II.3. More detailed information can be found in books by Skelland (1967), Sherman (1970), Whorlow (1980), Walters (1980) and Barnes et al (1989). Model fluids and the equipment for measuring rheological properties used in this study are presented in Section II.4. The rheological characteristics of these fluids can be found in Section II.5, and a brief discussion is given in Section II.6.

II.2 GENERAL THEORY OF FLUID FLOW

Considering a small element of a liquid undergoing steady motion between the wall of a stationary cylindrical vessel and that of a rotating coaxial cylinder (*Figure II.1*) the stress tensor (τ_{ij}) can be defined by nine components:

$$\tau_{ij} = \begin{bmatrix} \tau_{xx} & \tau_{xy} & \tau_{xz} \\ \tau_{yx} & \tau_{yy} & \tau_{yz} \\ \tau_{zx} & \tau_{zy} & \tau_{zz} \end{bmatrix} \qquad (II.1)$$

τ_{xy}, τ_{xz}, τ_{yz}, τ_{yx}, τ_{zx}, τ_{zy} are the shearing stresses where

$\tau_{xz} = \tau_{zx} = 0$, $\tau_{yz} = \tau_{zy} = 0$ - the relative motion between the cylinders being in the x- direction, $\tau_{xy} = \tau_{yx}$.

τ_{xx} , τ_{yy} ,and τ_{zz} are the normal stresses. τ_{yx} varies in the y- direction and is in most texts denoted simply as τ. This will also be used for the rest of this thesis. The flow curve of a fluid is obtained plotting shear stress (τ, Pa) as a function of shear rate ($\dot{\gamma}$, s^{-1})- i.e. the change of shear strain per unit time, (*Figure II.2*). The constitutive equation relating the shear stress to the shear rate :

$$\tau = \mu \dot{\gamma} \qquad (II.2)$$

is linear for Newtonian fluids and passes through the origin. The coefficient of shear rate (or the slope of the flow curve) is the Newtonian viscosity (μ, Pa s), which is only dependent on temperature and pressure. At constant temperature and pressure, Newtonian behaviour is characterised as follows (Barnes et al, 1989) :

i) The shear stress is the only stress generated in simple shear flow.

ii) The shear viscosity is not dependent on the shear rate.

ii) The viscosity does not vary with the time of shearing and the stress in the liquid falls to zero immediately after the shearing is stopped. The viscosity from any subsequent shearing - regardless of the period of time between the measurements - is as before.

Figure II.1 Stress components around a rotating coaxial cylinder

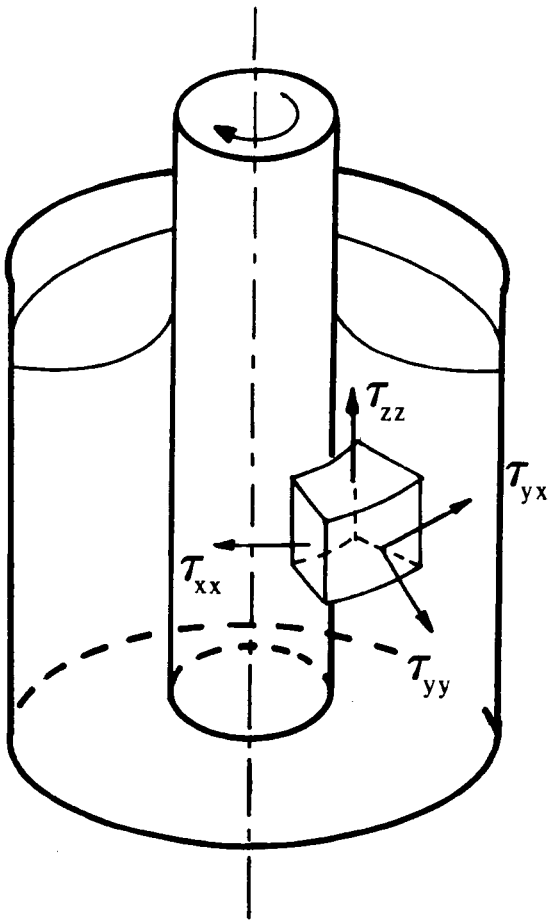

iv) The viscosity measured in different types of deformation (for example, uniaxial extensional flow and simple shear flow) are always in simple proportion to one another.

All liquids showing deviations from the above behaviour are non-Newtonian - some examples are shown in *Figure II.2*. The viscosity of a non-Newtonian fluid is not a coefficient of the shear rate but a function of it and is called the apparent viscosity :

$$\mu_a = \frac{\tau}{\dot{\gamma}} \qquad \text{(II.3)}$$

Non-Newtonian fluids can usefully be classified into three main categories (Skelland, 1967) even though in some cases sharp distinction between these groups is difficult :

i) Time independent fluids : the shear stress at any point is dependent only upon the instantaneous shear rate at that point.

ii) Time dependent fluids : the shear stress, and hence the viscosity, either increases or decreases with the duration of the shearing. These changes may be reversible or irreversible.

iii) Viscoelastic fluids : have both elastic solid and viscous fluid characteristics. They exhibit partial elastic recovery after a deforming shear stress is removed.

II.2.1. Time-independent fluids

The majority of non-Newtonian fluids are found to be pseudoplastic under this category (*Figure II.2*). The viscosity of pseudoplastic fluids decreases with increase in shear rate, therefore they are also called shear-thinning fluids. The characteristic of the flow curve is the linearity at very low and very

high shear rates where constant viscosities are measured. As *Figure II.3* also indicates, the "zero shear" viscosity (μ_0) is obtained at very low shear rates (section A), and the "high shear limiting" viscosity (μ_∞) which has a much lower value than μ_0 at high shear rates (section C). The pseudoplastic fluid flow behaviour can be modelled by the Cross or the Carreau equations which contain both the μ_0 and μ_∞ or the Ellis model which is a simplified form of these[4,16]. Amongst various models, that of Oswald-de-Waele (or the power law model), which predicts shear thinning behaviour within a range of shear rates, has been very widely used:

$$\tau = K (\dot{\gamma})^n \qquad (II.4)$$

K (kg m^{-1} s^{n-2}) is the consistency index and n the flow behaviour index. The deviation of n from 1 is a measure of the departure from Newtonian behaviour and for shear thinning fluids $0 < n < 1$. The expression for the apparent viscosity (μ_a) can be obtained combining equations (II.3) and (II.4) :

$$\mu_a = K (\dot{\gamma})^{n-1} \qquad (II.5)$$

where the apparent viscosity is linearly proportional to the shear rate on logarithmic scale (section B on *Figure II.3*).

For dilatant fluids, $n > 1$. Rheological dilatancy refers to increasing viscosity with increasing shear rate. Therefore, these fluids are also called shear thickening.

Pseudoplastic and dilatant fluids begin to flow as soon as a stress is applied. For plastic fluids, a yield value (τ_y) has to be exceeded so that flow occurs (*Figure II.2*). Several models - Bingham model, Herschel-Bulkley model, Casson model - have been proposed to characterise the

Figure II.2 Flow curves of Newtonian and non-Newtonian fluids

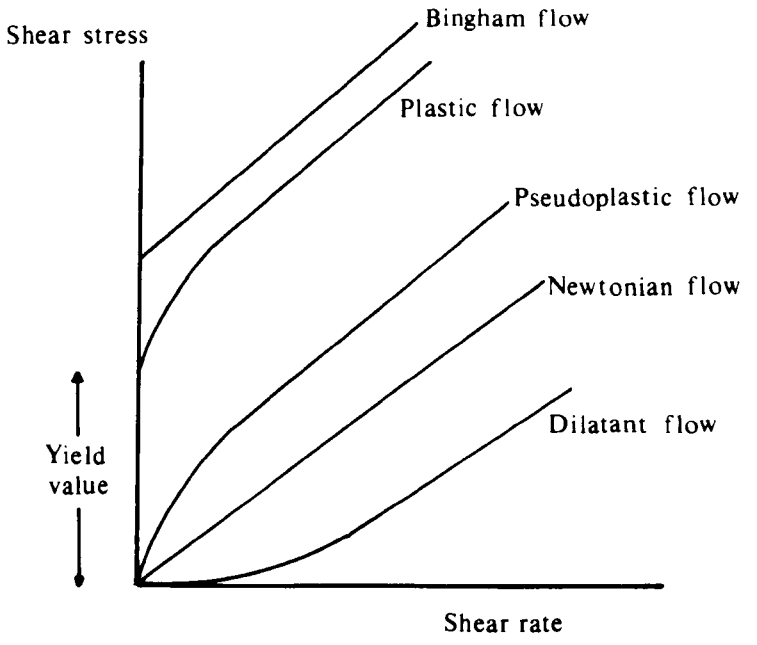

Figure II.3 Shear viscosity as a function of shear rate for a pseudoplastic fluid, showing regions of low shear limiting viscosity ($\dot{\gamma}_0$), high shear limiting viscosity ($\dot{\gamma}_\infty$) and power law behaviour.

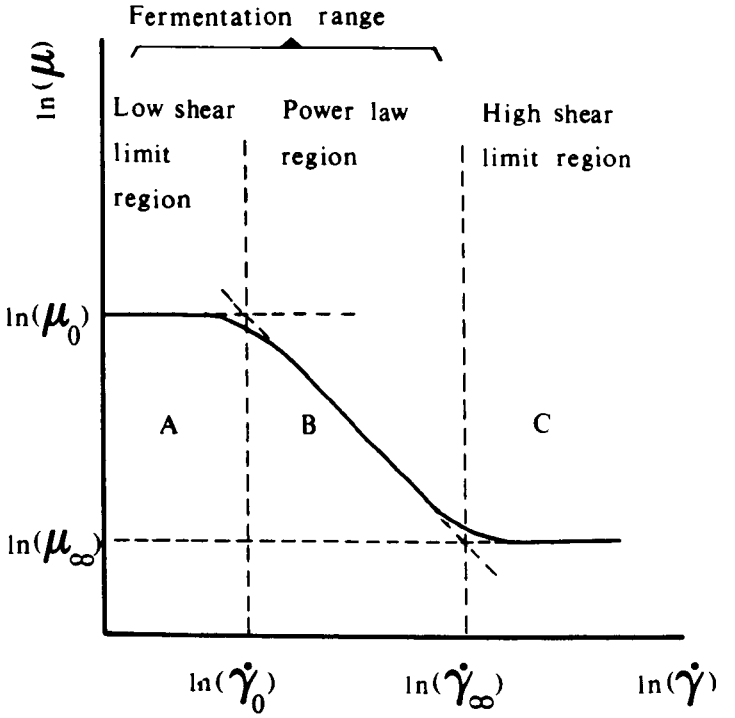

flow behaviour of these fluids.

II.2.2. Time dependent fluids

Thixotropic and rheopectic fluids are found in this group. When a shear stress is applied to a thixotropic fluid, the viscosity decreases gradually and when the stress is removed a gradual recovery is recorded. An opposite behaviour is observed with rheopectic fluids : gradual increase of viscosity followed by recovery upon the removal of stress.

II.2.3. Viscoelastic fluids

These materials exhibit elastic and viscous properties simultaneously.

Normal stresses generated under simple shear flow : τ_{xx} , τ_{yy} , and τ_{zz} are illustrated on *Figure II.1.* The magnitude of these normal stresses varies with the shear rate. It is usual to work in terms of normal stress differences rather than normal stresses themselves :

$$\tau_{xx} - \tau_{yy} = N_1(\dot{\gamma}) \qquad (II.6)$$

N_1 (Pa) is the first normal stress difference, and

$$\tau_{yy} - \tau_{zz} = N_2(\dot{\gamma}) \qquad (II.7)$$

N_2 (Pa) is the second normal stress difference. In viscoelastic fluids, non-zero normal stress differences are generated; the two normal stress differences are nill in Newtonian fluids.

The first and second normal stress difference coefficients, ψ_1 and ψ_2 (Pa s^2) respectively, are defined as:

$$\psi_1 = N_1 / \dot{\gamma}^2 \qquad (II.8)$$

and

$$\psi_2 = N_2 / \dot{\gamma}^2 \qquad (II.9)$$

Similar to the relationship between the shear stress and the shear rate, the first normal stress difference can conveniently be related to the shear rate with a power law :

$$N_1 = A \dot{\gamma}^b \qquad (II.10)$$

The typical range for b is $1 < b \leq 2$ (though lower values were reported for some fluids).

The Weissenberg number (Wi) compares the magnitude of elastic stresses to shear stresses. Though a number of definitions for this dimensionless number can be found in the literature depending on how the viscoelastic and/or shear thinning properties are characterised, that used in this thesis is :

$$Wi = \frac{N_1}{\tau} \qquad (II.11)$$

N_1 and τ can be substituted by the expressions in equations (II.8) and (II.3) :

$$Wi = \frac{\psi_1 \dot{\gamma}}{\mu_a} \qquad (II.12)$$

or by the expressions from equations (II.10) and (II.3) :

$$Wi = \frac{A\,(\dot{\gamma}^{\,b-n})}{K} \qquad (II.13)$$

The second normal stress difference is generally conceded to be much smaller than N_1 and negative[4]. Previously N_2 was assumed to be zero - known as the Weissenberg hypothesis. It has only recently been possible to measure non-zero values of N_2 using modern rheometers with a reasonable degree of precision and $|N_2|$ is found to be less than about 10 % of N_1 (Barnes et al, 1989). Although in some situations N_2 proves to be very important, for many other applications - for example those related to mixing- it has little practical significance and has therefore been neglected[116].

The generation of non-zero normal stress differences is the most outstanding manifestation of viscoelasticity in steady state flows and hence is remarkably significant in interpreting the role of viscoelasticity in stirred vessels. Normal stress differences are associated with non-linear viscoelastic effects and these are the quantified viscoelastic fluid property in this study. Therefore, linear viscoelasticity and methods to determine linear viscoelasticity (creep tests, oscillatory methods, wave propogation techniques, etc) are not described here. It is, however, worth mentioning briefly some other manifestations of viscoelasticity. The characteristic material time or the relaxation time may play a role in the vicinity of the impeller if the magnitude of this fluid property is comparable to the periodicity of the impeller- which is related to the speed and number of blades of the impeller. Another manifestation of viscoelasticity is the elongational viscosity (also called extensional viscosity or Trouton's viscosity) which may be many hundred times greater than the shear viscosity.

Elongational viscosity often exhibits a different behaviour from that of the shear viscosity: in polymer solutions that have a viscosity which decreases with increasing shear rate (shear thinning), the elongational viscosity increases with increasing elongational rate[4]. This plays a role in the process of bubble break-up and affects the rate of bubble coalescence[116]. It is in general far more difficult to measure this fluid property than the shear viscosity.

An observable consequence of the non-zero normal stress differences is the tendency of the fluid to climb along a rotating shaft at elevations far above the contact of the solution with the vessel wall. This is known as the Weissenberg effect (or the rod-climbing effect) and has long been taken as the only criterion of fluid elasticity. Since modern equipment allowing precise quantification of viscoelasticity has been available, it is known that the shaft climbing may not be observed in fluids of measurable viscoelasticity depending on the magnitude of elastic forces compared to that of inertial forces. It has also been reported that fluids possessing a yield stress have a reduced tendency to climb the shaft[35].

II.3 MODEL FLUIDS

II.3.1 Model fluids commonly used

Table II.1 lists some examples of the model fluids used in mixing experiments for simulating the properties of rheologically complex fluids handled in industry. Among these properties, pseudoplasticity and viscoelasticity are very commonly encountered and they generally accompany each other. Yield value (or apparent yield value) is another important fluid property that results in the formation of well mixed zones confined to the impeller region (caverns). Model fluids that exhibit most of these properties may be good representatives of real biological media, but results obtained with these

fluids have most times been difficult to interpret in terms of one fluid property or the other. Silicone oils, that have a shear independent viscosity, were therefore used in some studies to investigate the effects of viscoelasticity alone. Another model viscoelastic fluid was prepared by Boger (1977) - the so-called Boger fluid which is highly viscous, viscoelastic and has an almost constant viscosity.

Table II.1 Model fluids simulating the rheology of fermentation broths

Fluid	Fluid property
Glycerol, corn syrup, sugar solutions	Viscous Newtonian
Carboxymethyl cellulose solutions	Shear thinning, viscoelastic depending on the concentration and molecular weight
PAA solutions	Shear thinning, viscoelastic
Carbopol	Shear thinning with a yield stress, may be mildly viscoelastic
Xanthan solutions	Shear thinning with a yield stress value, viscoelastic
Paper pulp	Simulates the rheology of filamentous fermentation broths

II.3.2 Boger fluids

Boger fluids are highly viscous glucose or maltose solutions containing very small amounts of a polymer - usually polyacrylamide[7,8,9]. In *Figure II.4*, shear stress and first normal stress difference data characterising a Boger fluid are presented. These fluids have the advantage of exhibiting viscoelasticity with an almost constant viscosity over a range of shear rates. The shear-thinning behaviour of Boger fluids is generally very low : $0.93 < n < 1$ (Chang and Denn, 1979; Oliver et al, 1984). The first normal stress difference data for a Boger fluid was reported to have a quadratic dependence on the shear rate. This is, however, confined to the low range of shear rates (*Figure II.4*).

Some researchers[1,28,82] used Boger fluids prepared with polyacrylamide in glucose for their studies in the field of mixing. Brito de la Fuente et al (1990) carried out mixing experiments with "organic Boger fluids" : a high molecular weight polyisobutylene in a Newtonian solvent consisting of a mixture of kerosene oil and polybutene. The properties of this fluid were previously reported by Keentok et al (1980), who measured the second normal stress difference to be virtually zero, and also by Prilutski et al (1983).

The viscoelastic fluids used in this study are also of the "Boger fluid" type. The properties of these fluids are reported in the following sections of this chapter.

Figure IV.4 Shear stress and first normal stress difference data of a Boger fluid (0.025 % PAA in corn syrup) Boger, 1980

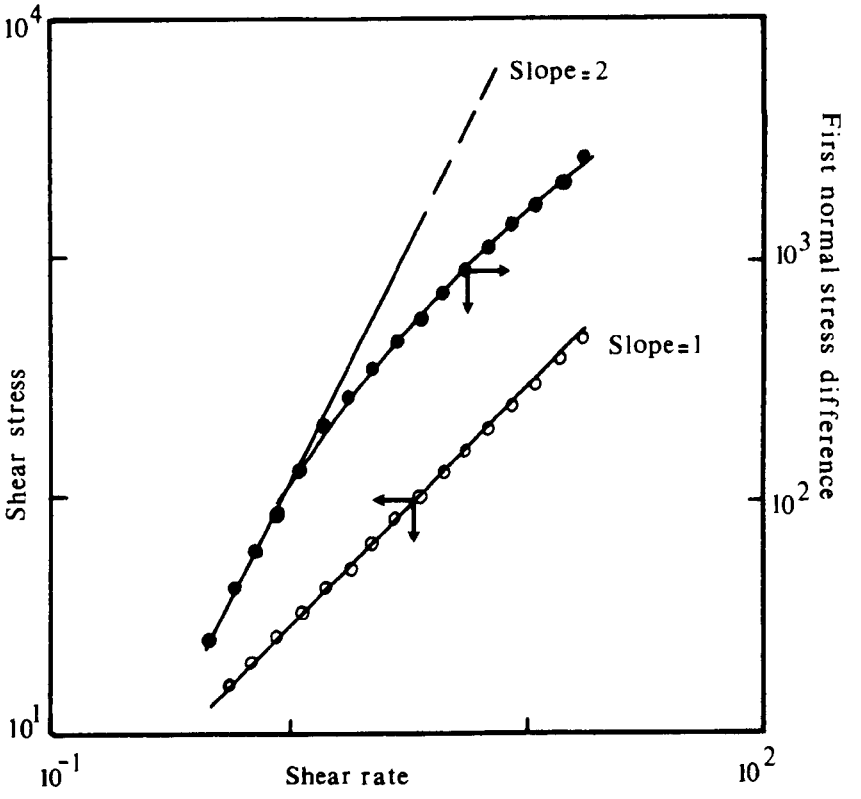

II.4 MODEL FLUIDS AND RHEOLOGY EQUIPMENT USED

II.4.1 Fluids used in mixing experiments

Demineralised water and undiluted glycerol (Sherman Chemicals Ltd., Sandy, U.K.) of 99% purity were the Newtonian fluids used in this work. Although sugar solutions are more popular as Newtonian viscous model fluids, they undergo microbial degradation very easily, and the viscosity of these solutions shows a strong dependence on temperature variations. Viscoelastic fluids were, therefore, prepared by adding trace amounts (ppm) of the polymer polyacrylamide into glycerol. Polyacrylamide supplied by Allied Colloids, Bradford, U.K. - Magnafloc LT25- had a molecular weight of around 2×10^7. In order to attain a desired viscosity, corn syrup (Tunnel Refineries, Greenwich, U.K.) was also added to some of these fluids.

Since most experiments were carried out under aerated conditions, these fluids, although more stable than sugar solutions, were prone to microbial contaminations which would alter their physical properties. Water is easily renewable but glycerol and glycerol based fluids had to be used for long periods. Therefore, 0.09% (v:v) Kathon DP (Rohm and Haas, Croydon, U.K.) was added as a preservative. This did not have any effect on the physical properties of the fluids.

II.4.2 Equipment used for rheology measurements

Density and viscosity of the Newtonian fluids were measured. For viscoelastic fluids, besides these two parameters, first normal stress measurements were also performed.

Density measurements were made using a picnometer.

II.4.2.1 Coaxial viscometer

Viscosity measurements of glycerol were performed using a coaxial cylinder

viscometer, Rheomat-30 (Contraves Ind. Products Ltd., Middlesex, U.K.) with a Rheoscan-30 programming unit. Measuring system B was used for all measurements.

II.4.2.2 Cone and plate viscometer

A Weissenberg rheogoniometer (Sangamo Weston Controls Ltd., Sussex, U.K.; Model R19) was used to measure both the shear stresses and first normal stress differences of viscoelastic fluids. The diameter of the bottom rotating cone and the top stationary plate was 5 cm and the gap angle was 2° 0' 9".

The shear rate range covered during the measurements with the Weissenberg rheogoniometer corresponded to the (average shear rate) range covered in the mixing vessels.

General details about these rheometers can be found in Whorlow (1980) and Barnes et al (1989).

II.5 RHEOLOGICAL CHARACTERISTICS OF MODEL FLUIDS USED

Mixing experiments carried out with different impeller types and geometries, lasted about ten to twenty days (with some blank days during which the fluid was left for degassification after aerated runs). A sample was taken each day experiments were conducted to measure the physical properties of fluids.

II.5.1 Viscous Newtonian glycerol

Glycerol had a viscosity of about 1 Pa s and a density of 1259 kg m^{-3}. Slight variations from these values after a period of time were taken into account in the calculation of relevant dimensionless numbers.

II.5.2 Viscoelastic fluids

Three viscoelastic fluids were prepared with various concentrations (w:w) of polyacrylamide: Fluid (1): 0.01 % PAA in glycerol;

Fluid (2): 0.02 % PAA in glycerol and about 20 % corn syrup;

Fluid (3): 0.03 % PAA in glycerol and about 30 % corn syrup.

These fluids were used for experiments of power consumption measurements, flow pattern and cavity observations. Results obtained are presented in Chapters IV and VIII.

II.5.2.1 Some observations during the preparation of viscoelastic fluids

To prepare these fluids, polyacrylamide supplied in powder form, was first dissolved in water as it did not readily dissolve in glycerol. When this thick solution was introduced into glycerol, it was captured in the zone of high turbulence around the impeller (*Photograph II.1*). During the initial stages of addition and mixing, the vessel contents composed of almost two separate fluids: the polyacrylamide solution around the impeller and the shaft exhibiting Weissenberg effect (*Photograph II.2*) and the glycerol as the main bulk. After further mixing, the Weissenberg effect was observed to decrease slowly and the fluid became clearer. Even a vortex was formed around the shaft. This was taken as the criterion of homogeneity. Although vigorous agitation was not applied, the suppression of the Weissenberg effect may also be due to a shear degradation of the polymer to a certain extent. Oliver et al (1984) and Collias and Prude'homme (1985) also reported an exceptional shaft climbing following the addition of PAA in glycerol, which decreased after 1-2 hours.

When preparing this viscoelastic fluid in the large vessel (T61), PAA was added gradually on several occasions to ensure a good homogeneity. It took 4 - 5 days to prepare the fluid at this scale.

Photograph II.1 Initial stages of mixing PAA in glycerol (0.03% w:w) - PAA captured in the impeller zone

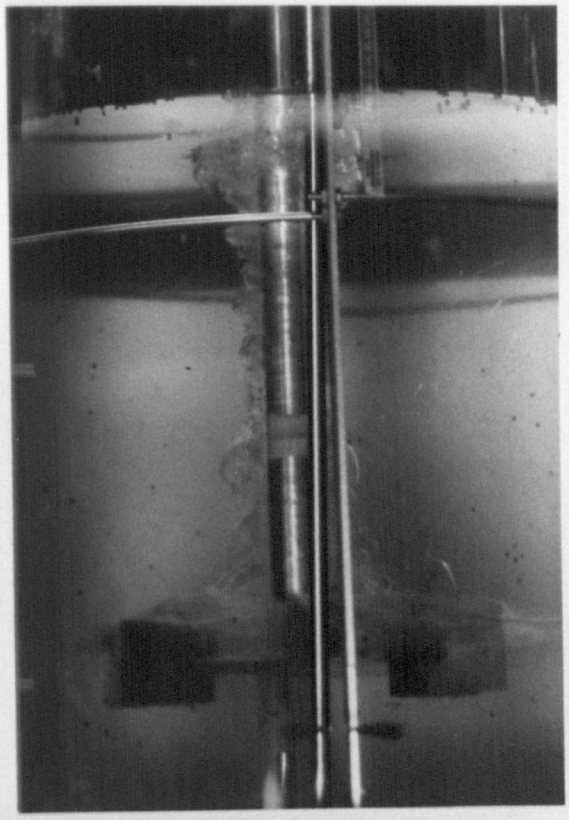

Photograph II.2 Weissenberg effect during the preparation of a solution of 0.03% (w:w) PAA in glycerol

II.5.2.2 Shear stress results

Figure II.5 presents the shear stress measurement results for one of the viscoelastic fluids. All viscoelastic fluids were only very slightly shear thinning which made it possible to investigate the elastic effects alone. Shear stress data were analysed fitting a power law model (eqn. II.4) and also a linear one (eqn. II.2). As *Table II.2* indicates, flow behaviour indices (n) were quite close to unity ($0.95 < n < 0.98$), and the correlation coefficients changed only very slightly when the shear stress was assumed to have a linear dependence on the shear rate. However, the slight shear thinning property of these fluids was taken into account for the calculation of dimensionless numbers that contain these data (e.g. Reynolds number, see Chapter IV).

Daily analysis of the rheological properties of all fluids showed that the shear stress data was quite reproducible over a period of more than ten days during which mixing experiments were carried out (*Figure II.5*).

Table II.2 Constitutive equations relating shear stress to the shear rate and the density of viscoelastic fluids used in this study

Fluid	ρ	Power law	Linear
1	1254.5	$\tau = 0.69\ \dot{\gamma}^{0.95}$ ($r^2 = 0.99$)	$\tau = 0.47\ \dot{\gamma}$ ($r^2 = 0.98$)
2	1276.5	$\tau = 0.64\ \dot{\gamma}^{0.98}$ ($r^2 = 0.98$)	$\tau = 0.58\ \dot{\gamma}$ ($r^2 = 0.98$)
3	1282.9	$\tau = 0.75\ \dot{\gamma}^{0.98}$ ($r^2 = 0.99$)	$\tau = 0.67\ \dot{\gamma}$ ($r^2 = 0.99$)

Figure II.5 Shear stress as a function of shear rate for one of the viscoelastic fluids of constant viscosity (Fluid 1)

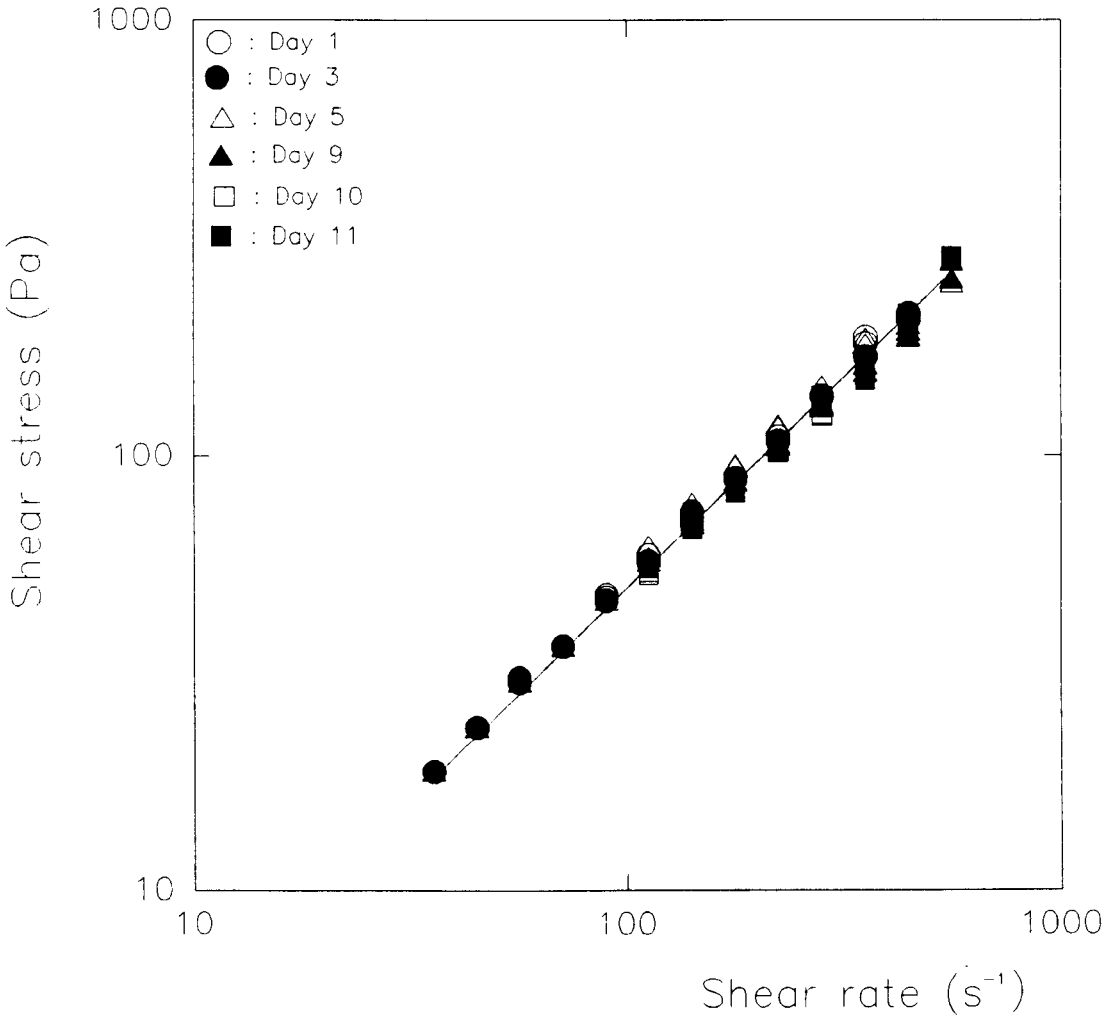

II.5.2.3 Normal stress results

First normal stress difference, on the other hand, was found to decrease with time (*Figure II.6*) - probably due to a certain extent of the shear degradation of the polymer. With the increase of polymer concentration the variation of elastic properties over a period of time decreased.

Power law parameters relating the first normal stress difference to the shear rate (eqn. II.8) are presented in *Table II.3* for all fluids. It can be noticed that though the dependence of the first normal stress difference on the shear rate was not precisely a second order one, however, the values of b were quite close to 2.0 varying between 1.6 - 1.9.

Increasing the polymer concentration (1 to 3 ppm) resulted in a mild increase of fluid elasticity. First normal stress difference was in general found to be higher than the shear stress in all the fluids.

Table II.3 Constitutive equations relating the first normal stress difference to the shear rate for one of the viscoelastic fluids of constant viscosity used in this study

Day	Fluid (1)	Day	Fluid (2)	Day	Fluid (3)
1	$N_1 = 0.032\ \dot{\gamma}^{1.59}$	1	$N_1 = 0.015\ \dot{\gamma}^{1.78}$	1	$N_1 = 0.037\ \dot{\gamma}^{1.74}$
3	$N_1 = 0.007\ \dot{\gamma}^{1.78}$	4	$N_1 = 0.026\ \dot{\gamma}^{1.68}$	2	$N_1 = 0.054\ \dot{\gamma}^{1.67}$
5	$N_1 = 0.005\ \dot{\gamma}^{1.79}$	5	$N_1 = 0.006\ \dot{\gamma}^{1.91}$	3	$N_1 = 0.026\ \dot{\gamma}^{1.79}$
9	$N_1 = 0.017\ \dot{\gamma}^{1.56}$	7	$N_1 = 0.012\ \dot{\gamma}^{1.75}$	4	$N_1 = 0.035\ \dot{\gamma}^{1.65}$
10	$N_1 = 0.007\ \dot{\gamma}^{1.55}$	8	$N_1 = 0.021\ \dot{\gamma}^{1.64}$	7	$N_1 = 0.020\ \dot{\gamma}^{1.7}$
11	$N_1 = 0.002\ \dot{\gamma}^{1.72}$	13	$N_1 = 0.008\ \dot{\gamma}^{1.76}$	8	$N_1 = 0.021\ \dot{\gamma}^{1.75}$

Figure II.6 First normal stress difference as a function of shear rate for one of the viscoelastic fluids (Fluid 2)

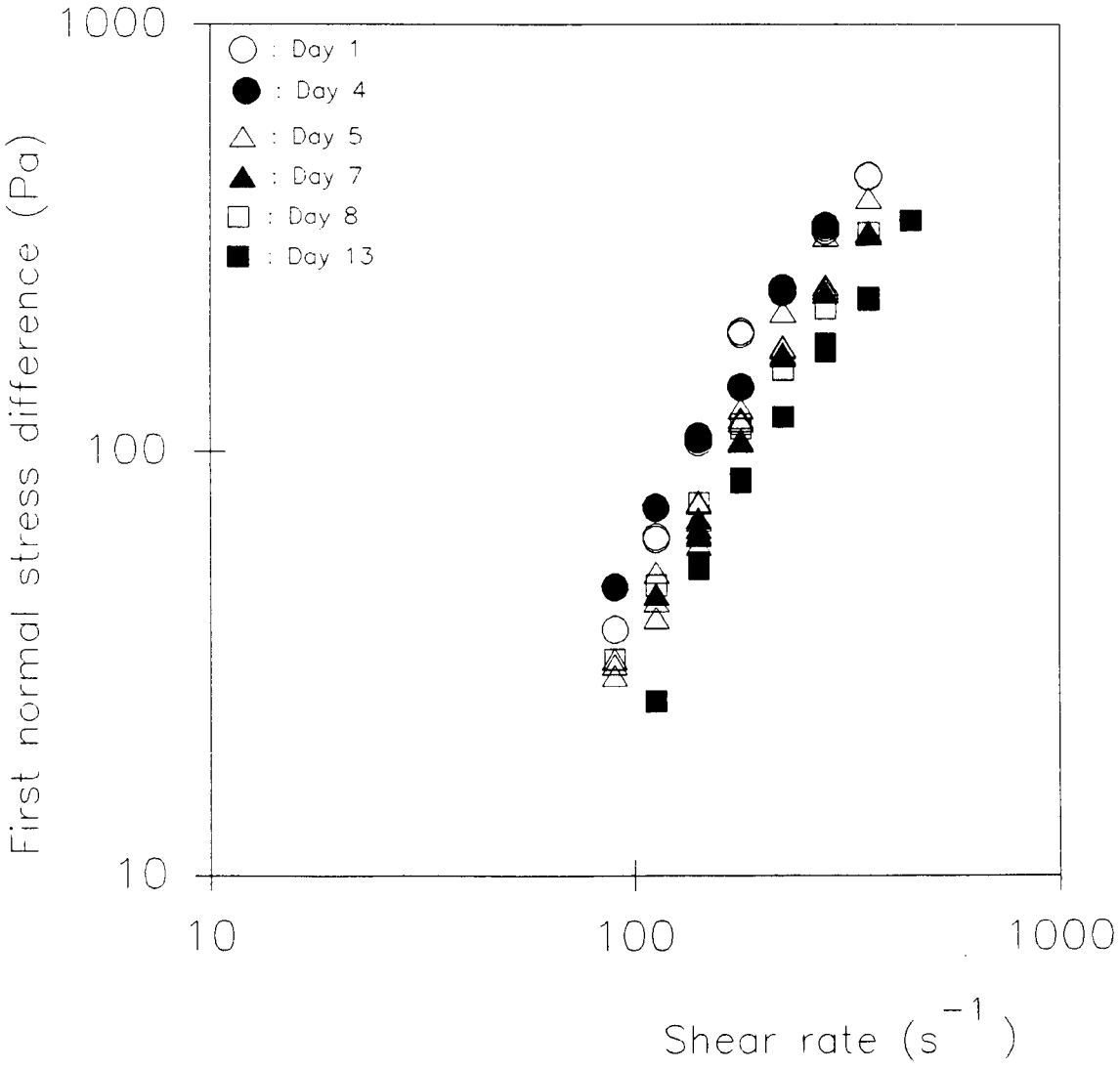

II.6 DISCUSSIONS

Model viscoelastic fluids used in this study were prepared adding trace amounts of polyacrylamide in glycerol. These were of the "Boger fluid" type exhibiting viscoelasticity but negligible shear thinning. Hence, they present the advantage of enabling the study of the impact of viscoelasticity independent of other rheological complexities.

The relation between the first normal stress difference and the shear rate was not found exactly to be a quadratic one in the range of shear rates covered. The values of the exponent "b" were slightly less than 2.0. In fact, the range of shear rates in which Boger (1977) reported a second order relation between the first normal stress difference and the shear rate was quite low ($\dot{\gamma} < 10\ s^{-1}$ as can be seen in *Figure II.4*), i.e. lower than those typically covered in mixing experiments.

Care should be taken during the preparation of these fluids to ensure a good homogenisation of PAA in a viscous bulk such as glycerol.

CHAPTER III SINGLE PHASE STUDIES IN NEWTONIAN FLUIDS: POWER CHARACTERISTICS AND FLOW PATTERNS

III.1 INTRODUCTION

This chapter is concerned with the mixing of Newtonian fluids under unaerated conditions- mainly the flow patterns generated and power dissipated by six bladed disc turbines and InterMIGs are dealt with. Following the theory and findings of some previous researchers in the field (presented in Section III.2), the mixing equipment used throughout this study is described in Section III.3. Experimental results on power consumption as well as flow pattern observations with six bladed disc turbines and InterMIGs in water and viscous Newtonian glycerol are presented in Section III.4. Section III.5 contains the related concluding remarks.

III.2 THEORETICAL CONSIDERATIONS AND PREVIOUS WORK

III.2.1 Power theory and dimensional analysis

The power dissipated by the impeller (P, W) depends on various independent variables such as:

$$P = fn\ (D,\ T,\ \mu,\ \rho,\ g,\ N,\ w,\ H,\ \text{other geometric simplexes}) \qquad (III.1)$$

The study of impeller power characteristics goes back to the late nineteenth century. The theory was developed basing on the very early work of various researchers (Thomson, 1855; Unwin, 1880; White et al, 1934 a,b and 1936; Hixson et al, 1933, 1935, 1937, 1942) who studied rotating discs or impellers in fluids to determine their resistance to motion- drag- and the power necessary to overcome it. Among these, White and his co-workers were the first to propose a dimensional analysis to correlate the impeller power. This was later elaborated by other researchers (Hixson et al, 1942; Rushton et al, 1950 a). Using the Buckingham pi theorem, the following dimensionless

equation could be obtained in its very general form:

$$\frac{P}{\rho N^3 D^5} = fn\left[\frac{\rho N D^2}{\mu}, \frac{N^2 D}{g}, \frac{T}{D}, \frac{w}{D}, \frac{H}{D}, \text{etc}\right] \qquad \text{(III.2)}$$

The dependent variable in this expression is the *Power number* (Po):

$$Po = \frac{P}{\rho N^3 D^5} \qquad \text{(III.3)}$$

also denoted as Np by some researchers. This dimensionless number represents the ratio of the power dissipated by the impeller to the inertial forces and is analogous to the drag coefficient or the friction factor.

The first independent variable in eqn (III.2) is the *Reynolds number* (Re):

$$Re = \frac{\rho N D^2}{\mu} \qquad \text{(III.4)}$$

which represents the ratio of inertial forces to viscous forces.

The second independent variable is the *Froude number* (Fr):

$$Fr = \frac{N^2 D}{g} \qquad \text{(III.5)}$$

which compares inertial forces to gravitational forces. The Froude number is important when a gross vortex is formed at the free liquid surface and thus the shape of the surface and flow patterns are affected by gravitational fields. This is an undesirable situation because when a vortex is formed the liquid follows large circular paths and consequently top to bottom motion is considerably reduced. The Froude number is not of much significance if a big

vortex is not observed and can be neglected. Then,

$$Po = fn\ (Re,\ geometrical\ ratios) \qquad (III.6)$$

For geometrically similar systems:

$$Po = fn\ (Re) \qquad (III.7)$$

The characteristic power curve is obtained plotting the Power number against the Reynolds number on a logarithmic scale. *Figure III.1* represents power curves of certain classical impellers. Different flow regimes can be identified on this curve. In the laminar flow regime -at Reynolds numbers below about 10- (also called the viscous flow regime or the creeping flow regime), viscous forces are dominant and the power curve is characterised by a slope of (-1) :

$$Po = K_p\ (Re)^{-1} \qquad (III.8)$$

At high Reynolds numbers (above about $2x\ 10^4$), flow is turbulent and the power number is essentially constant provided there is no surface aeration:

$$Po = constant \qquad (III.9)$$

There exists a range of Reynolds numbers in between these flow regimes where a gradual change from laminar to fully turbulent conditions takes place. In this transitional flow regime, the relation between the power number and the Reynolds number cannot be defined by any simple mathematical expression.

III.2.2 Importance of geometric factors

As the geometry and scale of operation generally vary in industrial applications, the effect of these parameters has been investigated by various researchers[5,65,40,17,18,19] mainly with Rushton turbines. These include the

Figure III.1 Characteristic power curves under unaerated conditions

(Bates et al, 1963)

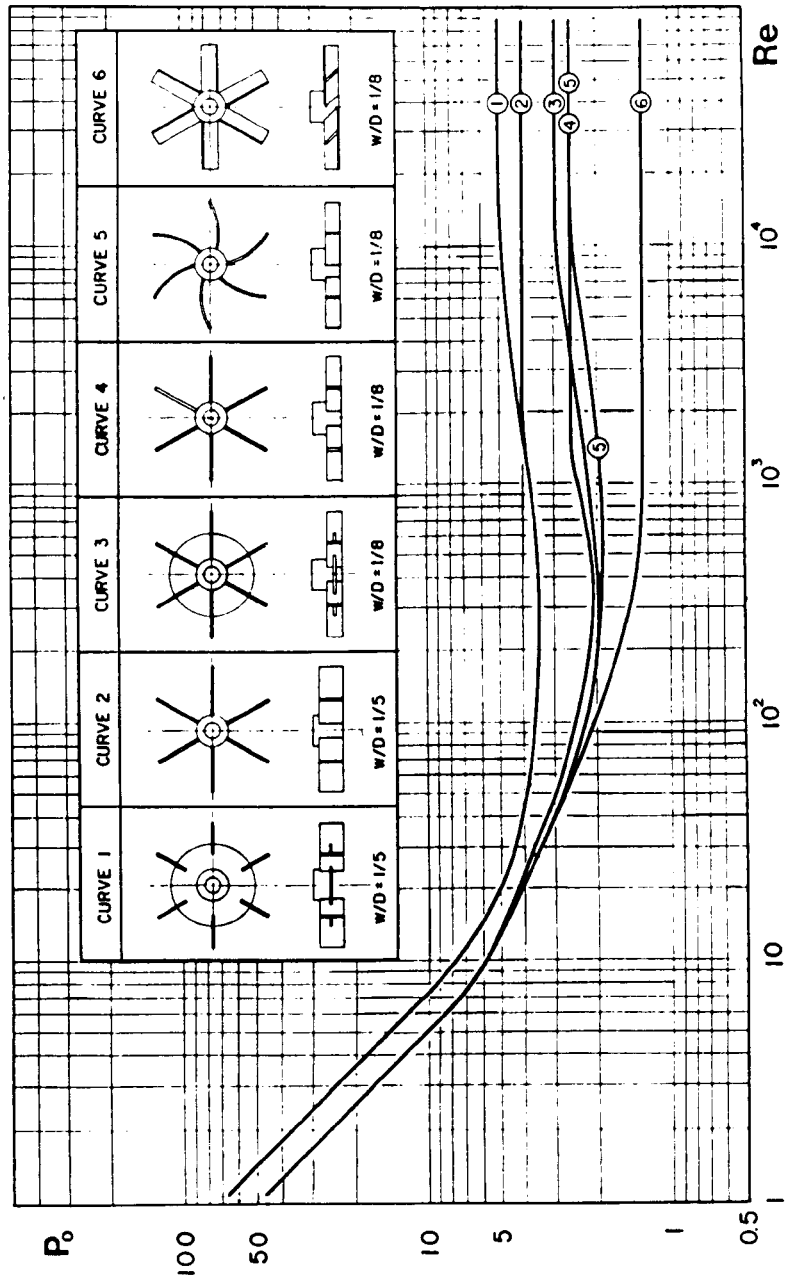

tank (T, m) and impeller diameters (D, m) and the impeller clearance from the vessel base (C, m). Nienow and Miles (1971) who made very accurate power measurements in the turbulent flow regime, obtained lower power numbers for smaller tank diameters or for smaller D/T ratios. The effect of D/T was pronounced especially when the disc thickness (x_1, m) was large compared to the blade width (w, m). When the impeller clearance was too low (C/T < 1/5), they observed changes in the flow patterns which were accompanied by a reduction in power. Following the work of Nienow and Miles (1971) who pointed out the importance of smaller dimensions such as the disc thickness (x_1) or blade thickness (x_2), Bujalski (1986) and Bujalski et al (1986 and 1987) published the effect of these geometric parameters. The correlation proposed for the power number in the turbulent regime obtained from a large amount of data over a range of scales was:

$$Po = 2.5\ (x_1/D)^{-0.2}\ (T/T_o)^{0.065} \qquad (III.10)$$

where T_o is a reference tank diameter equal to 1 m.

III.2.3 Flow patterns in Newtonian fluids under unaerated conditions

The overall flow pattern in a stirred vessel is determined by the geometrical configuration of the impeller, liquid properties and to a certain extent by the impeller speed.

Three main flow patterns that can be described in a mixing vessel are the primary, secondary and tertiary flow patterns. The primary flows for all agitator types are in the tangential direction following the rotation of the impeller. In the viscous flow regime, which is conceded to be almost inertialess, the overall features of the flow patterns are defined by the primary flows. At speeds high enough to exceed the viscous flow regime,

centrifugally driven forces generated by the primary flows gain more importance and give rise to secondary flows. The fluid flow heading away from the impeller reach the vessel walls and baffles, generate the inertially driven secondary flow patterns. These have axial and radial components. The dominant feature of the secondary flow patterns (whether axial, radial or other) depends on the geometry of the impeller and for certain impeller types on the direction of rotation.

Tertiary flow patterns are related to the stagnation flow on the upstream face of a blade giving rise to the vortex flow on the downstream face. An extensive study of the tertiary flows over the blades of disc turbines was carried out by van't Riet and Smith (1973) and Nienow and Wisdom (1974) following the earlier work by Takeda and Hoshino (1966) and Rennie and Valentin (1968). Nienow and Wisdom (1974) demonstrated the resemblance of the stagnation zones in front of and behind the blades of a Rushton turbine to that over an aerofoil or hydrofoil. The two research groups (van't Riet and Smith, 1973 and Nienow and Wisdom, 1974) showed the gentle flow in the region of high pressure on the front face of the blade and the presence of a pair of trailing vortices on the rear face. The capture of gas in these zones of low pressure behind the blades forming gas filled cavities under aerated conditions will be dealt in Chapter VI.

Flow patterns in non-Newtonian fluids may have entirely different features from those generated in a Newtonian fluid even of comparable consistency agitated with the same type of impeller. The effects of non-Newtonian fluid properties - mainly viscoelasticity- on the flow patterns are presented in Chapter IV. The quality of mixing is directly related to the flow patterns. This is expanded in Chapter V where mixing time studies are presented.

III.3 EQUIPMENT USED IN MIXING EXPERIMENTS

The equipment described in this Section has been used for mixing studies presented throughout this thesis. Some of these equipment were also used by previous researchers[58,25,1,19], who reported more details. Additional equipment and experimental techniques employed are described in the following relevant chapters.

III.3.1 Description of the pilot plant (*Photograph III.1*)

III.3.1.1 Mixing vessels

Experiments were carried out in a cylindrical, fully baffled, flat bottomed Perspex tank, of 0.61m diameter. Total liquid volume was 0.1783 m^3 (H = T). Other dimensions are given in *Figure III.2.* Water was circulated in the outer jacket (also made of Perspex) in order to maintain temperature control. This square outer jacket also provided a distortion- free view.

Figure III.2 Dimensions of the mixing vessel

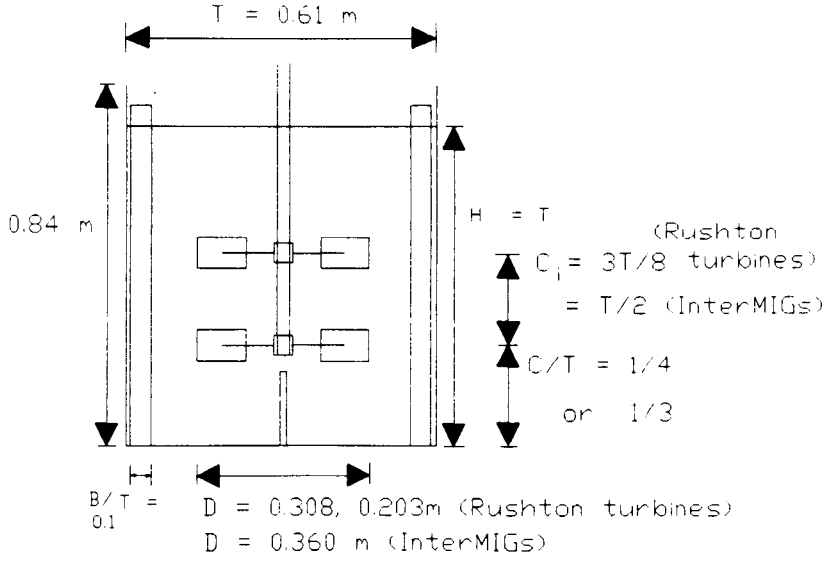

Photograph III.1 Pilot plant

a) Mixing vessel

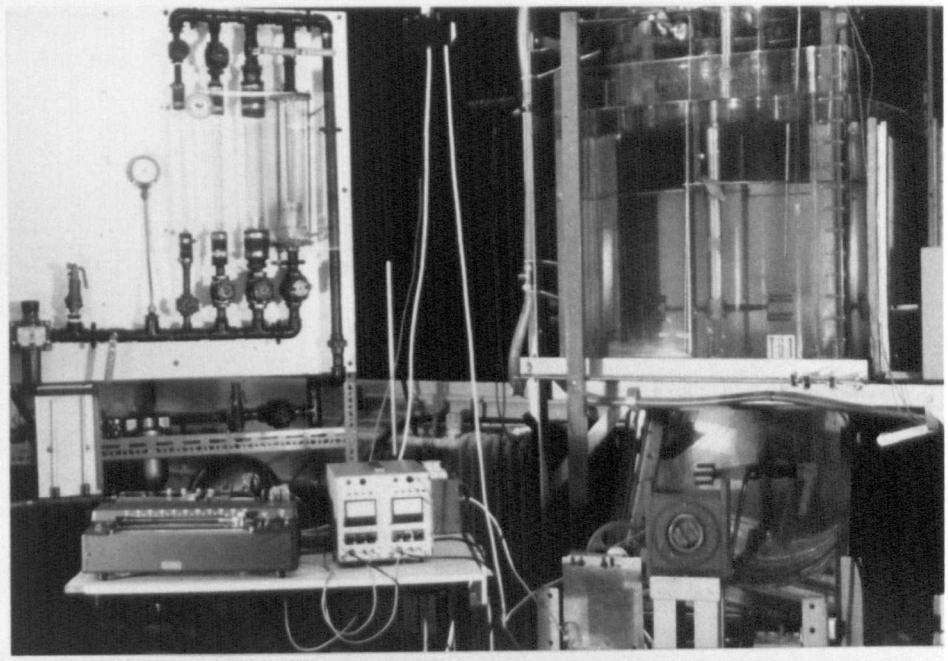

b) Impellers

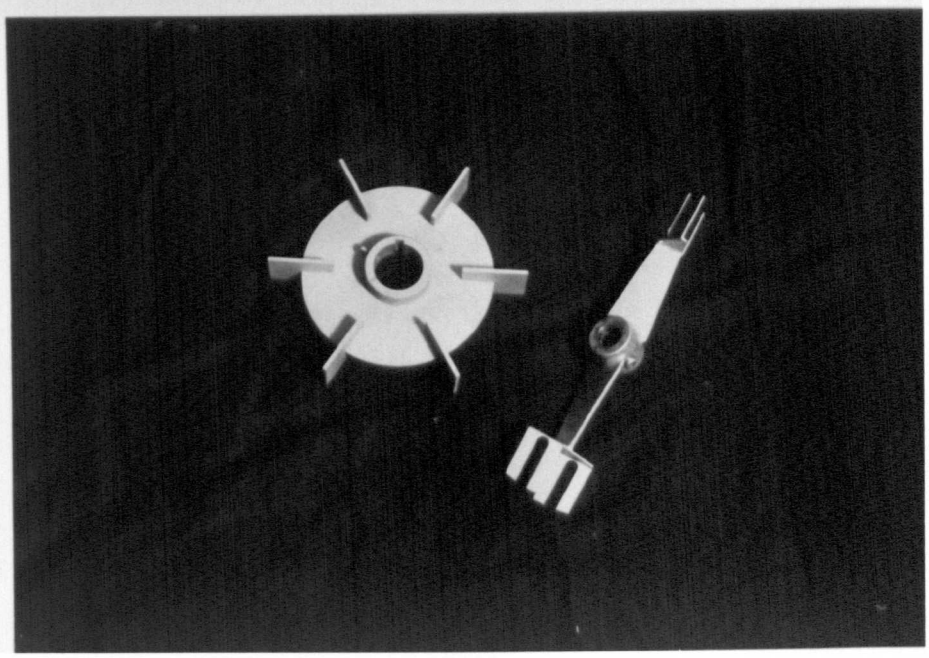

Some experiments were also carried out in a smaller but geometrically similar vessel of 0.29 m diameter. The liquid volume in this one was 0.0192 m^3.

These vessels are referred to as T61 and T29 later on in the text.

III.3.1.2 Impellers

Two types of impellers were used: the InterMIGs (from EKATO Ltd.) and the classical six bladed disc turbines (Rushton turbines).

Rushton turbines of diameters of D= T/2 and T/3 were used either singly or as a pair. The clearance from the tank base was C= T/3 or T/4 for a single turbine, and T/4 when multiple impellers were used. The inter-impeller spacing between two Rushton turbines was C_i= 3T/8 (i.e. C_i/ D = 1.13 for the small diameter Rushton turbine and C_i/ D = 0.75 for the larger one) and for InterMIGs C_i= T/2 (i.e. C_i/ D = 0.85). More details about the geometry of impellers can be found in *Figure III.3*.

The InterMIGs (D= 0.60 T) were always used as a pair, mounted at 90° with respect to each other. In most experiments, they were rotated in the sense recommended by the manufacturers, i.e. anti- clockwise rotation from the bottom view. This is referred to as "forward rotation" later on in the text. For a few experiments, they were rotated in reverse.

III.3.1.3 Power supply system

Power was supplied to the impeller by a D.C. electric motor (4kW for T61 and 1.5 kW for T29). A system of pulley cones enabled a maximum power output from the motor to be delivered to the shaft over a wide range of impeller speeds. The direction of rotation could be changed through a control box.

Figure III.3 Geometry of impellers

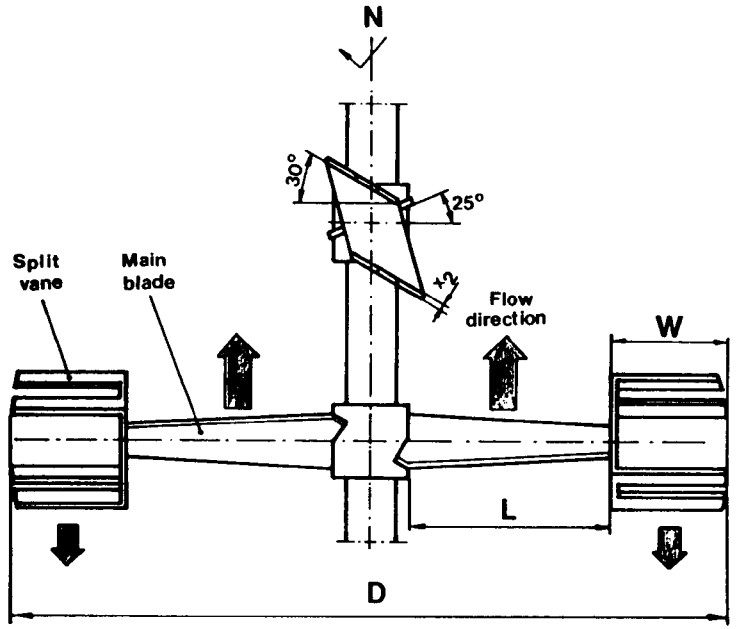

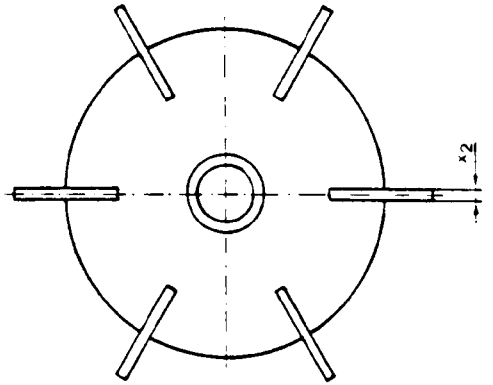

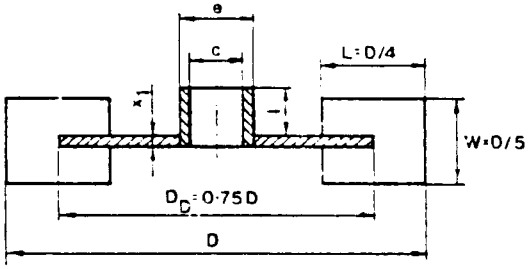

T(m)	Type of impeller	D(m)	D/T	D_d(m)	L(m)	W(m)	x_1(m)	x_2(m)
0.61	Rusht. turb	0.203	0.33	0.150	0.052	0.041	0.0033	0.0033
	Rusht. turb	0.308	0.50	0.227	0.077	0.061	0.0033	0.0033
	InterMIGs	0.360	0.60	-	0.097	0.056	0.0030	0.0030
0.29	Rusht. turb	0.101	0.35	0.076	0.027	0.020	0.0032	0.0032
	Rusht. turb	0.150	0.52	0.113	0.038	0.030	0.0032	0.0032
	InterMIGs	0.175	0.60	-	0.047	0.028	0.0020	0.0020

III.3.2 Measurement of impeller speed and torque

III.3.2.1 Tachometer (Photograph III.2)

The impeller speed was measured with an optic sensor. A wooden crown, having 60 holes, was mounted around the shaft outside the vessel. The holes allowed light to strike an infrared optical relay switch which was thus activated 60 times for every revolution of the shaft. The read-out had a precision to $\pm 0.02\ s^{-1}$.

III.3.2.2 Torque measurement

The larger vessel (T61) was equipped with a strain gauge-telemetry system for torque measurements. The strain gauges work on the principle that the electrical resistance of a metal changes according to the strain imposed on it. A full bridge of two pairs of strain gauges was mounted on opposite sides of the shaft, coated with protective layers. The torque (the twisting force acting against the direction of rotation of the impeller) is measured by the electrical resistance change of a Wheatstone bridge circuit. The gauges (Welwyn Strain Measurements Ltd., Basingstoke, U.K.) were connected to the transmitter unit of the telemetry equipment (Astech Electronics Ltd., Farnham, U.K.). The transmitter unit (*Photograph III.3*), which was mounted on a Perspex disc at the top of the shaft, generated a square wave oscillation the frequency of which is proportional to the change in the resistance of the strain gauge. The signal picked up by an aerial (*Photograph III.3*) was converted back to voltage and amplified by a receiver unit. The output, which was proportional to the torque, was monitored continuously on a chart recorder.

Stain gauges, mounted above the liquid level and above the lower impeller, enabled the total power consumption as well as the power consumption of individual impellers to be measured.

Photograph III.2 Tachometer (T61)

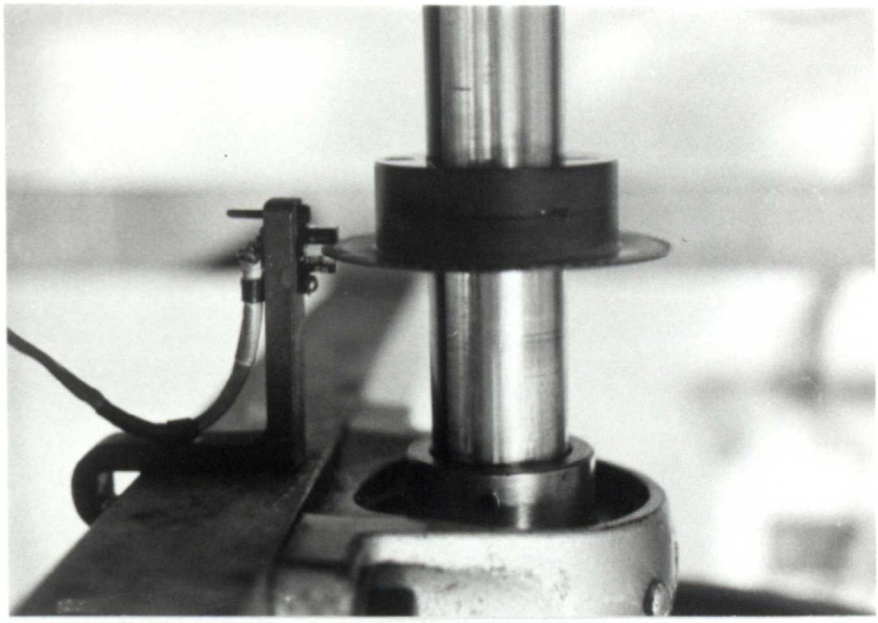

Photograph III.3 Transmitter unit and the aerials (T61)

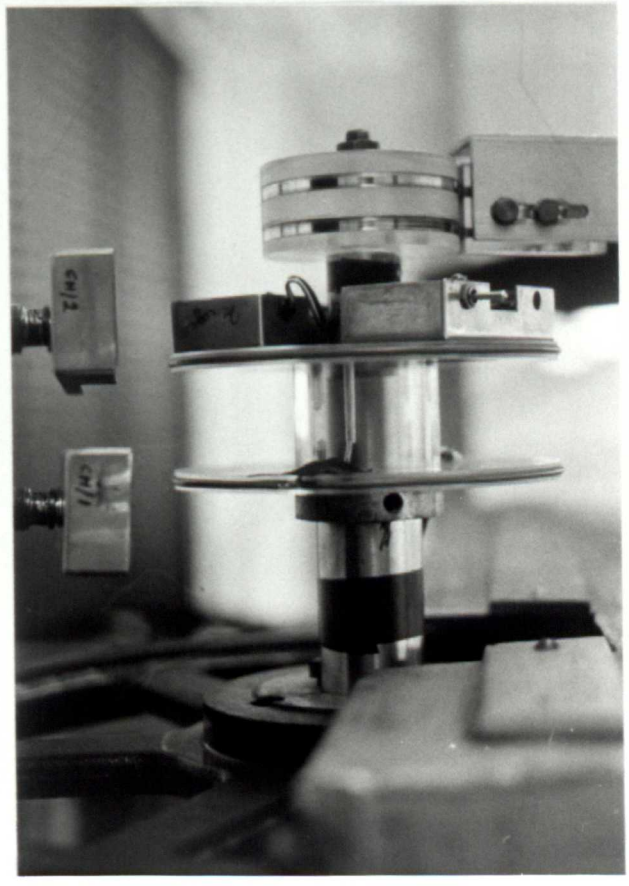

Calibration was carried out with the shaft de-mounted and positioned horizontally along a bench. The shaft was supported by two bearings above the bench and a six bladed disc turbine was fitted on. A series of weights were hung from a thread attached to one of the blades. A static torque on the shaft was created by passing the thread clockwise over the other five blades and allowing it to hang freely. The calibration was repeated passing the thread counter-clockwise over the blades. The torque (M, N m) was calculated as :

$$M = m\ g\ r$$

r (m) being the impeller radius, g (m s^{-2}) the acceleration due to gravity, and m (g) mass. Calibration coefficients obtained for different voltage ranges were later used to calculate the torque during mixing experiments and the power consumed (P, W) can be obtained by :

$$P = 2\ \pi\ N\ M$$

Torque measurements on the small vessel (T29) were carried out using an air bearing- load cell technique, details of which were given by Nienow and Miles (1969).

III.3.3 Studies of the hydrodynamics within the vessel

Flow patterns under unaerated conditions were visually observed using plastic beads in the bulk as flow followers. These beads, having a density slightly higher than that of water and slightly lower than that of glycerol, were not exactly neutrally buoyant. However, the path they followed gave an overall view of the fluid flow patterns. Video recordings were also made during some runs.

III.4 RESULTS AND DISCUSSIONS

Experiments in water were carried out to confirm the previous findings with single Rushton turbines, which have been studied thoroughly and to extend the limited amount of information obtained with dual Rushton turbines and InterMIGs. These results cover a Reynolds number range of about $3x10^4$ to $8x10^5$ in the turbulent flow regime depending on the impeller type and diameter. Data obtained with undiluted glycerol are more representative of fermentation broths in terms of the viscosity and Reynolds number range. Reynolds numbers from 40 to 600 were covered in the transitional flow regime. Operational conditions for these experiments are presented in *Table III.1.*

III.4.1 Flow patterns in Newtonian fluids

In the following paragraphs, visual observations of secondary flow patterns in Newtonian fluids with six bladed disc turbines and InterMIGs are reported. Video recordings were also made and a tape is available at the University of Birmingham- School of Chemical Engineering.

III.4.1.1 Rushton turbines

The main flow pattern observed with Rushton turbines was the typical radial discharge. Observations with glycerol in the transitional flow regime have shown that the tangential component of flow was more pronounced.

III.4.1.2 InterMIGs

Flow patterns for InterMIGs were only reported for low viscosity fluids in previous work: the fluid is pumped in opposite directions (upwards and downwards) by the inner and outer blades following the different inclinations of these. Since a counter - flow is thus generated and the InterMIGs are mounted at 90° with respect to each other, the flow patterns were rather

Table III.1 Operational conditions of unaerated experiments with Newtonian fluids

T61	Single 6DT				Two 6DT		InterMIGs	
D/T	1/3		1/2		1/3	1/2	0.60	
C/T	1/3	1/4	1/3	1/4			Forw.	Rev.
W A T E R								
N_{max} (s^{-1})	6.67	6.67	2.83	3.12	4.33	2.67	5.83	4.00
N_{min}	0.83	1.00	0.67	0.50	1.50	0.67	1.00	1.00
P_{max} (W)	556.5	539.5	359.06	470.22	219.10	432.92	648.62	241.02
P_{min}	1.07	1.84	4.46	1.83	10.04	7.08	3.33	3.48
Re_{max} ($x10^{-4}$)	27	28	27	30	18	25	76	52
Re_{min}	3.4	4.1	6.3	4.7	6.2	6.3	15	13
G L Y C E R O L								
N_{max} (s^{-1})	9.67	9.33	3.67	3.33	7.33	2.75	4.83	3.33
N_{min}	1.00	0.75	0.50	0.67	1.17	0.67	1.00	1.0
P_{max} (W)	1350	1231	584	447	559	203	398	303
P_{min}	1.71	0.81	1.63	3.52	2.42	3.18	6.08	12.9
Re_{max}	483	480	430	463	408	335	766	415
Re_{min}	50	39	59	93	60	81	159	125

chaotic and difficult to observe visually - especially at high speeds. General features of the flow patterns observed in this study can be described as follows. When rotated in the "forward" direction (i.e. anti-clock wise rotation viewing from the vessel base), a gentle flow pattern was established at low speeds (1- 1.5 s^{-1}): the fluid pumped downward by the outer blades was circulated back to the tip of these blades and the flows from the inner blades were in the upward direction (*Figure III.4 a).* The circulation loop associated with the outer blades of the upper impeller was larger than that from the lower impeller which was limited by the clearance from the vessel base. As the speed was increased (above about 1.7 s^{-1}), the flows generated by the two impellers as well as those from the different blades of the same impeller started to interact (*Figure III.4 b*). Most of the fluid pumped downward by the lower impeller was circulated back towards the outer blades, but some of it was entrained in the upward stream of flow generated by the inner blades of this impeller. At those relatively high speeds, the flow from the inner blades engaged with the flows from the top impeller. A part of the fluid pumped downwards by the upper impeller was captured in the fluid flows generated by the lower impeller.

At even higher speeds, flows from various blades intermingled more. In the "reverse" rotation sense (i.e. clockwise rotation viewing from the vessel base), the outer blades pumped upwards and the inner blades downwards.

InterMIGs can be described as counter-flow axial impellers in the turbulent regime. However, observations in viscous glycerol revealed a remarkable change of the pumping mode of the outer blades which started to discharge the liquid radially outwards in the transitional flow regime (*Figure III.5*). The downward circulation loop was much larger than the upper one. Compared to the circulation loops generated by Rushton turbines, those of InterMIGs covered a shorter distance because InterMIGs were larger in

Figure III.4 Flow patterns around InterMIGs in the turbulent flow regime (water)

a)

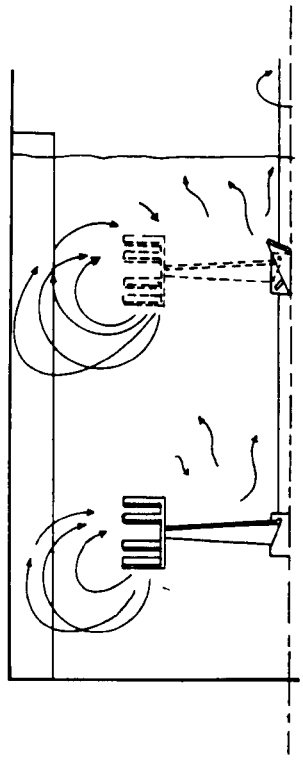

b)

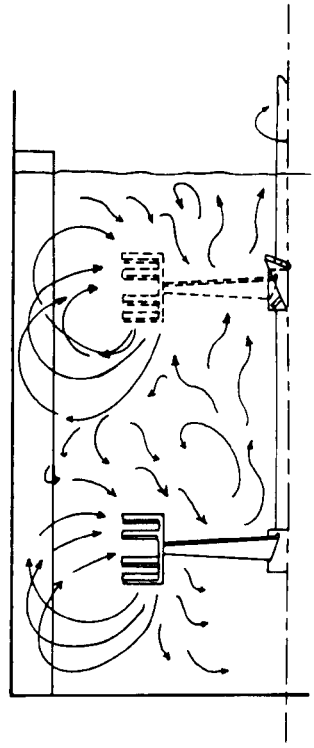

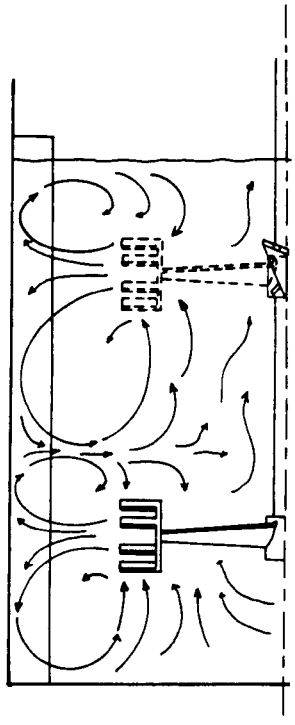

Figure III.5 Flow patterns around InterMIGs in the transitional flow regime (glycerol)

diameter and the radial discharge was associated only with the outer blades. As the speed was increased, the upper loop became smaller, especially the one of the lower impeller due to the interaction of the lower loop of the top impeller.

III.4.2 Surface aeration observations

Surface aeration started with the entrainment of a few bubbles from the free liquid surface. With the increase of impeller speed one or more swirling vortices were formed from which bubbles were first drawn and distributed in the upper half of the vessel (around the top impeller for multiple impellers), then throughout the bulk. The liquid surface was in general very wavy with InterMIGs in water (even before surface aeration started) because of the opposed pumping modes of the different blades. Vortices were, therefore, formed at various places on the liquid surface. In viscous glycerol, this mainly happened around the shaft. *Table III.2* contains impeller speeds (N_{SA}) and corresponding Froude numbers at which surface aeration was observed with the formation of swirling vortices. Some of the air was captured behind the blades of impellers forming cavities of very small size (see Chapter VI for the definition of cavities), but this did not affect the overall power consumption. Indeed, Bujalski (1986,a) had reported that the effect of surface aeration on the power consumed would start only when speeds 1.5- 2.0 N_{SA} were exceeded where clinging cavities were formed. Such high speeds were not achieved in this study. However, especially in glycerol, when the vortex reached the upper impeller occasionally, torque values fluctuated.

As *Table III.2* indicates, surface aeration started at a lower impeller speed for larger diameters and when two impellers were mounted compared to a single one of the same diameter. N_{SA} was lower for low

viscosity fluids. For a given fluid, air was entrained more easily when InterMIGs were rotated in reverse than in forward direction.

Table III.2 Operational conditions at which surface aeration is observed

T61	Single 6DT				Two 6DT		InterMIGs	
D/T	1/3		1/2		1/3	1/2	0.60	
C/T	1/3	1/4	1/3	1/4			Forw.	Rev.
W A T E R								
N_{SA} (s^{-1})	4.83	4.83	2.50	2.50	3.58	2.00	4.08	2.75
Fr	0.48	0.48	0.20	0.20	0.27	0.13	0.61	0.28
G L Y C E R O L								
N_{SA} (s^{-1})	5.67	5.67	3.10	3.00	4.25	2.20	4.50	3.00
Fr	0.67	0.67	0.30	0.29	0.37	0.15	0.74	0.33

III.4.3 Characteristic power curves in Newtonian fluids

Figure III.6 shows the power curves for Rushton turbines and InterMIGs in the transitional and turbulent flow regimes although there is a range of Reynolds numbers in between, which was not covered. Power numbers of Rushton turbines first decreased in the transitional regime, then after a minimum at a Reynolds number of about 240- 270, started to increase. Similar values for this critical Reynolds number were found by previous researchers[103,5,11,69]. In the turbulent flow regime power numbers were almost constant.

For a single Rushton turbine of a given diameter, changing the clearance from the vessel base did not have a significant effect on the power consumed (*Figure III.6*). The effect of this geometric factor on the power consumption was found to be important only at very low clearances where the two circulation loops were replaced by a single one[65]. The two clearances studied in this work were those widely used in industrial operations: C= T/3 and T/4. This variation was in fact too small to result in any major modifications of the flow patterns and thus the power consumption. Power numbers were only slightly higher for the larger impeller when used singly or as a pair. This is in agreement with the findings of Nienow and Miles (1971) who reported on the effect of this geometric parameter as well as those of Bujalski (1986) who evaluated the importance of impeller diameter in relation with other minor dimensions such as the disc and blade thicknesses. The results of the latter indicate that the effect of D/T becomes less important as the scale of operation increases.

Power numbers obtained with InterMIGs were in general much lower than those of Rushton turbines. In the turbulent flow regime, the overall power number with a pair of InterMIGs was 0.55- a value nearly ten times less than that for a single Rushton turbine. The power curve of these impellers had a very distinctive feature. In the transitional flow regime, power numbers

Figure III.6 Characteristic power curves obtained in Newtonian fluids

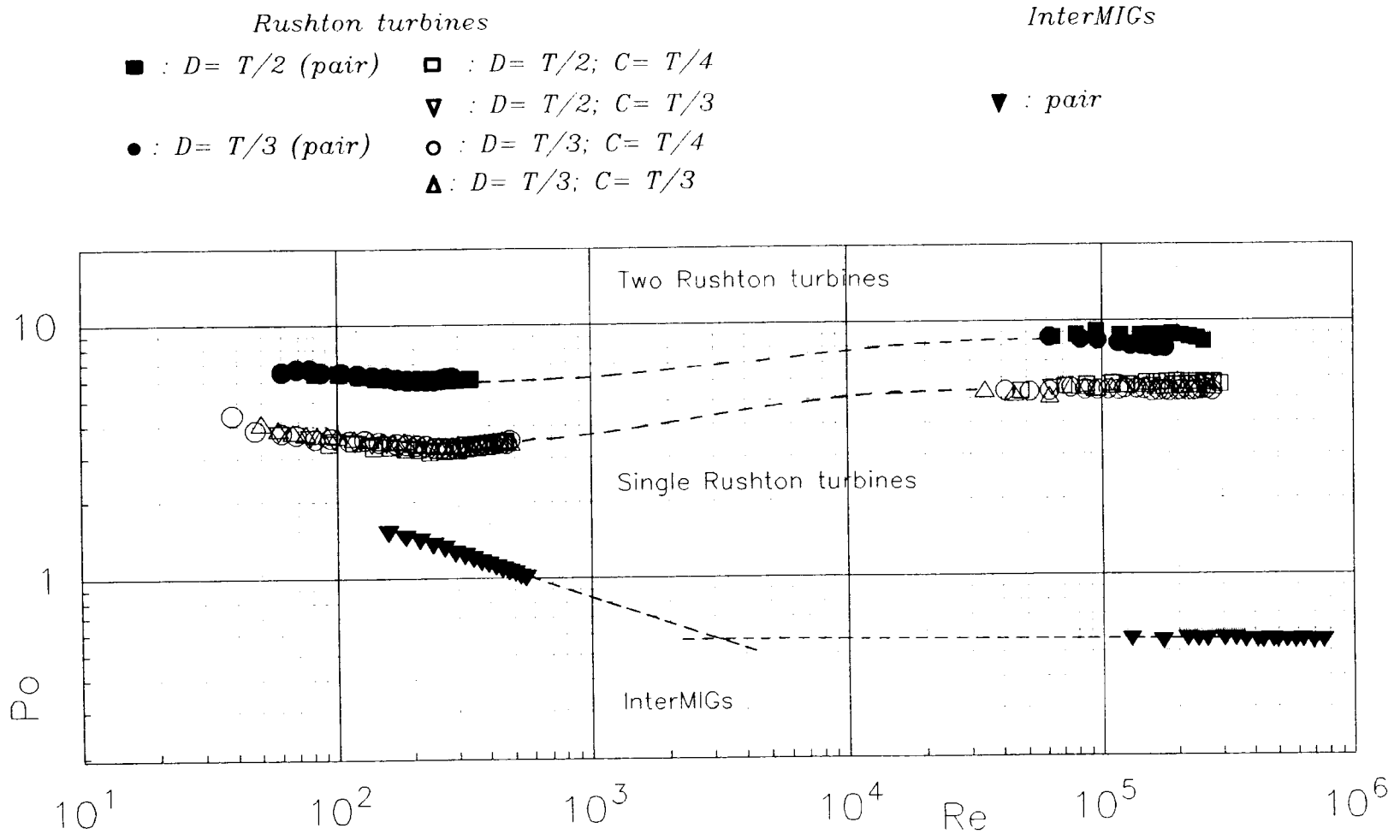

decreased with almost a constant slope (from Po= 1.50 at Re= 159 to Po= 0.88 at Re= 766) before attaining a very stable value in the turbulent flow regime. The Reynolds number at which this change of slope of the power curve took place was not within the range covered in this study. However, it can be expected that this shift corresponds to the change of pumping mode of the outer blades from radial discharge in the transitional regime to downward pumping in the turbulent regime. It should be noted that the shape of the power curve for InterMIGs bear certain resemblances to that for a pitched blade turbine (*Figures III.6* and *III.1*).

When InterMIGs were rotated in reverse (i.e. inner blades pumping downwards), power consumption was found to be slightly higher than that in the forward rotation sense (*Figure III.7*).

The power consumed by the upper and lower impellers of InterMIGs were almost identical. The overall power consumption by two Rushton turbines was nearly twice that of a single turbine in the transitional flow regime : $Po_{pair} = = (1.8 - 1.9)\ Po_{single}$. In the turbulent flow regime of important liquid velocities, the inter-impeller spacings used in this study (see Section III.3.1.2) gave way to an interaction of the circulation loops from the upper and lower impellers. Hence conforming with the findings of previous researchers[49,50,80] $Po_{pair} = (1.5\text{-}1.6)\ Po_{single}$.

Figure III.7 Power curves of InterMIGs rotated in "forward" (inner blades pumping upwards) and in "reverse" direction in Newtonian fluids

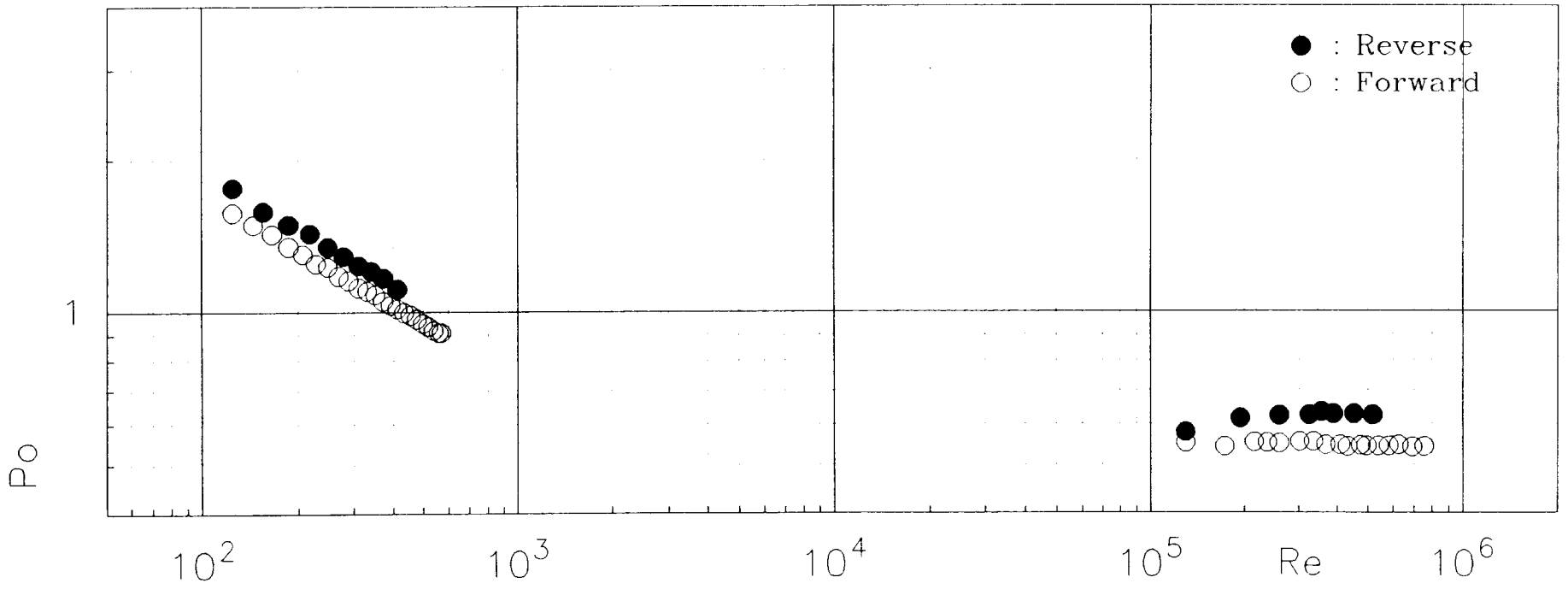

III.5 CONCLUDING REMARKS

Visual observations have shown two distinctively different flow patterns associated with the outer blades of InterMIGs in the transitional and turbulent flow regimes. In forward rotation, inner blades always pumped the fluid upward while the outer blades were observed to discharge the fluid radially outwards in the transitional flow regime, but thrust downwards in the turbulent flow regime. This was accompanied by a change in the slope of power curve where power numbers decreased almost constantly in the transitional region and acquired a constant value in the turbulent region. Considering the shape of the power curves, the prediction of power consumption can be more straightforward with InterMIGs than with Rushton turbines- especially in the transitional flow regime.

A range of Reynolds numbers between 10^3 to 10^5 could not be covered in this study. It could be envisaged to investigate this range where the change of the slope of power curve occurs and the modification of the flows associated with the outer blades of InterMIGs takes place.

Studies with these impellers have revealed that rotating in reverse presents certain disadvantages: power consumption was higher than in forward sense and surface aeration started at a much lower speed, thus limiting the range of operational conditions.

Slight changes in the power number were found with the changes in the geometry of Rushton turbines in agreement with previous findings. When these impellers were replaced with a pair of InterMIGs, the power numbers obtained were considerably lower.

These results provide essential information for the following chapters where the effects of fluid elasticity are investigated in comparison with the power consumed in Newtonian fluids (Chapter IV), impeller efficiencies are compared on the basis of power per unit volume (Chapter V) and the aerated

power characteristics are studied in relation to unaerated power consumption (Chapters VI and VII).

CHAPTER IV SINGLE PHASE STUDIES IN VISCOELASTIC FLUIDS : FLOW PATTERNS AND POWER CHARACTERISTICS

IV.1 INTRODUCTION

In most of the early work the importance of fluid viscoelasticity remained unrevealed due to the difficulties in experimentally quantifying this fluid property. Results obtained with fluids of significant elasticity were interpreted ignoring elastic effects or only qualitatively stating the presence of viscoelasticity where the Weissenberg effect was visually observed. Since the late seventies, more research on mixing (notably by Ulbrecht and his colleagues[115,96] and Nienow and his colleagues[69,71,82]) has been carried out to investigate the effects arising from various rheological properties of fluids. However, the coexistence of viscoelasticity with other fluid properties has, most times, made it difficult to identify the effects of viscoelasticity. Findings of different researchers especially regarding the impact of viscoelasticity on the power consumed vary considerably.

In this study, the role of viscoelasticity was investigated with viscoelastic model fluids that have an almost constant viscosity over a wide range of shear rates. Hence, the consequences of this fluid property could be studied in the absence of other rheological complexities. This chapter is confined to the studies of the effect of viscoelasticity on flow patterns and power characteristics under unaerated conditions. The background theory and previous work are introduced in Sections IV.2 and IV.3. In Section IV.4 results on power consumption with Rushton turbines and InterMIGs are discussed in relation to fluid elasticity and flow patterns. Concluding points are presented in Section IV.5.

IV.2 THEORETICAL CONSIDERATIONS - INTERPRETING VISCOELASTICITY

IV.2.1 Average shear rate theory of Metzner and Otto

Almost all viscoelastic fluids also exhibit shear thinning properties. The

non-linear relationship between the shear stress and the shear rate for these fluids was given in Chapter II (eqn. II.4). In a shear thinning fluid under agitation there exists a spectrum of shear rates that give rise to a range of local viscosities. For various, mainly practical reasons, an average shear rate ($\dot{\gamma}_{av}$, s^{-1}) was defined by Metzner and Otto (1957) which was related to the impeller speed :

$$\dot{\gamma}_{av} = k_s N \qquad \text{(IV.1)}$$

The constant k_s is characteristic of the impeller type and is determined by performing power consumption measurements with a Newtonian and a shear thinning fluid in the viscous flow regime. The theory is based on the assumption that in the viscous flow regime, shear thinning is the only fluid property that would account for the difference in power numbers obtained with a Newtonian and a shear thinning fluid and this assumption is valid inasmuchas the nature of viscous flow regime is inertialess. The value of k_s is obtained so that the characteristic power curves (Po versus Re) of these fluids superimpose. The procedure is detailed by Metzner and Otto (1957).

Some criticisms were made of the average shear rate approach of Metzner and Otto (mainly regarding its limitations with dilatant fluids or for important changes in scale of operation) by various researchers including Metzner and Taylor (1960) and Metzner et al (1961). However, it is widely used in the field of mixing.

The apparent viscosity, defined in equation (II.3), can then be calculated for the shear thinning contents of a mixing vessel :

$$\mu_a = \frac{\tau}{k_s N} \qquad \text{(IV.2)}$$

When τ in this equation is replaced by the expression in equation (II.4):

$$\mu_a = \frac{K\,(k_s\,N)^n}{k_s\,N} = K\,(k_s\,N)^{n-1} \qquad \text{(IV.3)}$$

IV.2.2 Dimensionless numbers

IV.2.2.1 Reynolds number

Reynolds number for a shear thinning fluid can conveniently be determined combining equations (IV.3) and (III.4) :

$$Re = \frac{N\,D^2\,\rho}{K\,(k_s\,N)^{n-1}} = \frac{N^{2-n}\,D^2\,\rho}{K\,k_s^{n-1}} \qquad \text{(IV.4)}$$

Clearly both equations (IV.3) and (IV.4) are valid in the ranges of shear rates where the shear thinning fluid obeys a power law (Section B on *Figure II.3*).

IV.2.2.2 Weissenberg number

Weissenberg number can be obtained in a mixing vessel by substituting the average shear rate in equation (II.10) :

$$Wi = \frac{A\,(k_s\,N)^{b-n}}{K} \qquad \text{(IV.5)}$$

This dimensionless number is characteristic of the rheological properties of a viscoelastic fluid containing parameters related to both the shear and normal stresses.

IV.2.2.3 Interpreting viscoelasticity- the Elasticity number

N_1 and Wi characterise viscoelasticity as a fluid property. The Weissenberg number contains the impeller speed, however, the effects of viscoelasticity may also depend on the characteristic length of flow, i.e. the impeller diameter. Elasticity number (El) defined as the ratio of the Weissenberg number to the Reynolds number:

$$El = \frac{Wi}{Re} \qquad (IV.6)$$

compares the magnitude of elastically driven forces to that of inertial forces. Substituting the expressions for the Reynolds number and the Weissenberg number from equations (IV.4) and (IV.5) in eqn. (IV.6), the Elasticity number can be obtained as:

$$El = \frac{A\,(k_s\,N)^{b-1}}{N\,D^2\,\rho} \qquad (IV.7)$$

Thus, the scale effects are incorporated in this dimensionless number with the impeller diameter raised to the power of two. For a viscoelastic fluid of given properties, dynamic similarity is respected maintaining the Reynolds number constant at different scales of operation. Considering two vessel sizes 1 and 2, dynamic similarity requires:

$$\left[\frac{(Re)_2}{(Re)_1}\right] = 1 \Rightarrow \left[\frac{(D)_2}{(D)_1}\right] = \left[\frac{(N)_1}{(N)_2}\right]^{1/2} \qquad (IV.8)$$

For viscoelastic fluids, an additional requirement is:

$$\left[\frac{(El)_2}{(El)_1}\right] = 1 \quad \Rightarrow \quad \left[\frac{(D)_2}{(D)_1}\right] = \left[\frac{(N)_1}{(N)_2}\right]^{1-(b/2)} \qquad (IV.9)$$

As the equality (IV.9) suggests, the value of b is crucially important for maintaining this similarity. It may therefore be useful to specify the range of the Elasticity number when interpreting the effects of viscoelasticity. Various expressions for this dimensionless number can be found in the literature depending on the definitions of Wi and Re. Therefore comparisons with previous work have to be made with caution.

IV.3 PREVIOUS WORK

IV.3.1 Flow patterns in viscoelastic fluids under unaerated conditions

Early work on the flows generated in viscoelastic fluids was confined to small scales where simple rotating bodies - such as spheres and discs - were studied.

Two research groups (Thomas and Walters, 1964; Walters and Waters, 1964; Walters and Savins, 1965 and Giesekus, 1964) reported that streamlines around a spinning sphere were under certain conditions reversed in viscoelastic fluids . They observed three distinctive flow patterns at different rotational speeds of the sphere or with different polymer concentrations. These corresponded well with their calculations determining the sign of the stream function (describing the streamline projections). *Figure IV.1* shows schematically the flow patterns in viscoelastic fluids which may either resemble those observed in Newtonian fluids (*Fig. IV.1 a*), or be reversed (*Fig. IV.1 b*) or have a bimodal feature with different flow

Figure IV.1 Flow patterns in viscoelastic fluids around a rotating sphere (IV.1 a, b, c [113,138,120,39,52,129] and IV.1 d [116] were reported by various research groups

a) Inertia dominated flow patterns

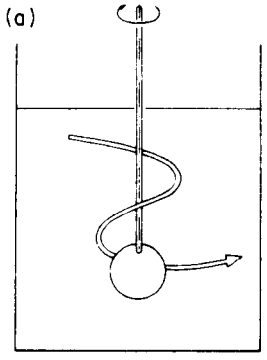

b) Flows dominated by viscoelastic forces (reversed flows)

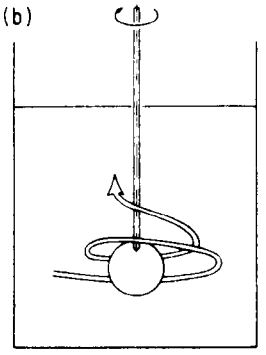

c) Intermediate flow patterns : viscoelastically forces dominant in the vicinity of the sphere (unshaded streamline), inertial forces outside this region (shaded streamline)

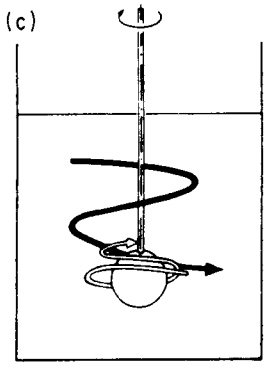

d) Intermediate flow patterns : inertial forces dominant in the vicinity of the sphere (unshaded streamline), reversed flow patterns outside this region (shaded streamline)

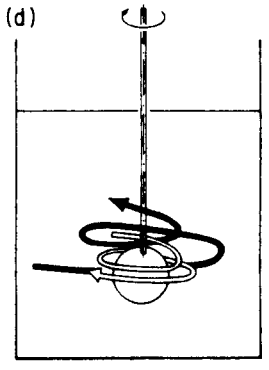

patterns in the vicinity of the rotating sphere and outside this region (*Fig. IV.1 c* and *d*).

Following the earlier work carried out mostly by rheologists, flow patterns in viscoelastic fluids were investigated with various agitators that have more complex geometry than spheres. In the viscous flow regime, which is dominantly characterised by primary flow patterns, normal forces generated in a viscoelastic fluid are not incompatible with the flows in the tangential direction. Hence, flow patterns are not remarkably affected by fluid viscoelasticity at low Reynolds numbers. Kelkar et al (1983) have shown that the tangential flow around a rotating body is not affected by the extent of fluid viscoelasticity provided the Reynolds number is less than about 5. When this flow regime is exceeded, inertially driven secondary flow patterns are generated as also explained in Chapter III for Newtonian fluids. In viscoelastic fluids, the nature of the secondary flows is not only determined by the inertially driven forces, but by an interaction of these with the viscoelastically driven forces. Very little information exists on the flow patterns in viscoelastic fluids for impellers other than Rushton turbines. With an axial flow impeller (screw propeller), it was reported that the propelling action being in the same direction as the viscoelastically driven flows, was reinforced in viscoelastic fluids and the flows were under no circumstance reversed[129]. With anchor impellers the vertical component of flow generated was observed to be enhanced for the same reason[91,107]. For a radially discharging impeller - such as the classical six bladed disc turbine- viscoelastically driven forces mutually oppose the inertial forces. Thus, the resulting secondary flow patterns depend on the relative magnitude of these forces. Elasticity number was, therefore, used as a key parameter by various researchers[52,116,129,28]. For low values of this dimensionless number inertial forces are dominant (similar to the situation presented in

Fig. IV.1 a) and the liquid is discharged radially outwards as in an inelastic fluid . On the other hand, the direction of inertially driven forces is reversed when the Elasticity number is sufficiently high and elastically driven forces are prevalent (similar to the situation in *Figure IV.1 b*). At intermediate values of the Elasticity number, secondary flow patterns break into two and segregated zones are formed around and outside the impeller region. This intermediate type of flow reported by previous researchers[110,111,78] who made observations in mixing vessels was similar to the flow patterns presented in *Figure IV.1 d*. Inertially driven forces prevailed in the vicinity of the impeller and with Rushton turbines the liquid was discharged radially outwards. Away from this region, fluid flows were reversed under the effect of viscoelastically driven forces. Formation of such segregated zones is clearly a very undesirable situation as the material exchange within the bulk is considerably reduced.

Various researchers[96,110,78] observed flow reversal with the rheologically complex fluids they used. However, conditions for the onset of different flow patterns were expressed in terms of Re, N_1, or Wi, but not the Elasticity number. A review of the effects of viscoelasticity on flow patterns is given by Ulbrecht and Carreau (1985).

The effects of viscoelasticity on the tertiary flow patterns have not been reported.

IV.3.2 Power consumption under unaerated conditions

Most of the viscoelastic fluids used by previous researchers were also highly viscous. Laminar and transitional flow regimes were therefore, covered and helical impellers have been of interest. Model viscoelastic fluids also exhibited other complex behaviour apart from a few studies[82,1,94,28,12,13] where elastic fluids of constant viscosity were used.

The power consumed in a stirred vessel is closely related to the flow patterns generated. Hence, in the viscous flow regime, where flow patterns are not substantially modified, the effect of viscoelasticity on power consumption would also be very little. Several researchers[137,26,116,98,47,48] reported that in the viscous flow regime, viscoelasticity did not noticeably affect the power consumed but pseudoplasticity did. Some researchers[71,28] found an increase in power in the late laminar region which suggested that viscoelasticity may alter the boundaries of the laminar flow regime.

Findings of various researchers regarding the effect of viscoelasticity on power consumption vary considerably in the transitional flow regime.

Ranade and Ulbrecht (1977) obtained power curves for viscoelastic pseudoplastic solutions below the Newtonian one (in the range $10 < Re < 300$) underlining the difficulty to distinguish the impact of these two rheological properties.

Höcker et al (1981 a,b) used both Rushton turbines and InterMIGs in viscoelastic PAA solutions. They reported an enhancement of power consumption with MIGs (a prototype of InterMIGs), but a reduction with Rushton turbines.

Oliver et al (1984) obtained power curves of wavy appearance in the laminar and transitional regions: power numbers with viscoelastic Boger fluids were higher or lower than those obtained with Newtonian fluids at arbitrary values of the Reynolds number. They interpreted this to be related to the elastic nature of the fluid. It should be noted that their power data was not reproducible for different runs under the same conditions.

Allsford (1985) studied Rushton turbines of 1/3 and 1/2 the tank diameter and reported that the power data for the large impeller was almost identical for viscoelastic (Boger fluids) and Newtonian fluids. For the small impeller, power consumption was suppressed in the range $5 < Re < 10$ with

elastic fluids but was slightly higher in the range 100 < Re < 1000.

Prud'homme and Shaqfeh (1984) and Collias and Prud'homme (1985) evaluated their data with Rushton turbines in terms of the Torque number (Γ) which they defined as :

$$\Gamma = (M\ \rho)/(\mu^2\ D)$$

In the ranges of Reynolds numbers between 10 and 45, they reported a substantial increase of the Torque number with Boger fluids. This enhancement was up to three to four times that with Newtonian fluids of identical viscosity depending on the scale of operation and the fluid properties. In the Elasticity number range they covered (El< 0.063), the flow patterns were similar to those observed in Newtonian fluids. Brito et al (1990, 1991) who used organic Boger Fluids reported similar findings for helical impellers.

Nienow et al (1981, 1983 c),and Nienow and Elson (1988) used a range of rheologically complex fluids and pointed out that the non-Newtonian power curve deviated from the Newtonian one in the transitional region (Re>10). They reported that the power consumption was less with these fluids especially in the range 50< Re < 1000.

Himmelsbach (1985) reported a slight reduction of power with Rushton turbines in xanthan solutions compared to that in Newtonian fluids and a slight increase in power with a pair of InterMIGs covering the transitional regime.

Some researchers[60,95] used aqueous polymer solutions and reported a reduction in power consumption in the turbulent flow regime. This "turbulent drag reduction" is also called the "Toms' effect".

IV.4 RESULTS AND DISCUSSIONS

In this section, experimental results concerning the influence of viscoelasticity on flow patterns and power characteristics of InterMIGs and Rushton turbines under unaerated conditions are presented. Rheological properties of the model fluids were reported in Chapter II. The mixing equipment used was described in Chapter III.

IV.4.1 Operational conditions, dimensionless numbers

Operational conditions and the ranges of the dimensionless numbers covered during experiments are presented in *Table IV.1* for viscoelastic fluids of different polymer concentrations at two scales of operation.

IV.4.1.1 Reynolds number

The viscoelastic fluids used in this study have an almost shear independent viscosity and therefore the dependence of the shear stress on the shear rate can be approximated to a linear one (*Table II.2*). The Reynolds number could then be calculated in two ways : *i)* assuming that this relation is strictly a linear one, i.e. taking viscosity values from the fourth column of *Table II.2*, and using the expression in equation (III.4), or *ii)* taking into account the slight shear thinning properties, i.e. substituting the K and n values from the third column of *Table II.2* in equation (IV.4). In the latter case, the value of k_s for Rushton turbines is taken as 11.5, relying on the previous data reported by various researchers, and 17.0 for InterMIGs as was found by the previous researchers in Birmingham University[1]. A plot of the characteristic power curve with the power number against the Reynolds number, calculated, in both ways is presented on *Figure IV.2*. For both InterMIGs and Rushton turbines, the power curves obtained from the two calculations almost coincide. The slight shear thinning properties are, however, taken into

Figure IV. 2 Characteristic power curves obtained in Fluid (1)

Reynolds number is calculated :

a) neglecting shear thinning effects (○ , △): $Re = (ND^2\rho/\mu)$

b) taking into account the slight shear thinning properties

(● , ▲): $Re = (N^{2-n} D^2 \rho / (K k_s^{n-1})$

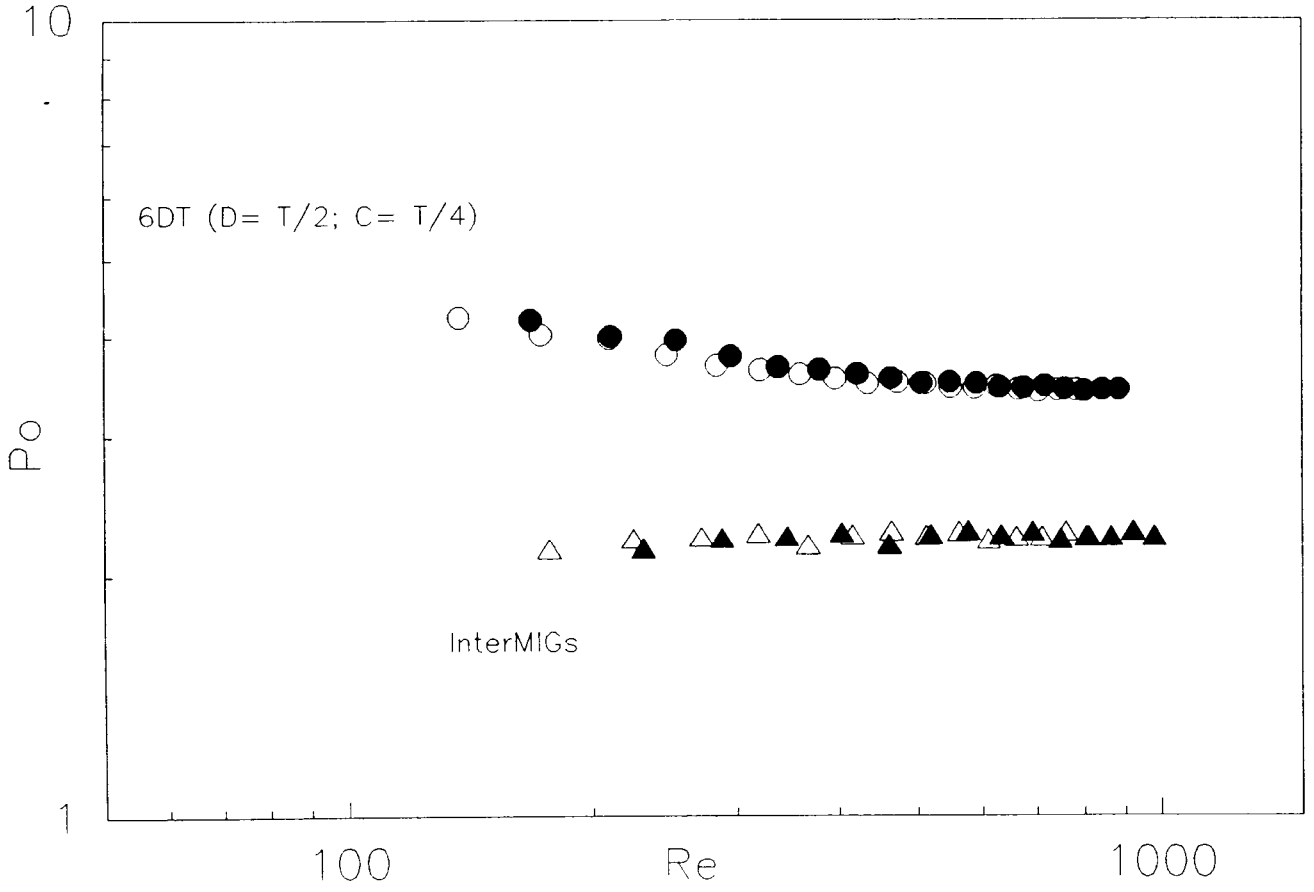

account for the rest of the calculations. These are the values given in *Table IV.1.*

It can be seen from *Tables III.1* and *IV.1* that the Reynolds numbers covered with Newtonian and viscoelastic fluids are almost in the same range which has allowed comparisons to be made.

IV.4.1.2 Weissenberg number and Elasticity number

The ranges of the Weissenberg number covered with viscoelastic fluids in this study are given in *Table IV.1.*

Figure IV.3 shows the evolution of the Elasticity number as a function of the Reynolds number for one of the viscoelastic fluids used. It was previously reported in Chapter II that elastic properties of the fluid decreased slightly from day to day. However, the effect of the impeller diameter, incorporated in the Elasticity number, is more important accounting for different ranges covered with the same fluid. This can be seen comparing *Figures II.6* and *IV.3.*

The ranges of the Elasticity numbers covered in this study are given in *Table IV.1.* Since the polymer concentration was increased only slightly from one fluid to another, the Elasticity number ranges also increased only very slightly.

Table IV.1 Operational conditions and dimensionless number ranges covered with the viscoelastic fluids

T61	Single 6DT				Two 6DT		InterMIGs
D/T	1/3		1/2		1/3	1/2	0.60
C/T	1/3	1/4	1/3	1/4			
FLUID 1							
N^{max}_{min} (s^{-1})	7.9 0.8	7.9 1.0	- -	3.5 0.7	6.3 0.7	2.7 0.7	2.8 0.7
P^{max}_{min} (W)	824 1	802 1	- -	510 4	666 1	417 3	385 5
Re^{max}_{min}	743 70	742 55	- -	726 127	588 55	546 127	810 178
Wi^{max}_{min}	0.14 0.04	0.40 0.09	- -	0.50 0.17	0.09 0.02	0.18 0.06	0.20 0.06
$El^{max}_{min} \times 10^3$	0.53 0.20	1.57 0.53	- -	1.40 0.69	0.30 0.15	0.40 0.32	0.34 0.25

Table IV.1 continued

T61	Single 6DT				Two 6DT		InterMIGs
D/T	1/3		1/2		1/3	1/2	0.60
C/T	1/3	1/4	1/3	1/4			
FLUID 2							
N_{min}^{max} (s^{-1})	-	8.4	3.5	3.3	6.8	2.5	2.5
	-	1.0	0.8	0.7	0.7	0.8	0.7
P_{min}^{max} (W)	-	1065	575	461	988	377	290
	-	2	9	4	1	11	6
Re_{min}^{max}	-	758	713	678	613	506	697
	-	86	165	131	57	148	181
Wi_{min}^{max}	-	0.45	0.28	0.42	0.59	0.25	0.55
	-	0.09	0.07	0.12	0.13	0.10	0.22
$El_{min}^{max} \times 10^3$	-	0.99	0.45	0.89	2.2	0.67	1.21
	-	0.60	0.40	0.62	0.96	0.50	0.79
FLUID 3							
N_{min}^{max} (s^{-1})	9.5	8.5	3.5	3.5	6.3	2.7	3.0
	0.8	1.0	0.7	0.8	0.7	0.7	0.7
P_{min}^{max} (W)	1262	1019	580	527	780	417	444
	1.3	2.22	5	7	1	7	5
Re_{min}^{max}	747	666	618	618	493	468	728
	62	75	113	128	49	113	156
Wi_{min}^{max}	1.26	1.12	0.58	0.83	0.80	0.77	0.58
	0.19	0.25	0.16	0.25	0.13	0.30	0.18
$El_{min}^{max} \times 10^3$	3.12	3.40	1.44	2.00	2.70	2.61	1.16
	1.68	1.68	0.94	1.30	1.62	1.65	0.80

Table IV.1 continued

T29	Single 6DT		Two 6DT	InterMIGs
D/T	1/3	1/2	1/3	0.60
C/T	1/4	1/4		
$N^{max}_{min}(s^{-1})$	8.25 1.3	9.8 1.0	5.55 0.5	5.1 1.0
$P^{max}_{min}(W)$	27 0.2	85 0.2	60 0.1	75 0.7
Re^{max}_{min}	187 29	224 22	278 24	349 66
Wi^{max}_{min}	0.44 0.09	0.51 0.07	0.31 0.04	0.40 0.10
$El^{max}_{min} x10^3$	3.20 2.30	3.40 2.30	1.70 1.10	1.53 1.16

Figure IV.3 Elasticity number as a function of Reynolds number (Fluid 2)

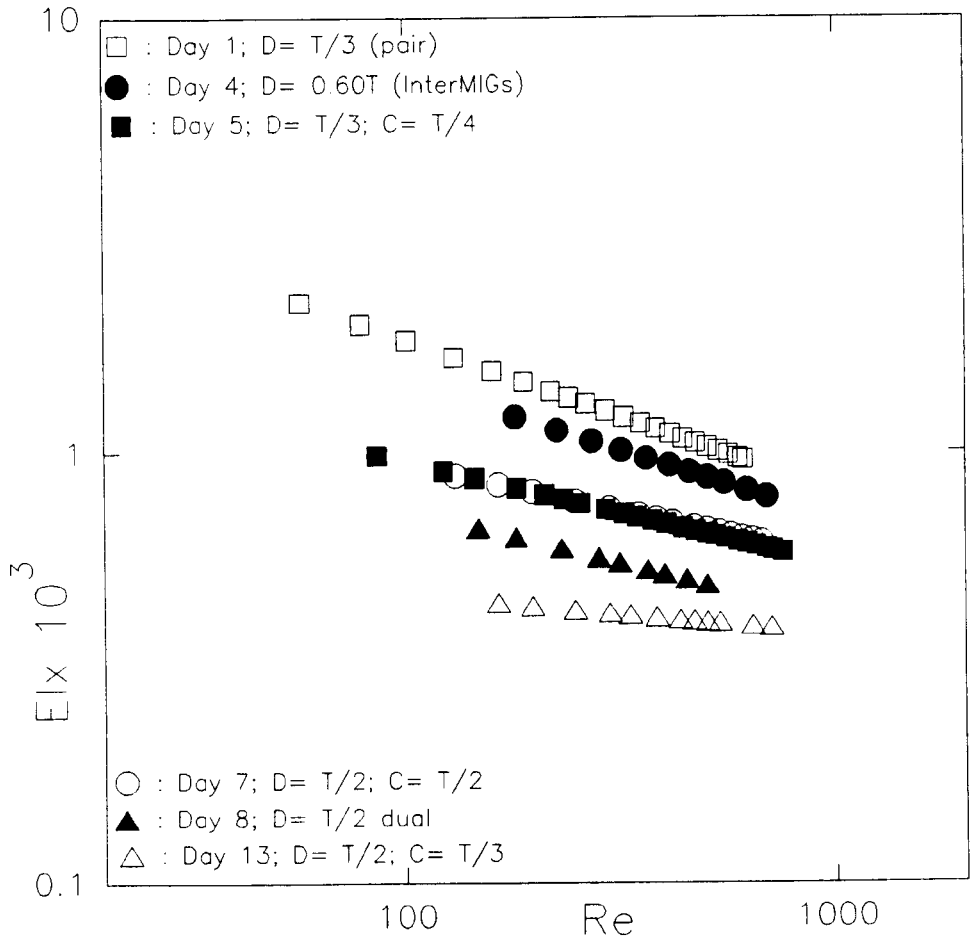

IV.4.2 Flow patterns under unaerated conditions

In the low range of Elasticity numbers covered, the magnitude of viscoelastically driven forces was not high enough to overcome inertially driven forces. Secondary flow patterns were in general similar to those observed in viscous Newtonian glycerol, with an important tangential component of flow.

The radial discharge from Rushton turbines was apparently constricted as the inertially driven forces were damped by the viscoelastically driven forces.

For InterMIGs, upward flows originating from the inner blades were reinforced being in the same direction as the viscoelastically driven forces. Hence, the effect of viscoelasticity, interfering with the radially outward flows from the outer blades, was enhanced.

Figure IV.4 schematically represents radially outward flows from the impellers being constricted under the effect of viscoelastically driven flows.

It was also observed that in viscoelastic fluids, the presence of forces normal to the plane of shear have retarded surface aeration. A noticeable vortex formation was not observed in viscoelastic fluids, although the range of impeller speeds covered were above those at which surface aeration gave rise to torque fluctuations in glycerol (see *Tables III.2* and *IV.1*).

Figure IV.4 A schematic representation of the interaction of viscoelastically driven flows with those imposed by the impellers

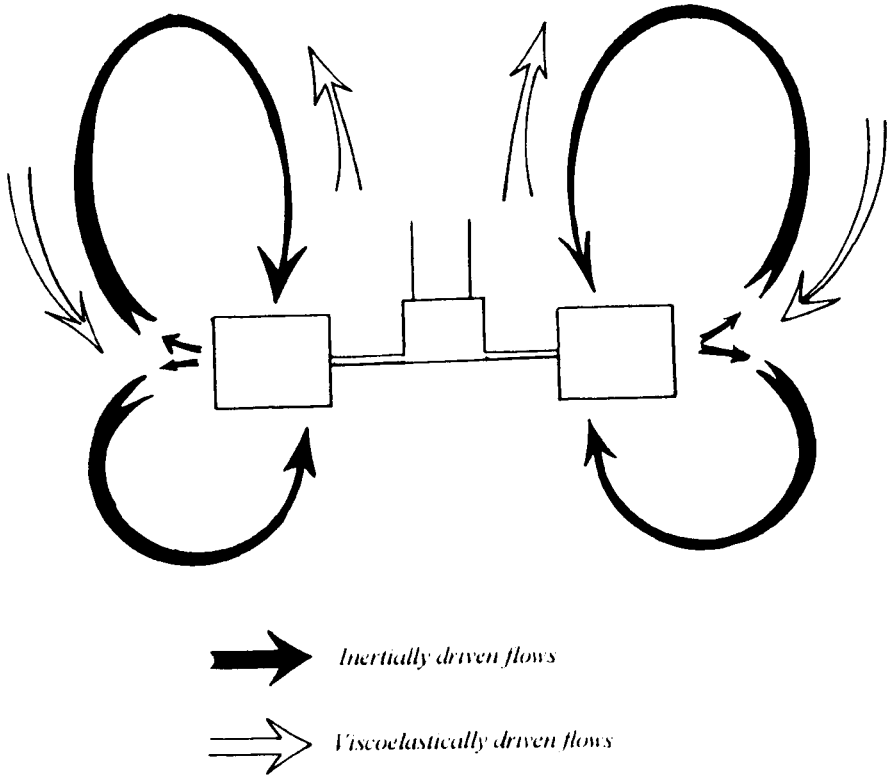

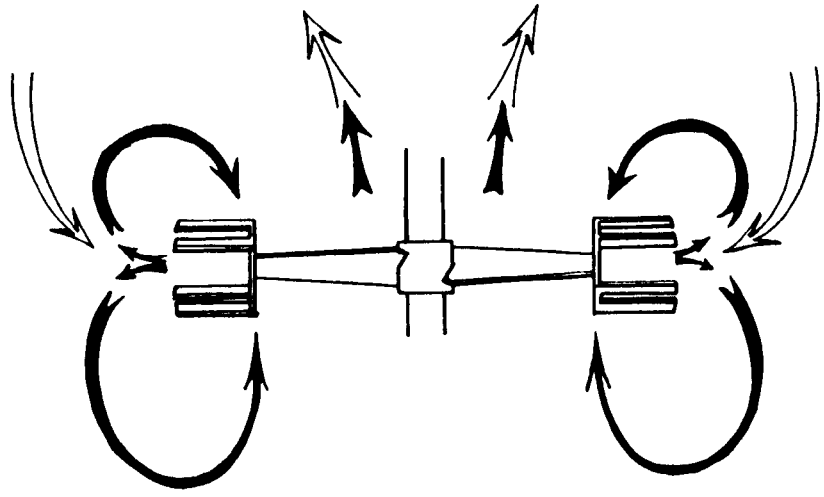

IV.4.3 Characteristic power curves in viscoelastic fluids

Characteristic power curves obtained in one of the viscoelastic fluids with various impeller geometries and types are presented in *Figure IV.5* . The trend followed in other fluids was similar.

Conforming with the results obtained in glycerol, the variation of the impeller clearances (C= T/3 and T/4) did not have a significant effect on the power consumed in viscoelastic fluids (*Figure IV.5*) as the flow patterns were also not modified. However, for higher or lower values than those investigated in this study, impeller clearance may be an important factor especially where segregated zones below and above the plane of the impeller are formed.

In Newtonian fluids, the effect of the impeller diameter on the power consumption was found to be negligible (see Chapter III). In viscoelastic fluids, power numbers were slightly higher for a single small Rushton turbine (*Figure IV.5*). This effect, however, was not evident for a pair of Rushton turbines: the power numbers for the two diameters (D= T/3 and D= T/2) were quite close. Hence, the overall power drawn by two large Rushton turbines was almost twice as that of a single one of the same diameter :

$Po_{dual} = (1.80 - 1.90)\ Po_{single}$, but for the small diameter impeller, this was:

$Po_{dual} = (1.50 - 1.65)\ Po_{single}$.

Power numbers for a pair of InterMIGs were in general much less than those obtained with even single Rushton turbines (*Figure IV.5*).

IV.4.3 Effects of viscoelasticity on power consumption

In *Figures IV.6* and *IV.7*, characteristic power curves obtained in viscous Newtonian glycerol and viscoelastic fluids are presented for a pair of Rushton turbine and InterMIGs respectively. The shape of the characteristic power curves obtained with Rushton turbines was similar in elastic and

Figure IV.5 Characteristic power curves obtained in one of the viscoelastic fluids (Fluid 1) with different impellers

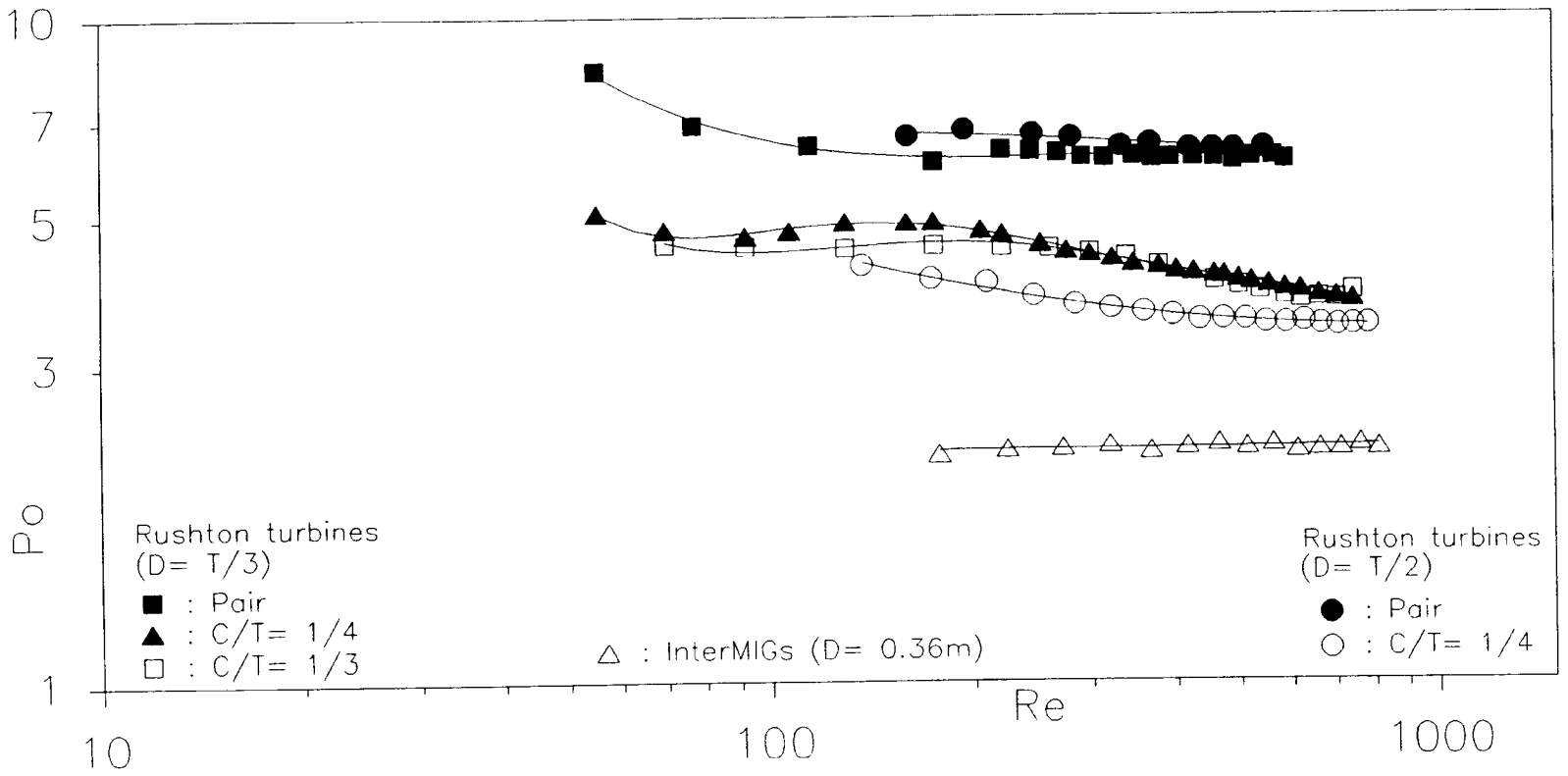

Newtonian fluids. However, for InterMIGs the continually decreasing power curve obtained in glycerol was replaced by an almost constant one in viscoelastic fluids.

Power numbers were in general found to be higher in viscoelastic fluids for all impeller types compared to inelastic glycerol (*Figures IV.6* and *IV.7*). This conforms with the findings of Collias and Prud'homme (1985) and Brito-de la Fuente et al (1990) who also used Boger fluids and obtained higher power numbers although the scale of operation of the former (T= 0.15-0.20 m) and the type of impeller used by the latter (helical ribbons) were different from those in this work. As the power consumed in a stirred vessel is closely related to the flow patterns generated, this enhancement can be interpreted in terms of the interaction of viscoelastically driven flows with those of inertially driven flows. Although the overall features of the secondary flow patterns were similar to those observed in Newtonian glycerol, the impeller had to overcome an additional elastic force in order to discharge the fluid almost radially as in an inelastic fluid. This required a higher power consumption. It can also be seen in *Figure IV.6* and *IV.7* that power numbers increased further for increasing levels of viscoelasticity (from Fluid 1 to 3). This enhancement was not very distinct as the polymer concentration and consequently the Elasticity number range increased only very slightly from one fluid to the other.

The difference in power numbers obtained with viscoelastic fluids and Newtonian glycerol was evaluated with :

$$\frac{|Po_{elast.} - Po_{Newtonian}|}{Po_{Newtonian}}$$

at a given Reynolds number. For both scales of operation (T29 and T61), this was found to be up to about 18 % for a pair of Rushton turbines; 32 % for a single large impeller (D= T/2) and 40 % for a single small impeller (D= T/3). For InterMIGs, as the shape of the power curve changed, the enhancement of power numbers was drastic; at high Reynolds numbers this was about 140 %. This is probably due to the complicated interaction of the viscoelastically driven flows with those associated with the inner and outer blades of InterMIGs.

Figure IV.6 Power curves obtained with a pair of Rushton turbines (D= T/3) in Newtonian glycerol and in viscoelastic fluids

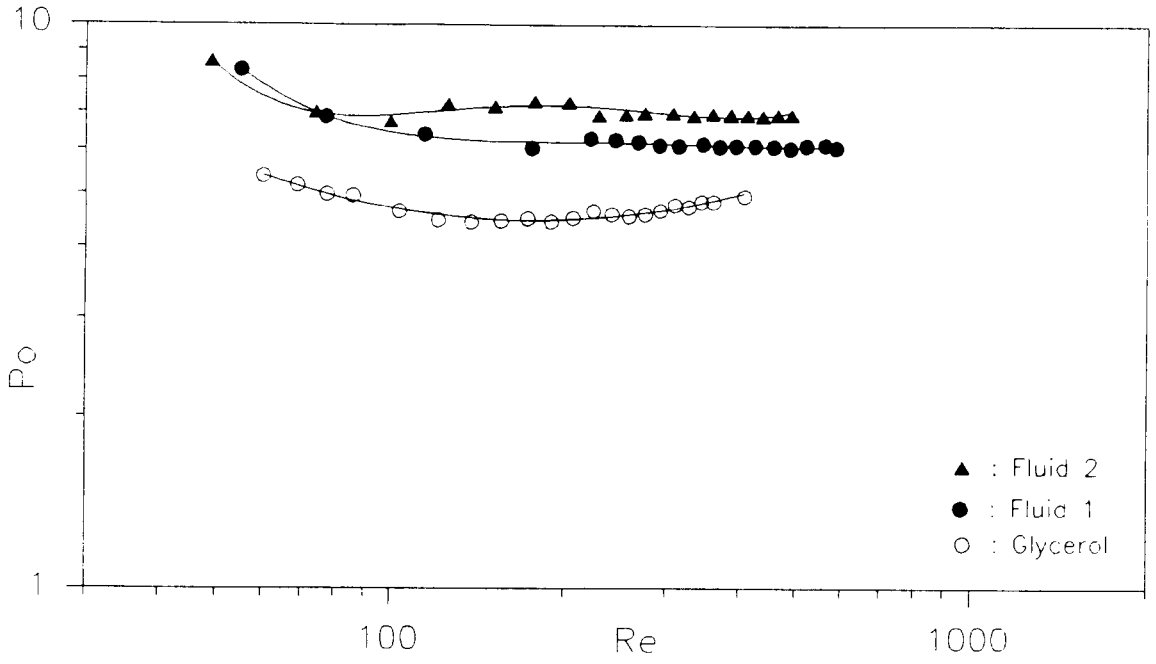

Figure IV.7 Power curves obtained with InterMIGs in Newtonian glycerol and in viscoelastic fluids

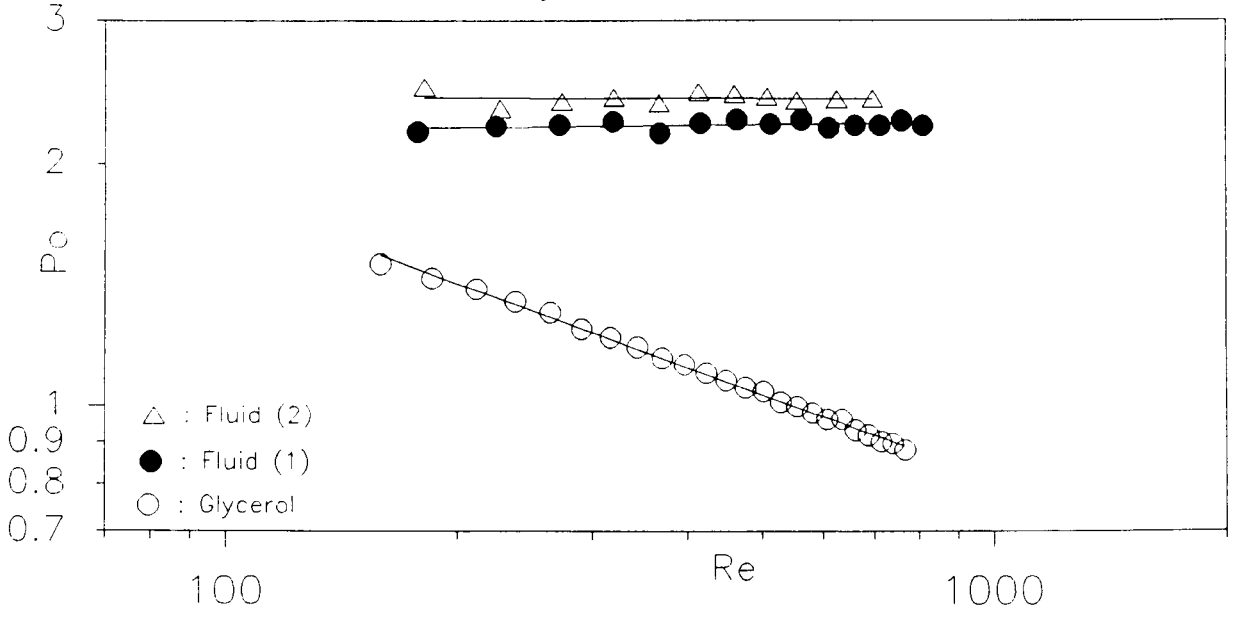

IV.5. CONCLUSIONS

The effects of fluid viscoelasticity on flow patterns and power consumption could be studied in the absence of other rheological complexities using model viscoelastic fluids of constant viscosity ("Boger fluids").

The Elasticity numbers covered with various impeller geometries and types (InterMIGs and Rushton turbines) in a range of PAA concentrations in glycerol were less than 3.5×10^{-3}. Visual observations have shown that, in this relatively low range, secondary flow patterns under unaerated conditions were not substantially modified in comparison to those observed in Newtonian glycerol. The radially outward flows from Rushton turbines and from the outer blades of InterMIGs were however constricted under the effect of mutually opposing viscoelastically driven forces.

The power required to sustain a radially outward discharge in viscoelastic fluids was therefore higher. Apart from a general enhancement of power consumption for all impeller types in the presence of fluid elasticity, a further enhancement was recorded with the increase of elasticity (increase of polymer concentration and thus the Elasticity number range). The enhancement of power numbers at a given Reynolds number was considerably more important for InterMIGs than Rushton turbines. The upward flows from the inner blades of InterMIGs were reinforced being in the same direction as that of viscoelastically driven flows which in turn reduced the extent of radially outward flows from the outer blades. This complicated interaction of the viscoelastically and inertially driven flows for InterMIGs resulted in a much larger increase in the power consumption as the shape of the characteristic power curve also changed markedly from a continuously decreasing to an almost constant one.

CHAPTER V MIXING TIME STUDIES

V.1 INTRODUCTION

A major task of agitation is to reduce inhomogeneities within the bulk. Poor mixing will lead to concentration and temperature gradients and thus adversely affect the product quality and yield. On the other hand, it would be desired to complete a given process with the minimum amount of energy expenditure ($E = P\ t_m$). A knowledge of the power input and the time for which it is applied is important as the efficiency of mixing ($1/\ P\ t_m$) is dependent on both of these parameters.

This chapter is concerned with the study of mixing time that provided a basis of comparison of the efficiency of different impellers in various fluids. Background information is given in Sections V.2 to V.4 where general concepts and experimental methods (Section V.2), data presentation (Section V.3) and findings of previous researchers (Section V.4) are presented. The technique and instrumentation used for measuring mixing time, which was installed during the course of this study, are described in Section V.5. Mixing time data obtained in various fluids with Rushton turbines and InterMIGs are reported in Section V.6.

V.2 DEFINITIONS AND EXPERIMENTAL METHODS

Although various definitions exist in the literature, *mixing time* can be defined as the time taken from the release of a tracer until the amplitude of the output signal fluctuations is within a set limit of the final reading; or if visual methods are used, the time for the disappearance of the last traces of gradients.

Where methods providing quantitative data are used, mixing time response curve often shows a periodicity *(Figure V.1)*. In practice, however, this periodicity may not be as ideally distinctive as represented in *Figure V.1*. *Circulation time* (t_c) is the time period elapsed between two subsequent peaks

Figure V.1 Evolution of concentration gradients in time - Mixing time curve

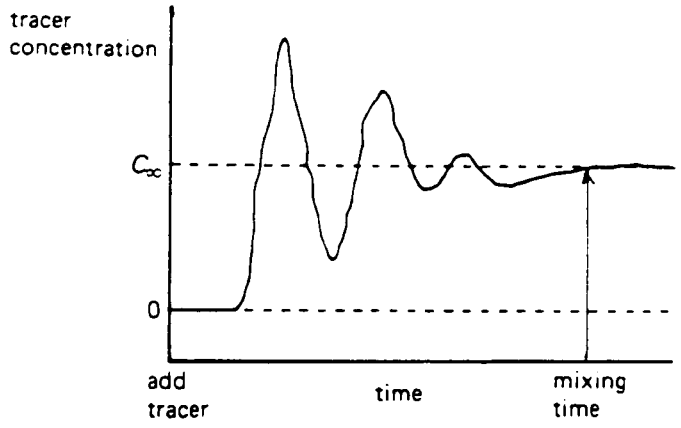

or troughs or where a suspended flow follower is observed, the time between two consecutive passages of the tracer from the impeller region. Circulation time reflects only the intensity of macro flow: the primary and secondary flows. The tertiary flows, i.e. flows associated with the upstream and downstream faces of the blade, do not contribute significantly to the value of the circulation time. Therefore, it is often considered that the circulation time is important when working with helical impellers but not so much with radially thrusting impellers[116].

The numerical value of mixing time experimentally determined, can vary considerably depending on the technique of measurement and the definition of mixing time[30,55]. Although it is not an absolute measurement, mixing time provides helpful information assigning a single value to the complex three dimensional flow field in a vessel.

Table V.1 Experimental methods for measuring mixing time

Method	Principle	Advantages	Disadvantages
Conductivity method	Monitoring the variation of conductivity after the addition of a salt, acid or base solution.	a) Objective results and an exact criterion for mixing. b) Fast response time probes c) Linear response probes over a wide range of liquid conductivities d) Stable probes over long period e) Continuous time history of fluctuations at sample points f) Known measuring volume	a) Rheological properties of some fluids change upon the addition of tracers b) Coalescence properties of the bulk are altered c) Conductivity or pH of the bulk increases
Dye addition method	Sample removal and analysis or visual observations after the addition of a dye.	Simple	a) Subjective results are obtained from visual observations b) Flow patterns are affected during sample removal c) Repetition are not possible with the same bulk.
Chemical reaction model	Colour changes due to a chemical reaction.	a) Final stages of mixing can be observed b) More sensitive than the dye addition method c) Suitable for small scale d) Flow pattern can be observed	a) Subjective b) Practical difficulties with strong acids c) Modifications of bulk rheology d) Observations difficult in the laminar regime (no sharp colour changes) e) Initial reactant must be homogeneously mixed before the run f)Observations difficult with opaque fluids
Tracer method	Determination of a uniform distribution of tracers throughout the bulk.	Different tracers allow the reuse of the same bulk	Practical difficulties
Thermal method	Monitoring the variation of temperature	a) The chemical composition of the fluid does not change b) Unlimited number of runs can be performed with the same bulk c) Reproducible quantitative data can be on large scale	a) Several practical requirements: - high sensitivity temperature measurements - vessel to be thermally insulated - probe of high thermal conductivity b) Rheological properties are substantially affected
Schlieren method	Optical inhomogeneities in inhomogeneous fluids.		a) Optical inhomogeneities may occur in a single agitated viscoelastic fluid b) Little knowledge regarding the time necessary to establish a stationary flow pattern

Various experimental methods for measuring mixing time and an evaluation of the advantages and disadvantages of these methods are summarised on *Table V.1*. More details on these techniques are given by Ford et al (1972). The choice of a technique of measurement will depend on several factors:

i. the effect of the addition of the tracer on the physical properties of the bulk liquid;

ii. the accuracy of the technique and the reproducibility of results;

iii. whether the bulk can be reused at the end of a run or not (this is important especially where costly fluids are used in large scale).

In any case, it is important to specify the manner and location of tracer addition, the end-point criterion, the position and the number of sensors, and the sample volume. Comparison of mixing time values obtained under different operational conditions can only be made if the same technique/ probe and end-point criterion are used.

The above experimental techniques present several shortcomings when used in highly viscous and/ or rheologically complex fluids *(Table V.1)*. The main disadvantage of using any of these techniques is that the physical properties of the bulk liquid are altered during (thermal method) and/ or after the run (dye addition, conductivity, etc). These result in significant discrepancies in the data obtained, and also require frequent renewal of the bulk which are both undesirable. The fluorescent dye- fiber optic technique was therefore used for mixing time measurements throughout this work since the quantity of the tracer to be added with this technique is only very small. Details of the technique and the actual set-up are given in Section V.5.

V.3 PRESENTATION OF MIXING TIME DATA

Mixing time experimentally measured depends on various variables such as:

$$t_m = fn\ (\rho,\ \mu,\ N,\ D,\ T,\ \text{other geometrical parameters}).$$

Data can be correlated in terms of the dimensionless mixing time ($N\ t_m$) which is the number of revolutions needed to attain an arbitrary but constant degree of homogeneity:

$$N\ t_m = fn\ (\rho\ N\ D^2/\mu,\ N^2\ D/g,\ T/D,\ \text{other geometrical ratios})$$

$$N\ t_m = fn\ (Re,\ Fr,\ \text{geometrical ratios})$$

For geometrically similar systems, geometrical ratios and when there is no vortex formation, the effect of the Froude number can be neglected :

$$N\ t_m = fn\ (Re).$$

A number of other groups were used by different researchers in attempt to relate mixing time to the power consumed:

$$(P\ t_m^2/D^3\ \mu) = fn\ (D^2\ \rho/t_m\ \mu) \qquad \text{Hoogendoorn and den Hartog (1967)}$$

$$(P\ D\ \rho^2/\mu^3) = fn\ (t_m\ \mu/\ D^2\rho) \qquad \text{Zlokarnik (1967)}$$

In this work, dimensionless mixing time ($N\ t_m$) is plotted as a function of Reynolds number to study the evolution of this number in the transitional and turbulent flow regimes. In order to evaluate the performance of different impellers in fluids of various rheological properties, energy requirements are taken into account and mixing time values are compared on the basis of

equal volumetric power input.

V.4 MIXING MISCIBLE LIQUIDS AND PREVIOUS WORK ON MIXING TIME

V.4.1 Mechanisms of mixing miscible Newtonian liquids

Two hydrodynamic effects that play a role in attaining a specified degree of homogeneity are the long range *convective flow (bulk flow, bulk diffusion* or *bulk dispersion)* and the *local turbulent diffusion (eddy diffusion* or *eddy dispersion). Molecular diffusion*, caused by the relative motion of molecules, determines the homogeneity of the system on a molecular scale. Local turbulent diffusion is related to the energy transfer from large groups of molecules- primary eddies- to smaller ones. The size of the large eddies is comparable to that of the impeller[73]. Large eddies, having an unstable motion, break up when they interact with slow moving streams, and generate smaller ones[14,15,73]. These small eddies further disintegrate giving rise to still smaller ones. Thus, a high proportion of the energy input by the impeller and transferred to large scale turbulent eddies is cascaded down to smaller scale eddies. The process continues producing smaller and smaller eddies until they are dissipated as heat under the effect of viscous forces. Bulk diffusion refers to all diffusion processes other than the molecular diffusion and the eddy dispersion. This mainly results from the pumping action of the stirrer. A good bulk or convective flow has to be ensured to reduce the stagnant zones in the vessel. The overall turbulent mixing process takes place by a complicated interaction of these mechanisms.

With highly viscous fluids where energy requirements are too high to create turbulent mixing, the laminar flow regime is covered. Mechanisms of mixing associated with laminar flow conditions are different in many aspects from turbulent mixing. As also explained in Chapter II, inertial forces being negligible, primary flow patterns characterise this flow regime. Among

various bulk diffusion processes, laminar shear flows which are at a higher velocity close to the rotating impeller reduce concentration differences by thinning layers, elongating threads and flattening lumps or agglomerates[14,73]. Rotational shear flows and extensional flows also contribute to the thinning and stretching of fluid elements increasing the surface area. As the process continues, the scale of fluid elements that are exposed to these flows is reduced. On molecular scale, diffusion takes place more slowly than under turbulent flow conditions. This is because other diffusional processes -shear and tensile deformations- that aid molecular diffusion are slower, also molecular diffusivity itself is low in highly viscous fluids.

The transitional flow regime- as the name suggests- is characterised by a combination of the mechanisms associated with both laminar and turbulent flow regimes. Truly laminar conditions were not studied in this work; the ranges of Reynolds numbers covered fall in the turbulent and transitional flow regimes.

V.4.2 Previous work on mixing time in Newtonian fluids

Various researchers[46,131,53,81,37,89,104,34,100,29,31], who used different impeller types and covered different flow regimes, reported that in Newtonian fluids the dimensionless mixing time is independent of the Reynolds number in the laminar flow regime, it decreases with increasing Reynolds number in the transitional regime before reaching a constant value in the turbulent flow regime *(Figure V.2)*. With six bladed disc turbines, the dimensionless mixing time was reported to attain a constant value at Reynolds numbers of about 3.3×10^3 to 6.0×10^3 by various researchers[46,55,29].

Figure V.2 Dimensionless mixing time of a Newtonian fluid in different flow regimes

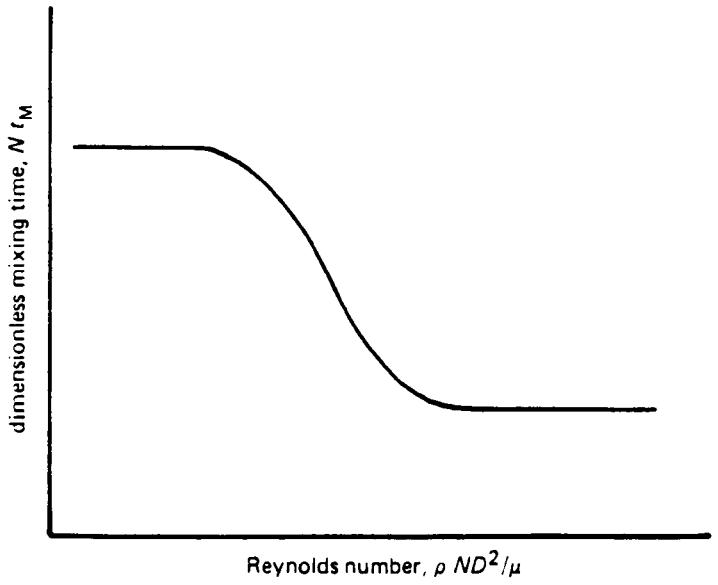

Pandit et al (1989), who covered the turbulent flow regime, reported the advantage of using a convex bladed mixed flow impeller which gives dimensionless mixing times almost equal to those obtained with other impellers (paddle, disc turbine, angle bladed turbine) but consuming considerably less power.

Allsford (1985) compared the performance of various impeller configurations in a glucose solution of 0.65 Pa s in the transitional flow regime, following the criterion proposed by Hoogendoorn and den Hartog (1967). Among the impellers tested, the combination of T/2 angle bladed impeller (pumping upwards) as the upper impeller and a disc turbine as the lower impeller was found to be the most energy efficient. A list of impeller configurations in order of decreasing efficiency can be found in Allsford (1985) and Nienow and Elson (1988).

A number of applications may require the addition of a liquid in a bulk of a different density that may also have a different viscosity. Studies on mixing fluids of different densities have shown that for additions made

outside the impeller region a light tracer will rise to the liquid surface and a heavy one will fall to the vessel base[109,101,10,20]. Depending on the impeller speed and the importance of density difference, only a part of the tracer may be drawn into the impeller region. In all these situations where all the tracer is not drawn into the impeller region, higher mixing times are required. Injection of the tracer in the impeller discharge or prior mixing of the tracer may eliminate such problems.

V.4.3 Previous work on mixing time in viscoelastic fluids

Mixing time studies carried out with viscoelastic fluids by previous researchers are generally confined to low Reynolds number ranges- due to high viscosity. Mostly helical impellers were used and measurements were made with the colourisation - decolourisation technique. It should also be noted that in most of these studies mixing time data were evaluated at equal speed or the dimensionless time at a given Reynolds number.

Findings of various researchers[26,21,37,28,92] indicate an important increase of mixing time in viscoelastic fluids: 2 to 7 times of that measured in inelastic fluids. Exceptionally, Brito et al, (1990, 1991) found similar mixing time data for viscoelastic fluids of constant viscosity and Newtonian fluids. Although they reported that viscoelasticity has a tendency to increase mixing time, the scatter in their data makes it difficult to draw any clear conclusions. This may be due to the technique employed - the thermal method - considering that the physical properties of the model fluids used are highly temperature sensitive.

Pörtner et al (1988) reported that the performance of InterMIGs and paddle impellers are comparable in Newtonian fluids and also in slightly elastic solutions of CMC. On the other hand, in highly elastic PAA solutions paddles were found to be more energy efficient than propellers with a draught

tube or InterMIGs .

The location of tracer addition is important particularly in viscoelastic fluids where segregated zones may be formed depending on the flow patterns generated. Collias and Prud'homme (1985) measured longer mixing times at the liquid surface, near the vessel wall and below the impeller level compared to a position above the impeller between the wall and the impeller. They also visually observed an important segregation of the liquid above and below the plane of the impeller.

In an attempt to quantify the impact of elasticity, Ulbrecht (1974), Ford and Ulbrecht (1976) and Carreau et al (1986) correlated mixing and circulation times for helical impellers to the Weissenberg number.

Mixing time measurements with fluids that possess a yield stress leading to cavern formation have little meaning as the exchange between the cavern contents and the rest of the bulk is governed by molecular diffusion. However, some attempts to measure mixing time and circulation time in such fluids have been made[38].

V.5 TECHNIQUE AND INSTRUMENTATION FOR MEASURING MIXING TIME

As also explained in Section V.2, conventional methods for the quantitative and qualitative evaluation of mixing time present various disadvantages when used in highly viscous fluids altering their physical properties. Therefore, the main concern in this study was to employ a technique that would avoid the frequent renewal of the bulk liquid because this is very costly considering the scale of the mixing vessel ($V = 0.178\ m^3$). Also, it is practically impossible to reproduce the rheological properties of viscoelastic fluids in different batches. A fluorescent dye - fiber optic technique, which requires the addition of a very small quantity of dye, was therefore adapted for this study. The technique was described by Bell (1972) for the determination of residence time distribution on distillation trays and also used by Collias and Prud'homme (1985) in a small scale mixing vessel.

V.5.1 Principle of the technique

This mixing time measurement technique requires the monitoring of the evolution of the intensity of light emitted from a fluorescent tracer which is proportional to the concentration of the tracer. The amplitude of the output fluctuations decreases as the fluorescent tracer is distributed in the bulk. A volume of the bulk fluid is illuminated at the primary excitation wavelength of the fluorescent tracer. After the addition of the tracer, the evolution of the intensity of the emitted fluorescent light at another wavelength is recorded.

V.5.2 The fluorescent tracer

A fluorescent dye, Rhodamine B500 (Hays Chemicals Ltd.,London, U.K.), was used as the tracer in this study. It is supplied as a water soluble powder which contains various impurities with about 30 % pure dye. The

concentrations given later in the text on are based on the weight of the impure powder as it is supplied. The primary excitation and emission wavelengths of the dye solution are 548 nm and 580 nm respectively.

The intensity of the fluorescent radiation, which is expressed in arbitrary units of deflection from zero in *Figure V.3*, is linearly proportional to the dye concentration up to a certain value. At higher concentrations, Rhodamine exhibits typical self extinction behaviour. This did not pose any practical problems with water as the bulk was frequently renewed and a reasonable number of experiments could be carried out in glycerol and viscoelastic "Boger" fluids before this maximum concentration was reached.

Figure V.3 Intensity of fluorescence as a function of dye concentration (Rhodamine B500)

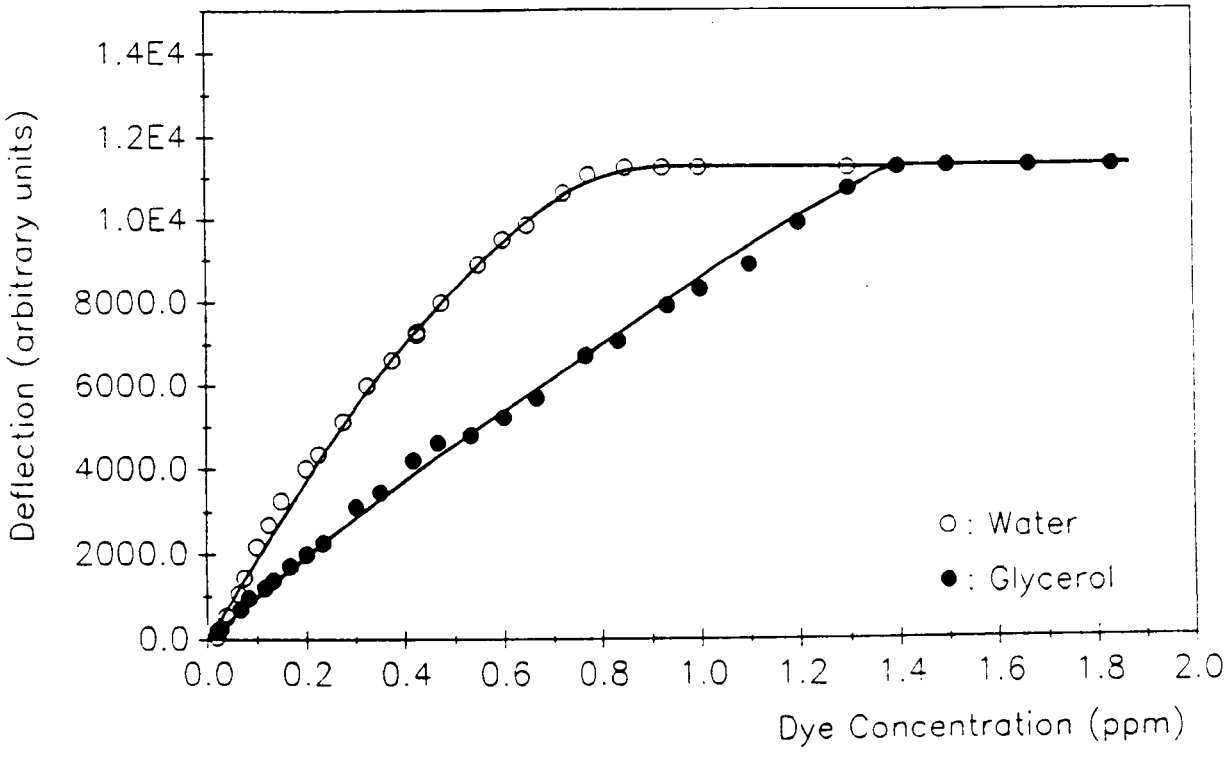

In order to avoid extremely long mixing times due to density and viscosity differences between the tracer and the bulk (see Section V.4.2), dye solutions were prepared in the same liquid as that in the vessel. In all cases, the density difference was less than 0.02 kg m^{-3}. For the same reason, the addition was made in the impeller region (see Section V.5.6). The quantity of dye added for each run was as low as 0.5-1.0 ml and dye concentrations used were 1-6 g/l.

V.5.3 Description of the photodetection system

The optical detection system schematically represented in *Figure V.4,* consists of a light source, a bifurcated fiber optic cable, a set of light filters and a photomultiplier detector.

Light from the source lamp passes through a primary filter. The transmitted light has a peak intensity at the primary excitation wavelength of the fluorescent dye and is conducted to the liquid through a fiber optic cable. A volume of the liquid is illuminated from the tip of this light pipe. Dye, when added to the bulk, absorbs this light to re-emit it at a longer wavelength as fluorescence. The emitted light received by the fiber optic cable is conducted through the other limb of the bifurcation to the photomultiplier tube after passing through a secondary filter which is opaque to primary light. As both excitation and emission wavelengths are in the visible range, experiments were carried out in the dark.

V.5.3.1 Excitation light source

A mercury arc lamp of 200 Watts (Zeiss, Germany) was used as a continuous light source.

Figure V.4 Experimental set-up for mixing time measurements

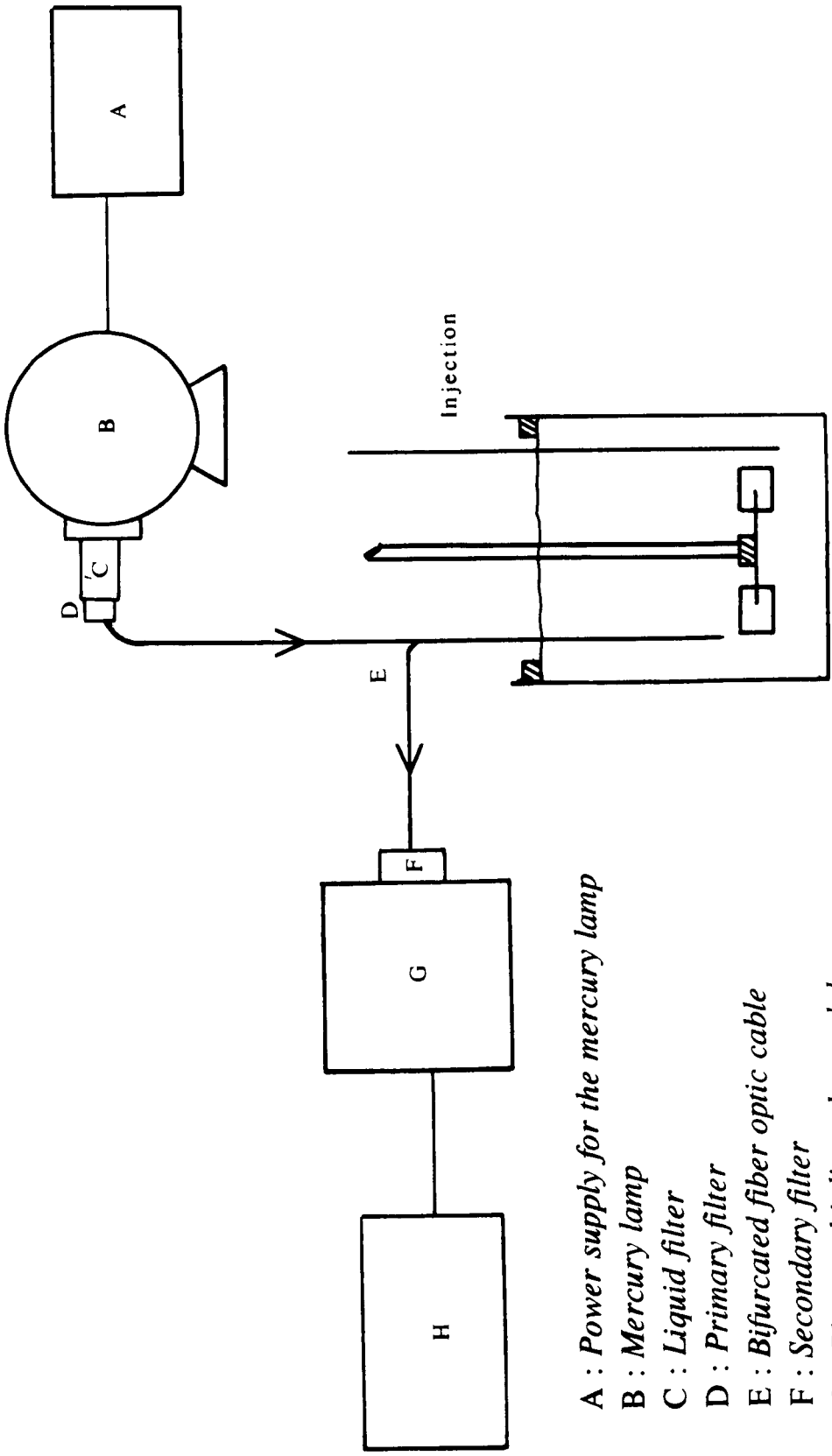

V.5.3.2 Light filters

A primary filter was mounted in front of the mercury lamp and a secondary filter in front of the photomultiplier detector to give peak transmission at the maximum excitation and emission wavelengths of the dye. Primary and secondary filters were carefully chosen so as to maximize sensitivity and minimize background. This is especially important when using Rhodamine, in order to avoid light scattered in the fluid enter the photomultiplier, as the excitation and emission maxima of this dye have only
a difference of 32 nm.

All filters were supplied by Oriel Scientific Ltd., Surrey, U.K. The primary filter was a narrow band mercury line filter (No. 56460) which has a centre wavelength of 547.8 nm with a peak transmittance of 61.6 %. The half peak band width of this filter is 9.7 nm. Maximum temperature of usage is specified as 80°C. Therefore a liquid filter (No. 61940) was mounted between the mercury lamp and the primary filter for protection. The secondary filter (No. 53910) had a centre wavelength of 581.2 nm with a peak transmittance of 65 % and a half peak bandwidth of 10 nm.

Filter holders and other fittings were manufactured in the Workshops of the School of Chemical Engineering, Birmingham University.

V.5.3.3 Fiber optics

The fiber optic cable (Dolan-Jenner Industries/ Oriel Scientific Ltd., Surrey, U.K.) used to transmit light is 1.85 m long and bifurcated at 0.1778 m. The core material of this bifurcated cable (No. EX 872) is flint glass and the cladding is of soda-lime. It has an interlocking stainless steel protective sheathing. The diameter of fiber bundles on the common leg is 3.18 mm and 2.24 mm on the bifurcated legs. The acceptance cone angle is 67° with a numerical aperture of 0.55 (nominal). In the range of wavelengths of

operation, each leg of bifurcation has a transmittance of about 35 %.

One branch of this bifurcation was used as an input to conduct the excitation light from the source lamp into the bulk liquid, and the other branch as an output to carry the fluorescent light to the secondary filter and the photomultiplier module.

V.5.3.4 Photomultiplier detector

A photomultiplier module (Heath photomultiplier module, (Model EU 701-30) converted the light transmitted from the secondary filter into an electrical signal which was amplified and measured.

V.5.4 Response characteristics

The response characteristics of this photodetection system were determined applying a step input change: the fiber optic cable was first immersed in water and a zero reading was adjusted, then plunged into a homogeneous dye solution. The response curve obtained was an exponential one with an initially zero output (c(t)) which finally became unity:

$$c(t) = 1 - e^{-t/t_f}$$

The time constant (t_f, s^{-1}) characterising this exponential response curve, i.e. the time for the response to reach 63.2 % of its total change, was first found to be extremely long: about 20 seconds. Increasing the gain of the electronics associated with the photomultiplier tube module, the time constant could be reduced to about 0.75 seconds. This approximately

corresponded to a frequency (f)

$$f = \frac{1}{2 \pi t_f}$$

of 0.2 Hz above which (or a period of 5 seconds below which) the output signal would be considerably deformed. This is not a negligible restriction, but increasing the gain more, would introduce undesirable noise in the signal, and it is almost impossible to take response characteristics into account when evaluating the mixing time output signal which is monitored on a chart recorder. However, since this probe was mainly installed to be used in viscous fluids where considerably longer mixing times are expected (and measured see Section V.6) along with a decay tail resulting from molecular diffusion.

Suggestions for further modifications that may improve this measurement system are given in Chapter IX.

V.5.5 Determination of the detection volume

The volume of the liquid that the probe can "see", has the shape of the frustrum of a cone. The altitude and base diameter of this frustrum were determined by immersing the fiber optic cable in the centre of a totally blackened beaker containing a given homogeneous dye concentration. Measurements of the output signal were taken varying the height of the probe from the bottom of the beaker *(Figure V.5)*. The altitude of the detection volume was determined as the height above which the probe could no longer see the bottom of the beaker and thus the reading did not change with height. The same experiment was carried out above this height, placing the probe at the wall of the beaker first, then varying the distance from the wall. Thus, the radial dimension of the detection volume was determined.

For a given light source and a light pipe used in this study, dye concentration in the bulk did not greatly affect the detection volume. The altitude of the cone was found to be about 5 cm and the base radius 3 cm both in water and glycerol. This confirmed the numerical aperture value of the fiber optics as stated by the manufacturers.

It is important to know the dimensions of the detection volume to position the probe in the vessel avoiding any wall effects.

Figure V.5 Intensity of fluorescence (Rhodamine B500) as a function of axial distance from wall

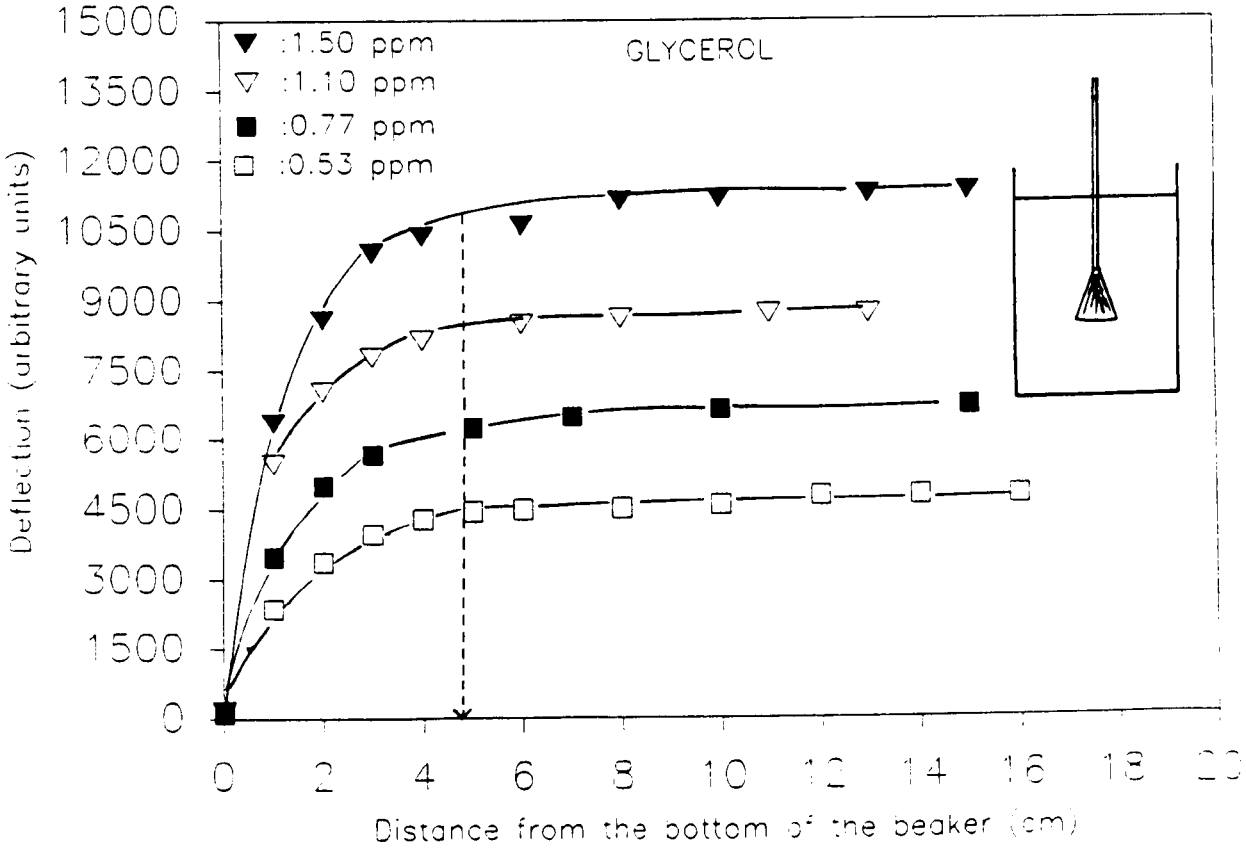

V.5.6 Injection and probe positions in the vessel

A stainless steel needle of 1.4 mm internal diameter supported in another stainless steel tube of larger diameter was used to inject the dye. The dye addition was made slightly below the (lower) impeller, 0.14m above the vessel base, midway between the baffles *(Figure V.6)*.

A practical problem (also reported by Smith and Schoenmakers, 1988) related to the addition of the tracer was encountered: following the injection of a known volume of dye, the remaining dye within the needle leaked from the tip. To prevent this, the dye in the needle was sucked back a short way immediately after the injection.

The probe -optical fiber- was also passed through a stainless steel tube in order to maintain enough rigidity to mount it in the vessel. It was positioned : *i)* avoiding sharp bends, as this would cause a loss of light intensity, and *ii)* wall effects- taking the detection volume into account. The tip of the probe was slightly above the level of the (lower) impeller, 0.255m high from the vessel base and 0.107m away from the vessel wall *(Figure V.6)*.

V.5.7 Results of preliminary tests

Prior to measuring mixing time in the large vessel (T61), some preliminary experiments were carried out in T29 where the detection volume and maximum dye concentration were determined.

Experiments under aerated conditions have shown that the presence of bubbles, which reflected light, caused an apparent fluorescence giving rise to an extremely noisy signal. This was more obvious under complete dispersion conditions. Therefore, in the large vessel mixing time measurements were made only under unaerated conditions.

Figure V.6 Injection and probe positions in the vessel

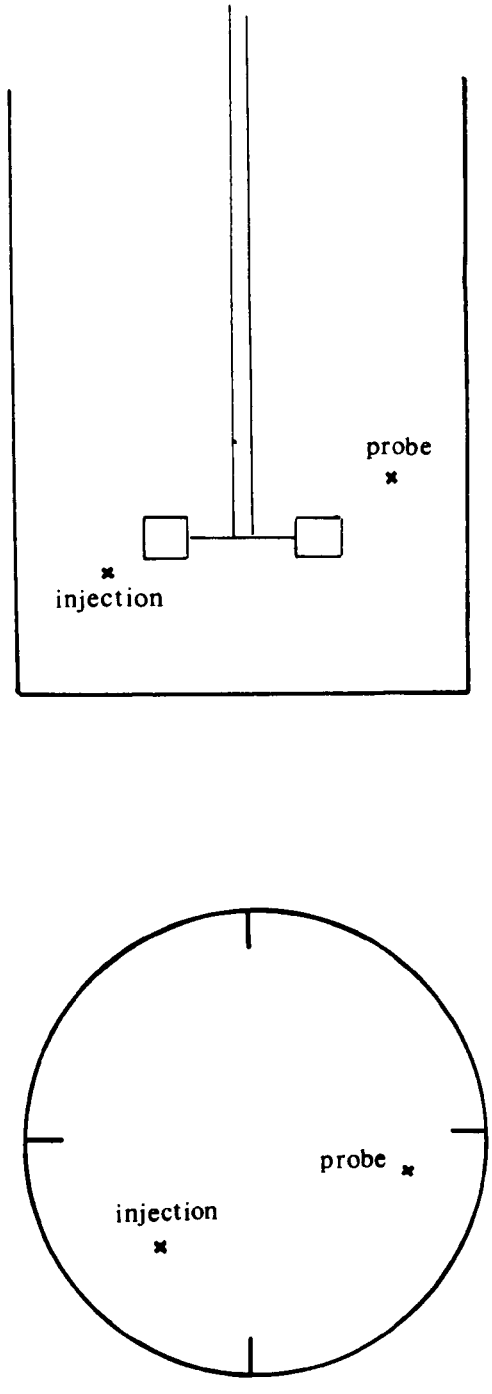

V.6 MIXING TIME STUDIES- RESULTS AND DISCUSSIONS

In this Section mixing time data obtained under unaerated conditions with various fluids and impellers are presented. The photodetection system described in Section V.5 was installed mainly for measuring mixing times in viscous fluids. However, measurements were also made with water in the turbulent flow regime. These are presented in Section V.6.1. Two viscous fluids used were undiluted glycerol (~ 1 Pa s) and a viscoelastic fluid. Results with these fluids can be found in Sections V.6.2 and V.6.3 respectively. The viscoelastic fluid had rheological properties similar to those described in Chapter II, having an almost shear independent viscosity in a range of shear rates:

$$\tau = 0.52\ \dot{\gamma}^{0.99}$$

and exhibiting viscoelasticity:

$$N_1 = 0.034\ \dot{\gamma}^{1.66}$$

The range of Elasticity numbers covered with this fluid was less than 1.5×10^{-3}.

Experiments were carried out in T61 using Rushton turbines and InterMIGs. Details of the geometry of these are given in Chapter III.

The mixedness criterion was taken as 95 % in this study although practical difficulties were encountered to determine the end-point in viscous fluids. Results are presented with an average value for 8 to 10 realisations of the same experiment.

V.6.1. Mixing time studies in water- turbulent flow regime

Figure V.7 shows dimensionless mixing times plotted against the Reynolds number. For an almost constant dimensionless mixing time in the turbulent

Figure V.7 Dimensionless mixing time as function of Reynolds number in the turbulent flow regime

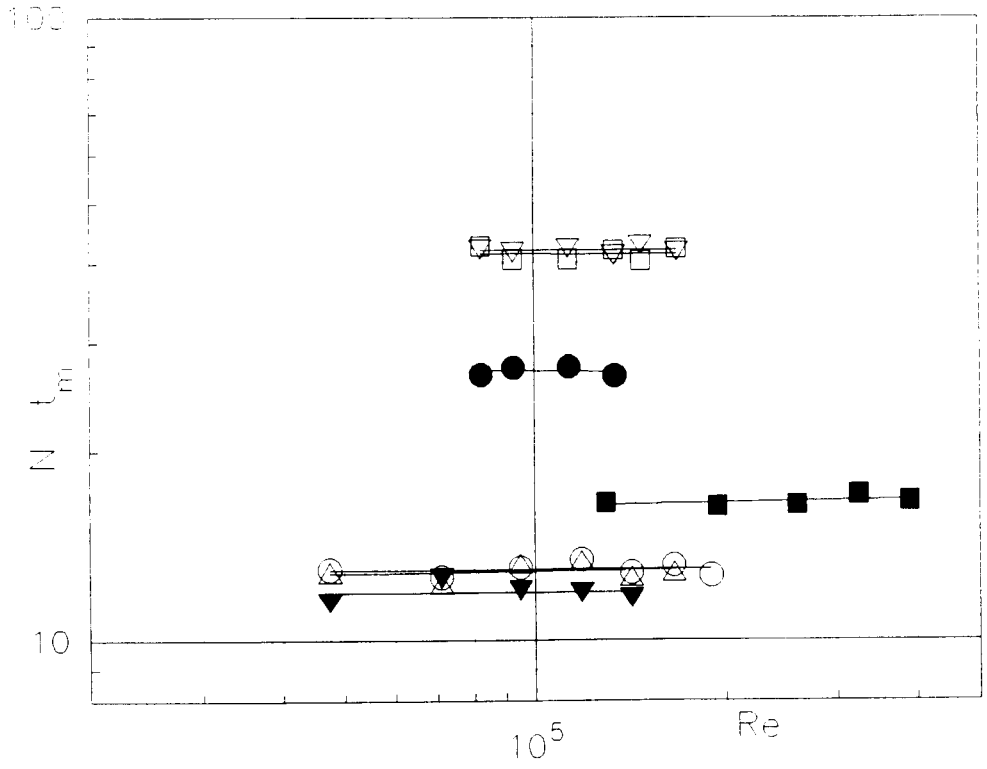

Symbol	Impeller	Geometry		N t_m
▼	Rushton turb.	Dual	D= T/2	11.93
△	Rushton turb.	C= T/3	D= T/2	12.95
○	Rushton turb.	C= T/4	D= T/2	12.97
■	InterMIGs	Dual	D= 0.60T	16.60
●	Rushton turb.	Dual	D= T/3	26.29
▽	Rushton turb.	C= T/3	D= T/3	41.89
□	Rushton turb.	C= T/4	D= T/3	41.17

Figure V.8 Mixing time as a function of impeller speed for different types and geometries of impellers studied in water

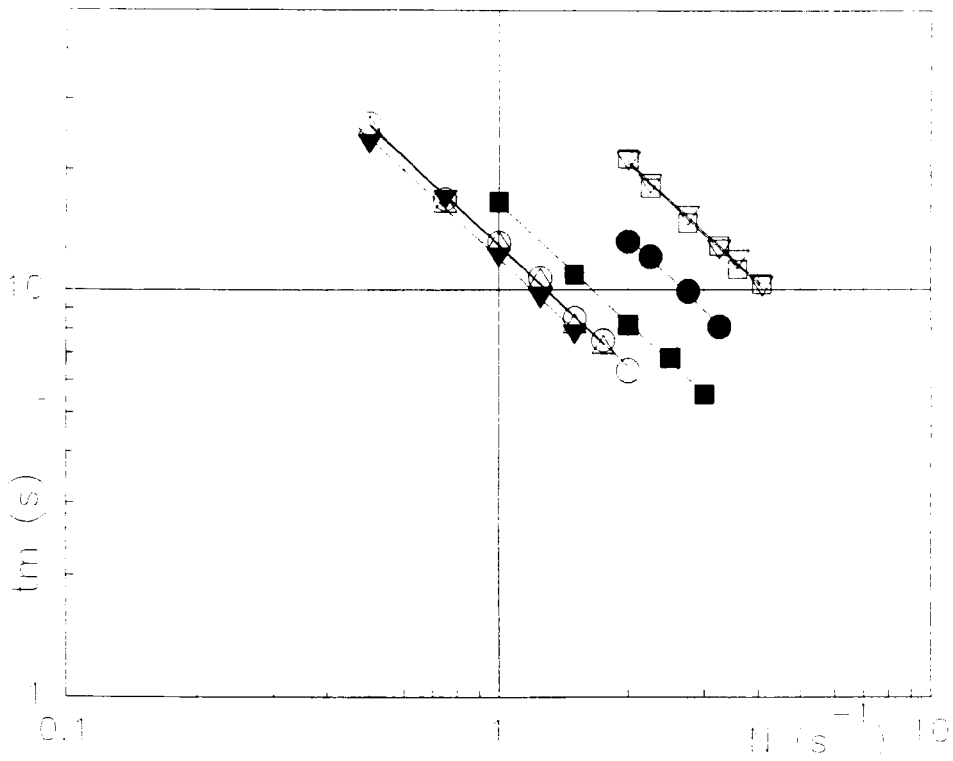

Symbol	Impeller	Geometry		t_m
▼	Rushton turb.	Dual	D= T/2	$t_m = 11.88\ N^{-1.00}$
△	Rushton turb.	C= T/3	D= T/2	$t_m = 12.91\ N^{-1.00}$
○	Rushton turb.	C= T/4	D= T/2	$t_m = 12.93\ N^{-0.99}$
■	InterMIGs	Dual	D= 0.60T	$t_m = 16.41\ N^{-0.99}$
●	Rushton turb.	Dual	D= T/3	$t_m = 26.23\ N^{-1.01}$
▽	Rushton turb.	C= T/3	D= T/3	$t_m = 41.83\ N^{-1.00}$
□	Rushton turb.	C= T/4	D= T/3	$t_m = 41.30\ N^{-1.01}$

Figure V.9 Comparison of mixing times at equal power per unit volume with different impellers and geometries in the turbulent flow regime

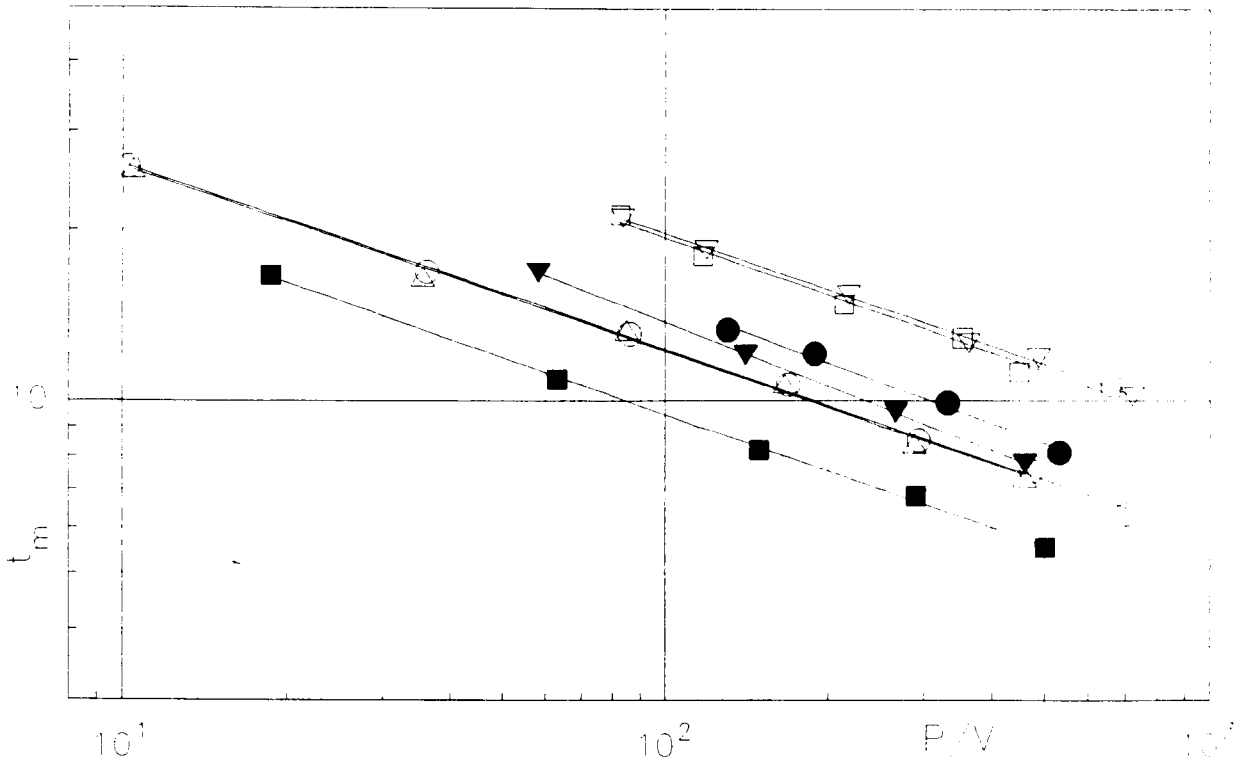

Symbol	Impeller	Geometry		t_m
■	InterMIGs	Dual	D= 0.60T	$t_m = 43.17\ (P/V)^{-0.33}$
△	Rushton turb.	C= T/3	D= T/2	$t_m = 56.34\ (P/V)^{-0.33}$
○	Rushton turb.	C= T/4	D= T/2	$t_m = 55.20\ (P/V)^{-0.33}$
▼	Rushton turb.	Dual	D= T/2	$t_m = 62.15\ (P/V)^{-0.34}$
●	Rushton turb.	Dual	D= T/3	$t_m = 74.24\ (P/V)^{-0.35}$
▽	Rushton turb.	C= T/3	D= T/3	$t_m = 90.36\ (P/V)^{-0.33}$
□	Rushton turb.	C= T/4	D= T/3	$t_m = 99.34\ (P/V)^{-0.35}$

flow regime, mixing time is inversely proportional to the impeller speed:

$$t_m \alpha N^{-1}$$

and this can be seen on *Figure V.8*. As the power number is also constant in the turbulent flow regime, power is proportional to the impeller speed by:

$$P \alpha N^3$$

Mixing time is then related to power or power per unit volume by:

$$t_m \alpha (P/V)^{-1/3}$$

This plot is presented in *Figure V.9* and was used as a basis of comparison to evaluate the performance of different impeller types and geometries. As can be seen on this Figure, InterMIGs were the most energy efficient impellers in reaching a required degree of homogenisation among those tested in this study. Chaotic flow patterns generated by these impellers have already been shown in Chapter III. A comparison of *Figure V.9* with *V.7* and *V.8* shows that the latter can be misleading in assessing impeller performance.

For Rushton turbines, the effects of changing : *i)* impeller diameter, *ii)* impeller clearance from the vessel base and *iii)* the number of impellers were investigated. Large diameter (D=T/2) turbines- either singly or as a pair- appeared to be a better choice in terms of energy expenditure (*Figure V.9*). Impeller clearances studied were those widely used for multi-purpose mixing operations : C= T/3 and T/4. Mixing time results obtained at these clearances with single turbines were found to be almost identical for a given diameter (*Figure V.9*). Two large Rushton turbines appear to be slightly less

Figure V.10 Dimensionless mixing time as a function of Reynolds number with a single Rushton turbine (D= T/2) and InterMIGs in Newtonian fluids

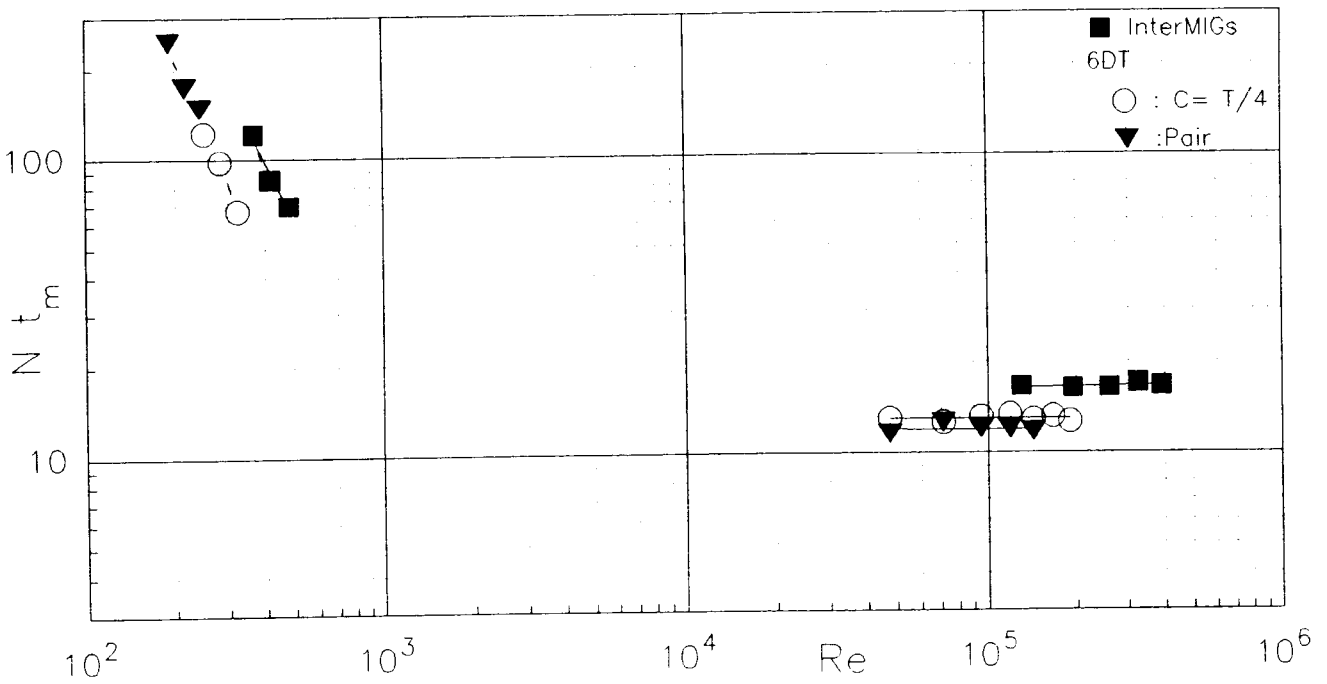

energy efficient than one (*Figure V.9*). A similar finding was also reported by Komori and Murokomi (1988) who found a D=T/2 paddle turbine more energy efficient than a pair especially when H_L= 2T. On the other hand, a single standard Rushton turbine (D= T/3), gave slightly higher mixing times than two at a given power per unit volume.

All impeller types and configurations could be tested in water which was renewed frequently. The number of runs that could be carried out in viscous fluids was limited by the dye concentration at which Rhodamine exhibits self extinction behaviour. Therefore, only the impellers that were found to be the most efficient in water were used in viscous fluids.

V.6.2 Mixing time studies in glycerol- transitional flow regime

Three impellers tested in glycerol were the InterMIGs, a single and a pair of large (D=T/2) Rushton turbines.

A range of Reynolds numbers from 190 to 500 was covered in the transitional flow regime. At these Reynolds numbers, mechanisms associated with mixing are complicated due to the transitional nature of the flow regime. Under fully turbulent conditions, inertially driven forces are sufficient to provide an adequate bulk flow, circulating the fluid from the impeller region throughout the vessel, then back to the impeller again. With a highly viscous fluid - such as 1 Pa s glycerol - where lower Reynolds numbers are attained, the importance of inertia is less hence are the fluid circulations. This could visually be observed in glycerol where the tangential component of flow was more pronounced, as also reported in Chapter III. Another important feature of turbulent mixing is eddy diffusion. This is a very fast process taking place every time the fluid passes through the impeller region of high shear rate where most of the energy introduced by the impeller is dissipated. In highly viscous glycerol, as the inertial forces

Figure V.11 Comparison of the efficiency of impellers in Newtonian glycerol

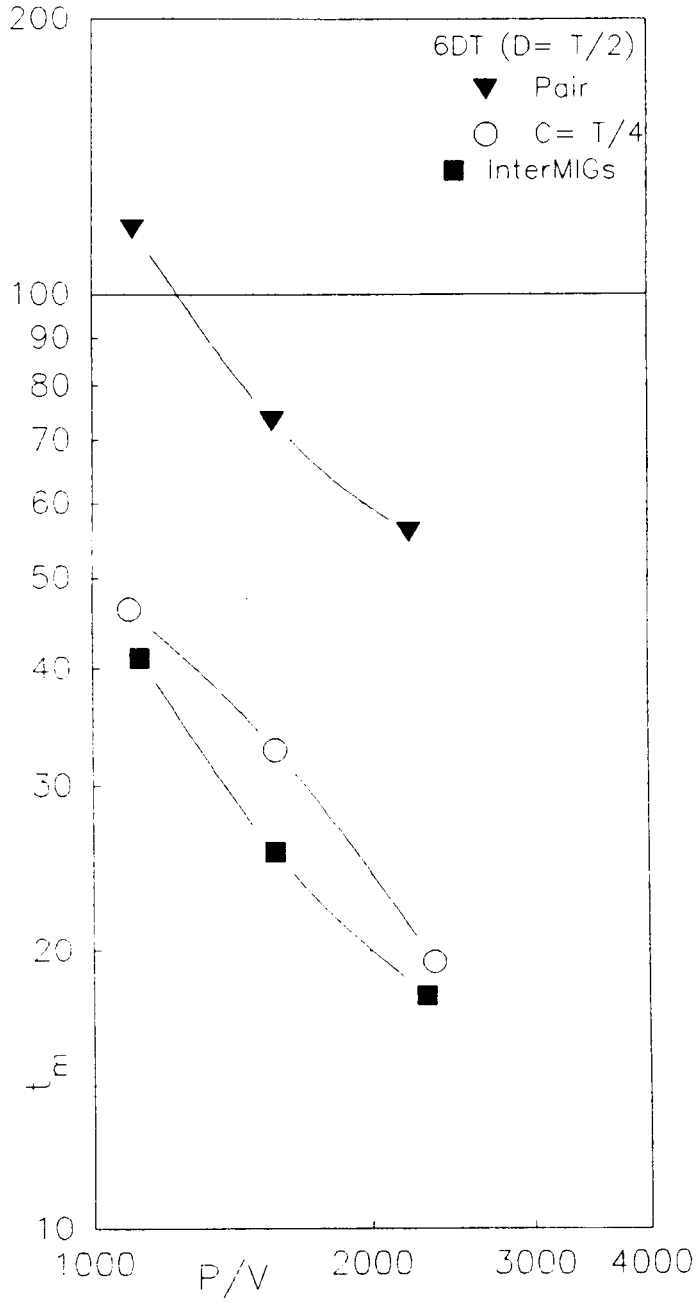

die out more quickly under the effect of viscosity, resulting in a less efficient bulk flow, eddy diffusion is in turn damped. The whole process becomes slower and slower, including molecular diffusion which gives long tails in the mixing time response curve. Hence, mixing times increase with decreasing Reynolds number. This can be seen in *Figure V.10* where constant dimensionless mixing times obtained in water are also plotted.

Figure V.11 compares mixing times obtained in viscous Newtonian glycerol at equal volumetric power input. The plot of mixing time as a function of power per unit volume provides straightforward information for the comparison of impeller efficiencies. However, it has to be used with caution. For different scales of operation, if the properties of the fluids (viscosity and density) also change, the ranges of Reynolds numbers - even the flow regime - covered may be entirely different. In these cases, a comparison on the basis of specific power input would not be meaningful, it may even lead to serious errors. In this study, the ranges of Reynolds numbers covered with different impellers were only slightly different, while the specific power input was held constant for the three impellers tested (*Figure V.10*). Hence, a general assessment of the efficiency of InterMIGs and Rushton turbines in glycerol could be made. The trend was similar to that found in water. In decreasing order of efficiency, they were ranked in the same way : *i)* a pair of InterMIGs, *ii)* one large (D=T/2) Rushton turbine and *iii)* a pair of large Rushton turbines.

V.6.3 Effect of viscoelasticity on mixing time

Mixing time measurements in the viscoelastic fluid were made using a pair of InterMIGs and a single large (D=T/2) Rushton turbine.

Mixing times in viscoelastic fluids were in general higher than those obtained in glycerol conforming with findings of previous

Figure V.12 Comparison of the efficiency of InterMIGs in Newtonian viscoelastic fluids in the transitional flow regime

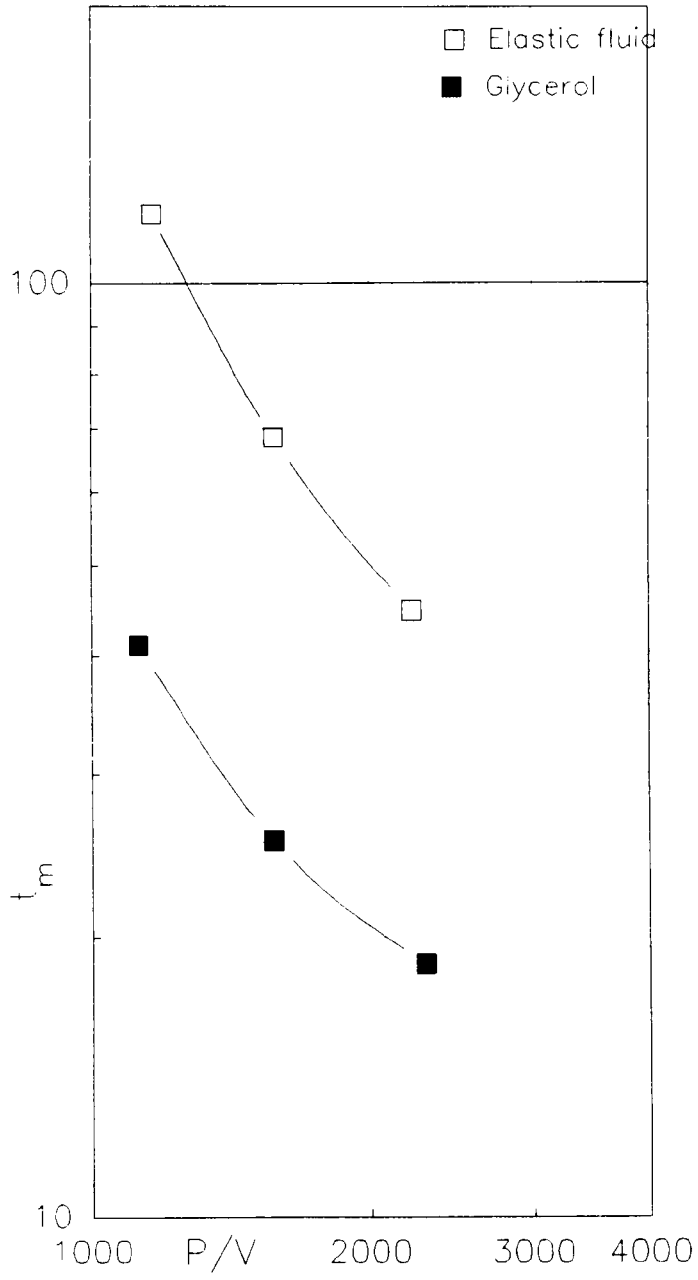

Figure V.13 Dimensionless mixing time as a function of Reynolds number for InterMIGs

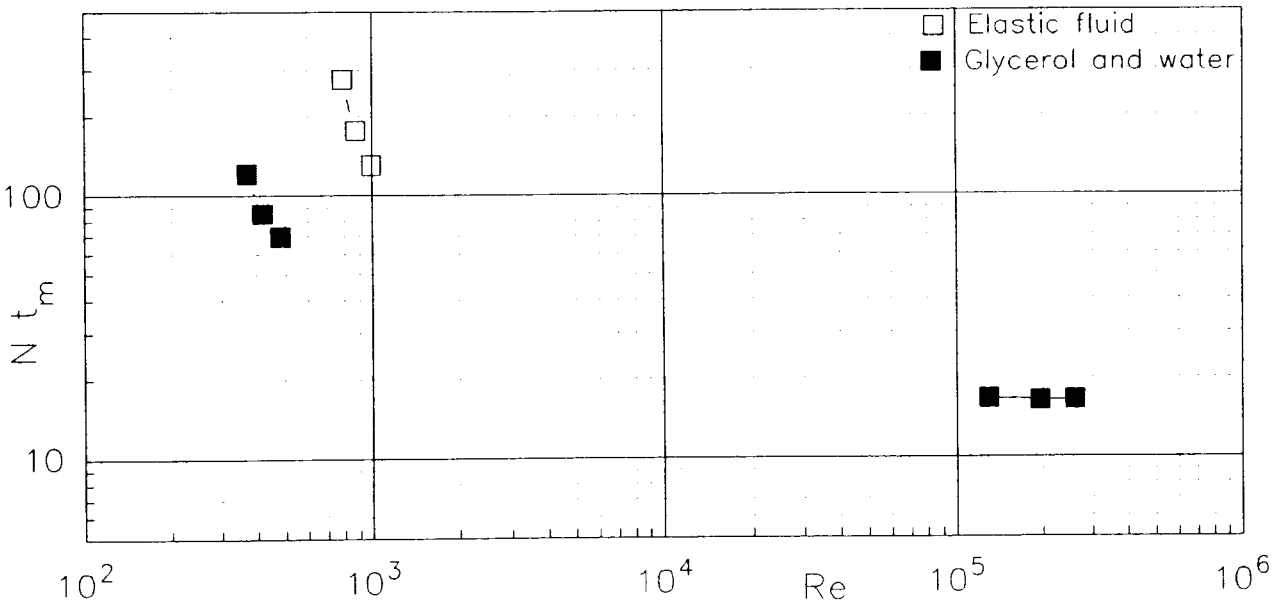

Figure V.14 Comparison of the efficiency of a pair of InterMIGs and a single Rushton turbine (D= T/2; C= T/4) in the viscoelastic fluid

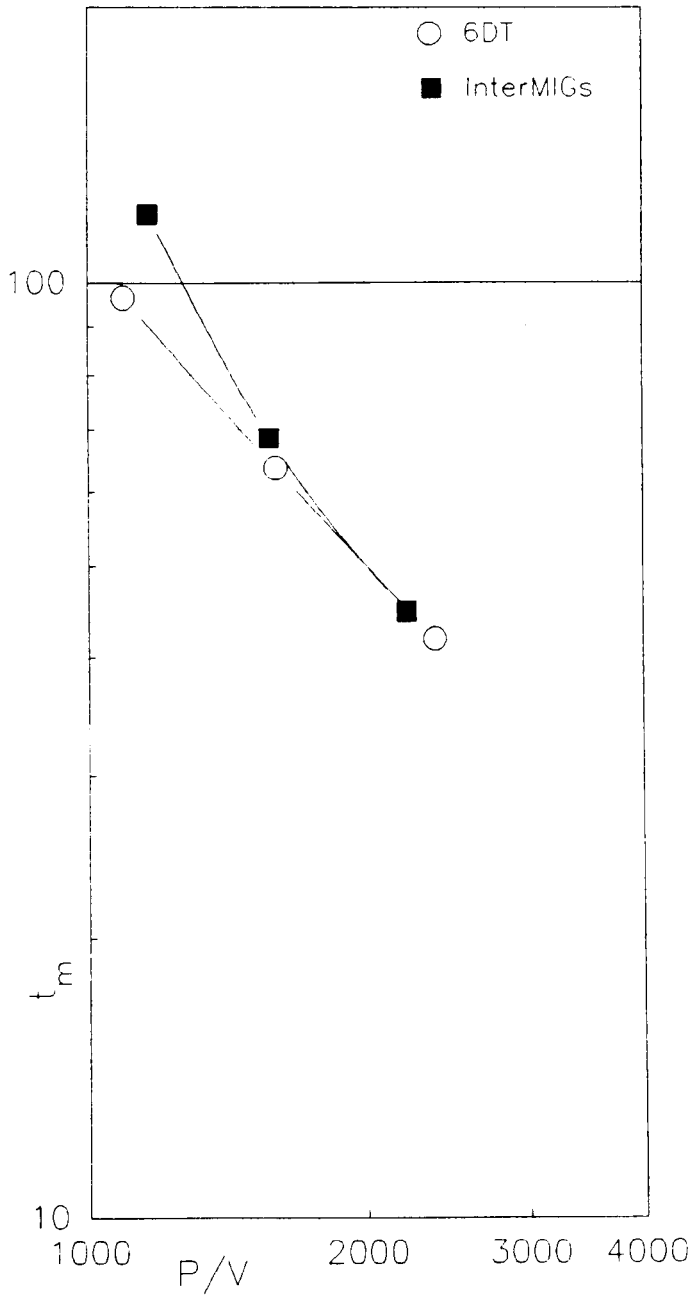

researchers[26,21,37,28,92]. Mixing time is closely related to the flow patterns generated in a stirred vessel. It would therefore be relevant to discuss mixing time data in relation to the flow patterns observed. The interaction of the elastically driven forces with the centrifugally driven forces was detailed in Chapter IV. Although the overall features of the flow patterns observed in viscoelastic fluids were similar to those generated in Newtonian glycerol, the radial discharge from Rushton turbines and from the outer blades of InterMIGs were constricted under the opposing action of viscoelastically driven forces. This resulted in longer mixing times. *Figure V.12* illustrates this for InterMIGs where data for both fluids are plotted. A quantitative evaluation to express this enhancement in terms of percentages has not been made as the Reynolds numbers covered with the two fluids do not coincide precisely (*Figure V.13*).

Figure V.14 compares mixing times obtained with a pair of InterMIGs and a single large (D= T/2) Rushton turbine at equal power per unit volume. Different from our findings in Newtonian fluids- of both low and high viscosity- where InterMIGs proved to be more energy efficient, in the viscoelastic fluid their performance was reduced. The complicated interaction of elastically driven forces with the counter-flows generated from the blades of InterMIGs was already discussed in Chapter IV. On the other hand, the study of viscoelastic effects on power consumption also showed that InterMIGs underwent viscoelastic effects more severely than Rushton turbines. It would therefore be expected that the enhancement of mixing time on account of fluid viscoelasticity would be the highest with these impellers.

V.7 CONCLUSIONS

The optical detection system installed for measuring mixing time with the fluorescent dye-fiber optic technique has been successfully used to perform a number of runs in highly viscous fluids without altering the physical properties of the bulk. Certain modifications can still be considered for further improvements of this system in future work. For some of the impeller geometries and fluids studied in common, results obtained with this technique were in line with those of previous researchers[1,78] who used the colourisation-decolourisation technique that provides a global evaluation of the mixing time.

In Newtonian fluids- both in the transitional and turbulent flow regimes InterMIGs were found to be more energy efficient than Rushton turbines. These impellers required shorter mixing times at a specific power input on account of the counter flows from their inner and outer blades generating chaotic patterns. Large diameter Rushton turbines (D=T/2) appeared to be the second best choice.

In viscoelastic fluids, the efficiency of the impellers tested were in general found to be reduced giving higher mixing times than those obtained in glycerol. The radial discharge from both the Rushton turbines and the outer blades of InterMIGs was restricted under the effect of viscoelastically driven forces. This effect was more pronounced with InterMIGs where upward flows from the inner blades superposed with the viscoelastically driven flows and intensified the effect of this fluid property. Thus, the efficiency of InterMIGs in viscoelastic fluids was found to be comparable to that of a single Rushton turbine. Future work to extend this study to a range of impeller types would be of interest.

CHAPTER VI TWO PHASE STUDIES IN THE TURBULENT FLOW REGIME: AIR-WATER

VI.1 INTRODUCTION

Various applications in chemical and para chemical industries (aerobic fermentations, waste water treatment, oxygenation and hydrogenation processes, etc) require the contact of a gaseous phase in a liquid - an operation most commonly carried out in a stirred vessel. Two phase mixing has therefore been subject to a number of studies where fluids of simple rheology- water or dilute sugar solutions were used. The impeller of interest was generally a six bladed disc turbine - known to be a good gas disperser in low viscosity fluids. Therefore, considerable information exists on the aerated mixing of low viscosity Newtonian fluids with a Rushton turbine. In this study, a limited number of experiments were carried out in water where multiple Rushton turbines and InterMIGs were also investigated prior to studies in viscous and viscoelastic fluids.

Following Chapters III to V on various aspects mixing under unaerated conditions, this Chapter is concerned with aerated mixing in the turbulent flow regime. In Section VI.2, relevant definitions and findings from previous work are briefly presented*. These provide the background information for the following sections of this Chapter as well as for Chapters VII and VIII where results obtained in the transitional regime with aerated viscous Newtonian and viscoelastic fluids are presented. Most of the equipment used for mixing experiments was described in Chapter III, details of others used during aerated experiments are given in Section VI.3. Section VI.4 contains observations of bulk flow patterns and cavities, and results on power characteristics in water with six bladed disc turbines and InterMIGs. Conclusions are given in Section VI.5.

---

* More detailed information can be found in the early publications of Nienow and his coll.[24,67,68,75,79] and Smith and his coll[16,108,122,123,124,75].

VI.2 DEFINITIONS, DATA PRESENTATION AND PREVIOUS WORK

Two operational conditions can be varied during aerated experiments: the impeller speed and gas flow rate (Q_G, $m^3\ s^{-1}$).* The hydrodynamic state of the impeller and consequently the power consumed depend on the relative value of these parameters. In this Section, the hydrodynamic states of an impeller under aerated conditions, different types of cavities formed behind impeller blades and certain relevant dimensionless numbers are briefly described- mostly in reference to six bladed disc turbines.

VI.2.1 Two phase hydrodynamics

Primary and secondary fluid movement described in Chapter III for single phase systems also occur in multi phase flow. The hydrodynamics of aerated turbines is however, more complicated as the gas flow rate affects the action of the stirrer on the fluid motion and at very high flow rates gas flow determines the overall features of the flow patterns. *Figure VI.1* schematically represents three distinctive hydrodynamic states observed around a six bladed disc turbine under aeration:

a) *Flooding*: The impeller is said to be flooded when the gas provided from the sparger rises to the liquid surface without being effectively dispersed and distributed by the impeller (*Figure VI.1.a*). This is clearly an undesirable situation.

b) *Loading*: The transition from flooding to loading takes place when the gas flow rate is decreased and/ or the impeller speed is increased. The impeller then starts to discharge the gas radially outwards which thereafter rises to the liquid surface (*Figure VI.1.b*). There is very little, if any gas

---

* Gas flow rate is also expressed in terms of the volume of gas per minute per liquid volume (Q_{GV}, vvm)

Figure VI.1 Flow patterns with Rushton turbines under aeration

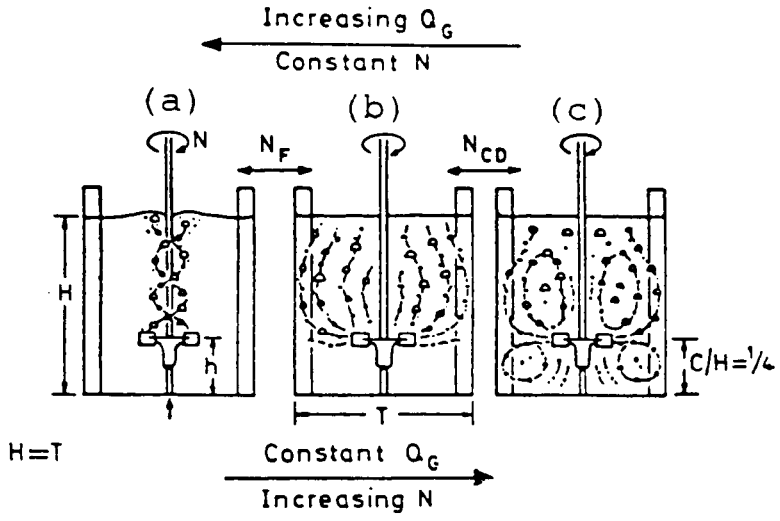

Figure VI.2 Gas filled cavity types (six bladed disc turbines/ air-water)

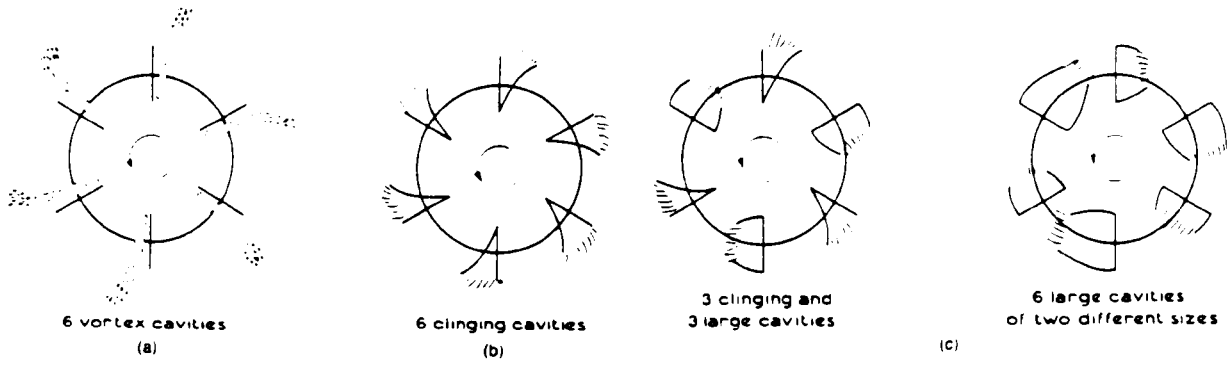

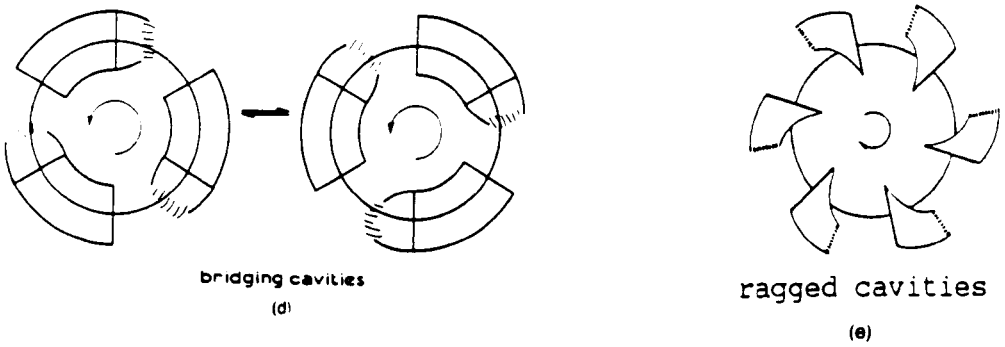

distributed in the region below the plane of the impeller.

c) *Complete dispersion*: Increasing further the impeller speed and/ or decreasing the gas flow rate, two circulation loops are formed above and below the impeller and bubbles broken up by the impeller are distributed throughout the vessel (*Figure VI.1.c*). This condition is referred to as "complete dispersion". At speeds above which complete dispersion (N_{CD}) is achieved, a recirculation loop is also formed.

Apart from the impeller speed and gas flow rate, geometric factors were also found to be important for the flooding-loading or complete dispersion transitions. High clearances from the vessel base require higher speeds, thus higher power consumption, to reach complete dispersion conditions and therefore may not be preferable. At very low impeller clearances, bubbles in the region above the impeller rise to the liquid surface as in a bubble column without being circulated. A clearance of C= T/4 was found to be optimum[67]. Other geometric parameters such as the impeller diameter (D/T) and disc and blade thicknesses (x_1/T and x_2/T) were in general included in the correlations proposed for the flooding-loading or complete dispersion transitions[67,75,17].

VI.2.2 Cavities

Tertiary flows around the blades of a six bladed disc turbine were described in Chapter III (Section III.2.3) for single phase systems. Under aeration, gas is captured in the zones of reduced pressure behind the blades. Gas pockets - *cavities*- are then formed resulting in a reduction in drag, hence the power consumption.

The size and shape of cavities formed depend on both the gas flow rate and the impeller speed. Three major types of cavities defined for Rushton

turbines in low viscosity fluids are presented in *Figure VI.2*[16,66] :

a) *vortex cavities* are formed at low flow rates where the gas is captured in the trailing vortices behind the blades (*Figure VI.2.a*). These reduce the power consumption very slightly.

b) *Clinging cavities*: The passage from vortex to clinging cavities occurs with the increase of gas flow rate at a given impeller speed (*Figure VI.2.a*). The power consumed is reduced as more gas is captured behind the blade and also due to a hydrodynamic smoothing of the blade. Bubble generation and dispersion takes place from the tip of clinging and vortex cavities.

c) *Large cavities:* At higher gas flow rates where large cavities are formed, the streamlining effect that decreases the stirrer friction is even more important. These cavities reduce the radial discharge from the impeller; gas bubbles are released from behind the blade. These large cavities generally form a *3-3 structure*[122] (*Figure VI.2.c*).

After flooding, *ragged cavities*[75] (*Figure VI.2.d*) and at very high gas flow rates cavities bridging two successive blades, *bridging cavities* (*Figure VI.2.e*) can be observed. Different cavity types are associated with different hydrodynamic states of the impeller.

VI.2.3 Dimensionless numbers and data presentation

Power number under aerated conditions (Po_g) is calculated using the aerated power consumption (P_g, W):

$$Po_g = \frac{P_g}{\rho N^3 D^5} \qquad (VI.1)$$

Figure VI.3 Characteristic power curves for Rushton turbines under aerated conditions

a) Power curves at constant impeller speed

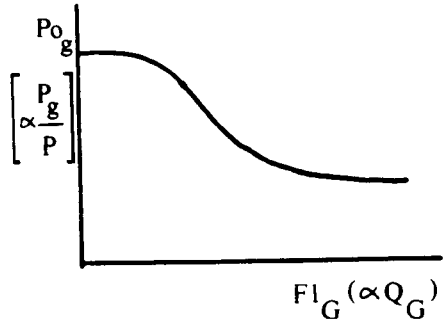

b) Power curves at constant gas flow rate

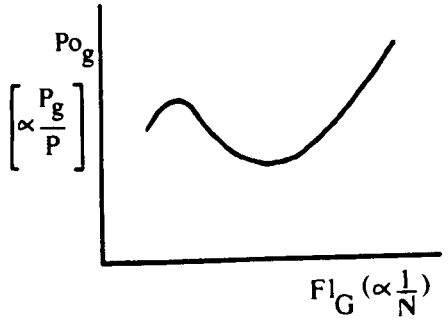

Another important dimensionless number is the *Gas Flow number* (or the *Aeration number*) (Fl_G):

$$Fl_G = \frac{Q_G}{N D^3} \qquad (VI.2)$$

which compares the volumetric gas flow rate to the volumetric discharge of the impeller.

Most correlations for the transitions of hydrodynamic states relate the Flow number to the Froude number in attempt to relate the axial flow induced by gassing to the radial flow due to the pumping action of the impeller. The correlations proposed by Nienow et al (1985) for Rushton turbines take into account scale effects for the flooding-loading:

$$(Fl_G)_F = 30\ (D/T)^{3.5}\ Fr_F \qquad (VI.3)$$

and complete dispersion transitions:

$$(Fl_G)_{CD} = 0.2\ (D/T)^{0.5}\ (Fr_F)^{0.5} \qquad (VI.4)$$

Conventionally characteristic power curves for aerated conditions are plotted with the relative power consumption [(P_g/P) or (Po_g/Po)] as a function of the Gas Flow number. *Figures VI.3.a* and *VI.3.b* show power curves obtained at constant impeller speed and constant gas flow rate respectively. Power numbers are also plotted as a function of the Gas Flow number as this shows the flooding- loading and complete dispersion transitions more obviously[67]. The latter is generally preferred in this study. Aerated and unaerated power numbers are also plotted as a function of the Reynolds number.

V.2.4 InterMIGs

InterMIGs have been subject to a number of studies where xanthan fermentations were successfully carried out[41,133,134]. Apart from the studies in fermentation broths, mixing studies on the characterisation of these impellers with model fluids were reported for viscous Newtonian and non-Newtonian fluids[1,47,48,56,125]. Results obtained in this study with viscous fluids are reported and compared with previous work in Chapters VII and VIII.

VI.3 EXPERIMENTAL EQUIPMENT

Equipment used for mixing studies was described in Chapter III. Here, only those specifically used during aerated experiments are given.

VI.3.1 Air supply

Air was provided through a point sparger positioned centrally below the impeller. The geometry of spargers is given in *Figure VI.4.* A humidification column was included in the aeration line to saturate the air before being sparged in the liquid. This humidification tank was bypassed during experiments with glycerol and glycerol based viscoelastic fluids as glycerol absorbs moisture very easily.

The air flow rate was adjusted using a set of rotameters calibrated with a gas meter. A flow rate range of 3.3×10^{-4} to 6.42×10^{-3} m^3s^{-1} (0.11- 2.16 vvm) in T61 and 8.3×10^{-5} to 1.1×10^{-3} m^3s^{-1} (0.26- 3.39 vvm) in T29 was covered, which roughly corresponds to the range covered in aerobic fermentations.

VI.3.2 Studies of two phase hydrodynamics

Under aerated conditions, the hydrodynamic state of the impeller (flooding-loading or complete dispersion transitions) was determined by visually observing the two phase flow patterns. Either the impeller speed or the gas flow rate was changed.

VI.3.3 Equipment used for the observation of cavities

Cavities formed behind the blades of the impeller in the presence of gas were observed from the bottom of the vessel through a pair of Dove prisms. Rotating the prisms at half the impeller speed froze the image of the impeller and the cavities. A 45° inclined mirror reflected the image of these.

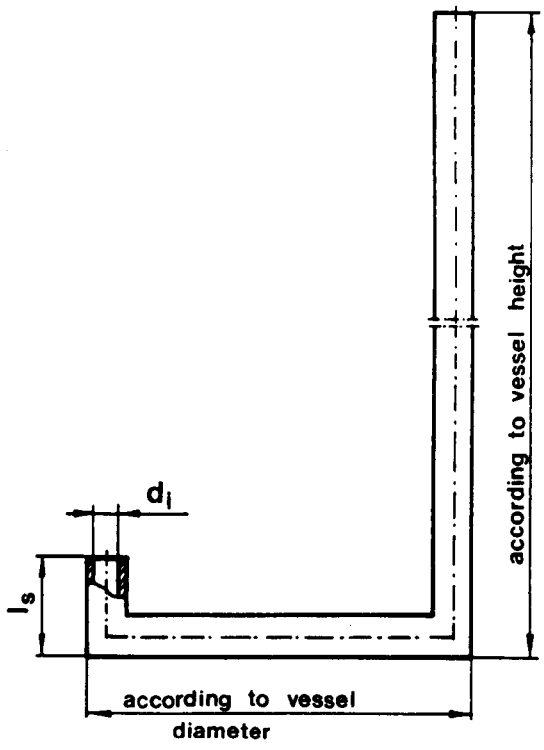

Figure VI.4 Geometry of spargers

T61: $d_i = 0.010$ m

$l_s = 0.076$ m

T29: $d_i = 0.004$ m

$l_s = 0.076$ m

Details of this experimental arrangement are given by Kuboi et al, 1983.

During these observations, the impeller region was illuminated with collimated beams from the opposite sides of the vessel at a plane horizontal to the impeller. Apart from visual observations through the "de-rotational prism", photographs using a Nikon FM camera were taken and some video recordings were also made.

VI.4 RESULTS AND DISCUSSIONS

Aerated experiments with water were confined to the turbulent flow regime: $4x10^4 < Re < 1x10^6$. In this Section experimental observations and results are presented with more emphasis on InterMIGs.

VI.4.1 Two phase fluid hydrodynamics with InterMIGs: air-water

VI.4.1.1 Flow pattern observations under aeration

Flow pattern observations around InterMIGs under unaerated conditions were reported in Chapter III (Section III.4.1.2). They tend to discharge the gas-liquid mixture in a similar way under aerated conditions: the inner blades pump upwards, the outer blades downwards in the forward direction and vis-versa in the reverse direction. The flooding- loading and complete dispersion transitions were not previously described for these impellers. This is partly because the definitions for conventional impellers do not hold for InterMIGs that induce counter-flows in the turbulent flow regime and partly because a limited number of studies were carried out with these impellers. In the following paragraph, two phase flow pattern observations with InterMIGs are reported at a given gas flow rate ($3 x10^{-3}$ m^3s^{-1} or 1 vvm) for increasing impeller speed. These are presented in *Figure VI.5*. Video recordings were also made in a range of operational conditions and a tape is available in The School of Chemical Engineering- University of Birmingham.

When gas was provided at a given flow rate into the bulk- without the impeller rotating- bubbles rose to the surface where some of them were broken up and circulated back in the liquid near the surface. Similarly, at very low impeller speeds ($N \cong 1.00- 1.25$ s^{-1}), some bubble motion could be observed only above the upper impeller (*Figure VI.5.a*) - a situation analogous to flooding conditions. As the speed was increased ($N \cong 1.50 - 1.95$ s^{-1}), gas from the sparger was drawn into the impeller region. Bubbles

started to extend along the main blades forming a cloud around the impeller (*Figure VI.5.b*). Under these conditions, the impeller was still not capable of dispersing gas effectively. When the speed was increased more ($N \cong 2.17$ s^{-1}), the downward pumping action of the outer blades could clearly be observed. Flows due to the upward pumping of the inner blades also became obvious although these were in general more gentle and difficult to observe. The impeller then started to discharge the gas efficiently and the transition from flooding to loading took place (*Figure VI.5.c*). The prominent feature of the flow patterns was the downward flows therefore bubbles were mostly concentrated in the regions below the impellers. Although there were still zones with no or very little gas dispersion between the upper and lower impellers, a compartmentalisation was not observed. Bubbles associated with the flows from the outer blades of the lower impeller occasionally integrated with the flows from the inner blades or those from the upper impeller and vice-versa. This interaction ensured a good exchange between the zones around the upper and lower impellers.

During studies on single phase flow, it was observed that the circulation loop associated with the outer blades of the upper impeller was bigger (Section II.4.1.2). Similarly, under aerated conditions at speeds above the flooding-loading transition, the volume of the liquid around the upper impeller in which intense bubble circulation took place was larger. This covered almost half the vessel height and touched the walls when the circulation loop from the lower impeller did not reach the vessel base or walls. As the speed was increased more, the fluid, pumped downwards by the upper impeller, hit the vessel wall and the flow split into two. Most of the gas rose along the vessel wall and was circulated back to the tip of the outer blades. Some moved short a way downwards to be circulated towards the bottom of the upper impeller. The outer blades of the lower impeller

Figure VI.5 Flow patterns with InterMIGs under aerated conditions (1 vvm)

a) N≅ 1.00- 1.25 s^{-1}

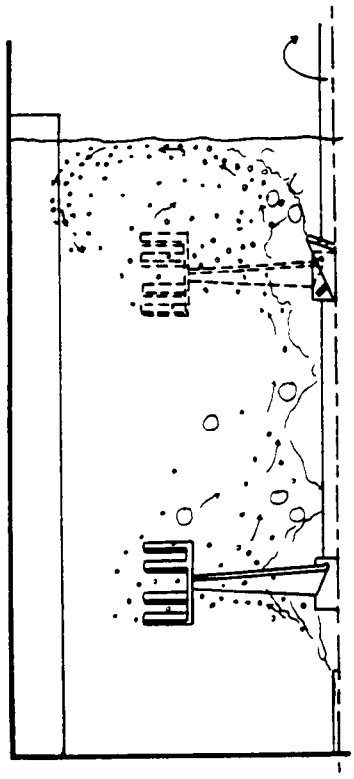

b) N≅ 1.50- 1.95 s^{-1}

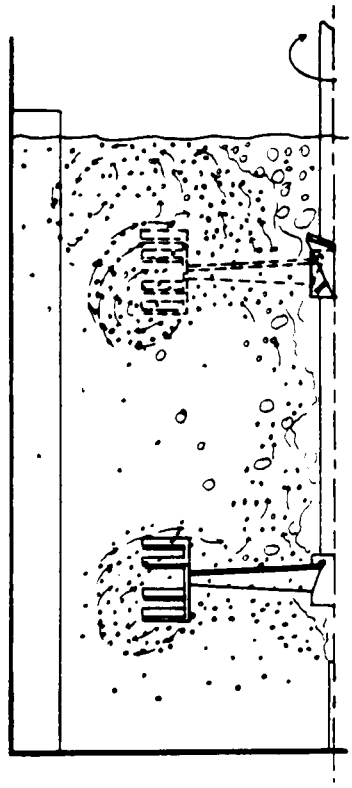

c) N≅ 2.17 s^{-1}

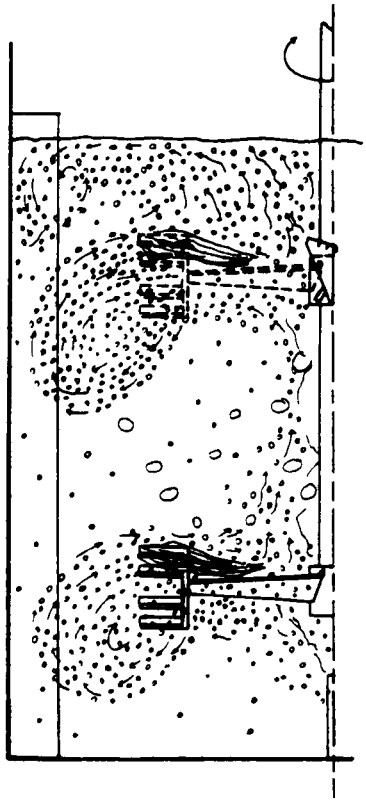

d) N= 4.16 s^{-1}

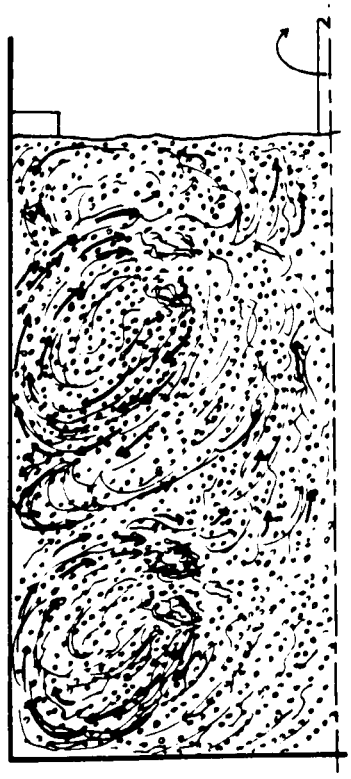

meanwhile always pumped downwards. A further increase of the impeller speed (N= 4.16 s^{-1}) led to complete dispersion (*Figure VI.5.d*). At such high speeds the visibility within the vessel was considerably reduced due to important circulation of small bubbles.

When rotated in the reverse direction, the pumping modes of the inner and outer blades were reversed. The dominant features of the fluid flows were still determined by the outer blades that pumped upwards. Therefore, even at very high speeds and/ or low gas flow rates, gas distribution below the lower impeller, hence, complete dispersion conditions could not be achieved.

VI.4.1.2 Complete dispersion transition

The passage between different hydrodynamic states was very gradual with InterMIGs; especially the flooding- loading transition was not as distinctive as with the six bladed disc turbines. This was therefore, difficult to determine and of less significance. The impeller speed and volumetric power input $(P_g/V)_{CD}$ to completely disperse gas were determined at a given gas flow rate. These are listed in *Table VI.1* which also contains the corresponding dimensionless numbers ($(Fl_G)_{CD}$ and Fr_{CD}) at the complete dispersion transition for different gas inflow rates. For comparison purposes, values for a six bladed disc turbine are also given.

Table VI.1 Operational conditions for the complete dispersion transition in water

$(Q_{GV})_{CD}$ (vvm)	N_{CD} (s^{-1})	$(Fl_G)_{CD}$ x 100	Fr_{CD}	$(P_g / V)_{CD}$ (kW m^{-3})
A pair of InterMIGs				
0.506	3.50	0.919	0.45	0.573
0.618	3.67	1.072	0.493	0.591
0.674	3.75	1.143	0.516	0.612
0.758	3.83	1.258	0.539	0.646
1.011	4.17	1.543	0.637	0.787
Six bladed disc turbine (D= T/2; C= T/4)				
0.506	1.42	3.624	0.063	0.195
0.618	1.58	3.963	0.079	0.252
0.674	1.67	4.107	0.087	0.280
1.011	2.03	5.050	0.130	0.437
1.348	2.33	5.867	0.171	0.573
1.573	2.53	6.305	0.202	0.679

In *Figure VI.6*, the variation of $(Fl_G)_{CD}$ with Fr_{CD} is presented and the corresponding correlations obtained for the scale and range of operation are :

$$(Fl_G)_{CD} = 0.031\ (Fr_{CD})^{1.490} \qquad r^2 = 0.992 \qquad (VI.5)$$

for a pair of InterMIGs and

$$(Fl_G)_{CD} = 0.133\ (Fr_{CD})^{0.490} \qquad r^2 = 0.997 \qquad (VI.6)$$

for a six bladed disc turbine. The latter is in fact a confirmation of correlation (VI.4) for the impeller diameter used in this study: for a D= T/2, correlations (VI.4) and (VI.5) are almost identical. A comparison of correlations (VI.5) and (VI.6) (and the plots in *Figure VI.6*) indicates that the dependence of the Flow number on the Froude number at the complete dispersion transition is stronger with InterMIGs than with Rushton turbines.

The above correlation can be used as a basic guideline to predict the operational conditions for the complete dispersion transition with InterMIGs in low viscosity Newtonian fluids. It is also important to be able to predict the power required for this transition which is generally correlated to the specific gas velocity based on the liquid volume (Q_{GV}, vvm). *Figure VI.7* shows the specific power input required to completely disperse gas in water for different gas flow rates. The correlations obtained for this transition are:

$$(P_g / V)_{CD} = 0.757\ (Q_{GV})_{CD}^{0.469} \qquad r^2 = 0.924 \qquad (VI.7)$$

for a pair of InterMIGs and

$$(P_g / V)_{CD} = 0.421\ (Q_{GV})_{CD}^{1.081} \qquad r^2 = 0.998 \qquad (VI.8)$$

for a six bladed disc turbine.

Figure VI.6 Complete dispersion transitions in water

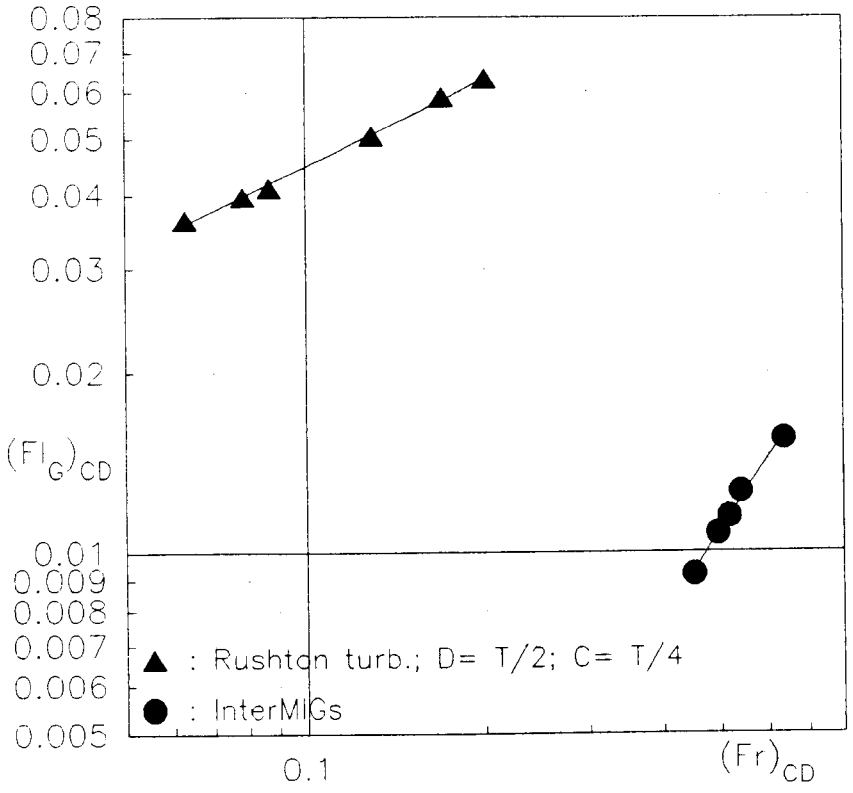

Figure VI.7 Specific power input at the complete dispersion transition in water

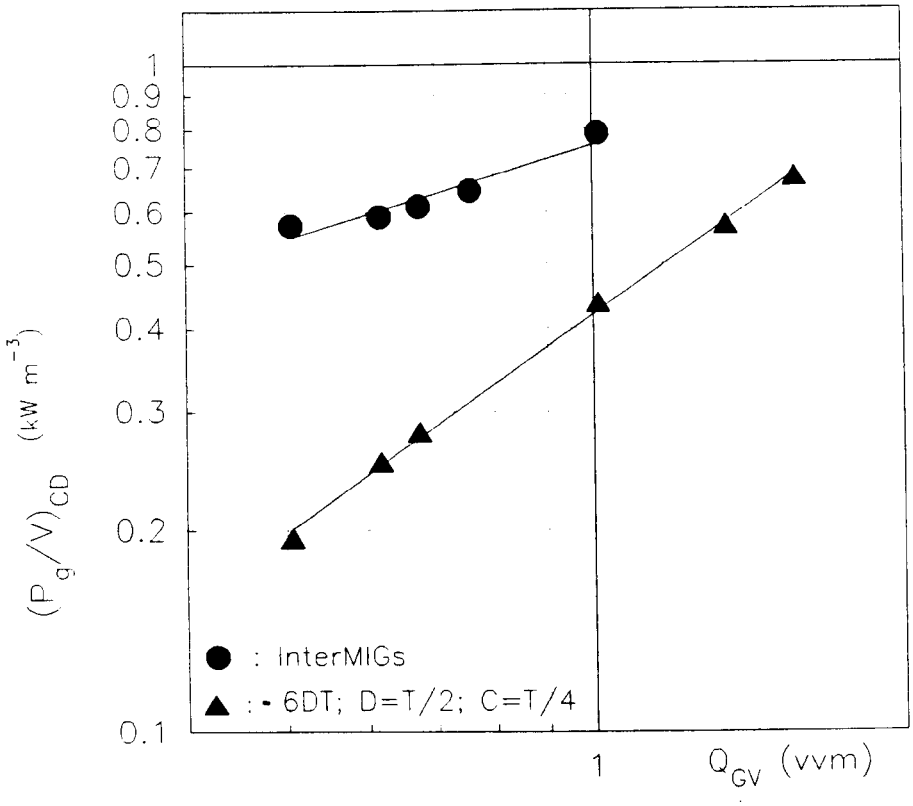

The values of the coefficient and the exponent in VI.7 are quite close to those obtained by Dawson (1992) for InterMIGs (with slight geometric variations) in water aerated through a point sparger. The relatively low value of the exponent of Q_{GV} for InterMIGs shows that $(P_g / V)_{CD}$ has a weak dependence on this parameter. The specific power input at the complete dispersion transition is higher for InterMIGs (*Figure VI.7*).

VI.4.2 Cavities

Cavities formed behind the blades were observed through the de-rotational prism described in Section VI.3.3. InterMIGs were studied rotating in forward rotation, i.e. inner blades pumping upwards.

At very low impeller speeds, where the pressure reduction behind the blades was not important, and at low gas flow rates only an accumulation of bubbles instead of cavities was observed behind the blades of Rushton turbines. A few small bubbles were attached behind the two upper split vanes of InterMIGs. These had negligible effect on the power consumed. At higher flow rates, vortex and clinging cavities were observed. A minimum impeller speed was required to allow the formation of large cavities that greatly reduce the power consumption. The corresponding Froude number (Fr_{min}) was characteristic for an impeller type - independent of its diameter, clearance from the vessel base or the number of impellers mounted. The value obtained for InterMIGs was: $Fr_{min} = 0.060$ higher than that for Rushton turbines $Fr_{min} = 0.045$.

Figure VI.8 shows the cavities formed behind the blades of InterMIGs above Fr_{min}. At low gas flow rates a sliver of gas was observed to attach behind each split vane and a small gas pocket was formed in the corner where the inner blade joins the outer blades (*Figure VI.8.a*). Increasing the gas flow rate, small cavities grew in size to engage with each other and form a

Figure VI.8 Cavities observed with InterMIGs in water

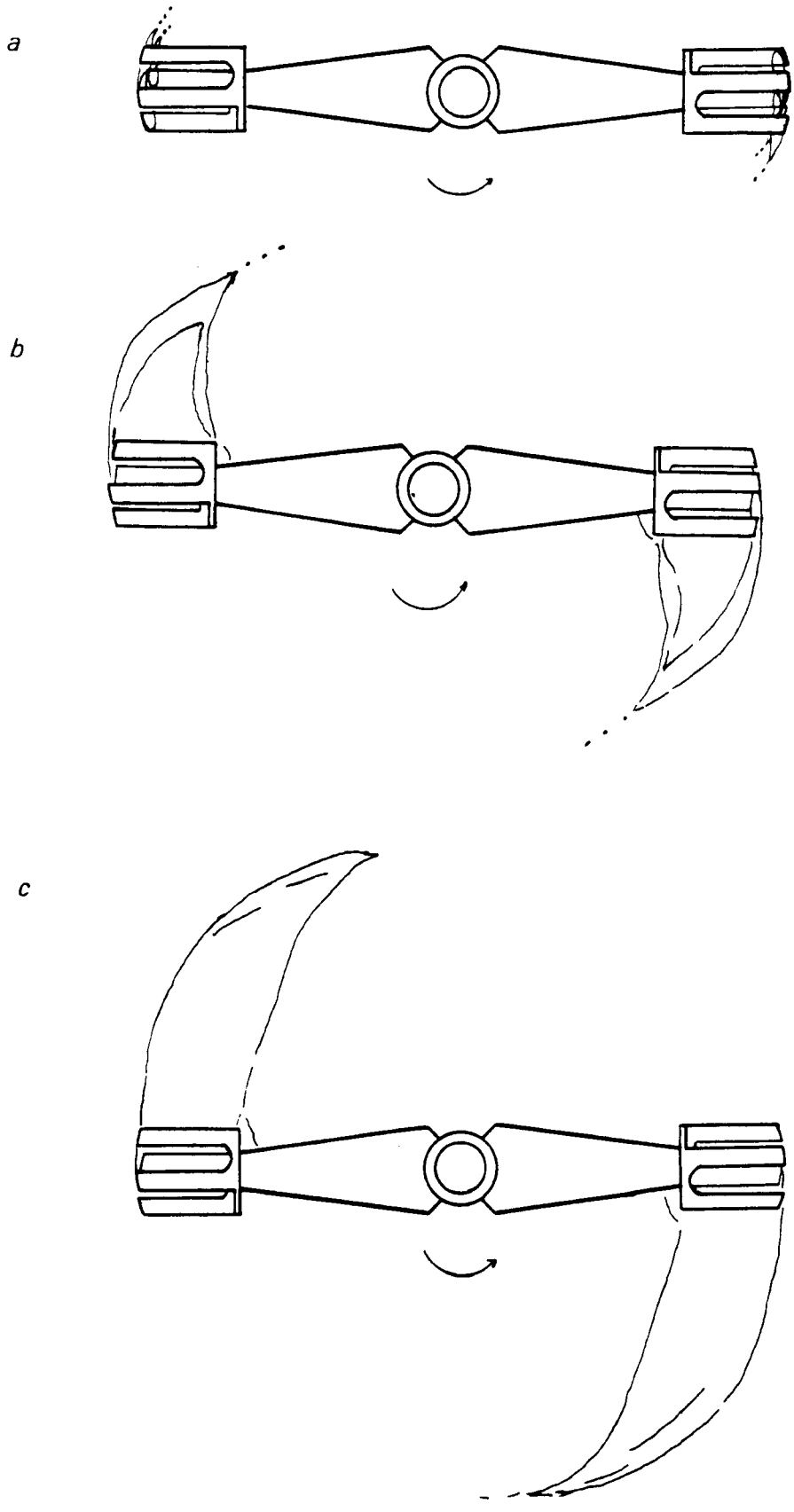

single cavity at each extremity of the impeller (*Figure VI.8.b*). Further increases in the gas flow rate resulted in a gradual increase of the cavity size (*Figure VI.8.c*).

VI.4.3 Power characteristics in the turbulent flow regime: air-water

Characteristic power curves are studied with the power numbers (Po_g) or relative power consumption (P_g/P or Po_g/Po) as a function of the Aerated Flow number. These are shown in *Figures VI.9* to *VI.13*. Power numbers are also plotted as a function of the Reynolds number for the data obtained at constant gas flow rate (*Figures VI.14* and *VI.15*).

VI.4.3.1 Experiments at constant impeller speed

Figure VI.9 shows power curves obtained at constant speeds with a six bladed disc turbine (D= T/2 and C= T/4). At low gas flow rates, where vortex cavities were formed, the power consumed was close to that under unaerated conditions. With the formation of clinging cavities at higher gas flow rates, power consumption was reduced. Increasing the gas flow rate more, led to the formation of a 3-3 structure of cavities prior to reaching an almost constant value of the power number. Power consumption could not be reduced further, increasing the gas flow rate. It can also be seen in this Figure that at low impeller speeds (Fr= 0.03) where only vortex and clinging cavities were formed, the power reduction was not very important (15-20 %). The power curves with Rushton turbines of different geometries (D, C, pair) were similar.

Apart from the general shape of the power curves, findings of previous researchers concerning the advantage of using a large diameter low clearance (D= T/2; C= T/4) were confirmed.

Figure VI 9 Power curves of a single Rushton turbine (D= T/2; C= T/4) in water at constant impeller speeds

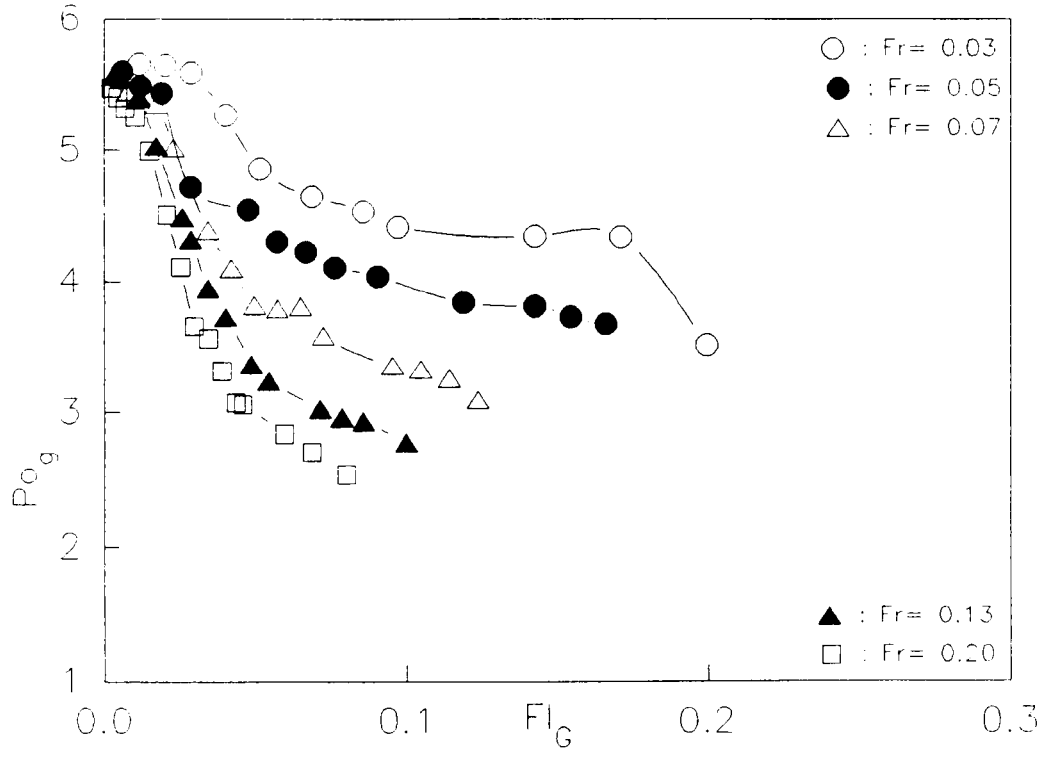

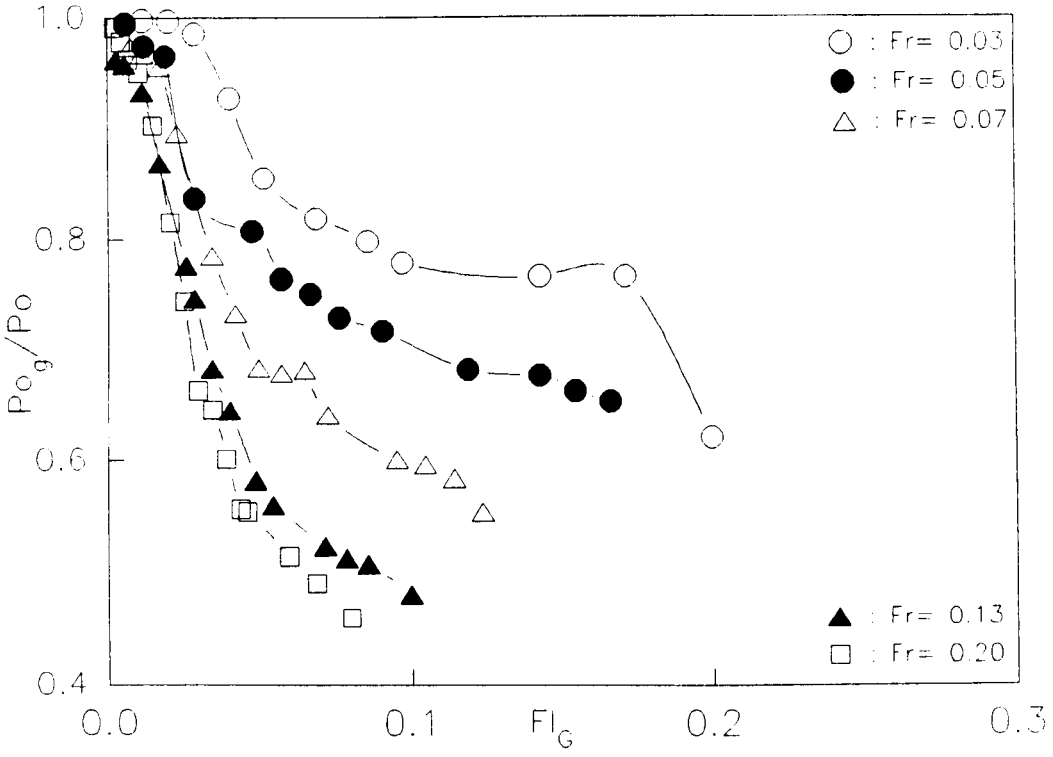

Figure VI.10 Power curves of a pair of InterMIGs in water at constant impeller speeds

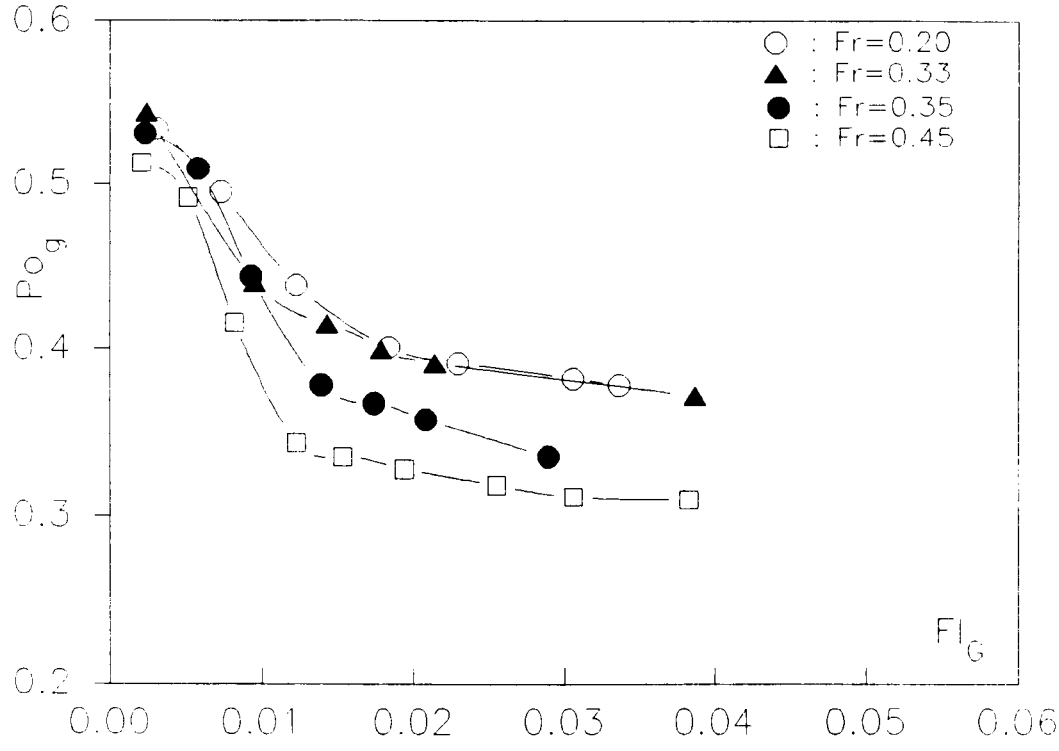

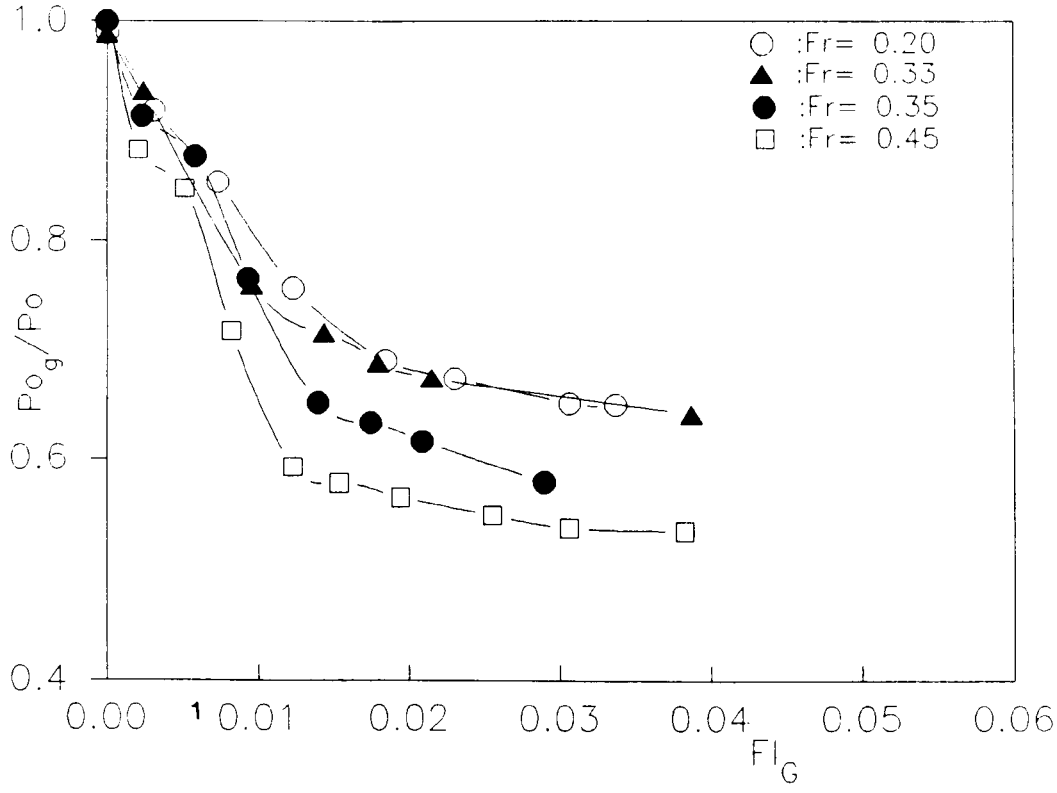

Figure VI.11 Power curves obtained with InterMIGs rotated in forward (inner blades pumping upwards) and in reverse.

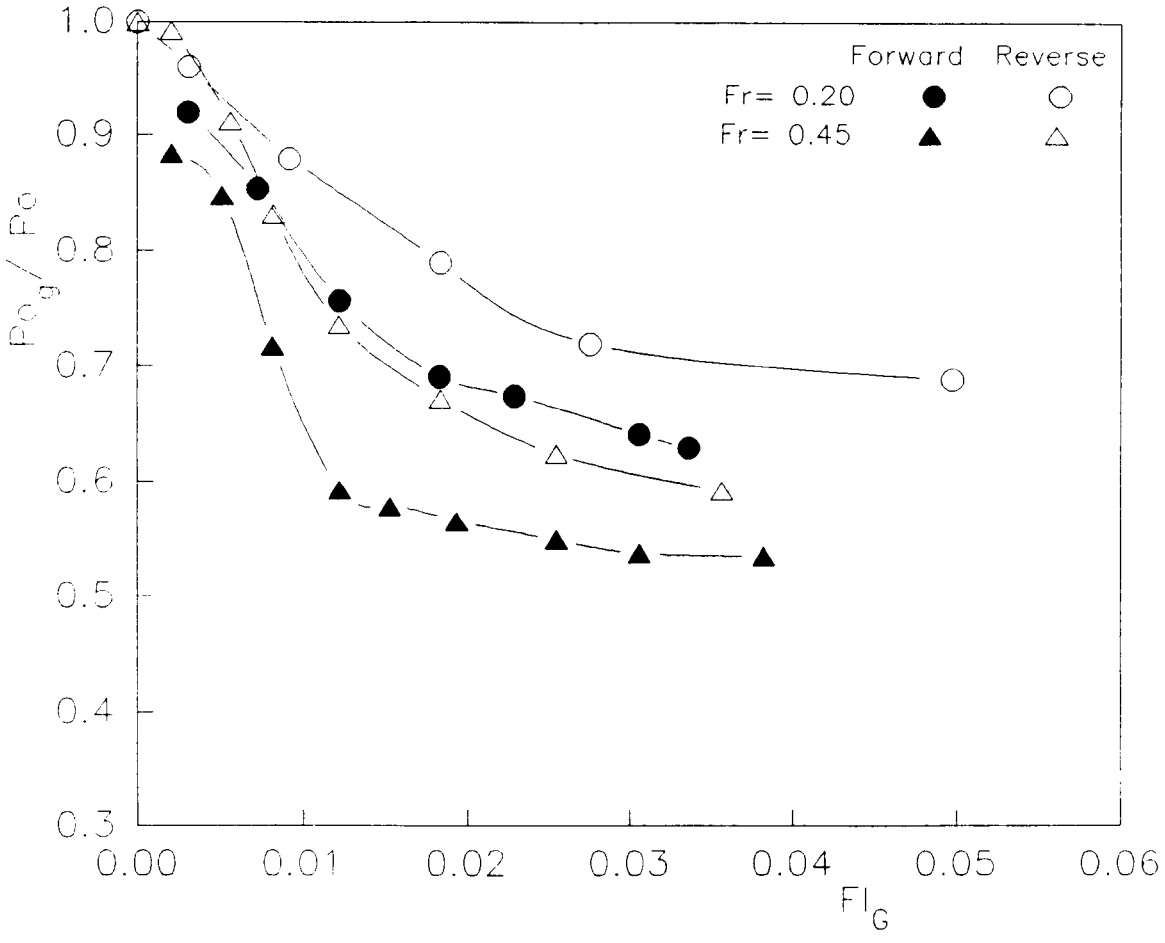

Conforming with the results obtained under unaerated conditions, the overall power consumed by two Rushton turbines at a given impeller speed was not precisely twice as that by a single one of the same diameter. Due to an interaction of the circulation loops associated with the upper and lower impellers at the inter-impeller spacings used in this study (C_1/D = 1.13 for the small diameter impeller and C_1/D = 0.75 for the larger one), this was : $(Po_g)_{pair}$ = 1.6 - 1.8 $(Po_g)_{single}$. This is not necessarily an undesirable situation as a certain extent of interaction between the upper and lower impellers prevents compartmentalisation within the vessel.

Characteristic power curves for a pair of InterMIGs obtained at constant impeller speed are presented in *Figure VI.10*. The initial power drop at low gas flow rates was almost linear with these impellers. Comparing *Figures VI.9* and *VI.10*, it can be seen that InterMIGs are characterised with fairly low power numbers compared to Rushton turbines.

A few experiments were also carried out rotating InterMIGs in reverse direction. *Figure VI.11* shows that the power consumption was higher when the inner blades pumped downwards and the outer blades upwards.

VI.4.3.2 Experiments at constant gas flow rate

Characteristic power curves obtained at different constant gas flow rates are presented in *Figure VI.12* for a six bladed disc turbine (D= T/3 and C= T/4). At low impeller speeds (or high Fl_G), where the impeller was observed to be flooded, Power numbers did not change much with increasing impeller speed (or decreasing Fl_G): they decreased very slightly. Beyond the flooding to loading transition, a steep power drop was noted. Power numbers decreased until a minimum, which corresponded to the complete dispersion transition, was reached. At speeds higher than N_{CD} (or at $Fl_G < (Fl_G)_{CD}$), where circulation loops above and below the plane of the impeller were established and the size

Figure VI.12 Power curves of a single Rushton turbine (D=T/3; C= T/4) in water at constant gas flow rates

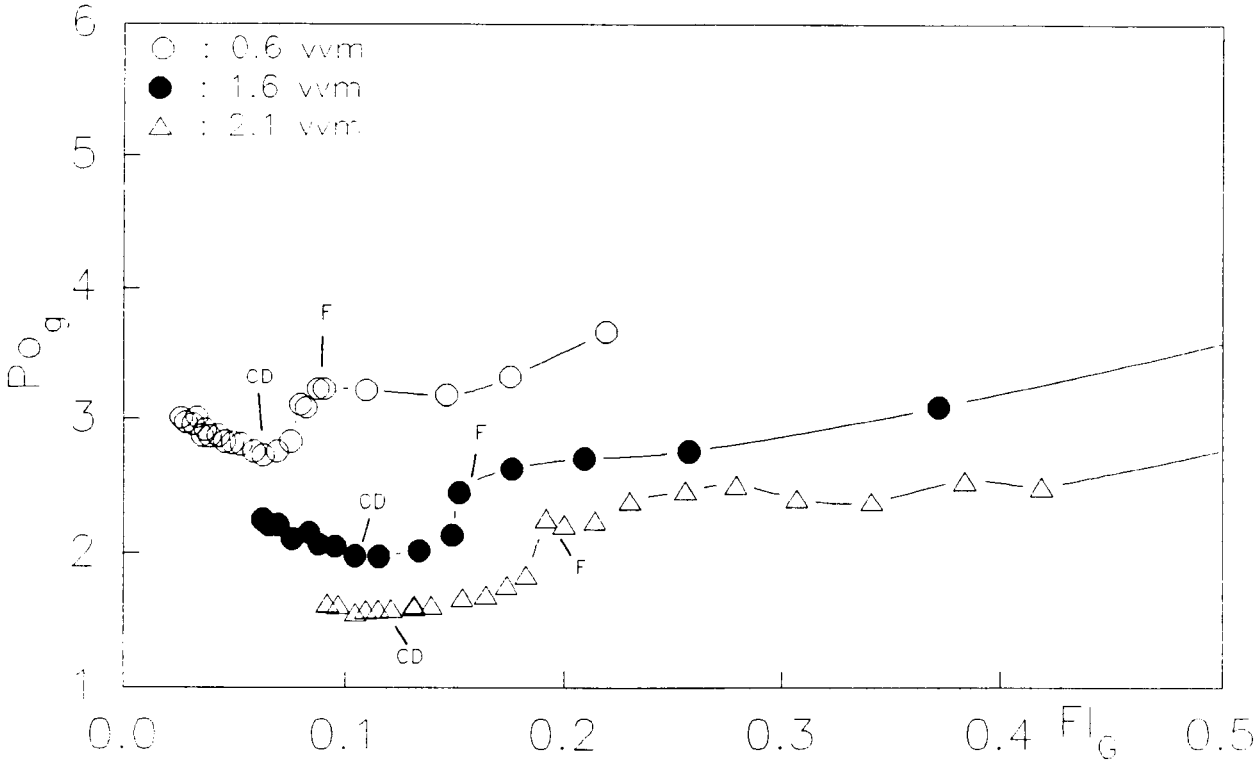

Figure VI.13 Power curves of a pair of InterMIGs in water at constant gas flow rates

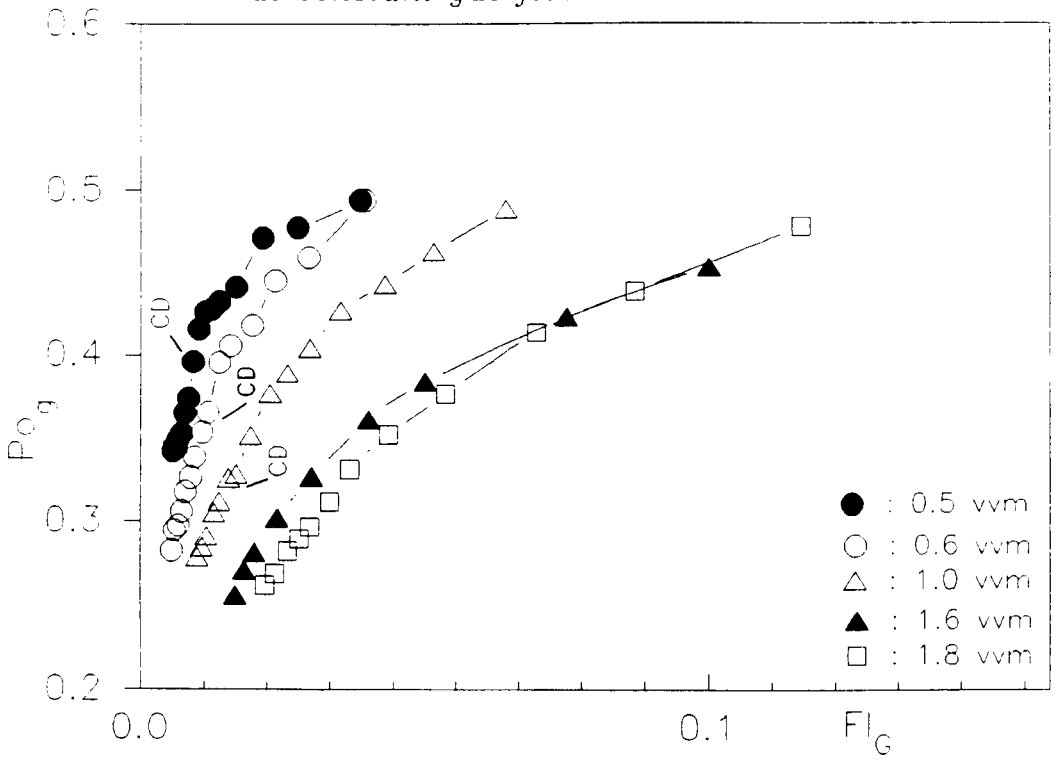

Figure VI.14 Unaerated and aerated Power numbers for a pair of InterMIGs in water

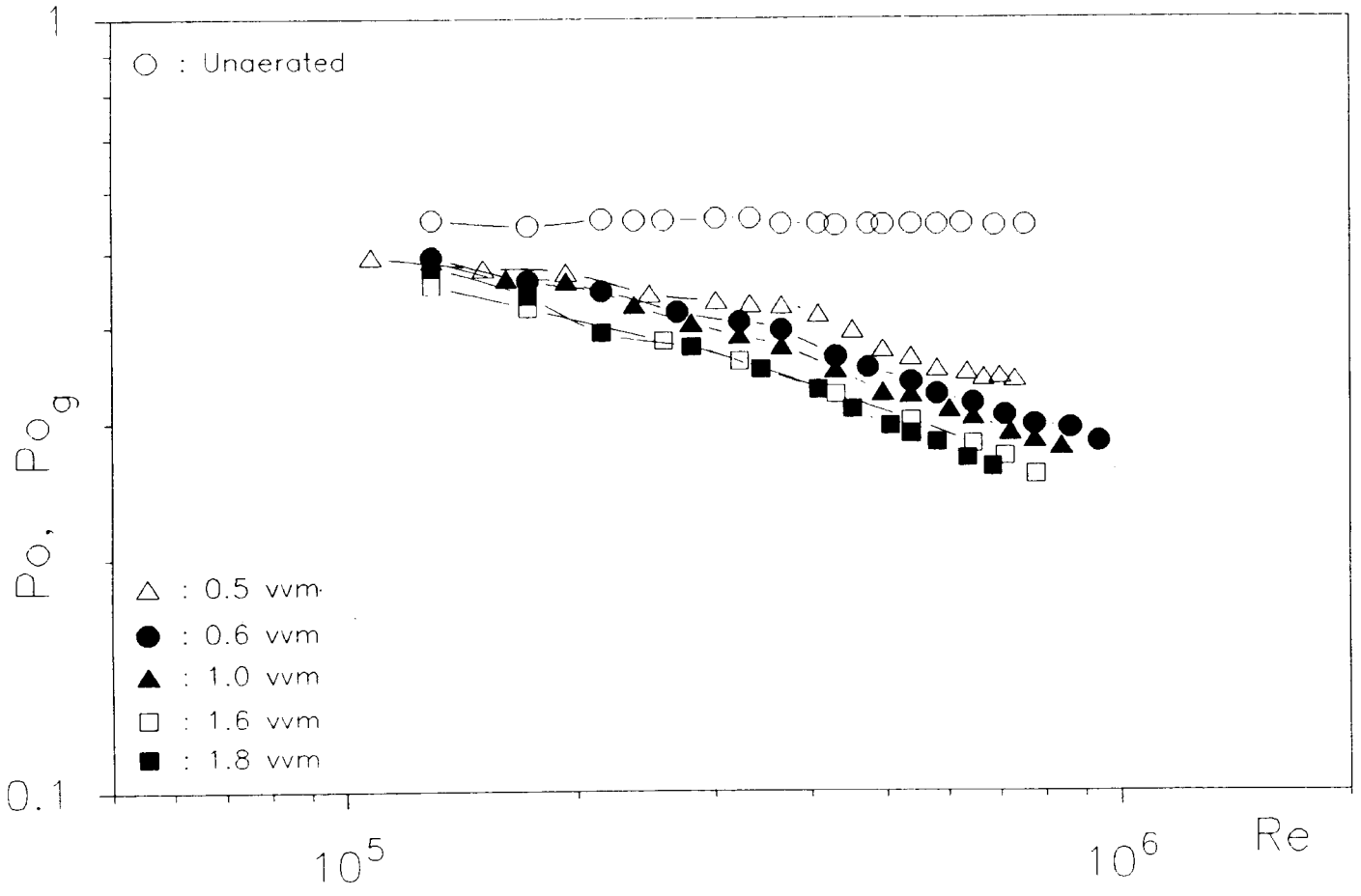

Figure VI.15 Unaerated and aerated Power numbers for a pair of Rushton turbines (D= T/2) in water

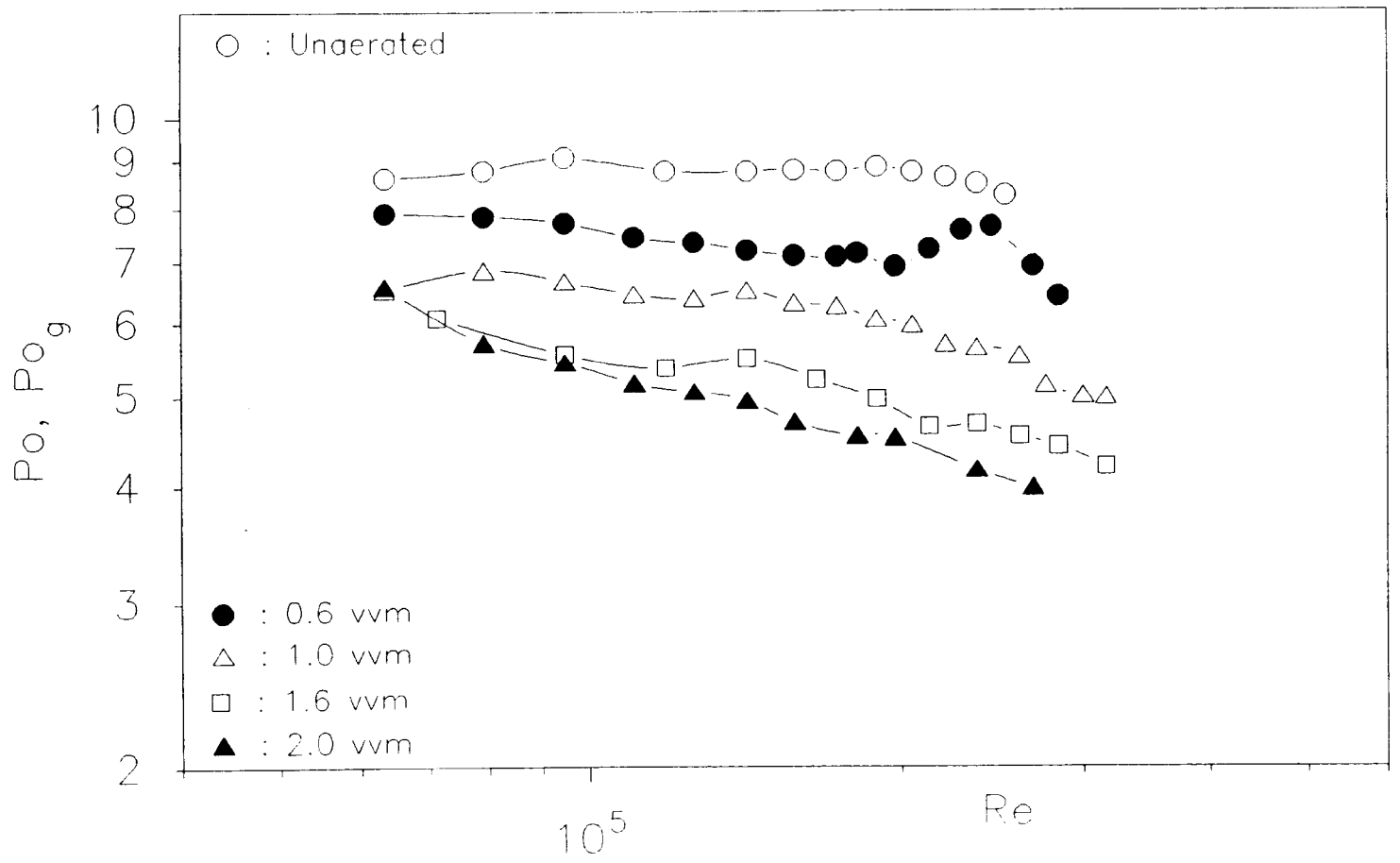

of the cavities behind the blades became smaller, gassed power consumption increased steeply (*Figure VI.12*).

Figure VI.13 shows the power curves obtained with a pair of InterMIGs. As reported in Sections VI.4.1 and VI.4.2, the changes in the impeller hydrodynamics and the cavity shape took place very gradually with InterMIGs. Conforming with these observations, power numbers also decreased gradually with increasing impeller speed. As an important characteristic of these impellers, it should be noted that the visually observed complete dispersion transition was not marked by a minimum in the power curve (*Figure VI.13*) as with the Rushton turbines (*Figure VI.12*).

Power numbers obtained with InterMIGs were much lower than those for Rushton turbines (*Figures VI.12* and *VI.13*).

In *Figures VI.14* and *VI.15*, plots of the unaerated and aerated power numbers as a function of Reynolds number are presented. With InterMIGs, the reduction of power consumption was not found to be as sensitive to the value of the gas flow rates as with Rushton turbines in a range from 0.5 to 2.0 vvm) . A similar finding regarding the complete dispersion was reported in Section VI.4.1.2.

VI.4.3.3 Power reduction under aeration

In order to assess the power reduction on account of aeration, the specific power input (P_g/V) corresponding to an unaerated power input of 1 kW m^{-3} is plotted against the gas flow rate (vvm). *Figure VI.16* shows this plot for different agitators.

As would be expected, the power reduction with a pair of Rushton turbines was less than that with a single one of the same diameter (*Figure VI.16*).

The specific power input by a pair of InterMIGs under aeration was

Figure VI.16 Specific power input under aeration corresponding to 1 kW m^{-3} under unaerated conditions

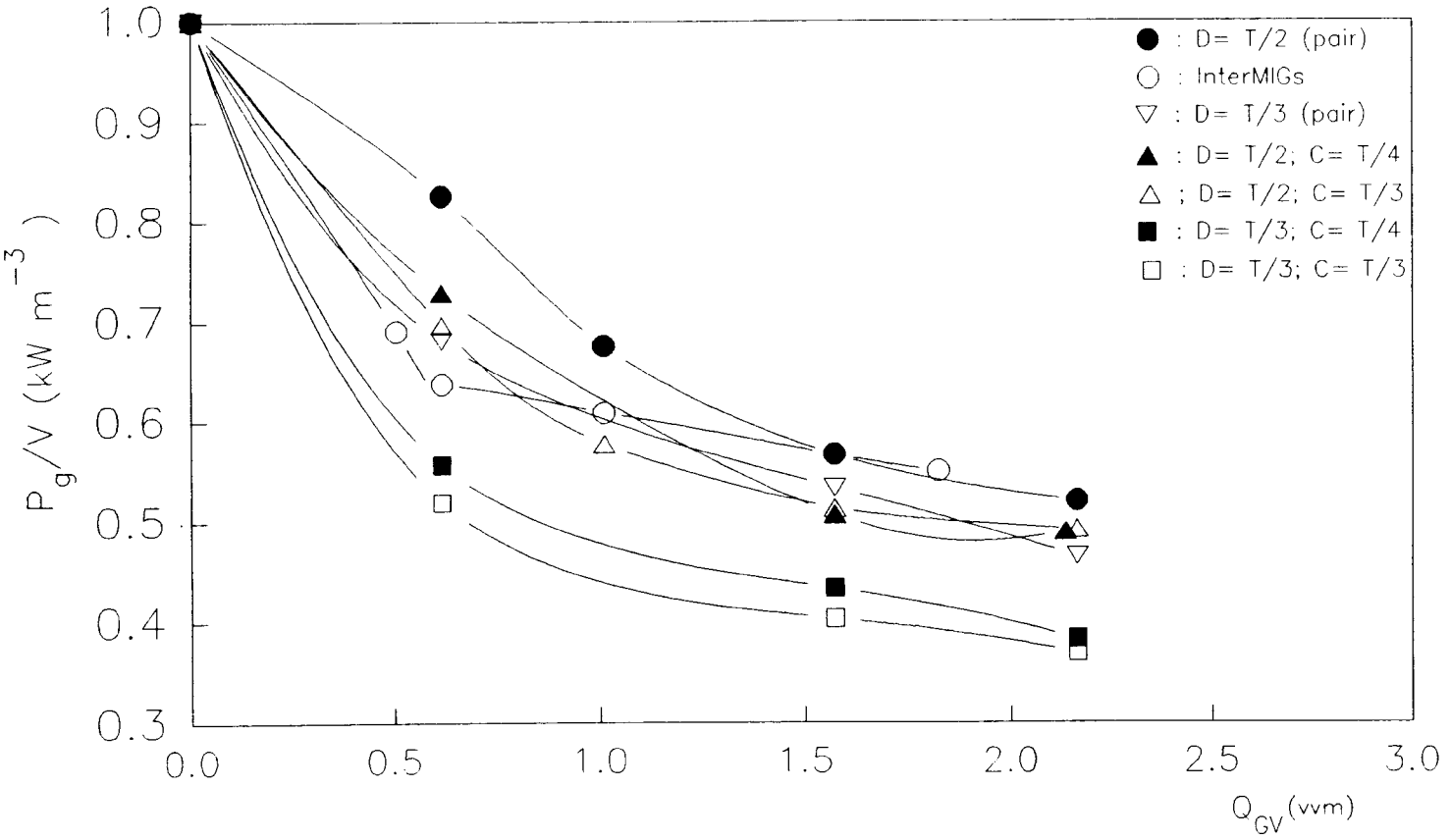

comparable to or slightly higher than that by a single large Rushton turbine for an equivalent unaerated power input (*Figure VI.16*). It can again be seen in this Figure that the aerated power consumption by InterMIGs is much less sensitive to the variation of the gas flow rate compared to Rushton turbines.

VI.5 CONCLUSIONS

Visual observations and power measurements in low viscosity Newtonian fluids have revealed that under aerated conditions InterMIGs are characterised by gradual changes in terms of the transitions between different hydrodynamic states, formation of different cavity types and power reduction- which are indicative of the advantages of using these impellers.

Similar to unaerated conditions, under aeration InterMIGs were observed to generate axial counter-flows. In a large range of operational conditions, the inner blades pumped upwards and the outer blades downwards in forward direction, i.e. anti clockwise rotation viewing from the vessel base. Only at very low speeds and very high flow rates, the sparged gas bypassed the impeller region. This situation, analogous to flooding described for classical impellers, was not encountered in the range of speeds and flow rates that would usually be covered. Due to the very gradual nature of the transition, operational conditions to prevent flooding could not be determined.

Correlations to predict the operational conditions to completely disperse gas and the specific power input at this transition were obtained. The power consumption at this transition was found to be higher than that for a single Rushton turbine and much less sensitive to the changes in the gas flow rate.

Both in forward (i.e. inner blades pumping upwards) and reverse rotation (outer blades pumping downwards) the dominant features of the fluid flows

were determined by the outer blades. In reverse rotation where these blades pumped upwards, it was not possible to achieve complete dispersion under any condition. Power consumption was also higher in this direction which therefore cannot be recommended.

Besides the transitions between different hydrodynamic states, the development of different cavity types also took place very gradually. As a result, Power numbers were found to decrease gradually with these impellers. The visually observed complete dispersion transition was not accompanied by a minimum in the power curve as with Rushton turbines.

The power reduction by InterMIGs was in general found to be much less sensitive to the changes in the value of the gas flow rate compared to Rushton turbines.

A comparison of the specific power input under aerated conditions, for an equivalent unaerated power input of 1 kW m^{-3}, has shown similar or slightly higher values for a pair of InterMIGs than those of a single large Rushton turbine.

CHAPTER VII AERATED POWER CHARACTERISTICS, HYDRODYNAMICS AND CAVITIES: VISCOUS NEWTONIAN GLYCEROL - TRANSITIONAL FLOW REGIME

VII.1 INTRODUCTION

Increase of viscosity is commonly encountered during many batch and semi-batch fermentations where viscosity is taken as the key parameter to monitor the evolution of the process. This Chapter is concerned with the mixing of highly viscous Newtonian fluids under aerated conditions. The model viscous Newtonian fluid used was undiluted glycerol ($\mu \cong$ 1 Pa s), with which the transitional flow regime was covered.

The definitions given in Chapter VI for low viscosity Newtonian fluids also provide a sufficient background for viscous Newtonian fluids. The experimental equipment used was described in Chapters III and VI. Hence, this Chapter only contains the results obtained in this study. Observations and results related to the hydrodynamics within the vessel and cavities formed behind the blades are presented in Sections VII.2 and VII.3. Studies on power characteristics in aerated viscous Newtonian glycerol can be found in Section VII.4 where results are compared to those obtained under unaerated conditions and discussed in relation to the previous work. Conclusions are given in Section VII.5.

VII.2 BUBBLE BREAK UP AND TWO-PHASE HYDRODYNAMICS IN THE TRANSITIONAL REGIME: AIR- GLYCEROL

Visual observations of both bulk flow patterns and cavities were considerably hindered in viscous fluids due to the presence of small bubbles retained in the bulk. Observations were therefore mostly confined to low gas flow rates: gas- liquid flow patterns reported in this Section are for a flow rate of $Q_{GV} < 0.5$ vvm. A video tape describing these is available at the University of Birmingham, School of Chemical Engineering.

VII.2.1 General observations

A range of bubble sizes- mainly a bimodal or a trimodal bubble size distribution- was observed in viscous Newtonian glycerol.

At low impeller speeds, most of the gas sparged into the vessel rose to the liquid surface along the rotating shaft in the form of gross bubbles (larger than those observed in water). These big bubbles had a short residence time. Bubble breakup took place- to a limited extent- at the liquid surface (as would be observed in a bubble column). Very small bubbles (of a diameter of about a millimeter or two), formed at the liquid surface, were retained in the viscous bulk and followed the liquid flows. The impeller then acted merely as a device that circulated and recirculated the small bubbles. The small bubbles that stay in the bulk for very long periods are generally conceded to be depleted of oxygen. These conditions are clearly unfavorable for oxygen mass transfer processes.

At sufficiently high speeds, a part of the gas provided by the sparger was drawn into the impeller region and broken up in this zone. Small bubbles were then produced at the impeller discharge and distributed within the bulk. Medium size bubbles (with a diameter of about a centimeter), were also formed through a partial break-up of gross bubbles. They rose towards the liquid surface from the tip of the blades without being circulated in the region below the plane of the impeller. This trimodal bubble size distribution is schematically presented in *Figure VII.1.*

At even higher speeds, medium size bubbles were discharged radially outwards. Those entrained in the upper circulation loop rose to the liquid surface. Some cap shaped bubbles stuck to the vessel walls one next to the other of decreasing size, the larger being behind the baffle.

The liquid surface was in general very wavy due to large bubbles that were observed even at very high speeds. These often splashed liquid out of

Figure VII.1 Figure VII.1 A schematic representation of bubble size distribution in viscous glycerol (1 Pa s; Re < 1000)

a) InterMIGs

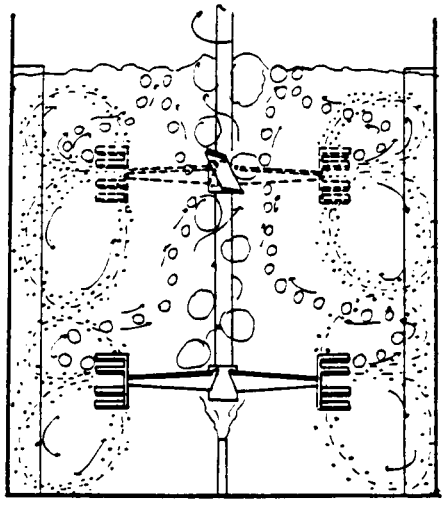

b) Rushton turbines

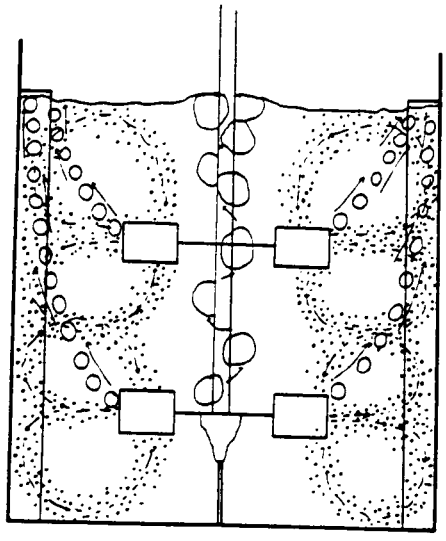

the vessel.

To summarise, bubble break-up in viscous glycerol took place through two mechanisms at two different locations: in the impeller region and at the liquid surface. Different from what was observed in low viscosity liquids, a discharge of small bubbles, could always be observed giving the impression of a "complete dispersion" state even though these may not have been produced by the impeller and a substantial amount of large bubbles escaped to the liquid surface. Hence, the hydrodynamic states defined for low viscosity fluids (in Chapter VI) would not be valid for highly viscous fluids. It can in general be recommended to work under conditions where medium size bubbles are generated and dispersed by the impeller.

An attempt to estimate the bubble size distribution with local hold-up measurements using an ultrasonic probe (dynamic gas disengagement technique) did not prove to be successful. The occasional liquid splash gave spikes in the output and due to the accumulation of tiny bubbles in the bulk, hold-up values obtained were time- dependent, but not typical to a given speed and gas flow rate.

VII.2.3 InterMIGs

The secondary flow patterns generated by InterMIGs in single phase systems were reported in Chapter III. Similarly, under aeration a change of the pumping mode of the outer blades from an axial flow in the turbulent flow regime (water- Chapter VI) to a radial discharge in the transitional flow regime (aerated glycerol) was observed. The lower circulation loops heading from these outer blades were larger than the upper loops especially for the top impeller (*Figure VII.1.a*). At low speeds where almost all the gas escaped to the liquid surface, the radial discharge was confined to the liquid phase. Gas break-up and the onset of trimodal bubble size distribution (*Figure*

VII.1.a) roughly corresponded to the speed at which cavities were formed.

VII.2.3 Rushton turbines

The discharge from Rushton turbines was radially outwards with an important tangential component of flow. Other observations were similar to those reported for InterMIGs. *Figure VII.1.b* schematically presents the bubble size distribution with these impellers.

VII.3 CAVITIES IN VISCOUS NEWTONIAN FLUIDS

Observations of cavities formed behind the blades could be made through the derotational prism described in Chapter VI for as long as the bulk remained transparent. Apart from visual observations, video recordings were also made and a tape is available at The University of Birmingham- School of Chemical Engineering.

VII.3.1 Formation of cavities

The Froude numbers corresponding to the minimum speed (N_{min}) of the formation of cavities that reduce power consumption were not different from those obtained in water : Fr_{min}= 0.040 for Rushton turbines and 0.060 for InterMIGs.

At speeds slightly higher than N_{min} , it was observed that cavities did not originate, as in water, from the inner corner of the rear of the blades of six bladed disc turbines, but from the middle of these. They mostly occupied the upper part of the blades (with respect to the disc). This suggests that the low pressure zones behind the blade were not the same above and below the disc which may be ascribed to the modifications of the tertiary flows as a result of the change of the flow regime within the bulk (transitional flow regime).

With InterMIGs, at low speeds a small gas pocket was first formed in the corner where the split vane joins the main blade. Some tiny bubbles were also observed to attach behind the tips of the outer blades.

VII.3.2 Cavity types in viscous Newtonian fluids

The type of cavity formed in a low viscosity fluid depends on the impeller speed as well as the gas flow rate. An interesting peculiarity of highly viscous fluids was the insensitivity of the type of cavities to the changes in the gas flow rate. A very low gas inflow rate was sufficient to form large cavities at a given impeller speed, further increases in the gas inflow rate had no effect. Even when the gas inflow rate was switched off, these cavities remained stable behind the blades. Thus, they were called the *"stable cavities"* (Bruijn et al, 1974; Ranade and Ulbrecht, 1977; Nienow et al, 1981; Allsford, 1985; Özcan, 1987; Özcan et al, 1988 and 1990).

VII.3.2.1 Cavities under aeration

Mainly two types of cavities were identified in the range of operational conditions that allowed visual observations. These are presented in *Figure VII.2* : *i)* at low speeds cavities originated from the middle of the blade where the blade joined the disc. Creeping up the blade they extended along the length of the blade, then formed a tail at the extremity of which bubbles were dispersed (*Figure VII.2.a*). As the speed was increased, these grew in size and the cavity tail was trailed a longer way behind (*Photograph VII.2.a*).

ii) With further increases in speed, the cavity described above became larger. It occupied mostly the upper part of the blade (with respect to the disc), some gas was also captured beneath the disc although this was difficult to observe. Bubbles were released from the extremities of the two

Figure VII.2 Cavities formed behind the blades of Rushton turbines in viscous Newtonian glycerol (Re< 1000)

(a)

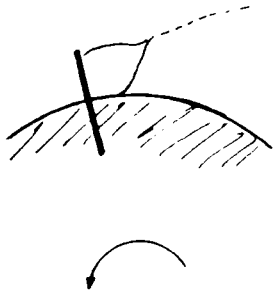

(b)

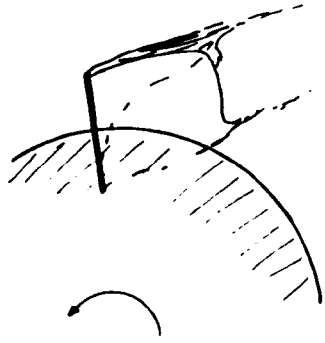

Figure VII.3 Cavities formed behind the blades of InterMIGs in viscous Newtonian glycerol (Re< 1000)

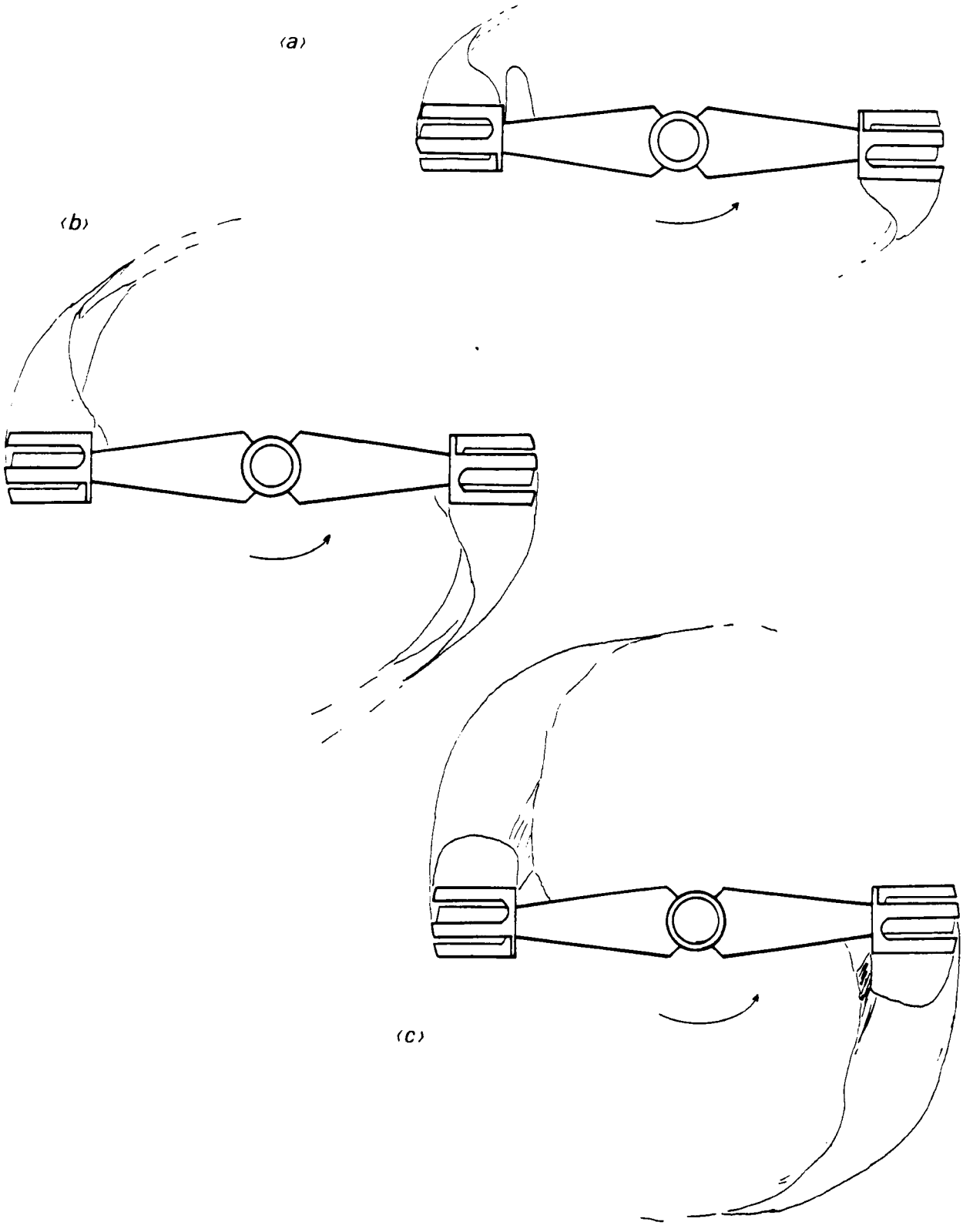

tails which occasionally touched the following blade. This cavity, schematically presented in *Figure VII.2.b* and also shown in *Photograph VII.3.a* had well defined boundaries.

When multiple impellers (a pair of Rushton turbines or InterMIGs) were used, only the cavities on the lower impeller could be studied in detail. Although under certain conditions, the cavities on the upper impeller could vaguely be seen, the fluid was in general not sufficiently transparent to get full information.

Figure VII.3 shows the cavities formed behind the blades of InterMIGs. The passage from one type to another was gradual with these impellers where the cavities changed size rather than shape as the speed was increased : *i)* At low speeds, individual bubbles were attached behind each split vane and a gas pocket was formed in the corner where the outer blades join the main blade. Increasing the speed resulted in the formation of a cavity behind the split vanes. The cavity in the corner of the blade was blunt; it did not have a tail like the cavities behind the split vanes from which bubbles were released.*Figure VII.3.a* and *Photograph VII.1* show these. This thumb shaped cavity was observed only on one of the main blades, and occasionally changed position from one blade to the other.

ii) At intermediate speeds, the size of these cavities fluctuated and the gas pocket in the corner of the blade (the thumb-like one) occasionally integrated with the cavity on the outer blades (*Figure VII.3.b*).

iii) At even higher speeds, only the cavities behind the split vanes could be observed which occupied a large volume along the track of the tail of the small cavity described above (*Figure VII.3.c*).

Various instabilities regarding the cavities formed behind the blades of InterMIGs can be listed as follows : *i)* at very low speeds only one small cavity was formed at one extremity of the impeller; *ii)* a thumb-like

Photograph VII.1 Cavities formed with InterMIGs at low speeds in glycerol (1 Pa s) : behind the split vanes and in the corner where the main blade joins the split vane

$N = 1.3\ s^{-1}$ $Q_{GV} = 0.3$ *vvm*

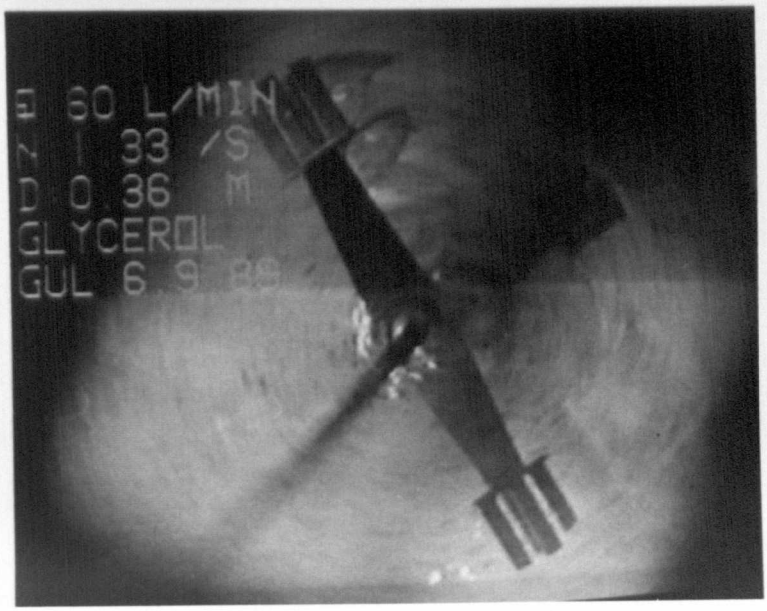

blunt cavity formed in the corner between the split vane and the main blade was observed only at one extremity of the impeller. This occasionally changed position from one main blade to the other or integrated with and disintegrated from the cavity behind the split vane; *iii)* at high speeds, the tail of the cavity at one extremity of the impeller shrunk when the one at the other extremity elongated and vice versa. However, these may not be considered to be of major importance as they were not accompanied by any instabilities or asymmetries in the main bulk flow patterns or on the characteristic power curves.

VII.3.2.2 "Stable cavities"

Under certain operational conditions, an important portion of gas filled cavities formed under aeration was observed to remain behind the blades for hours after the air supply was switched off and retain the power consumption low. In previous work, the stability of cavities was attributed to the fluid viscoelasticity or to the presence of a yield value since most of the model fluids used were also non-Newtonian. However, stable cavities were recently reported in Newtonian fluids for sufficiently high viscosities (Özcan, 1987; Özcan et al, 1988 and 1990).

As the fluid became opaque in the presence of tiny bubbles, stable cavities could not always be observed visually. The range of operational conditions in which cavities remained stable was determined as follows: *i)* following a period of mixing under aerated conditions, the air supply was switched off, the impeller was left to rotate. If any cavities remained stable behind the blades, they were released almost immediately after the impeller was stopped and the corresponding gas bubbles could be observed at the liquid surface; or

ii) by continuous power measurements prior to aeration, under aeration, and

Figure VII.4 Power consumption in the presence of stable cavities with a pair of Rushton turbines D= T/2; N= 1.5 s^{-1}

I: prior to aeration

II: during aeration

III: after the air supply is switched off

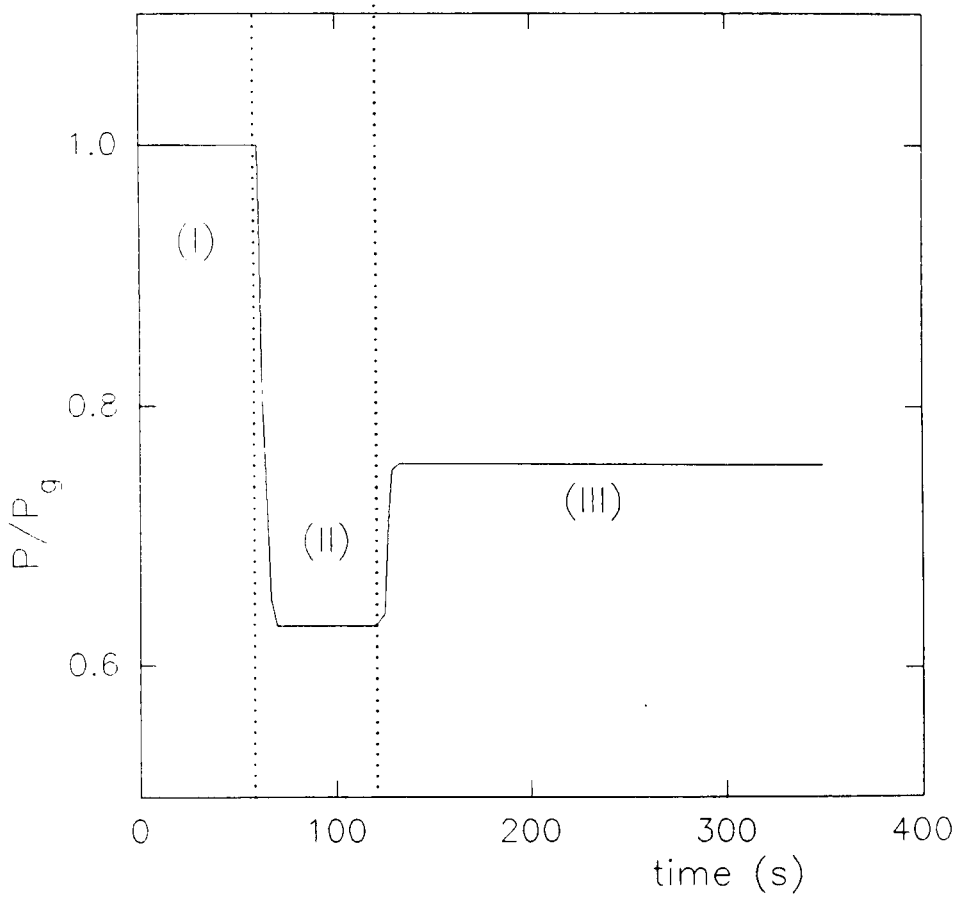

Photograph VII.2 Cavities formed with a pair of Rushton turbines (D= T/2) in glycerol: N= 1.3 s^{-1}

a) cavities formed during aeration: Q_{GV}= 0.3 vvm

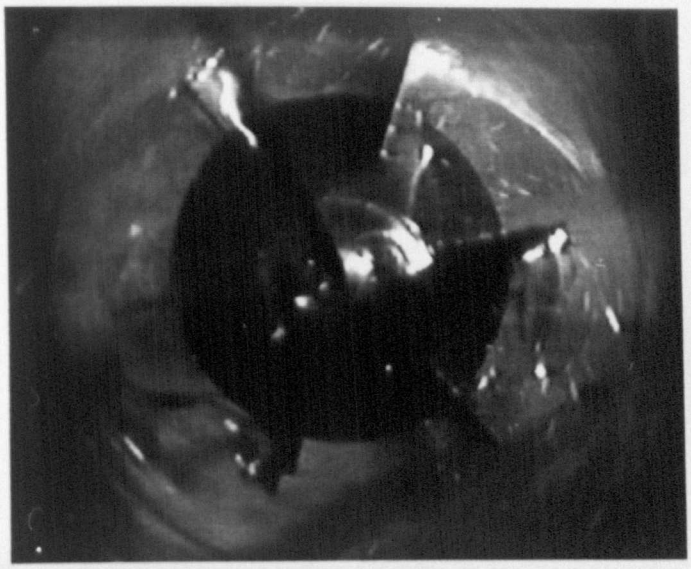

b) cavities that remain stable after the air supply is switched off: Q_{GV}= 0 vvm

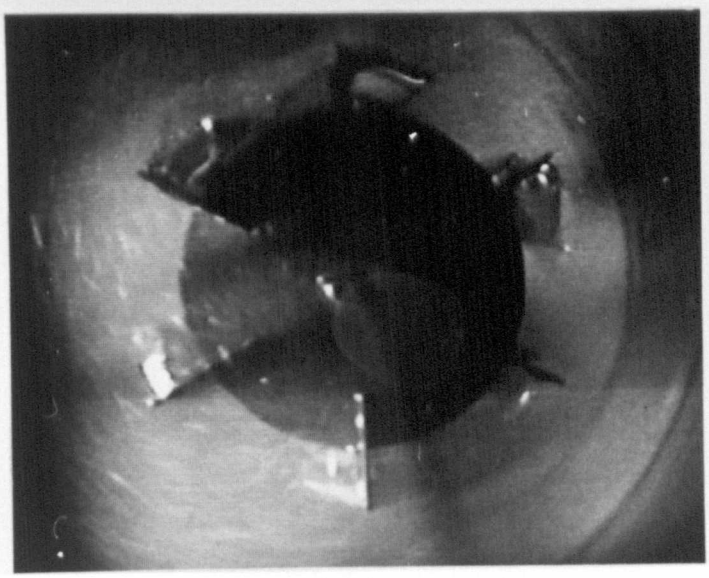

Photograph VII.3 Cavities formed with a pair of Rushton turbines (D= T/2) in glycerol: N= 1.5 s^{-1}

a) cavities formed during aeration: Q_{GV}= 0.3 vvm

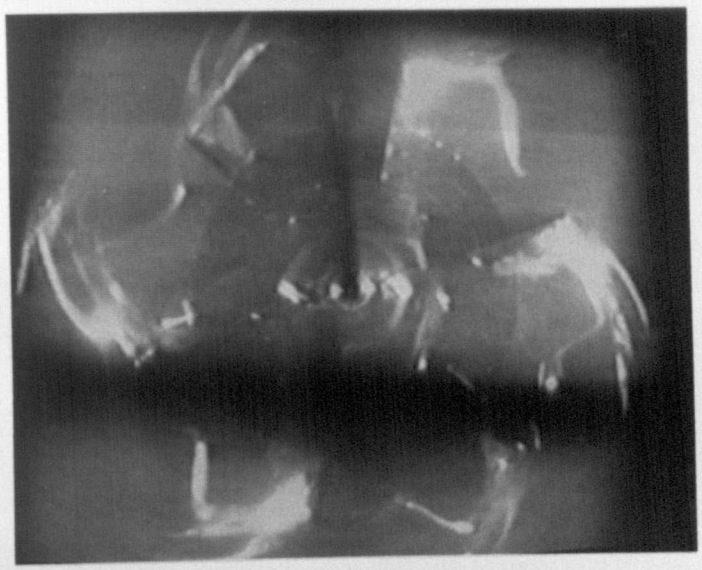

b) cavities that remain stable after the air supply is switched off: Q_{GV}= 0 vvm

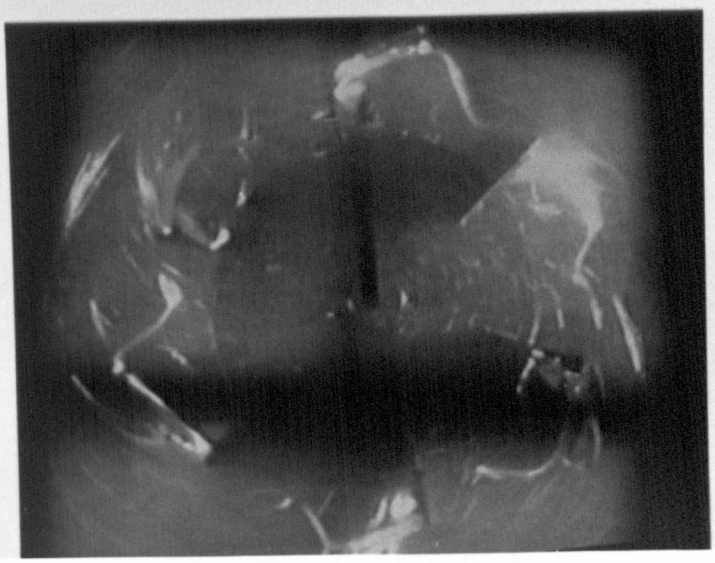

II). If the operational conditions allowed these cavities to remain after the air supply was turned off, the power also remained low (*Figure VII.4- region III*).

Once cavities were formed above Fr_{min}, they were retained behind the blades after the air supply was switched off, provided the liquid viscosity was sufficiently high and the impeller diameter and speed were low. All three parameters appearing in the Reynolds number, the operational conditions beyond which stable cavities were not observed could be expressed in terms of this dimensionless number: Re_{max} (Özcan, 1987). Conforming with the findings of Özcan (1987), Re_{max} was found to be about 400 for single Rushton turbines. This value could not be determined for a pair of Rushton turbines since at speeds corresponding to Re ≅ 400- 500, the system was aerated by air entrained from the free liquid surface after the main gas supply was switched off.

Studies in low viscosity Newtonian fluids have already shown that the dependence of the power drawn by InterMIGs on the value of the gas flow rate is weak in comparison to Rushton turbines (Chapter VI). Similarly, in viscous glycerol, the stability of cavities with regard to the changes in the gas flow rate was more pronounced with InterMIGs. At the highest Reynolds number attained with glycerol, 1050, cavities were still observed to remain behind the blades.

Photographs VII.2 and *VII.3* illustrate examples of cavities formed under aerated conditions with a pair of Rushton turbines (*Photograph VII.2.a* and *VII.3.a*) that remain stable after the air supply is switched off (*Photographs VII.2.b* and *VII.3.b*) As can be seen in these Photographs, cavities became smaller in size after the air supply is switched off, due to a partial loss of gas from behind the blades, which resulted in a slight, gradual increase of the power (*Figure VII.4, region III*). Once a residual

cavities became smaller in size after the air supply was switched off, due to a partial loss of gas from behind the blades, which resulted in a gradual increase of the power(*Figure VII.4*, region *III*). Once a residual size was achieved, the power consumption also attained a stable value.

VII.4 POWER CHARACTERISTICS IN AERATED VISCOUS NEWTONIAN FLUIDS

With undiluted glycerol ($\mu \cong$ 1 Pa s), Reynolds numbers between 50 to 1050 were covered in the transitional flow regime.

Characteristic power curves obtained in viscous Newtonian glycerol are presented in *Figures VII.5*, *VII.6* and *VII.9*, *VII.10* where power numbers are plotted against the Aerated Flow number. For experiments carried out at constant gas flow rate, power numbers are also plotted as a function of the Reynolds number (*Figures VII.7* and *VII.8*) along with the unaerated data.

VII.4.1 The effect of impeller speed on the power consumed in aerated viscous Newtonian fluids

At very low speeds, where a substantial cavity formation was not observed, power consumption was not reduced under aeration. Unaerated and aerated Power numbers were almost identical at low Reynolds numbers as can be seen in *Figures VII.7* and *VII.8* and for low Froude numbers as shown in *Figures VII.9* and *VII.10*.

Above Fr_{min} (0.040 for Rushton turbines and 0.060 for InterMIGs), power consumption was reduced on account of aeration. Power numbers decreased with increasing impeller speeds as result of an increase in the size of cavities (*Figures VII.5* and *VII.6*).

With Rushton turbines, similar to the results obtained in the turbulent flow regime (*Figure VI.12*), the power curve also made a minimum in the transitional flow regime (*Figure VII.5*). In water, this minimum was

Figure VII.5 Power curves of a 6DT (D= T/2; C= T/4) at constant gas flow rates (glycerol– transitional flow regime)

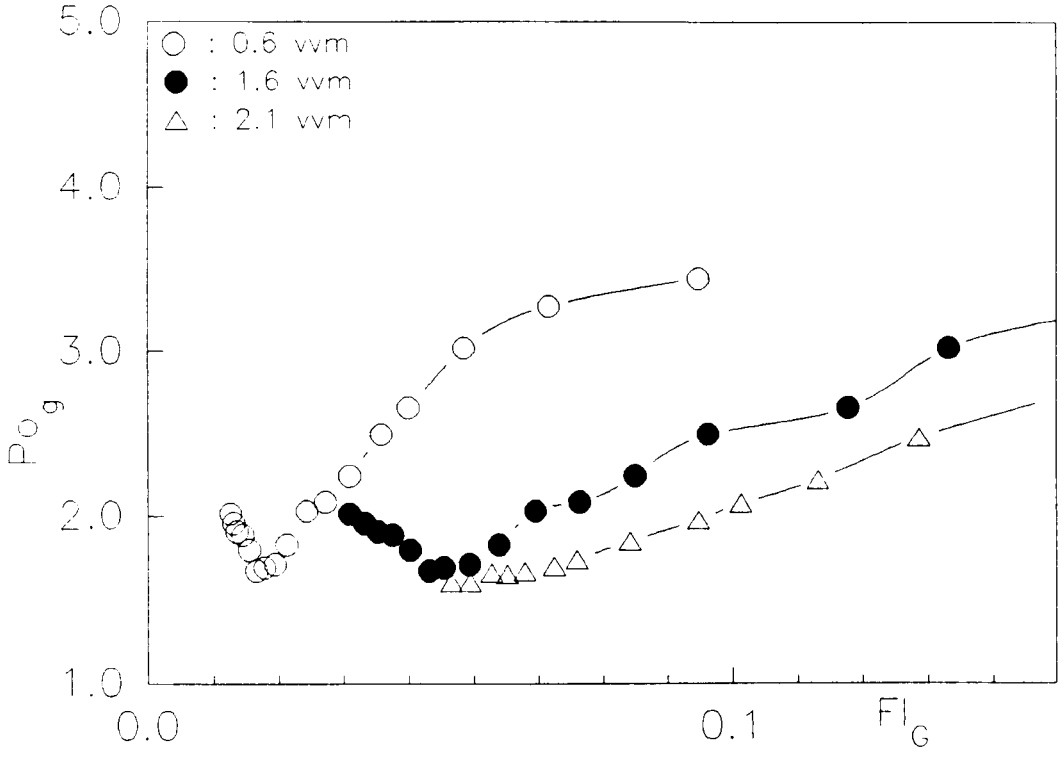

Figure VII.6 Power curves of a pair of InterMIGs at constant gas flow rates (glycerol – transitional flow regime)

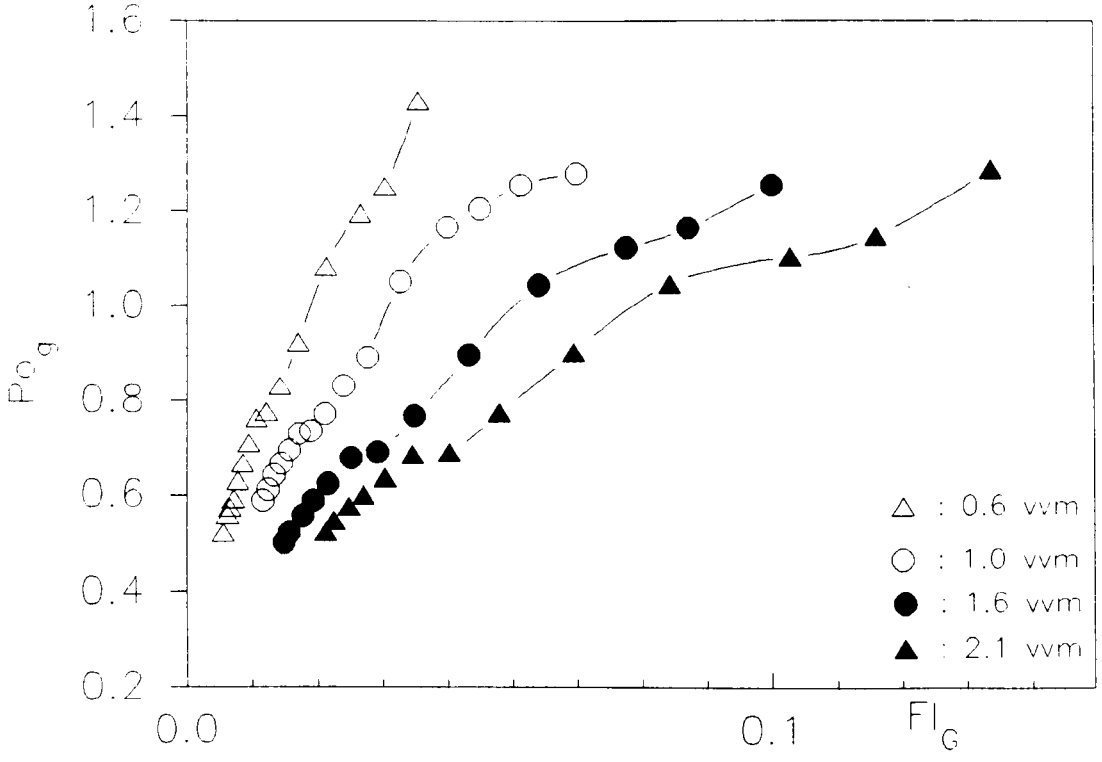

observed to correspond to a change in the impeller hydrodynamics: the complete dispersion transition. At speeds above this transition where the impeller became more efficient in dispersing gas from behind the blades, cavities became smaller in size and the power consumption increased. Although the minima in the power curves obtained with glycerol cannot be interpreted as the "complete dispersion" transition (as defined for low viscosity liquids), for reasons explained in Section VII.2, it certainly corresponds to a more efficient gas dispersion capacity of the impellers by analogy to low viscosity fluids. The speed to reach the minimum in glycerol (~ 1 Pa s) was found to be about three times higher than that obtained in water. This corresponds well with the findings of a previous work[74] where the dependence of the speed to reach the minimum on the fluid viscosity was reported as $N_{mini} \propto \mu^{0.15}$.

Minima were not obtained in the power curves of InterMIGs; power numbers decreased with increasing speeds (*Figure VII.6*). This does not suggest an inefficiency of these impellers as even in the turbulent flow regime, the visually observed complete dispersion transition was not either marked with a minimum in the aerated power curve (*Figure VI.13*).

Figure VII.7 Unaerated and aerated Power numbers for a pair of Rushton turbines (D= T/2) in glycerol

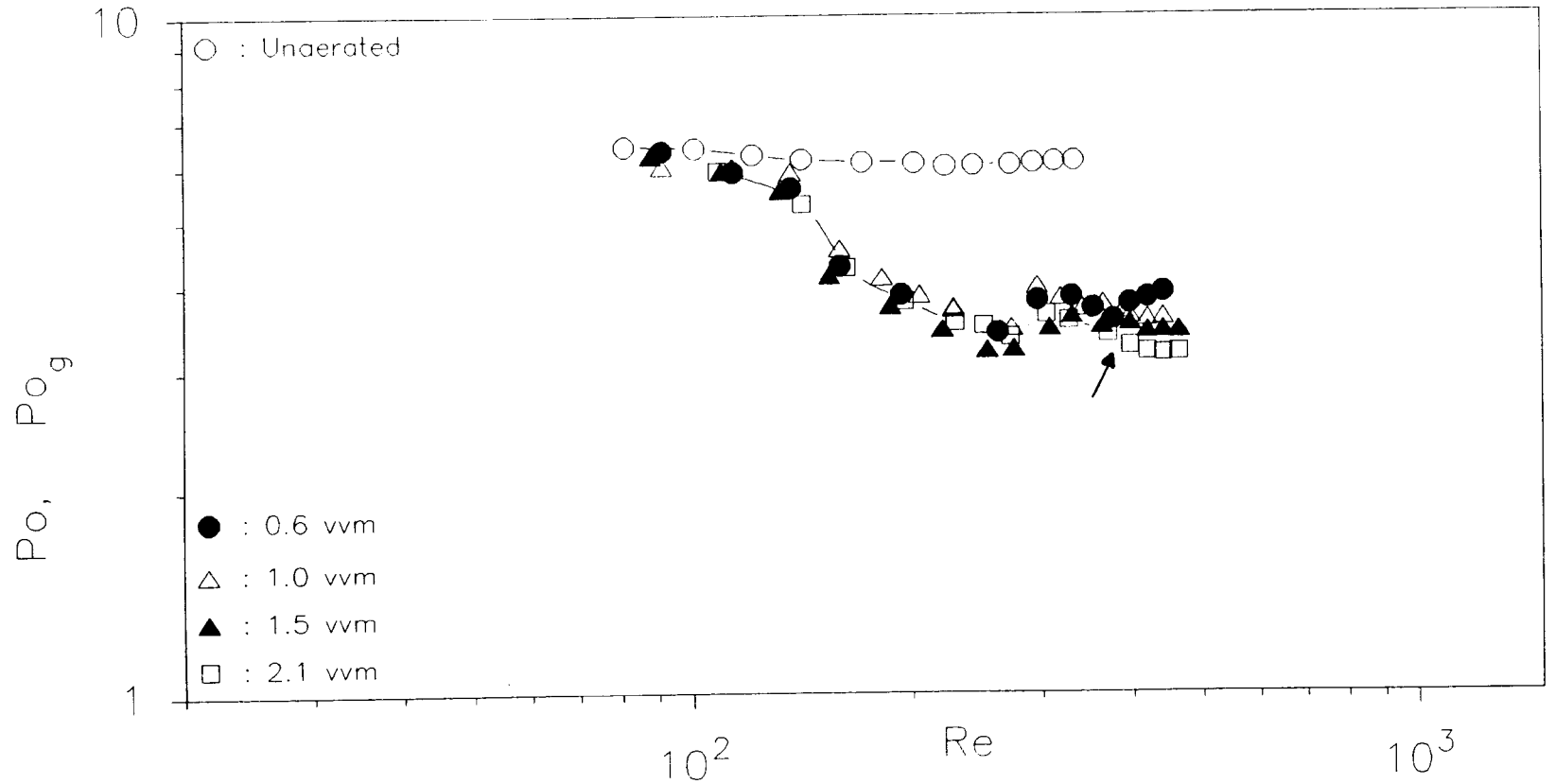

Figure VII.8 Unaerated and aerated Power numbers for a pair of InterMIGs in glycerol

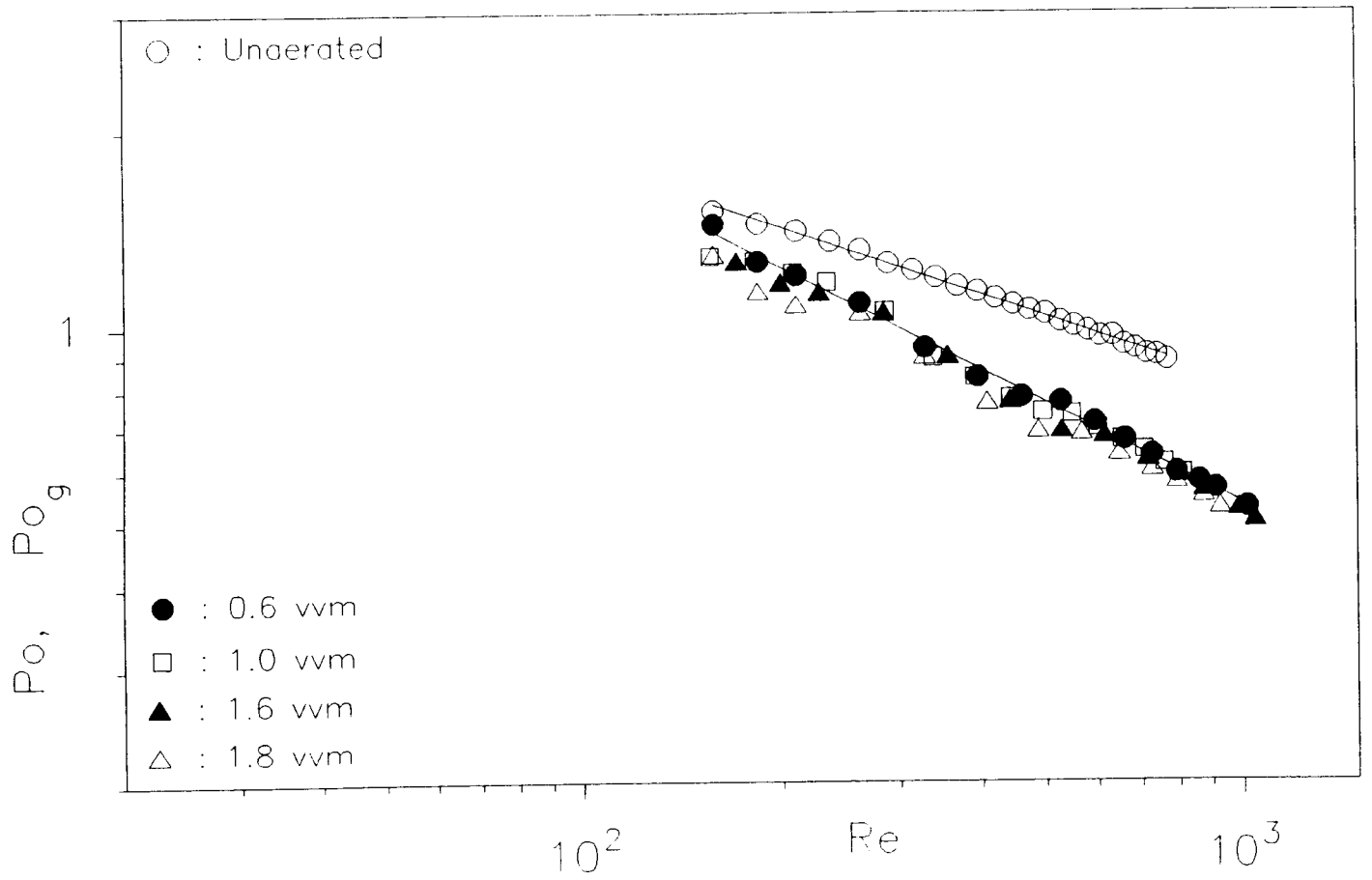

VII.4.2 The effect of gas flow rate on the power consumed in aerated viscous Newtonian fluids

In the above paragraphs the effect of impeller speed on the power consumed in aerated glycerol is reported. Gas flow rate, on the other hand, had no impact on the power consumption in a large range of operational conditions. Flat power curves obtained at constant impeller speed show this in the most striking way (*Figures VII. 9* and *VII.10*). Similar findings in viscous Newtonian fluids were previously reported by Özcan,1987; Özcan et al,1988; for Rushton turbines and by Kipke, 1978 and Höcker et al, 1981 for MIGs and InterMIGs. As reported in Section VII.3, even at very low gas flow rates, cavities formed had already attained their ultimate size. These were stable to the changes in the gas flow rate and therefore led to the maximum power reduction for a given impeller speed. It can be seen in *Figures VII.9*, *VII.10* as well as *VII. 7* and *VII.8* that the power reduction above Fr_{min} was only dependent on the impeller speed; power curves obtained for gas flow rates from 0.6 to 2.1 vvm superposed in a large range of Reynolds numbers.

With Rushton turbines, at about a Reynolds number of 400, aerated power curves separated from one another (*Figure VII.7*). The power consumption was then also dependent on the value of the gas flow rate: lower power numbers were obtained for high gas flow rates. This value of the Reynolds number at which a branching of the power curves took place ($\simeq$ 400) corresponded to the maximum Reynolds number above which the cavity stability against the changes in the gas flow rates was lost, in coherence with the findings of previous work (Özcan, 1987; Özcan et al, 1990).

Observations have shown that cavities were stable in a larger range of Reynolds numbers with InterMIGs. Parallel to this, at Reynolds numbers as high as 1000 the power numbers obtained for different gas flow rates were almost identical (*Figure VII.8*).

Figure VII.9 Power curves for a pair of Rushton turbines (D= T/3) at constant speeds (glycerol–transitional flow regime)

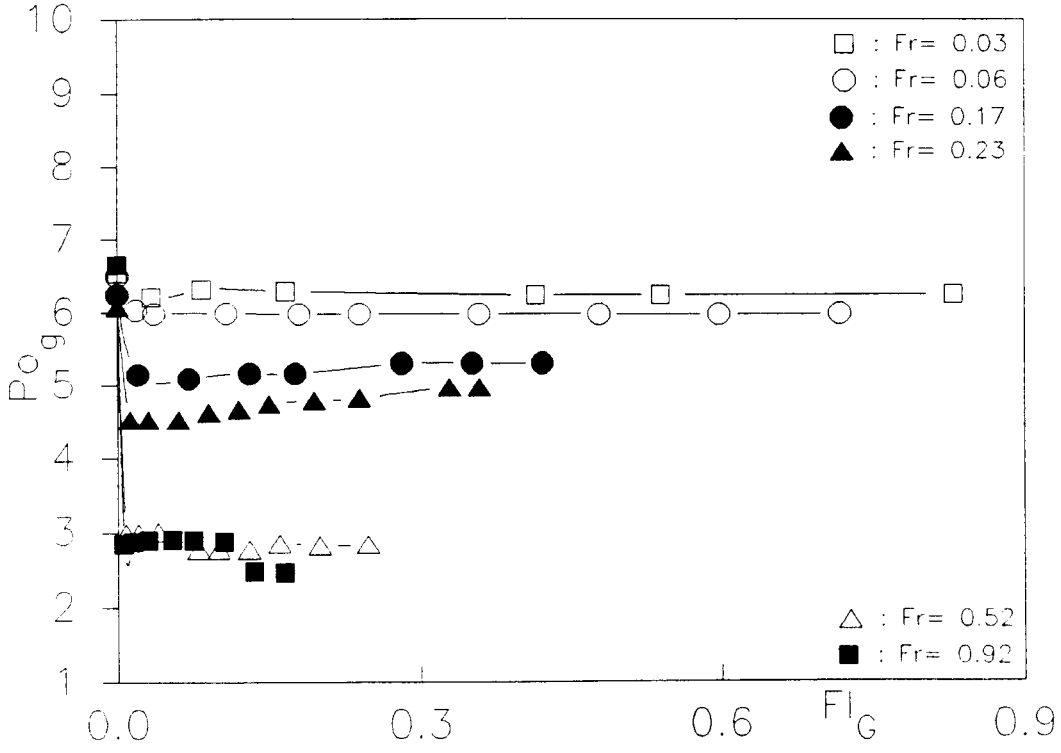

Figure VII.10 Power curves of a pair of InterMIGs at constant impeller speeds (glycerol– transitional flow regime)

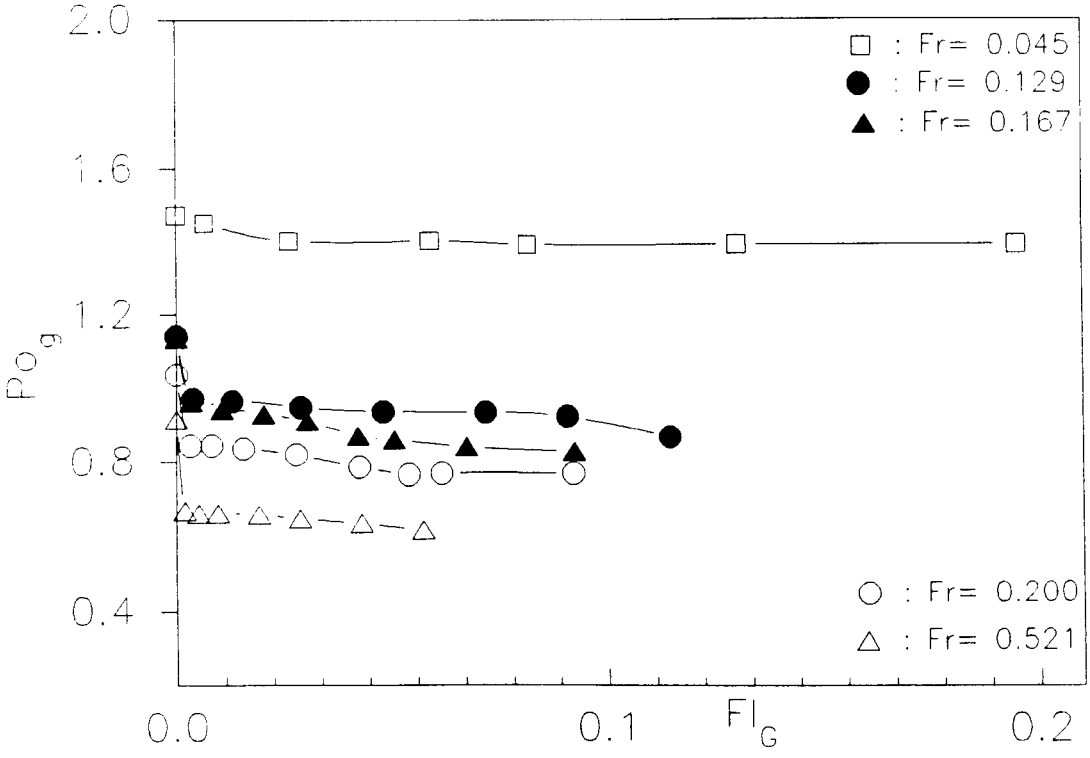

A comparison of the power data for Rushton turbines and InterMIGs in the range of Reynolds numbers where power consumption was only dependent on the impeller speed, this dependence appears to be very weak for InterMIGs (*Figures VII.7*, *VII.8* and *VII.9 VII.10* - it should be noted that the y-axis range in these Figures are not the same for InterMIGs and Rushton turbines).

VII.4.3 Effect of geometric parameters on power consumption

Conforming with the previous findings, large Rushton turbines when used singly or as a pair acquired higher power numbers at a given Reynolds number. Impeller clearance from the tank bottom did not seem to have a significant effect either.

Power reduction under aeration $\dfrac{(Po - Po_g)}{Po}$

was therefore almost the same for a given impeller diameter irrespective of the impeller clearance from the tank bottom and the number of impellers mounted on the shaft. The highest reduction was obtained with small Rushton turbines (D= T/3). At a given Reynolds number of around 300, power reduction with small Rushton turbines was 56- 61 % under aerated conditions, 37% with larger turbines (D= T/2) and only 24% with a pair of InterMIGs.

VII.5 CONCLUSIONS

In viscous Newtonian glycerol, mainly a bimodal or a trimodal bubble size distribution was observed depending on the operational conditions. Different from low viscosity fluids, two distinct sizes of bubbles were formed under all conditions: gross bubbles escaped to the liquid surface even at very high speeds and the tiny ones entrapped in the viscous bulk followed liquid flows. These small bubbles, produced at the liquid surface or by the impeller, gave the impression of a "complete dispersion" state under all conditions. Hence, impeller hydrodynamics in viscous fluids could not be assessed as in low viscosity fluids. The bimodal bubble size distribution at low speeds with big bubbles of short residence time and small bubbles depleted of oxygen is clearly not favourable for oxygen mass transfer processes.

The onset of trimodal bubble size distribution corresponded roughly to the speeds where cavities were formed. The medium size bubbles then produced were discharged radially outwards by the impellers at higher speeds. It can therefore be recommended- as a rough guide- to exceed the conditions where a trimodal bubble size distribution is generated.

The secondary flow patterns generated by Rushton turbines and InterMIGs in aerated glycerol were in general similar to those observed under unaerated conditions in the transitional flow regime. Rushton turbines were characterised by a radial discharge with an important tangential component of flow, and the axial flows associated with the outer blades of InterMIGs were replaced with a radial discharge in the transitional flow regime.

Cavity types observed in glycerol were different from those found in water especially for Rushton turbines. A more important aspect of mixing viscous fluids was that cavities and consequently the power consumption were stable against the variations in the gas flow rate. Hence, the power consumed was only dependent on the impeller speed in a range of operational

conditions. A low value of gas flow rate was sufficient in order for the cavities to reach their ultimate size at a given impeller speed. Further increases or decreases of the flow rate did not affect the size, type of cavities or the corresponding power consumption. An important portion of these cavities was retained even after the air supply was switched off provided the Reynolds number is sufficiently low.

An estimate of the power consumed for viscous aerated fluids can therefore be made more easily as this only depends on the impeller speed in a range of conditions in the transitional flow regime. When operated in the zone of stable cavities, changing the gas flow rate or even a total failure of gas supply will not result in a drastic increase of the power consumed. It should however, be noted that in such viscous systems power consumption measurements made after the air is switched off, will considerably underestimate the power demand for truly unaerated systems.

A general comparison of InterMIGs with Rushton turbines has shown that the aerated power consumption with these impellers - due to their configuration, is not only stable against the changes in the gas flow rate in a larger range of Reynolds numbers, but also much less dependent on the impeller speed.

CHAPTER VIII EFFECTS OF VISCOELASTICITY UNDER AERATED CONDITIONS

VIII.1 INTRODUCTION

Following chapters on the effects of viscoelasticity in single phase systems and gas-liquid mixing in Newtonian fluids, this chapter is concerned with the studies on the effects of viscoelasticity under aerated conditions. Hence, the results presented are most relevant to aerobic fermentations of complex rheology.

The model fluids used were prepared by adding trace amounts of the polymer polyacrylamide in glycerol. Three viscoelastic fluids containing different polymer concentrations had an almost shear independent viscosity which allowed the study of viscoelastic effects alone. The rheological properties of these were detailed in Chapter II. All three viscoelastic fluids and glycerol had comparable consistency, hence comparisons could be made in a given range of Reynolds numbers in the transitional flow regime (Re< 1300). Results for aerated conditions were also compared to those for single phase systems which were detailed in Chapter IV. This Chapter covers the observations and results on two phase bulk flow patterns (Section VIII.2), cavities (VIII.3) and power characteristics (Section VIII.4) obtained in this study. Conclusions can be found in Section VIII.5.

VIII.2 TWO PHASE FLUID HYDRODYNAMICS IN VISCOELASTIC FLUIDS

A spectrum of bubble size distribution- mainly bimodal or trimodal- was observed in viscoelastic fluids as in viscous glycerol. Medium size bubbles of a diameter of more than about 1 cm were observed to be deformed under elastic effects. In Newtonian fluids, bubble shape was in general spherical although some cap shaped or oblate ellipsoidal ones were observed. These slight deformations were mainly due to inertial effects. The deformation due to elastic effects gave bubbles of prolate ellipsoid shape as shown in *Photograph VIII.1* obtained in a small scale.

Photograph VIII.1 Prolate ellipsoid bubble shape in viscoelastic fluids

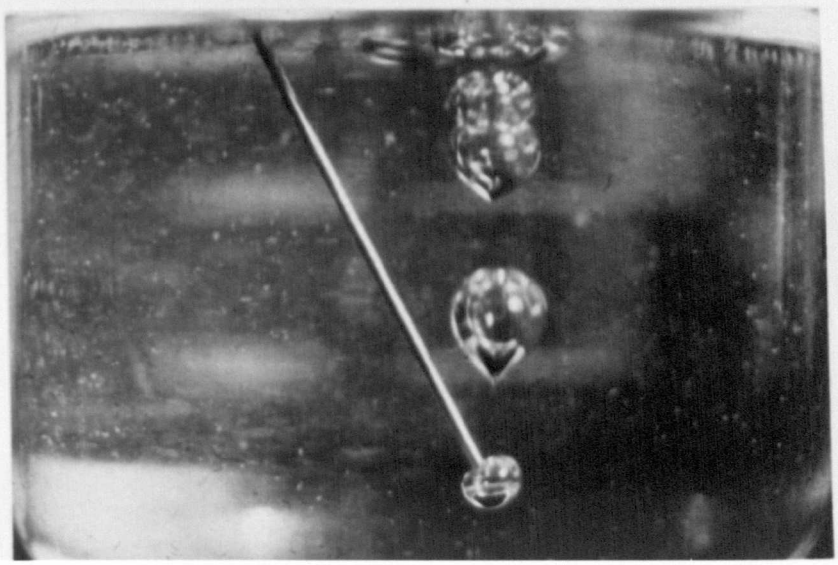

General features of the bulk flow patterns as visually observed were similar to those reported for viscous Newtonian glycerol: radially outwards from Rushton turbines and from the outer blades of InterMIGs. Bubbles of 1-2 cm diameter discharged radially outwards by the impeller and circulated in the zones below the impeller plane were observed to attach to the vessel walls in glycerol. This did not happen in viscoelastic fluids where the secondary flows were reduced. Liquid surface was also less wavy compared to glycerol.

VIII.3 CAVITIES IN VISCOELASTIC FLUIDS

The equipment used for the observation of cavities was described in Chapter VI. A video tape of the recordings of cavities formed in viscoelastic fluids is also available at The University of Birmingham- School of Chemical Engineering.

VIII.3.1 Cavities formed under aeration

At low impeller speeds, bubble agglomerates were observed behind the blades; these did not affect the power consumed. Although it was reported[74] that higher speeds are required for the formation of cavities in viscous and rheologically complex fluids, in this study the values of the Froude number at which cavities were formed in viscoelastic fluids were found to be the same as those obtained in Newtonian fluids of low and high viscosity : 0.040 and 0.060 for Rushton turbines and InterMIGs respectively. The minimum Froude number required for cavity formation proved to be an impeller characteristic independent of fluid properties.

The shape and type of cavities were only dependent on the impeller speed in viscoelastic fluids as in viscous glycerol, and similar problems in observing cavities in a range of operational conditions were met in the

Figure VIII.1 Cavities formed in viscoelastic fluids with Rushton turbines

a)

b)

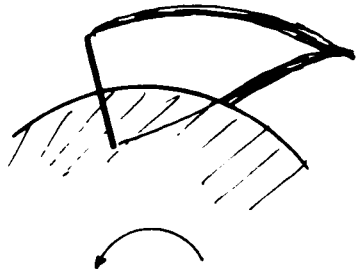

Figure VIII.2 Cavities formed in viscoelastic fluids with InterMIGs

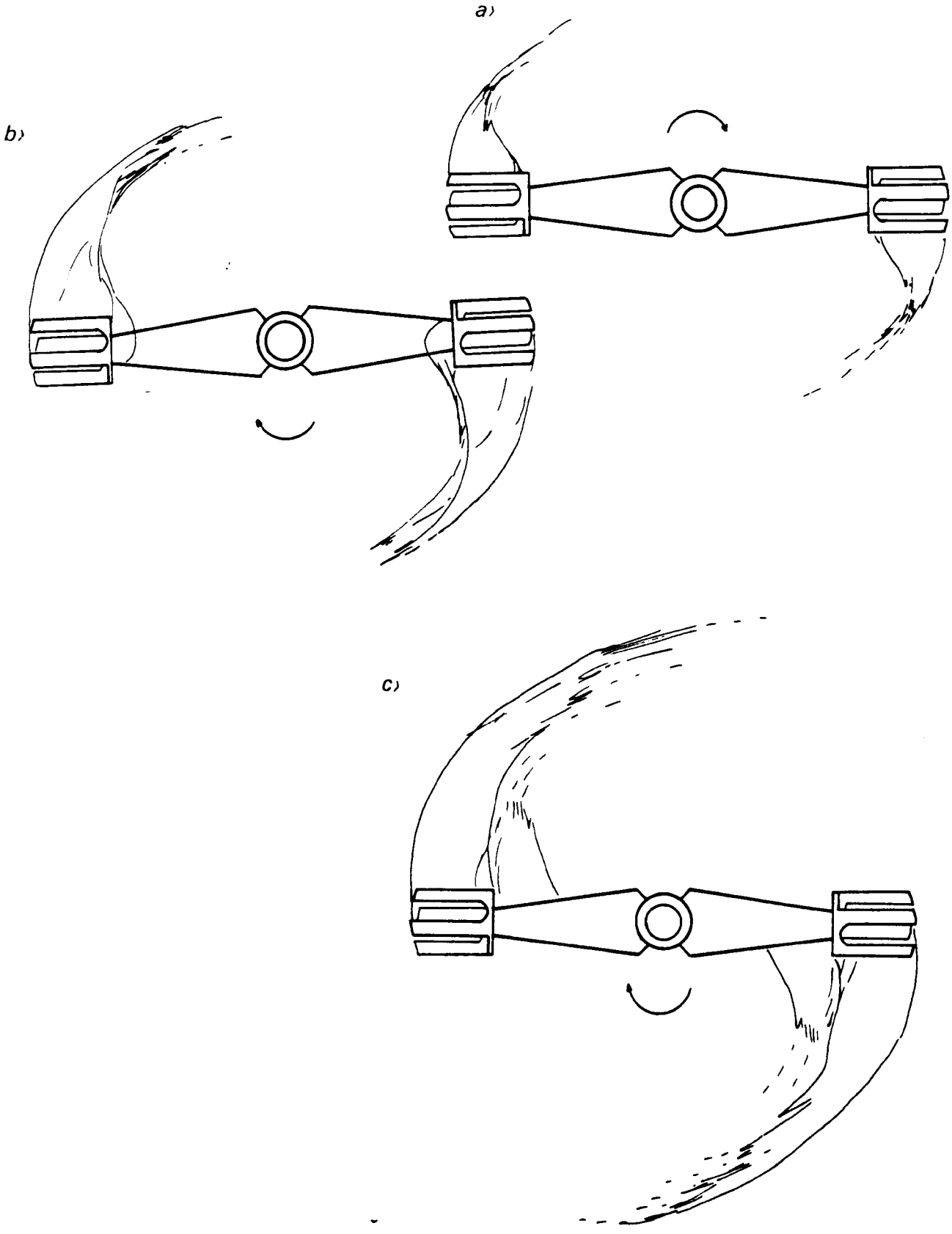

presence of tiny bubbles. With Rushton turbines, cavities formed in the transitional flow regime with viscous Newtonian glycerol were different from those observed in the turbulent flow regime. In viscoelastic fluids, mainly two other types of cavities were observed with Rushton turbines: *anvil* (or *split*) and large cavities as reported previously by Ranade and Ulbrecht (1977) and Nienow et al (1983). Anvil cavities are schematically presented in *Figure VIII.1.a* and shown in *Photograph VIII.2.a*. Large cavities can be found in *Figure VIII.1.b* and *Photograph VIII.3.a*. Cavities formed behind the blades of InterMIGs are presented in *Figure VIII.2*. The major difference of these cavities from those observed in Newtonian fluids was that the tip of the cavities were not smooth. Examples are also given in *Photographs VIII.4.a* and *VIII.5.a*.

VIII.3.2 Stable cavities in viscoelastic fluids

The stability of cavities in viscous Newtonian fluids against the changes in the gas flow rate was reported in the previous chapter (Section VII.3.2). Cavities formed under aeration above Fr_{min} (0.040- 0.045 for Rushton turbines and 0.060 for InterMIGs) remained stable also in viscoelastic fluids and even in a larger range of Reynolds numbers. The maximum Reynolds number for observing stable cavities was 400 in viscous Newtonian fluids, in viscoelastic fluids the stability was maintained until a Reynolds number of about 1000. The enhancement of the stability of cavities in viscoelastic fluids was probably a result of the tendency of the fluid to flow towards the impeller and the reduced dispersion capacity of the impeller on account of the mutually opposing viscoelastic and inertial forces.

It should also be noted that despite a great difference in the values of Re_{max} obtained with Newtonian glycerol and viscoelastic fluids, the same value of Fr_{min} was obtained in the three viscoelastic fluids and

Photograph VIII.2 Cavities with a single Rushton turbine (D= T/3) in one of the viscoelastic fluids (0.03% PAA in glycerol): N= 3.33 s^{-1}

a) cavities formed during aeration: Q_{GV}= 0.33 vvm

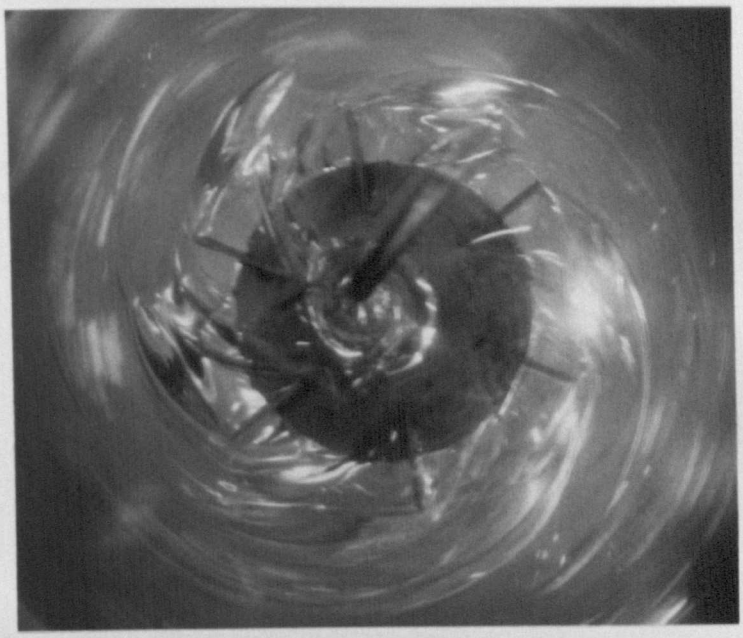

b) cavities that remain stable after the air supply is switched off: Q_{GV}= 0 vvm

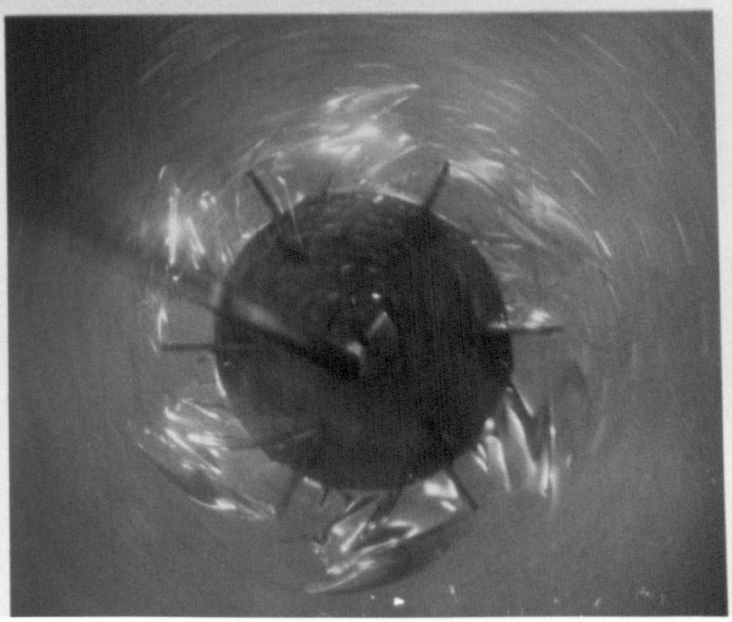

Photograph VIII.3 Cavities with a single Rushton turbine (D= T/3) in one of the viscoelastic fluids (0.03% PAA in glycerol): N= 5.0 s^{-1}

a) cavities formed during aeration: Q_{GV}= 0.33 vvm

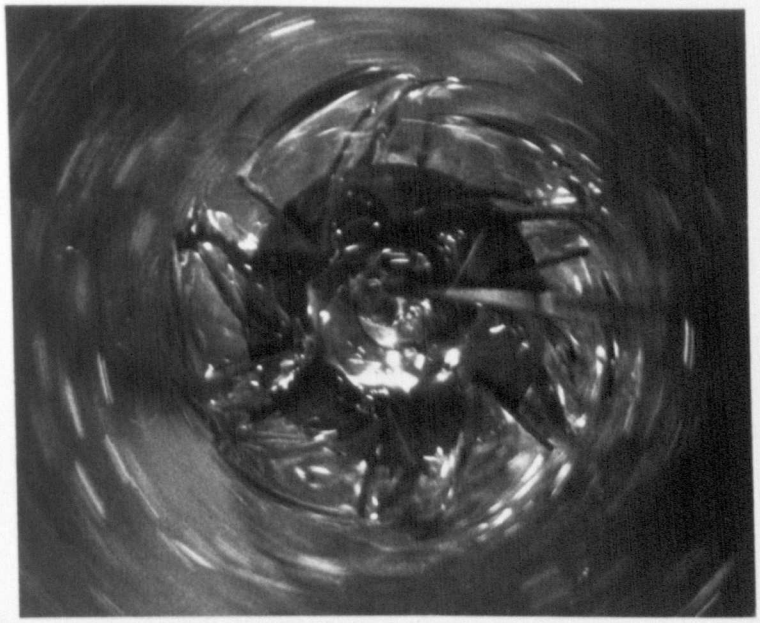

b) cavities that remain stable after the air supply is switched off: Q_{GV}= 0 vvm

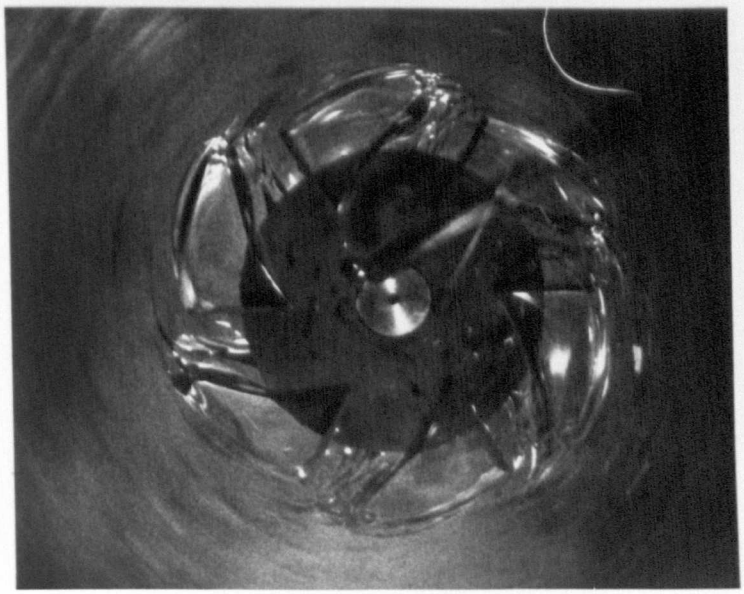

Photograph VIII.4 Cavities with a pair of InterMIGs in one of the viscoelastic fluids (0.03% PAA in glycerol): N= 2.0 s^{-1}

a) cavities formed during aeration: Q_{GV}= 0.33 vvm

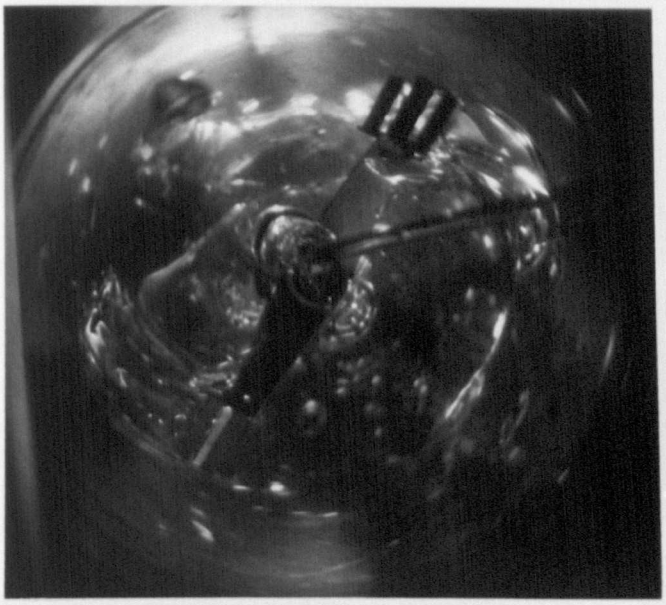

b) cavities that remain stable after the air supply is switched off: Q_{GV}= 0 vvm

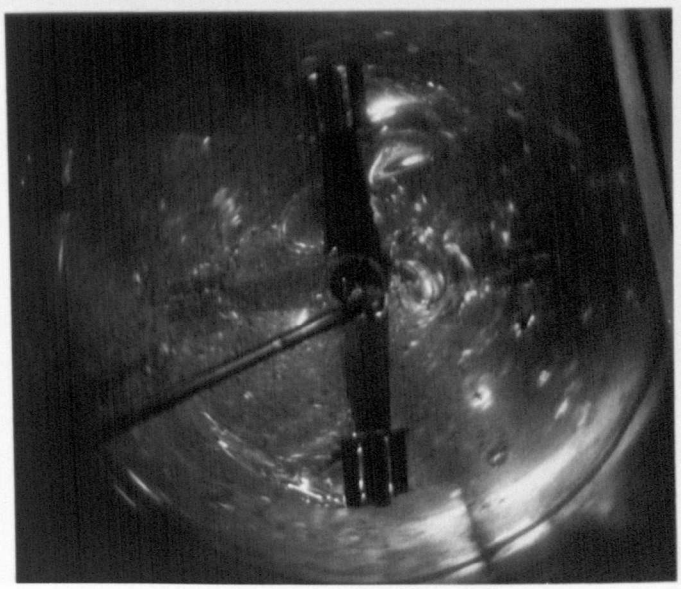

Photograph VIII.5 Cavities with a pair of InterMIGs in one of the viscoelastic fluids (0.03% PAA in glycerol): N= 2.5 s^{-1}

a) cavities formed during aeration: Q_{GV}= 0.33 vvm

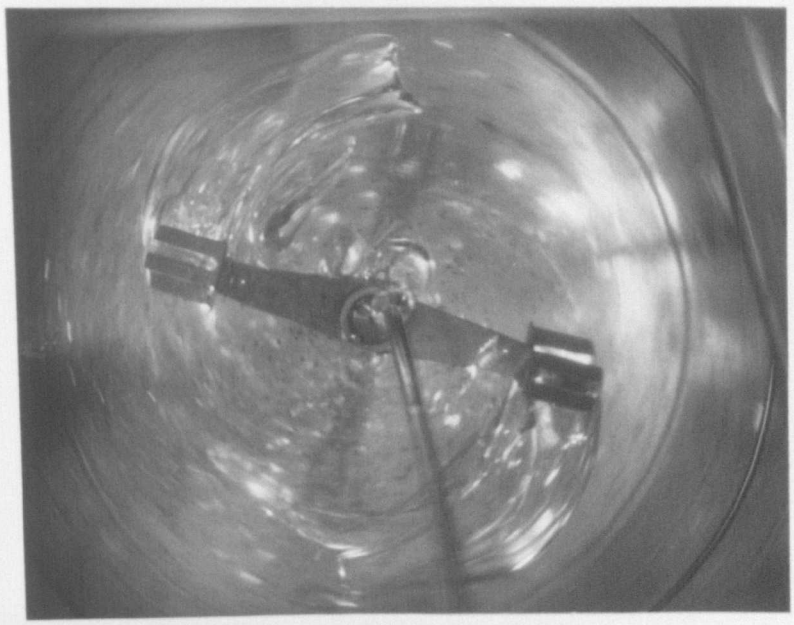

b) cavities that remain stable after the air supply is switched off: Q_{GV}= 0 vvm

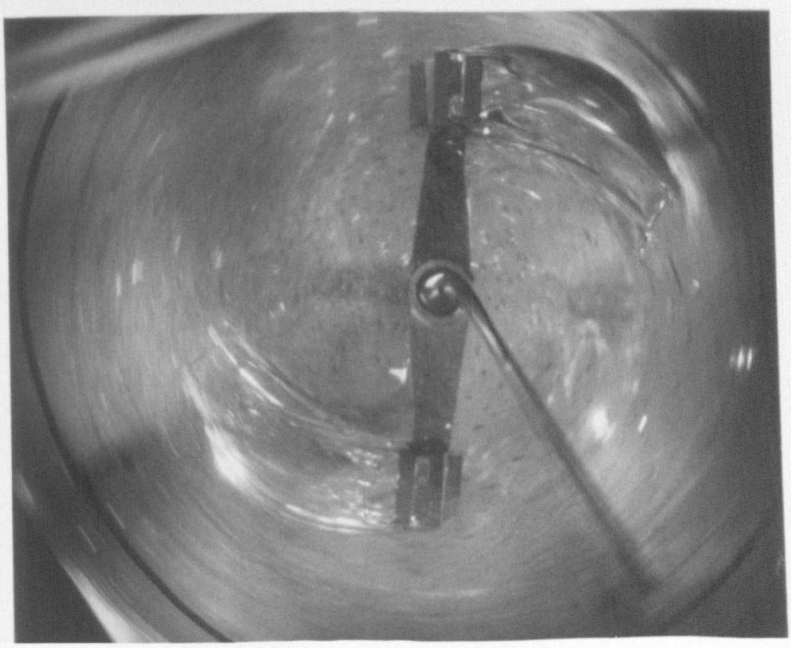

glycerol. Slightly different values for Fr_{min} were given by previous researchers: 0.017 (Bruijn et al, 1977), 0.08 (Ranade and Ulbrecht, 1978).

Photographs VIII.2.b, VIII.3.b VIII.4.b and *VIII.5.b* show some examples of stable cavities with Rushton turbines and InterMIGs.

VIII.4 POWER CHARACTERISTICS IN AERATED VISCOELASTIC FLUIDS

A range of Reynolds numbers between 40 to 1300 in the transitional flow regime was covered with the three viscoelastic fluids and the Elasticity numbers were less than 3.5×10^{-3}. The rheological properties of these fluids can be found in Chapter II. The equipment used was described in Chapters III and VI.

VIII.4.1. Effect of impeller speed and gas flow rate on the power consumed

Some examples of power curves obtained in viscoelastic fluids with Rushton turbines and InterMIGs are presented in *Figures VIII.3* to *VIII.8*. A comparison of the findings on the effects of impeller speed and gas flow rate in viscoelastic fluids with those obtained in viscous Newtonian glycerol is reported in the following paragraphs.

A minimum impeller speed allowing the formation of a substantial cavity size (Fr_{min}; 0.040 for Rushton turbines and 0.060 for InterMIGs) had to be exceeded in order for the power consumption to be reduced under aeration. As in glycerol (*Figures VII.9* and *VII.10*) aerated and unaerated Power numbers were almost identical at lower speeds (*Figures VIII.5* and *VIII.7*).

At speeds above Fr_{min}, power numbers decreased almost constantly for increasing impeller speeds due to growing cavity size (*Figures VIII.3, VIII.4, VIII.5* and *VIII.6*). A minimum in the power curve was not obtained with either Rushton turbines or InterMIGs. In Newtonian fluids (in both water

Figure VIII.3 Power curves of a Rushton turbine (D= T/2) at constant gas flow rates (viscoelastic fluid 1)

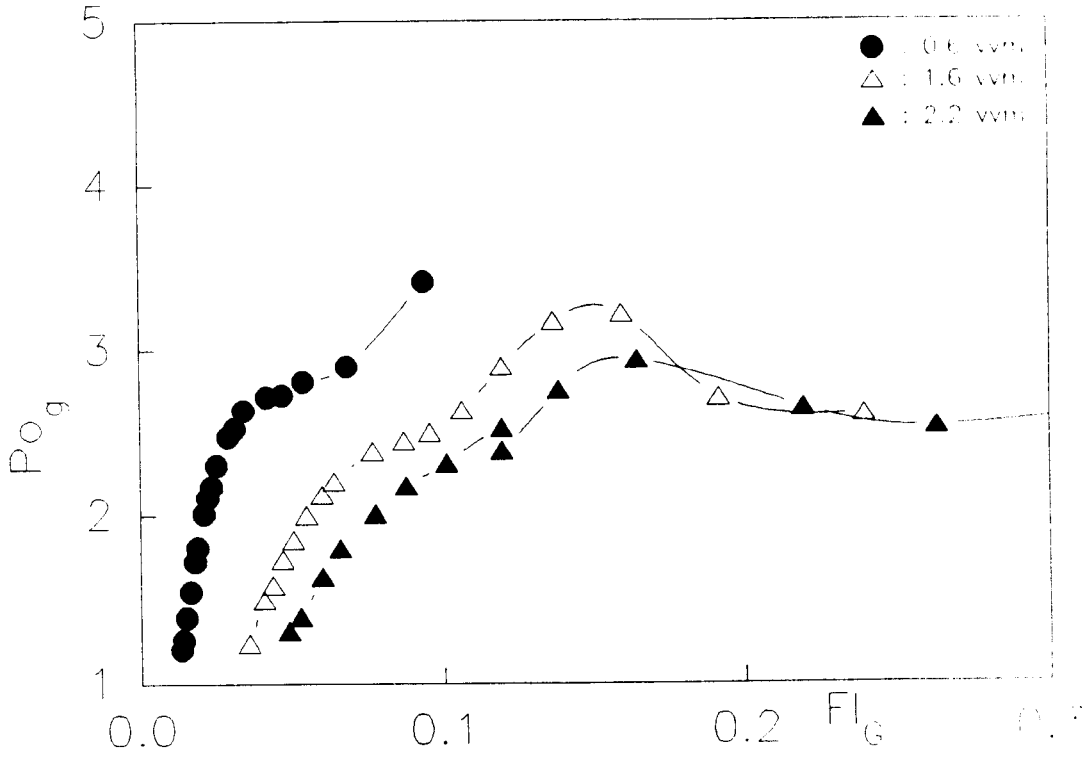

Figure VIII.4 Power curves of a pair of InterMIGs at constant gas flow rates (viscoelastic fluid 1)

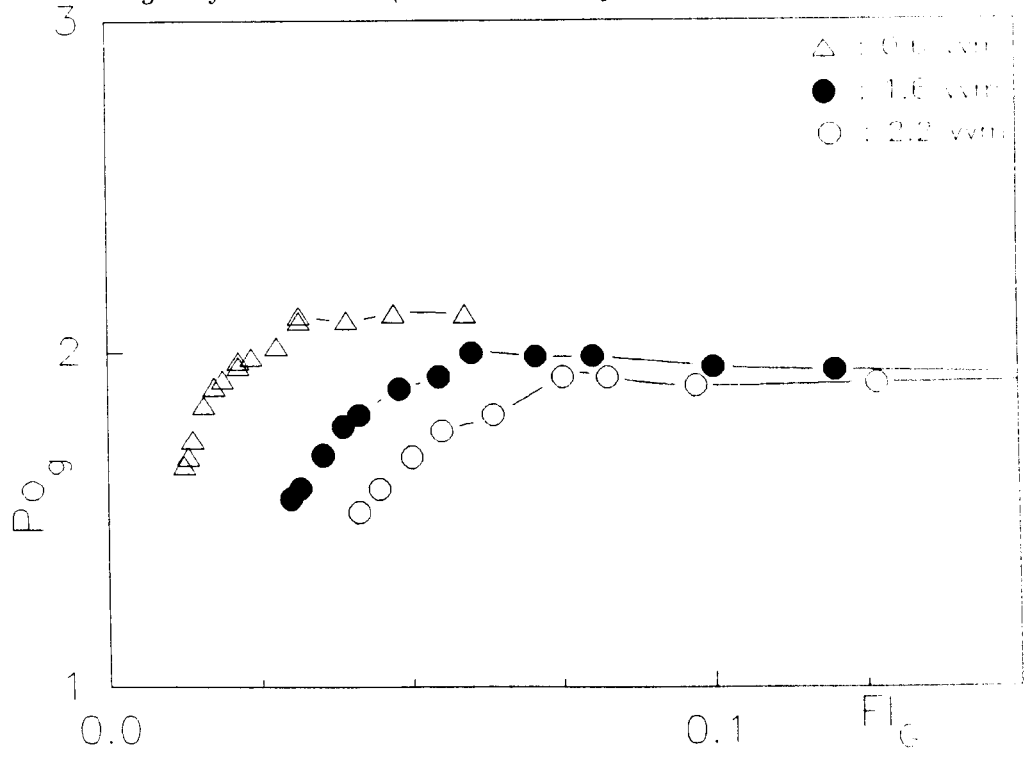

Figure VIII.5 Unaerated and aerated Power numbers for a pair of Rushton turbines (D= T/3) in a viscoelastic fluid of constant viscosity (Fluid 3)

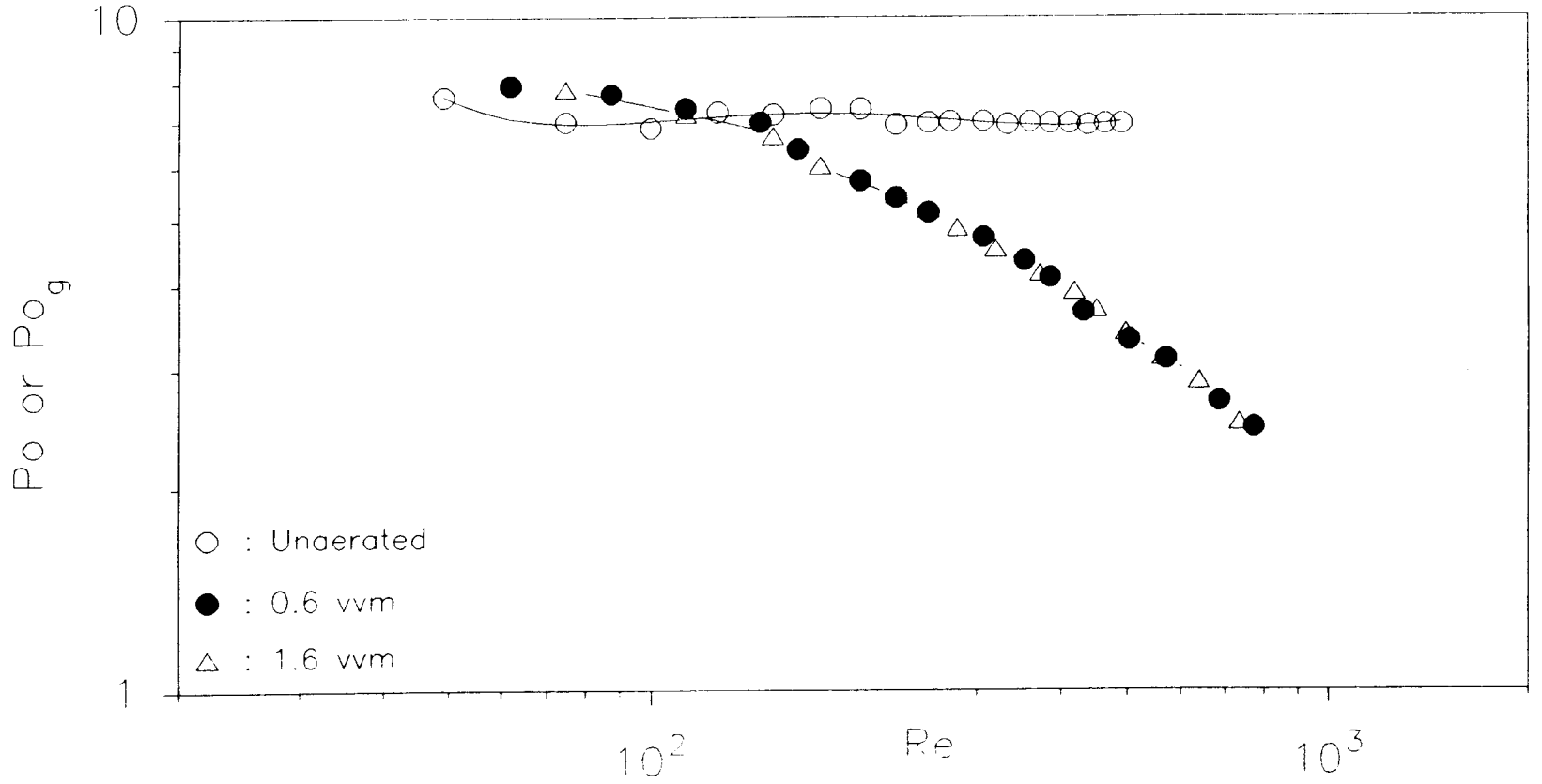

Figure VIII.6 Unaerated and aerated Power numbers for a pair of InterMIGs in a viscoelastic fluid of constant viscosity (Fluid 1)

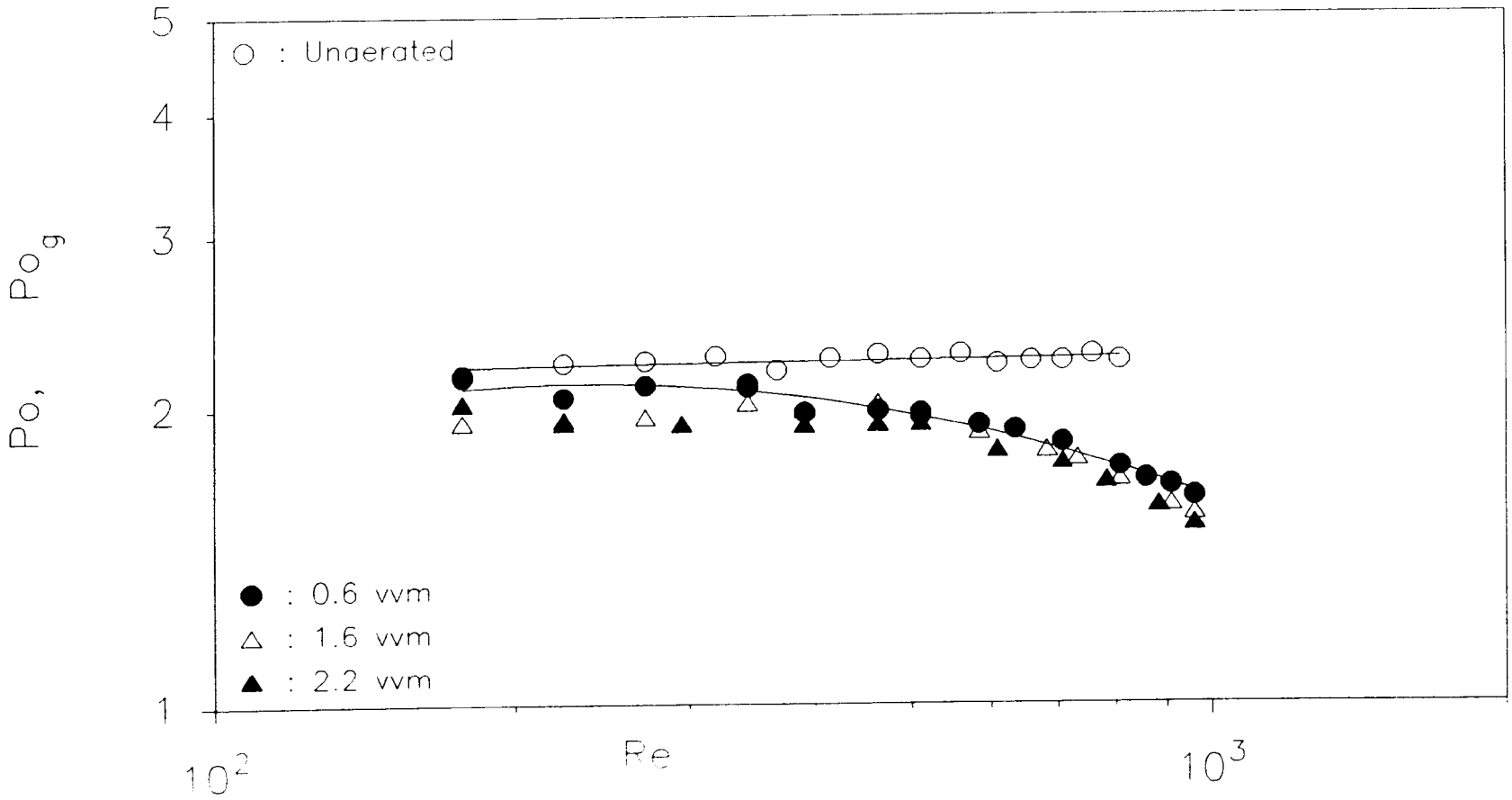

and glycerol), however, the power curves of Rushton turbines were characterised with minima (see Chapters VI and VII). These corresponded to the complete dispersion transitions in water. On account of their different geometric configuration, the power curves of InterMIGs did not make a minimum although the complete dispersion transition was visually observed in water. The absence of minima for Rushton turbines was confined to viscoelastic fluids (*Figures VIII.3* and *VIII.5*). This may be linked to the impeller hydrodynamics although it is in general difficult to assess local impeller hydrodynamics in highly viscous fluids where a wide spectrum of bubble size distribution is observed in a range of operational conditions and tiny bubbles retained in the bulk blur the vision. This is also true for the interpretation of the absence of a minimum Power number in viscoelastic fluids as power measurements could not be coupled with flow pattern observations. It can, however, be explained through the large size of cavities and the constricted secondary circulations. In viscous fluids the pumping capacity of the impellers is reduced by the large size cavities that form even at very low gas flow rates. This was probably accentuated in viscoelastic fluids where secondary flows were opposed by the viscoelastically driven flows. Consequently, the minimum was delayed and higher speeds were required to reach this transition.

Similar to the findings in viscous Newtonian fluids, aerated power numbers were independent of the gas flow rate also in viscoelastic fluids. The power consumption was only dependent on the impeller speed. This can be seen in *Figures VIII. 5* and *VIII.6*, where aerated power curves for different gas flow rates are superimposing as well as in *Figures VIII.7* and *VIII.8* which show the flat power curves obtained in a range of gas flow rates. However, in viscoelastic fluids the power consumption was independent of the value of the gas flow rate over a larger range of Reynolds numbers as would

Figure VIII.7 Power curves of a Rushton turbine (D= T/ 2) at constant impeller speeds (viscoelastic fluid 3)

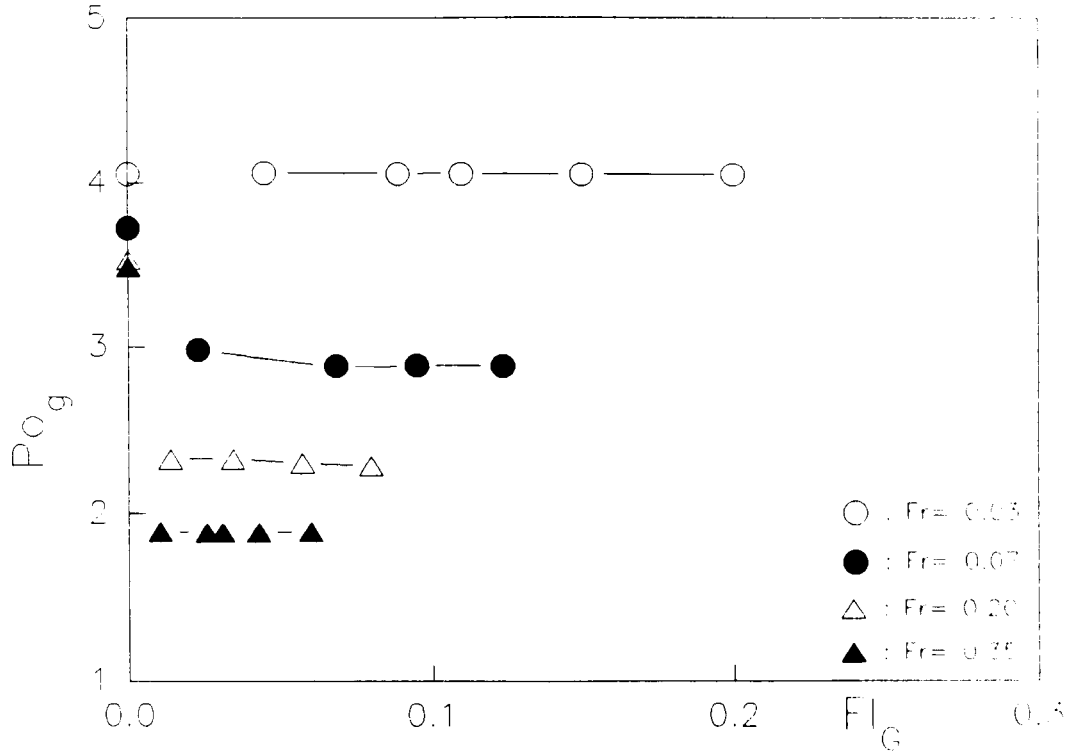

Figure VIII.8 Power curves of a pair of InterMIGs at constant gas flow rates (viscoelastic fluid 3)

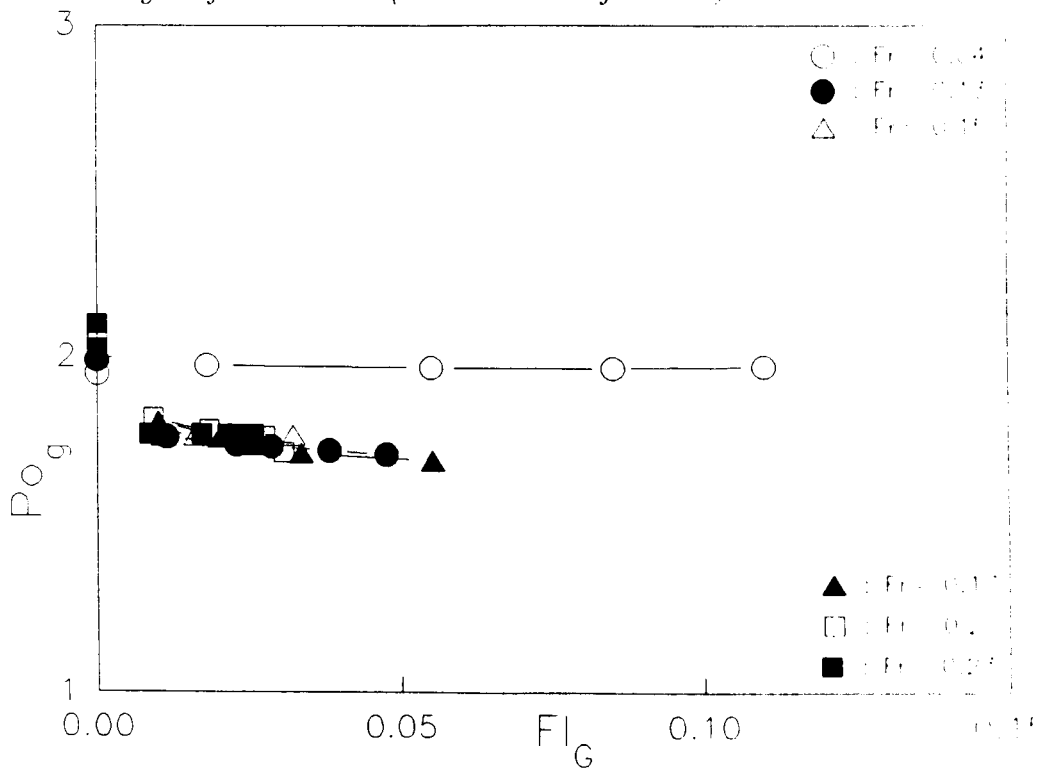

be expected from the enhanced cavity stability. In Newtonian glycerol, the power curves of Rushton turbines separated from each other according to the value of the gas flow rate above a maximum Reynolds number of about 400, (see Chapter VII). In viscoelastic fluids Re_{max} was about 1000 - a value that corresponds to previous findings[69,71] with rheologically complex fluids. The maximum Reynolds number at which this branching of power curves occurs could not be attained with InterMIGs. As a characteristic of these impellers, the power consumed was in general more stable to the changes in the gas flow rate in both glycerol and viscoelastic fluids.

The dependence of power consumption on the impeller speed with InterMIGs was also much weaker compared to Rushton turbines (*Figures VIII.6* and *VIII.8*) conforming with the findings in glycerol and water.

VIII.4.2 Power reduction under aeration

As explained above, the power reduction under aeration was independent of the value of the gas flow rate over a large range of Reynolds numbers due to viscous and viscoelastic fluid properties. As an impeller characteristic, the power consumed by InterMIGs had also a very weak dependence on the speed. Hence, the power was reduced much less with these impellers compared to Rushton turbines. The highest power reduction [(Po- Po_g)/ Po] was obtained with a small Rushton turbine. For an overall comparison made at a Reynolds number of about 580, the power reduction was about 60 - 65% for a single small Rushton turbine (D= T/3), and 55% for a pair of these; 45% for a single large Rushton turbine (D= T/2), 35% for two large turbines and only 14% for a pair of InterMIGs.

Power reduction on account of aeration was in general less with viscoelastic fluids than with Newtonian glycerol and this reduction decreased slightly for increasing levels of elasticity.

VIII.4.3 Effects of viscoelasticity on aerated power consumption

Aerated power numbers were in general higher in viscoelastic fluids compared to those obtained in Newtonian glycerol. This can be seen in *Figures* from *VIII.9* to *VIII.12* where power curves obtained in Newtonian glycerol and viscoelastic fluids are plotted together. Data obtained in a range of experiments with InterMIGs and Rushton turbines at constant gas flow rates or constant impeller speeds are presented in these Figures. An enhancement of power numbers with viscoelastic fluids was also found in single phase systems where power numbers increased further for increasing levels of viscoelasticity (see *Figures IV.6* and *IV.7*). However, under aerated conditions, viscoelastic effects manifested themselves regardless of this fluid property : aerated power curves for the three viscoelastic fluids were superimposed above the inelastic one as can be seen in *Figures VIII.9* to *VIII.12*.

The power consumed in single phase system is closely related to the secondary flow patterns generated. Hence, the higher power drawn under unaerated conditions would be associated to the interaction of the viscoelastically driven flows with those of inertially driven flows. Under aerated conditions, tertiary flows and the cavities formed behind the impeller blades predominantly determine the power consumption as explained in Chapter VI. Tertiary flows behind impeller blades were not studied previously in viscoelastic fluids. However from a previous work[116], it is known that the wake behind fins is suppressed in viscoelastic fluids. The results in this study also suggest that the flow around the impeller blades and the size of cavities formed were modified in viscoelastic fluids and the size of cavities were smaller. A low level of viscoelasticity was sufficient for this, further increases had only a slight effect, if any.

Figure VIII.9 Power curves for inelastic glycerol and viscoelastic fluids with a pair of 6DT (D=T/2) at a constant gas flow rate of 1.6 vvm

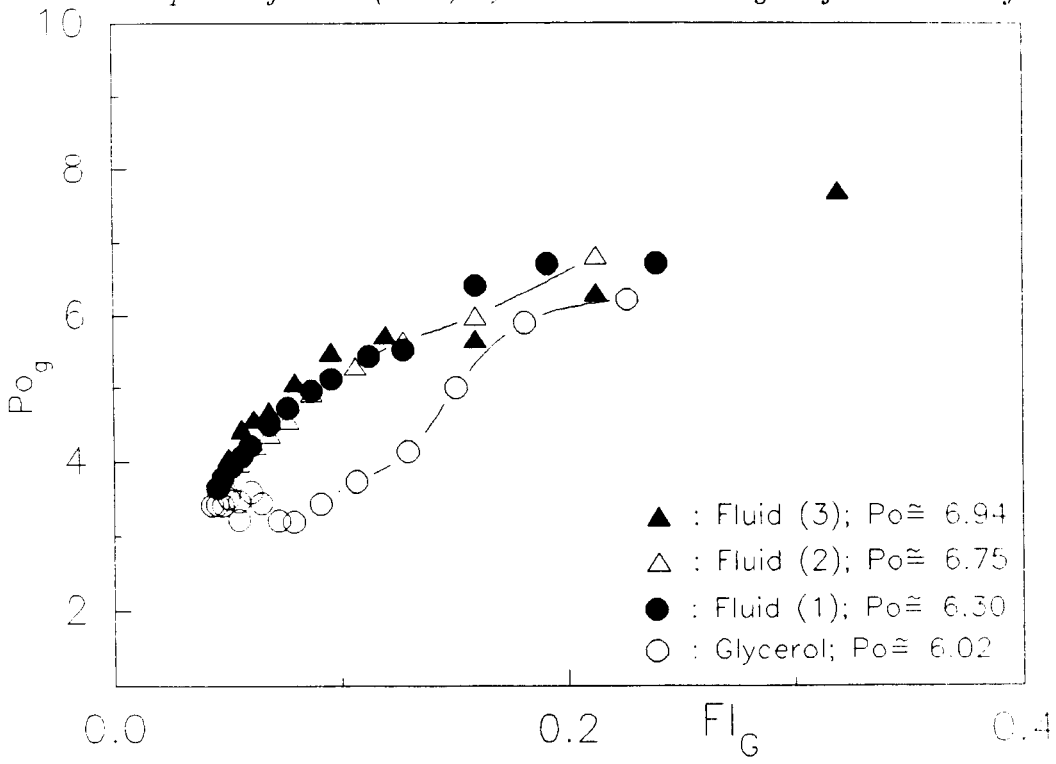

Figure VIII.10 Power curves for Newtonian glycerol and viscoelastic fluids with a pair of InterMIGs at a constant gas flow rate of 1.6 vvm

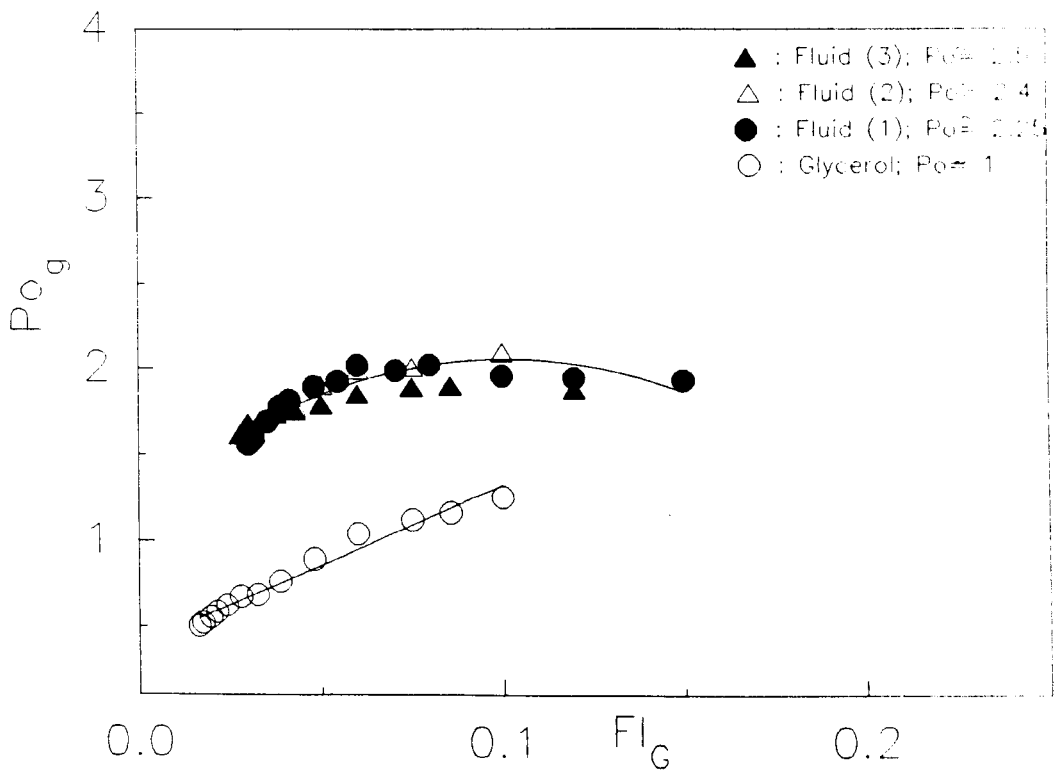

Figure VIII.11 Power curves for inelastic glycerol and viscoelastic fluids with a 6DT (D= T/3) at a constant speed of 1.7 s^{-1}

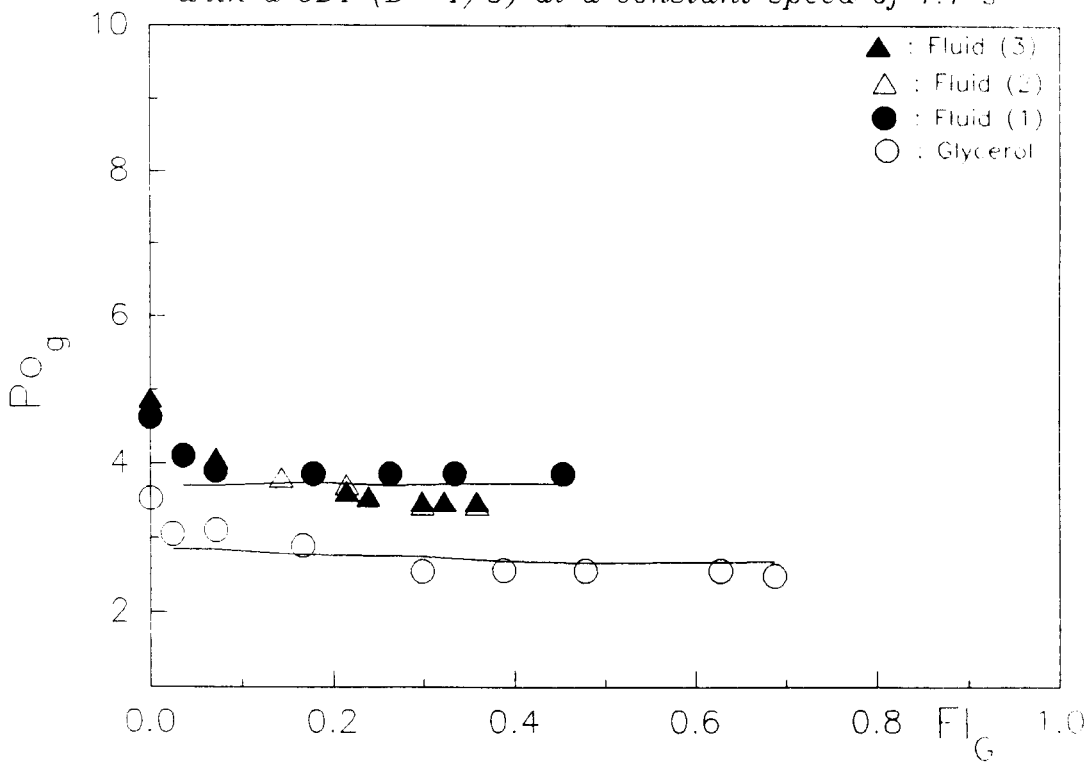

Figure VIII.12 Power curves for Newtonian glycerol and viscoelastic fluids with a pair of InterMIGs at a constant impeller speed of 2.3 s^{-1}

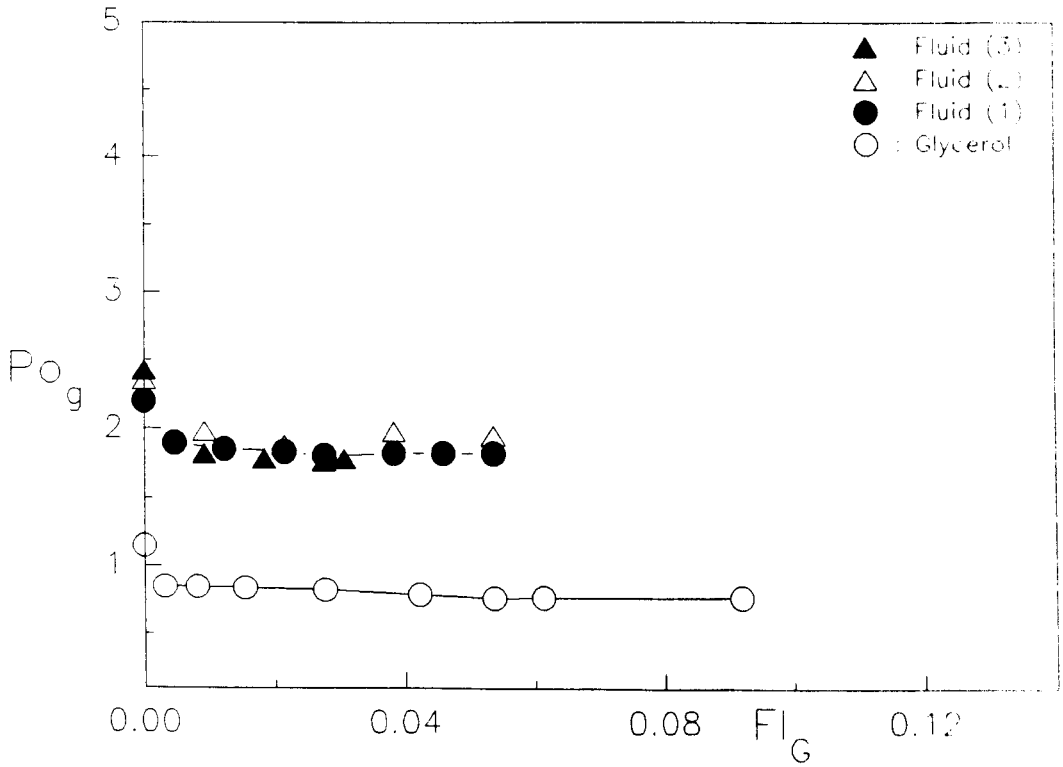

The difference in Power numbers obtained with viscoelastic fluids and Newtonian glycerol was evaluated with

$$\frac{|Po_{elast.} - Po_{inelast.}|}{Po_{elast.}}$$

at a given Reynolds number. Parallel to the findings under unaerated conditions, the enhancement of Power numbers was more pronounced with InterMIGs: up to 70%. With Rushton turbines, the increase was found to be more important for two impellers compared to a single one of the same diameter: up to about 50% with a single small Rushton turbine (D= T/3) and 60% with a pair of this; 27% with a large impeller (D= T/2) and 40% with a pair.

VIII.5 CONCLUSIONS

Bulk flow patterns, cavities and power consumption were studied under aerated conditions using viscoelastic fluids of shear independent viscosity. A comparison of these results with those obtained in Newtonian glycerol has enabled to study the effects of viscoelasticity in the absence of other rheological complexities.

The overall features of bulk flow patterns were similar to those in viscous Newtonian glycerol where the outer blades pumped radially outwards and the inner blades upwards. The hydrodynamic state of the impeller could not be determined since a spectrum of bubble size distribution was observed in a range of operational conditions. The secondary flows were in general found to be constricted due to the mutually opposing action of viscoelastically and inertially driven flows and also on account of the cavities that surrounded the impeller and reduced the pumping capacity of

this.

Cavities, hence the power consumed, were stable against the changes in the gas flow rate similar to the findings in viscous Newtonian glycerol. Viscoelasticity accentuated this stability and the power consumed was dependent on the impeller speed in a larger range of Reynolds numbers. With InterMIGs, power consumption was found to be much less sensitive to the variations in the gas flow rate and even the impeller speed conforming with the findings in water and glycerol. This appears to be an impeller characteristic.

Aerated power numbers in viscoelastic fluids were higher than those in Newtonian fluids as was also found in single phase systems. However, under unaerated conditions an enhancement of power numbers was noted for increasing levels of viscoelasticity whereas under aeration this enhancement was independent of the polymer concentration. A certain level of fluid viscoelasticity was sufficient to modify the tertiary flow patterns and the size of cavities behind the impeller blades; further increases did not have any effect.

IX. GENERAL CONCLUSIONS

This Chapter consists of two sections where major findings and conclusions from various aspects of this study are presented (Section IX.1) and suggestions are made to extend this work in future studies (Section IX.2).

IX.1 CONCLUSIONS

Before a general evaluation of the findings and conclusions, some of the interesting experimental aspects of this work can be highlighted as follows:

i) Model fluids prepared adding trace amounts of the polymer polyacrylamide in a viscous Newtonian fluid- glycerol, exhibited viscoelasticity with an almost shear- independent viscosity. These "Boger fluids" offered the advantage of studying the effects of viscoelasticity in the absence of other rheological properties. Comparisons of the data could be made easily with those obtained in viscous Newtonian glycerol covering the transitional flow regime (Re< 1300). Trends obtained previously regarding the effects of viscoelasticity in the transitional flow regime, where fluids of complex rheology were used, vary considerably. In a few recent studies, Boger fluids were used but these were mostly confined to unaerated conditions. In this study, non-linear viscoelastic properties- first normal stress differences- were quantified and in the relatively large scale of operation (T= 0.61m) the Elasticity numbers were less than 3.5×10^{-3}. The effects of viscoelastic fluid properties under both unaerated and aerated conditions could be identified in this range.

Another advantage of these fluids was that the dependence of the first normal stress difference on the shear rate was close to a quadratic one, b values ranging from 1.7 to 1.9, which meant that the dependence of the Elasticity number the impeller speed and hence Reynolds number was not very

important.

ii) A new experimental technique (fluorescent dye- fiber optic technique) was adapted to measure mixing times in viscous fluids. Most conventional methods cannot be used in viscous fluids, others present various shortcomings. Fluorescent dye-fiber optic technique could successfully be used in viscous fluids to measure mixing times without altering the physical properties of the bulk.

iii) A relatively new type of impeller, InterMIGs, were studied to compare their characteristics with those of Rushton turbines. Previous studies with these impellers were mostly carried out in relation to xanthan fermentations on account of their potential advantages in systems where the viscosity and the rheological properties of the bulk change.

Prior to studies in viscous fluids in the transitional flow regime, experiments were conducted in water for a preliminary characterisation of InterMIGs.

A pair of InterMIGs was found to acquire much lower power numbers than a single Rushton turbine in all the three types of fluids (water, glycerol and viscoelastic fluids).

InterMIGs were flooded in water only at very low impeller speeds and high gas flow rates. They discharged the gas in a range of operational conditions and the flooding- loading transition was not as obvious as with Rushton turbines. Correlations to predict the operational conditions to completely disperse gas in water and the specific power input at this transition were obtained. The visually observed complete dispersion transition was not marked with a minimum in the power curve as with Rushton turbines. One advantage of these impellers was that they were characterised by gradual changes in terms of the transitions between different hydrodynamic

states, formation of different cavity types and power reduction under aeration not only in water but also in viscous fluids. Another advantage of using InterMIGs was that on account of their geometry, the power demand for the complete dispersion transition in water and in general aerated power consumption in all Newtonian and viscoelastic fluids was much less sensitive to the changes in the gas flow rate. These impellers proved to be more stable to the changes in the gas flow rate which makes the prediction of aerated power consumption easier.

Manufacturers' claims regarding the direction of rotation of InterMIGs were confirmed: rotating anticlockwise, as viewed from the vessel base, is recommendable.

When rotated in this direction, the inner blades pumped upwards, the outer blades downwards in water. In viscous fluids, the outer blades were observed to discharge radially outwards. In the relatively low range of Elasticity numbers covered, these secondary flow patterns were not reversed, but the radially outward flows from Rushton turbines and from the outer blades of InterMIGs were constricted.

Since the extent of secondary flow patterns were reduced in viscoelastic fluids, mixing times (at equal power per unit volume) were higher than those measured in Newtonian glycerol. InterMIGs were more energy efficient in reaching a required degree of homogeneity in low and high viscosity Newtonian fluids. In viscoelastic fluids, the upward flows from the inner blades of InterMIGs were reinforced being in the same direction as that of viscoelastically driven flows which in turn enhanced the effect of viscoelasticity interfering with the radially outward flows from the outer blades. Hence, the enhancement of mixing times in viscoelastic fluids was more important with InterMIGs and their efficiency was comparable to that of

a single Rushton turbine.

Under unaerated conditions, the power required to sustain a radially outward discharge despite the opposing action of viscoelastically driven flows was higher (at a given Reynolds number) for all impeller types. Power consumption increased further for increasing levels of viscoelasticity. The complicated interaction of the viscoelastically and inertially driven flows for InterMIGs resulted in a more important increase in the power consumption.

Power numbers in viscoelastic fluids were also found to be higher under aerated conditions than in Newtonian fluids. Since the aerated power consumption is closely related to the cavities formed behind impeller blades, this enhancement can be interpreted in terms of the modification of the tertiary flows and cavities by viscoelastic fluid properties. For aerated conditions, the enhancement of power numbers was independent of the level of fluid viscoelasticity.

An interesting aspect of mixing viscoelastic fluids under aeration was the stability of cavities and consequently the power consumption with respect to the variations in the gas flow rate. This stability was in general more pronounced with InterMIGs. In viscous fluids, power consumption was dependent only on the impeller speed in a range of Reynolds numbers. Hence, when operated in this stable zone, changing the gas flow rate or a total failure of the gas supply will not result in a drastic increase of the power consumed. Viscoelasticity was found to accentuate this stability.

Apart from a better understanding of the importance of viscoelasticity in stirred tanks for a given range of Elasticity numbers, InterMIGs were characterised in relation to viscous and viscoelastic fluid properties in this study. These impellers presented various advantages in low and high viscosity Newtonian fluids in comparison to Rushton turbines. They were found

to undergo viscoelastic effects more severely on account of their geometry and their performance was therefore comparable to that of a single large Rushton turbine. They appear to be a better choice for processes where bulk liquid viscosity and other rheological properties change over the course of time.

Suggestions to extend this study further are made in the following section.

IX.2 SUGGESTIONS FOR FUTURE WORK

In this Section a number of suggestions are made as guidelines to extend the findings of this study in future:

1) Single phase fluid hydrodynamics: In this study, the effects of viscoelasticity on impeller performance were investigated in relation to fluid hydrodynamics where fluid flow patterns were only visually observed. This can be extended by carrying out local fluid velocity measurements with a laser-doppler anemometer. Such quantitative analysis of velocity fields will contribute to the understanding of the interaction of viscoelastically and inertially driven flows especially for impellers of complicated geometry such as InterMIGs. It can then be envisaged to numerically predict the flow fields for viscous and viscoelastic fluids as previous work carried out in the field is mostly confined to classical impellers.

2) Mixing equipment: This study on the effect of fluid viscoelasticity on impeller performance was focused on InterMIGs to compare their performance with the classical six bladed disc turbines. It was revealed that the elastically driven flows interacted in a complicated way with the inertially driven flows originating from the inner and outer blades of InterMIGs that pump in different directions. Simple axial flow impellers can be studied for

a better understanding of the impact of viscoelasticity on axial flows induced by the impeller- although axial flow impellers may not be a potentially better choice for retrofitting where viscoelastic fluids are concerned (axial flows are more liable to promote segregated zones below and above the plane of the impeller). The study can also be extended to other impeller types- e.g. a combination of an axial and a radial impeller.

Two phase studies were mostly carried out with a point sparger. Previous studies in water have shown that large ring spargers enhance the gas handling capacity of impellers prior to flooding (Nienow et al, 1988,b). Other sparger types can be investigated although in viscous fluids, where cavity formation and gas dispersion processes are different, sparger type may not be as important as in low viscosity fluids.

3) Mixing time measurements: Various modifications can be considered to improve the experimental arrangements for mixing time measurements in future work:

a) For mixing time measurements, it is important to ensure short and reproducible injection times. The quantity of dye added with the fluorescent dye- fiber optic technique was very small compared to that in other methods. Therefore errors due to manual injection with a syringe can be considered minimal. However, an automatic injection system can be devised for future work.

b) Coupling this measuring device to a digital computer can greatly enhance data acquisition and analysis functions. The accuracy of the mixing time readings can thus be improved. On the other hand, an up - to - date data acquisition unit of high accuracy and sampling rate will enable to store large quantities of data points on which detailed analysis can be accomplished, e.g. corrections taking into account response characteristics

may be made.

c) The PMT module used was one already available in the Department. Recent models may have faster response characteristics. Further modifications other than increasing the gain can also be considered to reduce the time constant.

d) In this study, mixing times were measured at the impeller discharge. Results obtained for the impeller types used in common with those in a previous work where the colorisation- decolorisation technique was used were comparable. However, it would in general be preferrable to make measurements at various locations in viscous fluids where stagnant zones may form and last for long periods, This is even more important with viscoelastic fluids especially if the range of Elasticity numbers that create segregated zones is covered.

4) On the effects of viscoelasticity: Results obtained on the effect of viscoelasticity can be complemented with heat and mass transfer studies. From the findings of this study, it can be expected that heat transfer and oxygen mass transfer will be reduced in the presence of viscoelasticity. It would, however, be interesting to obtain the quantitative data as previous studies in this area are limited. It should be noted that this would also require measurements at various positions in the bulk.

SYMBOLS

A	Constant in eqn. II.9	(kg s^{b-2} m^{-1})
b	Constant in eqn. II.9	(dimensionless)
C	Impeller clearance from the vessel base	(m)
C_i	Inter-impeller spacing for a pair of impellers	(m)
D	Impeller diameter	(m)
E	Energy	(J, kg s^{-2} m^2)
El	Elasticity number (eqn. IV.6)	(dimensionless)
Fl_G	Aerated Flow number	(dimensionless)
Fr	Froude number (eqn. III.5)	(dimensionless)
g	Acceleration due to gravity	(m s^{-2})
H_L	Liquid height in the vessel	(m)
k_s	Constant in eqn. IV.1	(dimensionless)
K	Consistency index	(Pa s^n, kg s^{n-2} m^{-1})
K_p	Constant in eqn. III.8	(dimensionless)
M	Impeller torque	(kg s^{-2} m^2)
n	Flow behaviour index	(dimensionless)
N	Impeller speed	(s^{-1})
N_1	First normal stress difference	(Pa, kg s^{-2} m^{-1})
N_2	Second normal stress difference	(Pa, kg s^{-2} m^{-1})
P	Power dissipated by the impeller	(W, kg s^{-3} m^2)
P_g	Power dissipated under aeration	(W, kg s^{-3} m^2)
Po	Power number (eqn. III.3)	(dimensionless)
Po_g	Power number under aeration (eqn. VI.1)	(dimensionless)
Q_G	Gas flow rate	($m^3 s^{-1}$)
Q_{GV}	Gas flow rate	(vvm)
Re	Reynolds number (eqn. III.4 and IV.4)	(dimensionless)
T	Tank diameter	(m)

T	Tank diameter	(m)
T_o	Reference tank diameter in eqn. III.10	(m)
t_c	Circulation time	(s)
t_m	Mixing time	(s)
V	Liquid volume in the vessel	(m^3)
w	Blade width	(m)
Wi	Weissenberg number (eqn. II.11 and IV.5)	(dimensionless)
x_1	Disc thickness of a six bladed disc turbine and inner blade thickness of InterMIGs	(m)
x_2	Blade thickness of a six bladed turbine and outer blade thickness of InterMIGs	(m)

Greek

ε	Specific power input	(kg s^{-3} m^{-1})
$\dot{\gamma}$	Shear rate	(s^{-1})
ρ	Fluid density	(kg m^{-3})
μ	Fluid viscosity	(Pa s, kg s^{-1} m^{-1})
μ_0	Zero shear limiting viscosity	(Pa s, kg s^{-1} m^{-1})
μ_∞	High shear limiting viscosity	(Pa s, kg s^{-1} m^{-1})
μ_a	Apparent viscosity	(Pa s, kg s^{-1} m^{-1})
τ	Shear stress	(Pa, kg s^{-2} m^{-1})
τ_y	Yield value for a plastic fluid	(Pa, kg s^{-2} m^{-1})
ψ_1	First normal stress diff. coefficient	(N $s^2 m^{-2}$)
ψ_2	Second normal stress diff. coeff.	(N $s^2 m^{-2}$)

Superscripts and subscripts

max	Maximum
min	Minimum
SA	Surface aeration
av	Average
F	Flooding
CD	Complete dispersion
g	Under gassed conditions

REFERENCES

1) ALLSFORD, K.V. (1985) Gas-liquid dispersion and mixing in mechanically agitated vessels with a range of fluids. PhD Thesis. Univ. of Birmingham

2) ANDERSON, C.; LE GRYS, G.A. and G.L. SOLOMONS (1982) Concepts in the design of large scale fermenters for viscous culture broths. The Chemical Engineer (February, 1982) p: 43- 49.

3) ATKINSON, B. and F. MAVITUNA (1991) Flow behaviour of fermentation broths (in "Biochemical Engineering and Biotechnology Handbook" M stockton press) p: 672-725.

4) BARNES, H.A.; HUTTON, J.F. and K. WALTERS (1988) An introduction to rheology. Elsevier.

5) BATES, R.L.; FONDY, P.L. and R.R. CARPSTEIN (1963) An examination of some geometric parameters of impeller power. Ind. Eng. Chem.- Proc. Des. Dev., Vol.2, No.4, p:310-314

6) BELL,R.(1972) Experimental determination of residence time distributions on commercial scale distillation trays using a fiber optic technique. A.I.Ch.E.J. (18), No.3, p: 491-497.

7) BOGER,D.V. (1977) A highly elastic constant viscosity fluid. Jrnl. of non-Newtonian Fl. Mech. (3) p:87-91

8) BOGER,D.V. and H. NGUYEN (1978) A model viscoelastic fluid. Polymer Eng. and Science, Vol.18, No.13, p:1037-1043

9) BOGER,D.V. (1980) Separation of shear-thinning and elastic effects in experimental rheology. 8th Int. Conf. on Rheology, Naples, Vol.1 (by Astarita, G.; Marucci,G. and L. Nicolais) Italy, p:195-218

10) BOUWMANS, I. and H.E.A. VAN DER AKKER (1990) The influence of viscosity and density differences on mixing times in stirred vessels. Fluid Mixing 4. I.Chem.E. Sypm. Series, No. 121 p: 1-12

11) BRAUER, H. (1979) Power consumption with aerated stirred tank reaction systems. Advances in Biochem Eng., Vol.18, p:87-119

12) BRITO DE LA FUENTE, E.; LEULIET, J.C.; CHOPLIN, L. and P.A. TANGUY (1990) Mixing and circulation times in rheologically complex fluids. Fluid mixing 4 I.Chem.E. Symp. Series No 121 p:75-96

13) BRITO DE LA FUENTE, E.; LEULIET, J.C.; CHOPLIN, L. and P.A. TANGUY (1991) On the role of elasticity on mixing with a helical ribbon impeller. Trans. I. Chem.E., (69) Part a, p: 324- 331.

14) BRODKEY, R.S. (1966) Fluid motion and mixing (in "Mixing: theory and practice"- Editors: Uhl, V.W. and J.B. Gray; Academic Press New York) p:7-105.

15) BRODKEY, R.S. (1985) Fundamentals of turbulent mixing and kinetics (in "Mixing of liquids by mechanical agitation" - Editors: Ulbrecht J.J. and G.K. Patterson; Gordon and Breach Publishers New York) p: 29-59.

16) BRUIJN, W.; VAN'T RIET, K. and J.M. SMITH (1974) Power consumption with aerated Rushton turbines. Trans. Inst. Chem. Eng. - Vol.52, p:88-104

17) BUJALSKI, W. (1986) Three phase mixing: Studies of geometry, viscosity and scale. Ph.D. Thesis, University of Birmingham.

18) BUJALSKI, W.; NIENOW, A.W.; CHATWIN, S. and M. COOKE (1986) The dependency on scale material thickness of power numbers of different impeller types. Colloque d'Agitation Mecanique (ENSIGC-Tolouse) p:1/37-1/47

19) BUJALSKI, W.; NIENOW, A.W.; CHATWIN, S. and M.COOKE (1987) The dependency on scale material thickness of power numbers of Rushton disc turbines. Chem. Eng. Sci., Vol.42, p:317-326

20) BURMESTER, S.S.H.; RIELLY, C.D. and M.F. EDWARDS (1991) The mixing of miscible fluids with large differences in density and viscosity. Proc. of the 7th Eur. Conf. on Mixing (18-20 Sept. 1991, Brugge) p: 9-16.

21) CARREAU, P.J.; PATTERSON, I. and C.Y. YAP (1976) Mixing of viscoelastic fluids with helical ribbon agitators I- Mixing time and flow patterns. The Can. J. of Chem. Eng. Vol. 54, p: 135-142.

22) CARPENTER, K. (1992) Interview- Towards a flexible impeller. The chemical Engineer. No. 527 (24 Sept.1992)

23) CHANG, J.C. and M.M. DENN (1979) An experimental study of isothermal spinning of a Newtonian and a viscoelastic fluid. Jrnl. of Non-Newt. Fl. Mech. (5) p:369-385

24) CHAPMAN, C.M.; NIENOW, A.W.; COOKE, M. and J.C. MIDDLETON (1983) Particle- gas- liquid mixing in stirred vessels Part2 :gas - liquid mixing. Chem. Eng. Res. Des. Vol.61, p: 82- 95.

25) CHATWIN, S. and A.W. NIENOW (1985) Successful power measurement in agitated vessels. Lab. Sci. and Tech. September p:19.

26) CHAVAN, V and J.J. ULBRECHT (1973) Power correlations for close clearance helical impellers in non-Newtonian liquids. Ind. Eng. Chem. Proc. Des. Dev. (12), p:472.

27) CHAVAN, V.V.; ARUMUGAM, M. and J.J. ULBRECHT (1975) On the influence of fluid elasticity in a vessel agitated by a combined ribbon screw impeller. A.I.Ch.E.J. (21), p: 613-615.

28) COLLIAS, D.J. and R.K. PRUD'HOMME (1985) The effect of fluid elasticity on power consumption and mixing times in stirred tanks. Chem. Eng. Sci., (40), 8, p:1495-1505.

29) COOKE, M.; MIDDLETON, J.C. and J.R. BUSH (1988) Mixing and mass transfer in filamentous fermentations. 2nd Int. Bioreactor Conf. on Bioreactor Fluid Dynamics (Cambridge 21-23 Sept.)

30) COYLE, C.K.; HIRSCHLAND, H.E.; MICHEL, B.J. and J. OLDSHUE (1970) Mixing in viscous fluids. A.I.Chem.E.J., (16), No.6, p: 903-906.

31) CRONIN, D.G. (1988) The design of a pilot scale proto fermenter and its

application to mixing, power consumption, heat transfer and mass transfer studies. Ph. D. thesis, Univ. of Birmingham

32) DAWSON, M. (1992) The influence of agitator type on fluid dynamics and oxygen mass transfer in a pilot scale mixing vessel. Ph.D. thesis University of Birmingham.

33) DESPLANCHES, H.; ESSAYEM, F. and M. BRUXELMANE (1986) Hydrodynamics and heat transfer in agitated, aerated Newtonian and highly viscous liquids in the transitional flow regime. 6th European Conf. on Mixing. (24-26 May, Pavia, Italy) p: 479-484.

34) EDWARDS, M.F. (1985) Mixing of low-viscosity liquids in stirred tanks. (in "Mixing in the Process Industries" ed. Harnby, N.; Edwards, M. F. and A. W. Nienow - Butterworth and Cod Ltd.) p:

35) ELSON, T.P.; SOLOMON, J.; NIENOW, A.W. and G.W. PACE (1982) The interaction of yield stress and viscoelasticity on the Weissenberg effect. Jrnl. of non-Newt. Fl. Mech., (11), p:1-22

36) FORD, D.E.; MASHELKAR, R.A. and J.J. ULBRECHT (1972) Mixing times in Newtonian and non-Newtonian fluids. Process Tech. Int., (17), 10, p:321-326.

37) FORD, D.E. and J.J. ULBRECHT (1976) Influence of rheological properties of polymer solutions upon mixing and circulation times. Ind. Eng. Chem., Proc. Des. Dev., (15), No 2, p: 321-326.

38) FUNAHASHI, H.; HARADA, H.; TAGUCHI, H. and T. YOSHIDA (1987) Circulation time distribution and volume of mixing regions in highly viscous xanthan gum solution in a stirred vessel. J. of Chem. Eng.of Japan, (20), No.3, p:277-282

39) GIESEKUS, H. (1964) Some secondary flow phenomena in general viscoelastic fluids. 4th Int. Cong. on Rheology, (1), p: 249-266.

40) GRAY, D.J.; TREYBAL, R.E. and S.M. BARNETT (1982) Mixing of two and single phase systems: power consumption of impellers. A.I.Ch.E. Jrnl., Vol.4, p:195-199

41) HERBST, H.; SUH, I.S.; PETERS, H.; SCHUMPE, A. and W.D. DECKWER (1989) Comparison of various fermenter types for production of xanthan. DECHEMA Biotechnology Conf. 3, Part A, p: 495- 498, VCH, Verlagsgesellschaft, Weinheim.

42) HIXSON, A.W. and G.A. WILKINS (1933) Ind. Eng. Chem. Vol.25 p:1196.

43) HIXSON, A.W. and A.H. TENNEY (1935) Trans. A.I.Ch.E. Vol.31 p: 113.

44) HIXSON, A.W. and V.D. LEUDEKE (1937) Ind. Chem. Eng. Vol.29, p:927.

45) HIXSON, A.W. and S.J. BAUM (1942) Ind Chem.Eng. Vol.34, p: 194.

46) HOOGENDOORN, C.J. and A.P. den HARTOG (1967) Model studies on mixers in the viscous flow region. Chem. Eng. Sci., (22) p: 1689- 1699.

47) HÖCKER, H. (1981) Power consumption of stirrers in non-Newtonian liquids. Ger. Chem Eng., (4), p: 113-123.

48) HÖCKER, H.; LANGER, G. and U. WERNER (1981) Mass transfer in aerated Newtonian and non-Newtonian liquids in stirred reactors. Ger. Chem Eng. (4), p:51-64

49) HUDCOVA, V.; NIENOW, A.W. and V. MACHON (1987) Gas- liquid dispersion with dual Rushton turbine impellers. CHISA (30 August- 4 September, Prague Czechoslavakia) pp. E6.3

50) HUDCOVA, V.; NIENOW, A.W. and V. MACHON (1989) Gas- liquid dispersion with dual Rushton turbine impellers. Biotechno. and bioeng., (34), p: 617-628.

51) HUPPLER, J.D.; ASHARE, E. and L.A. HOLMES (1967) Trans. Soc. Rheol., Vol 11, p:159-179

52) IDE, Y. and J.L. WHITE (1974) Rheological phenomena in polymerisation reactors. Jrnl. Appl. Polym. Sci., (18), p:2997-3018.

53) JOHNSON, R.T. (1967) Batch mixing of viscous fluids. I.and Chem Proc

Des. and Dev. (6), No 3, p:340-345.

54) KEENTOK, M.; GEORGESCU, A.G.; SHERWOOD, A.A. and R.I. TANNER (1989) The measurement of second normal forces for polymeric solutions. Jrnl. of non-Newt. Fluid Mech. (6) p:303- 324 (in Barnes et al., 1989)

55) KHANG, S.J. and O. LEVENSPIEL (1976) New scale-up and design method for stirrer agitated batch mixing vessels. Chem. Eng. Sci. (31) p: 569-577.

56) KIPKE, K. (1980) Gas dispersion in non-Newtonian liquids. Int. Symp. on Mixing- Mons, p: C5 1-22.

57) KOMORI, S. and Y. MURAKOMI (1988) Turbulent mixing in an unbaffled stirred tank with double impellers. 6th Europ. Conf. on Mixing (24-26 May Pavia, Italy) p: 63 - 68.

58) KUBOI, R.; NIENOW, A.W. and K. ALLSFORD (1983) A multipurpose facility for flow visualisation and dual impeller power measurement. Chem Eng.Comm. (22), p:29-39

59) MACHON, V.; VLECK, J.; NIENOW, A.W. and J. SOLOMON (1980) Some effects of pseudoplasticity on hold-up in aerated, agitated vessels. The Chem. Eng. Jrnl. (19) p:67-74

60) MASHELKAR, R.A.; KALE, D.D. and J.J. ULBRECHT (1975) Rotational flows of non-Newtonian fluids. Part 2- Torque Suppresion With Agitators. Trans. Instn. Chem. Engrs. (53), p:150-153

61) METZNER, A. B. and R. E. OTTO (1957) Agitation of non-Newtonian fluids. A.I.Ch.I Journal (3) No.1, p:3-10

62) METZNER, A.B. and J.S. TAYLOR (1960) Flow patterns in agitated vessels. A.I.Ch.I Journal (6) No.1, p:109-114

63) METZNER, A.B.; FEEHS, R.H.; RAMOS, H.L.; OTTO, R.E. and J.D. TUTHILL (1961) Agitation of viscous Newtonian and non-Newtonian fluids. A.I.Ch.I Journal (7) No.1, p:3-9

64) NIENOW, A.W. and D. MILES (1969) A dynamometer for the accurate measurement of mixing torque. J. Sci. Inst. (J. Phys. E.) Series 2, Vol 2, p: 994-995.

65) NIENOW, A.W. and D. MILES (1971) Impeller power numbers in closed vessels. Ind. Eng.Chem.Proc.Des.Devel.- Vol.10 No.1,p:41-43

66) NIENOW, A.W. and D.J. WISDOM (1974) Flow over disc turbine blades. Chem. Eng. Sci., Vol.29 p:1994-1997

67) NIENOW, A.W.; D.J. WISDOM and J. C. MIDDLETON (1977) The effect of scale and geometry on flooding, recirculation and power in gassed stirred vessels. 2nd Europ. Conf. on Mixing (30 March- 1 April Cambridge, U.K.) p:F1-1 F1-16.

68) NIENOW, A.W. and M.D. LILLY (1979) Power drawn by multiple impellers in sparged agitated vessels. Biotechnology and Bioeng. Vol.XXI, p:2341-2345

69) NIENOW, A.W.; WISDOM, D.J.; SOLOMON, J.; MACHON, V. and J. VLECK (1981) The effect of rheology on power consumption in an aerated agitated vessel. Chisa Congress,Prague, paper:A-2-3,p:1-13

70) NIENOW, A.W.; ALLSFORD, K.V. and R. KUBOI (1983 a) Using a derotational prism for studying gas dispersion processes. 9th Eng. Found. Conf.on Mixing

71) NIENOW, A.W.; WISDOM, D.J.; SOLOMON, J.; MACHON, V. and J. VLECK (1983) The effect of rheological complexities on power consumption in an aerated agitated vessel. Chem. Eng. Comm. (19) p: 273-293.

72) NIENOW, A. W. (1984) Mixing studies on high viscosity fermentation processes- xanthan gums. The World Biotech. Report, Vol.1, p:293-304

73) NIENOW, A.W.; EDWARDS M.F. and N. HARNBY (1985) Introduction to mixing problems (in "Mixing in the Process Industries" ed. Harnby, N.; Edwards, M. F. and A. W. Nienow - Butterworth and Cod Ltd.) p: 2-9.

74) NIENOW, A.W. and J.J. ULBRECHT (1985) Gas- liquid mixing and mass transfer in high viscosity fluids (in "Mixing of Liquids by Mechanical Agitation" ed. Ulbrecht, J.J. and G.K. Patterson, Gordon and Breach Sci.

Publishers) p: 203-238.

75) NIENOW, A.W.; WARMOESKERKEN, M.M.C.G.; SMITH J.M. and M. KONNO (1985) On the flooding - loading transition and the complete dispersal condition in aerated vessels agitated by a Rushton turbine. 5th European Conference on Mixing (Wurzburg, Germany) pp: 15, p: 143-154.

76) NIENOW, A. W. (1987) Gas dispersion performance in fermentation operations: a critical review. A.I.Ch.E. Annual Meeting paper 174a

77) NIENOW, A. W. (1987) Stirred tank bioreactors. Bioreactor Engineering Course, Yugoslavia

78) NIENOW, A.W. and T.P. ELSON (1988) Aspects of mixing rheologically complex fluids. Chem.Eng.Res.Des. (66),p:5-15

79) NIENOW, A.W.; HUOXING, L.; HAOZHUNG, W.; ALLSFORD, K.V.; CRONIN D. and V. HUDCOVA (1988) The use of large ring spargers to improve the performance of fermenters agitated by single and multiple standard Rushton turbines. 2nd Int. Conf. on Bioreactor Fluid Dynamics-Cambridge paper D2, p:159-177

80) NOCENTINI, M.; MAGELLI, F. PASQUALI, G. and D. FAJNER (1988) A fluid dynamic study of a gas- liquid, non- standard vessel stirred by multiple impellers. The Chem. Eng. Jrnl. (37), p: 53-59.

81) NOVAK, V. and F. RIEGER (1977) Influence of vessel to screw diameter ratio on the efficiency of screw agitators. Trans. I. Chem.E. (55), p:202-206.

82) OLIVER, R.D.; NIENOW, A.W.; MITSON, R.J. and K. TERRY (1984) Power consumption in the mixing of Boger fluids. Chem. Eng. Res. Des., (62), p: 123-127.

83) ÖZCAN, N.G. (1987) The influence of viscosity on power characteristics in agitated aerated vessels (Influence de la viscosité sur les caractéristiques de puissance des milieux agités et aérés. Mémoire de DEA) M.Phil. Thesis. Université Technologique de Compiègne.

84) ÖZCAN, N.G.; DECLOUX, M. and M. BRUXELMANE (1988) Power characteristics of agitated aerated viscous fluids. 6th European Conf. on Mixing. (24-26 May, Pavia, Italy) p: 361-368.

85) ÖZCAN, N.G.; DECLOUX, M. and M. BRUXELMANE (1990) Effect of viscosity on cavity formation and power characteristics of an agitated aerated Newtonian fluid. Chem. Trans. I. Chem. E. (68) Part A, p:63-68.

86) ÖZCAN, N.G. and A.W. NIENOW (1991) Viscoelastic effects on power consumption and cavity formation in mechanically agitated vessels. 7th European Conf. on Mixing (18-20 Sept., Brugge, Belgium) p: 359-366.

87) ÖZCAN-TASKIN, N.G.; CHATWIN, S. and A.W. NIENOW (1992) Les caractéristiques de puissance des InterMIGs et des turbines Rushton dans les fluides viscoelastiques à viscosité constante. Agitation Industrielle (27-29 January, Toulouse France) pp: II-10

88) ÖZCAN-TASKIN, N.G.; BARTLETT, G. and A.W. NIENOW (1993) Mixing time studies in highly viscous fluids. I.Chem.E. Research Event (5-6 January Birmingham, U.K.) p:672-674.

89) PACA, J.; ETTLER, P. and V. GREGR (1976) Hydrodynamic behavior and oxygen transfer rate in a pilot plant fermenter. J. Appl.Chem. Biotechnology, 26, p:309-317

90) PANDIT, A.B.; RIELLY, C.D.; NIRANJAN, K. and J.F. DAVIDSON (1989) The convex bladed mixed flow impeller: a multi-purpose agitator. Chem. Eng. Sci. (44), No.11, p: 2463-2474.

91) PETERS, D.C. and J.M. SMITH (1969) Mixing in anchor agitated vessels. Can. J. Chem. Eng. (47), p: 268-271.

92) PÖRTNER, R.; LENGER, G. and U. WERNER (1988) Homogenisation of non-Newtonian fluids in stirred tanks. Proc. of the 6th Eur. Conf. on Mixing (24-26 May, Pavia, Italy) p: 521-526.

93) PRILUTSKI G., GUPTA R.K., SRIDHAR T.and M.E. RYAN (1983) Model viscoelastic liquids. Jrnl. of non-Newt. Fl. Mech. (12) p: 233-241

94) PRUD'HOMME, R. K. and E. SHAQFEH (1984) Effect of elasticity on mixing torque requirements for Rushton turbine impellers. A.I. Chem. E. Jrnl. (30), p: 485-486.

95) QURAISHI, A.Q.; MASHELKAR, R.A. and J.J. ULBRECHT (1976) Torque suppression in mechanically strirred liquids and multiphase liquid systems. Jrnl. of non-Newt. Fl. Mech. (1), p:223-245.

96) RANADE, V.R. and J.J. ULBRECHT (1977) Gas dispersion in agitated viscous inelastic and viscoelastic liquids. 2nd Eur. Conf. on Mixing, p: F6 83-100.

97) RENNIE, J. and F.H.H. VALENTIN (1968) Chem. Eng. Sci., Vol. 23, p: 663.

98) RIEGER, F. and V. NOVAK (1974) Power consumption for agitating viscoelastic fluids in the viscous flow regime. Trans. Inst. Chem. Eng. (52), p: 285-286.

99) RIELLY, C.D. and R.E. BRITTER (1985) Mixing times for passive tracers in stirred tanks. 5th Eur. Conf. on Mixing (Wurzburg, 10-12 June) p: 365-375

100) RIELLY, C.D. and R.E. BRITTER (1985) Mixing times in stirred tanks. I.Chem.E. Symp. Series No.94.

101) RIELLY, C.D. and A.B. PANDIT (1988) The mixing of Newtonian fluids with large density and viscosity differences in mechanically agitated contactors. Proc. of the 6th Eur. Conf. on Mixing (24-26 May, Pavia) p: 69-77.

102) RUSHTON, J.H.; COSTICH, E.W. and H.J. EVERETT (1950) Power characteristics of mixing impellers - Part I. Chem. Eng. Prog., Vol.46, No.8, p: 305-404,

103) RUSHTON, J.H.; COSTICH, E.W. and H.J. EVERETT (1950) Power characteristics of mixing impellers - Part II. Chem. Eng. Prog., Vol.46, No.9, p: 467-476

104) RUSZKOWSKI, S.W. and M.J. MUSKETT (1985) Comparative mixing times for stirred tank agitators. Proc. of the 5th Eur. Conf. on Mixing (10-12 June, Wurzburg) p:

105) SHERMAN, P. (1970) Industrial rheology. Academic Press.

106) SKELLAND A.H.P. (1967) Non-Newtonian flow and heat transfer. John Wiley and Sons Inc. New York.

107) SMITH, J.M. (1970) Secondary flow phenomena in mixing viscous and viscoelastic fluids. The Chem. Eng. (March), p:45-49.

108) SMITH, J.M. and M.M.C.G. WARMOESKERKEN (1985) The dispersion of gases in liquids with turbines. 5th Europ. Conf. on Mixing, (10-12 June) Wurzburg, Germany, pp:13, p:115-126.

109) SMITH, J.M. and A.W. SCHOENMAKERS (1988) Blending of liquids of differing viscosity. Chem. Eng. Res. Des. Dev. (66), p:16-21.

110) SOLOMON, J. (1980) Mixing, aeration and rheology of highly viscous fluids. Ph.D. Thesis, University College London.

111) SOLOMON J.,NIENOW A.W., PACE G.W. (1981) Flow patterns in agitated plastic and pseudoplastic viscoelastic fluids. I. Chem. Eng. Symp. Series, No: 64, p:A1-13.

112) TAKEDA, K. and T. HOSHINO (1966) Kagaku Kogoku, Vol.4, p:394.

113) THOMAS, R.H. and K. WALTERS (1964) The motion of an elasticoviscous liquid due to sphere rotating about its diameter. Quart. Jrnl. Mech and Appl. Math. (17). Part 1, p:39-53.

114) THOMSON, J. (18555) Proc. Roy. Soc. Vol.7, p:509.

115) ULBRECHT, J.J. (1974) Mixing of viscoelastic fluids by mechanical agitation. The Chem Eng. p: 347-354.

116) ULBRECHT, J.J. and P. CARREAU (1985) Mixing of viscous non-Newtonian liquids (in 'Mixing of liquids by mechanical agitation' Gordon and Breach, New York. eds. ULBRECHT, J.J. and G.K. PATTERSON) p: 93- 135.

117) UNWIN, W.C. (1880) Proc. Roy. Soc. A31, p:54.

118) vAN'T RIET, K. and J.M. SMITH (1973) The behavior of gas-liquid mixtures near Rushton turbine blades. Chem.Eng. Sci.- Vol.28, p:1031-1037

119) WALTERS, K. and N.D. WATERS (1964) The interpretation of experimental resultsobtained from a rotating sphere elastoviscometer. Brit. J. Appl. Phys. (15), p:989-991.

120) WALTERS, K. and J.G. SAVINS (1965) A rotating sphere elastoviscometer. Trans of the Soc. of Rheol. (9). p:407- 416.

121) WALTERS, K. (1980) Rheometry: Industrial applications. John Wiley and Sons Inc.

122) WARMOESKERKEN, M.M.C.G.; FEIJEN, J. and J.M. SMITH (1981) Hydrodynamics and power consumption in stirred gas- liquid dispersions. I.Chem.E. Symposium Series No.64, p:J1-14

123) WARMOESKERKEN, M.M.C.G.and J.M. SMITH (1982) Description of power curves of turbine stirred gas- liquid dispersions. 4th Europ. Conf. on Mixing, (27-29 April, Noordwijkerhout, The Netherlands), pp G1, p:237-246.

124) WARMOESKERKEN, M.M.C.G. and J.M. SMITH (1985) Flooding of disc turbines in gas- liquid dispersions: a new description of the phenomenon. Chem. Eng. Sci. Vol.40, No.11,p:2063-2071

125) WERNER, H. (1985) Investigation on heat and mass transfer and homogenization in agitated fermenters, on the example of xanthan. Chem. Ing. Tech. (57), No: 6, p: 548-549.

126) WHITE, A.M. and E. BRENNER (1934) Trans. A.I.Ch. E. Vol.30, p:585.

127) WHITE, A.M.; BRENNER, E.; PHILLIPS, G.A. and M.S. MORRISON (1934) Trans. A.I.Ch.E. Vol.30, p: 570.

128) WHITE, A.M. and S.D. SOMERFORD (1936) Chem. and Met. Eng., Vol.43, p:370.

129) WHITE, A.M.; SIRIKALAYA, C. and Y. IDE (1977) Rheological behaviour and

flow patterns around agitators in polymer solutions. Trans. Soc. Rheol. (21), 1, p: 1-18.

130) WHORLOW, R.W. (1980) Rheological techniques. John Wiley and Sons Inc.

131) ZLOKARNIK, M. (1967) Suitability of stirrers for the homogenisation of liquid mixtures. Chem. Ing. Tech., (39) p: 539-548

132) ELSON, T.P.; CHEESMAN, D.J. and A.W. NIENOW (1986) X-ray studies on cavern sizes and mixing performance with fluids possessing a yield stress. Chem.Eng.Sci., Vol.41,No.10, p:2555-2562

133) HERBST, H; SCHUMPE, A. and W.D. DECKWER (1989) Xanthan production in stirred tank fermenters: oxygen transfer and scale-up. DECHEMA (30-31 May, Frankfurt Germany)

134) PETERS, H.; HERBST, H; SUH,I.; SCHUMPE, A. and W.D. DECKWER (1989) The influence of fermenter hydrodynamics on xanthan production by Xanthomonas campestris. (in "Biomedical and Biotechnological Advances in Industrial Polysaccharides" ed. V. Crescini- Gordon and Breach) p: 275-281.

135) CHARLES, M. (1978) Technical aspects of the rheological properties of microbial cultures. Adv. Biochem.Eng. (8) p:1-28.

136) KELKAR, J.V.; MASHELKAR, R.A. and J.J. ULBRECHT (1973) A rotating sphere viscometer. J. Appl. Polym. Sci. (17), p: 3069.

137) KELKAR, J.V.; MASHELKAR, R.A. and J.J. ULBRECHT (1972) On the rotational viscoelastic flows around simple bodies and agitators. Trans. Inst. Chem. Engrs. (50), p:343-352.

138) WATERS, N.D. and M.J. KING (1971) The steady flow of an elastico-viscous liquid induced by a rotating spheroid. Quart. Jrnl. Mech. and Applied Math. (24), part: 3, p:331-346.